Imidazole-Containing Polymerized Ionic Liquids for Emerging Applications: From Gene Delivery to Thermoplastic Elastomers

Michael H. Allen, Jr.

Dissertation submitted to the faculty of the Virginia Polytechnic Institute and State University in partial fulfillment of the requirements for the degree of

Doctor of Philosophy
In
Chemistry

Timothy E. Long
Robert B. Moore
Kevin J. Edgar
Tijana Z. Grove

November 30, 2012
Blacksburg, VA

Keywords: Block Copolymers; Controlled Radical Polymerization; Imidazole; Nonviral Gene Delivery; Polyelectrolytes

Imidazole-Containing Polymerized Ionic Liquids for Emerging Applications: From Gene Delivery to Thermoplastic Elastomers

Michael H. Allen, Jr.

ABSTRACT

Novel imidazole-containing polyelectrolytes based on poly(1-vinylimidazole) (poly(1VIM)) were functionalized with various hydroxyalkyl-substituents to investigate the influence of charge density and hydrogen bonding on nonviral DNA delivery. Copolymers with higher charge densities exhibited increased cytotoxicity, whereas increased hydroxyl concentrations remained nontoxic. DNA binding affinity increased with increased charge densities and increased hydroxyl content. Dynamic light scattering determined the copolymers which delivered DNA most effectively maintained an intermediate binding affinity between copolymer and DNA. Copolymers containing higher charge densities or hydroxyl concentrations bound DNA too tightly, preventing its release inside the cell. Copolymers with lower charge densities failed to protect the DNA from enzymatic degradation. Tuning hydrogen bonding concentration allowed for a less toxic and more effective alternative to conventional, highly charged polymers for the development of nonviral DNA delivery vehicles. The synthesis of amine-containing imidazolium copolymers functionalized with low concentrations of folic acid enabled the investigation of additional polymer modifications on nonviral gene delivery.

Functionalization of 1VIM with various hydroxyalkyl and alkyl groups and subsequent conventional free radical polymerization afforded a series of imidazolium-containing polyelectrolytes. Hydroxyl-containing homopolymers exhibited higher thermal stabilities and lower T_g's compared to the respective alkyl-analog. X-ray scattering demonstrated the polarity of the hydroxyl group facilitated solvation of the electrostatic interactions disrupting the

nanophase-separated morphology observed in the alkylated systems. Impedance spectroscopy determined hydroxyl-containing imidazolium homopolymers displayed higher ionic conductivities compared to the alkyl-containing analogs which was attributed to increased solvation of electrostatic interactions in the hydroxyl analogs.

Beyond functionalizing 1VIM monomers and homopolymers to tailor various properties, the synthesis of novel architectures in a controlled fashion remains difficult due to the radically unstable *N*-vinyl propagating radical. The regioisomer 4-vinylimidazole (4VIM) contains two resonance structures affording increased radical stability of the propagating radical. Nitroxide-mediated polymerization (NMP) and atom transfer radical polymerization (ATRP) failed to control 4VIM homopolymerizations; however, reversible addition-fragmentation chain transfer (RAFT) demonstrated unprecedented control. Linear pseudo-first order kinetics were observed and successful chain extension with additional 4VIM suggested preservation of the trithiocarbonate functionality.

Effectively controlling the polymerization of 4VIM enabled the design of amphoteric block copolymers for emerging applications. The design of ABA triblock copolymers with 4VIM as a high T_g supporting outer block and di(ethylene glycol) methyl ether methacrylate (DEGMEMA) as a low T_g, inner block, required the development of a new difunctional RAFT chain transfer agent (CTA). The difunctional CTA successfully mediated the synthesis of the ABA triblock copolymer, poly(4VIM-*b*-DEGMEMA-*b*-4VIM), which exhibited microphase separated morphologies. The amphoteric nature of the imidazole ring required substantially lower concentrations of outer block incorporation compared to traditional triblock copolymers to achieve similar mechanical properties and microphase separated morphologies.

ACKNOWLEDGEMENTS

I would first like to acknowledge my advisor, Prof. Tim Long, for his support and trust in me these past four years. His advice and ideas greatly enhanced my research during my time here at Virginia Tech. The constant quip in my first couple of years, "You will not graduate from my group an expert in biology; you will graduate as an expert in polymer chemistry," resonated strongly with me and helped to direct my research projects appropriately. His research advice and writing critiques will serve me well in my future endeavors as a scientist. I also like to thank the rest of my committee: Dr. Robert Moore, Dr. Tijana Grove, and Dr. Kevin Edgar. Their assistance and support throughout my time at Virginia Tech was extremely helpful. I am also grateful to the other Virginia Tech present and former faculty whose helpful interactions enhanced my research while at Virginia Tech: Dr. Abby Whittington, Dr. Teresa Reineke, and Dr. S. Richard Turner.

I also thank the funding agencies whose financial assistance supported my graduate research and helped me avoid the dreaded GTA responsibilities for most of my semesters at Virginia Tech. The Army Research Office for the ILEAD MURI and the NSF for the MILES-IGERT fellowship provided financial assistance and materials throughout the years. I also thank Procter & Gamble who provided me with a summer internship and the numerous scientists I interacted with during my time there.

Additionally, the support of numerous staff at Virginia Tech made life much easier over the past four years. Laurie Good, Tammy Jo Hiner, Valerie Owens, and Naya Sou all put forth much time and effort into answering constant questions and requests for me. Without their help with Tim's schedule, paperwork, and constant attention to my stipend, I would still be struggling trying to find Tim during his busy days.

Obviously, I owe much gratitude and appreciation to the members of the Tim Long group in helping me accomplish my research goals and objectives. Without them, I would still be trying to successfully recrystallize a product or distill a monomer. The CRC crew: Matt Green, Eva, Steve, Mana, Ali, David made my first couple years extremely enjoyable and welcoming when I joined the group. The Friday morning breakfasts definitely helped build group camaraderie. I also owe a significant amount of my graduate school successes to the ICTAS II gang: Nancy, Sean, Adam, Ashley, Alex, Chainika, and Dan. Nancy helped keep graduate school light hearted and her fun, always happy personality made coming into work that much more enjoyable. Sean and Adam, my co-inventors, I pretty much owe all my research accomplishments and subsequently the "dream job" I obtained at Adhesives Research to them. Their strong friendship and ingenuity experienced on a daily basis will surely be missed. I cringe when I think of where my research projects would be without their interaction. I also thank Becca Brown and the two Matts, Green and Hunley, who were essentially my unofficial mentors and helped me hit the ground running. I am truly indebted to them and happy to call them lifelong friends. There are numerous other students whom I have interacted with over the years that I would like to thank including: John, Sharlene, Tomonori, Emily, Gozde, Tianyu, Shijing, Renlong, Alie, Keren, and Evan. Additionally the postdocs I interacted with: Kevin Miller, Gene Joseph, Sean Ramirez, Chris, Erin, and Philippe helped me through the trials and tribulations of grad school. I have to also thank the undergraduate and graduate students I mentored: Hiwote, Kelsea, and John. Mentoring the three of them reminded me how much I love science and how truly exciting science can be.

Lastly and most importantly, I have to thank my wife and family for their love and support over these years. Priscilla kept life fun and easy, well I struggled through graduate

school, constantly running errands without me so I could focus on preparing for a group talk or writing a paper. She truly exemplifies unconditional love. My parents Mike and Mary, knew how to keep me going during my first year struggles. Their support was immensely appreciated and quite obvious with either my Dad and his Donovan McNabb email or my mom with her attempts at being consoling over the phone. I also thank my in-laws, Dave and Kathy, who made me feel like I was the most brilliant scientist in the world. It certainly helped do wonders for my confidence when it was constantly being shattered by graduate school. Without the support of these five, I most certainly would not have made it through graduate school.

ATTRIBUTION

Prof. Timothy E. Long
: Professor of Chemistry, Virginia Tech

Dr. Matthew Green
: Former graduate student in the Long Research Group, my mentor as a first year graduate student and collaborator on several research projects involving nonviral gene delivery

Dr. Matthew Hunley
: Former graduate student in the Long Research Group, my other mentor as a graduate student and collaborator on electrospinning projects

Sean Hemp
: Graduate student in the Long Research Group, collaborator on several research projects presented in Ch. 5, 6, 7, and 8

Dr. Adam Smith
: Former research scientist in the Long Research Group, taught RAFT polymerization techniques and collaborated on projects presented in Ch. 7 and 8

Nancy Zhang
: Graduate student in the Long Research Group, performed AFM in Ch. 8 and provided numerous helpful discussions

John Herlihy
: Graduate student in the Long Research Group, synthesized small molecules utilized in Ch. 8

Mingqiang Zhang
: Graduate student in Dr. Robert Moore's research group, performed X-ray scattering of polymers described in Ch. 8

Prof. Robert Moore
: Professor, Virginia Tech, advised Mingqiang Zhang, collaborated on the block copolymer morphology discussed in Ch. 8

Sharon Wang
: Graduate student at University of Pennsylvania, performed X-ray scattering of polymers described in Ch. 6

Prof. Karen Winey
: Professor, University of Pennsylvania, advised Sharon Wang and provided helpful discussions on polymer morphology discussed in Ch. 6

Hiwote Getaneh

Undergraduate student of the chemistry department, performed DNA gel shift assays presented in Ch. 4

Kelsea Day

Undergraduate student of the chemistry department, synthesized copolymers and performed biological assays presented in Ch. 5

Table of Contents

List of Figures

List of Tables

List of Schemes

Chapter 1: Introduction

1.1 *Dissertation Overview*

The central theme of this dissertation encompasses incorporating the imidazole ring into various macromolecules for nonviral gene delivery, electroactive membranes, and thermoplastic elastomers. The second chapter details ring-opening polymerization of various substituted alkylene oxides for emerging applications and concludes with recent work on designing novel imidazole-containing epoxide monomers. The development of imidazole epoxides inspired the polymerization of vinyl-containing imidazole monomers for numerous applications. The third chapter reviews macromolecules containing 1-, 2-, and 4-vinylimidazole and highlights recent developments including water purification, synthetic enzymes, nonviral gene delivery, and controlled radical polymerization.

The fourth chapter focuses on the influence of charge density and hydrogen bonding of imidazolium copolymers on nonviral DNA delivery. Imidazolium copolymers were synthesized with a variety of charge densities and hydroxyl concentrations to tailor polymer-DNA binding affinity through electrostatic interactions and hydrogen bonding. We determined an intermediate binding affinity (25% charge density, 1 hydroxyl group) produced the most efficient DNA delivery vehicles as the polymer released its genetic cargo inside the cell and protected the nucleic acid from enzymatic degradation. The fifth chapter describes the incorporation of folic acid onto imidazolium copolymers for the potential treatment of chronic diseases such as cancer and tumors which commonly over-express folate receptors. Folic acid conjugation onto primary amine-containing imidazolium copolymers dramatically increased nucleic acid gene delivery efficiency in immortalized cervical cancer cells. Copolymers lacking folic acid failed to transfect cells. Fluorescence microscopy determined folic acid functionalized copolymers transfected similarly to positive controls Superfect™ and poly(ethyleneimine).

Chapter six describes the synthesis and characterization of hydroxyalkyl-containing imidazolium homopolymers for electroactive devices. Anion selection and alkyl chain length controlled the thermal transitions and thermal stabilities of the homopolymers. Impedance spectroscopy determined that the incorporation of hydrogen bonding substituents increased ionic conductivities dramatically compared to alkyl-containing imidazolium homopolymers. X-ray scattering demonstrated that the (hydroxy)alkyl chain length influenced backbone-to-backbone spacing, and more importantly, showed hydroxyl incorporation diminished the nanophase-separated morphology present in the alkyl analogs.

The seventh chapter introduces a regioisomer of the commercially available 1-vinylimidazole. 4-Vinylimidazole studied in the late 1970s and early 1980s, lacks commercial production, preventing its widespread use. However, 4-vinylimidazole contains two resonance contributors for its propagating radical. Reversible addition-fragmentation chain transfer demonstrated effective control of the homopolymerization of 4-vinylimidazole. High molecular weight polymers were obtained with narrow polydispersities and linear pseudo-first order kinetics. The eighth chapter describes the synthesis of ABA triblock copolymers which incorporated 4-vinylimidazole in the outer blocks. A new difunctional chain transfer agent enabled the synthesis of the triblock copolymers. These novel, amphoteric block copolymers generated phase separated morphologies with sufficient mechanical properties. The ninth chapter summarizes the accomplishments of the dissertation and the tenth chapter describes the future directions of this research with a strong focus on synthetic design for emerging applications.

Chapter 2: Ring-Opening Polymerization of Substituted Alkylene Oxides for Emerging Applications

2.1 *Abstract*

The ring-opening polymerization of substituted alkylene oxide monomers with various functionalities offers potential for application in numerous emerging fields. The most widespread substituted alkylene oxide monomers remain propylene oxide and styrene oxide; however, the variety of novel substituted alkylene oxide monomers has increased dramatically. Anionic, cationic, coordination, and photo-initiators enable the synthesis of well-defined macromolecules with precise molecular weight control. Substituted alkylene oxide monomers which generate unique macromolecules include glycidyl ether monomers and their derivatives, carbazolyl-containing epoxides, phosphorus-containing epoxides, fluorine-containing epoxides, and silicon-containing epoxides. Ring-opening polymerization of glycidyl ether monomers and their derivatives and silicon-containing epoxides affords polymers for biological and electroactive device applications. Carbazolyl-containing epoxides are also commonly polymerized for electroactive membrane applications while phosphorus-containing polymers exhibit high thermal stabilities and flame retardant behavior. The use of fluorine-containing epoxides has become popular for numerous hydrophobic and low surface energy applications.

2.2 *Introduction*

Alkylene oxide monomers undergo anionic and cationic-initiated ring-opening polymerization (ROP) due to the ring strain in the three-membered ring. Figure 2.1 depicts commonly polymerized alkylene oxide monomers.

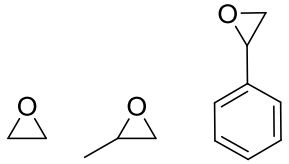

EO PO SO

Figure 2.1. Common alkylene oxide monomers: ethylene oxide (EO), propylene oxide (PO), styrene oxide (SO).

The 60° bond angles induce ring strain in these monomers as compared to the preferred bond angles of 110° for the two carbon atoms and 105° for the oxygen atom.[1] This significant bond angle difference creates a large amount of ring strain, and torsional strain introduces additional ring strain. Torsional strain originates from the eclipsed methylene hydrogen atoms which result from the planar conformation of the epoxide ring. Thermodynamically, polymerization of a three-membered ring is highly favored due to the release of this ring strain resulting in a ΔH_{lc} (liquid monomer to crystalline polymer) of -113.0 kJ mol^{-1} and ΔG_{lc} of -92.5 kJ mol^{-1}.[2] Table 2.1 compares the thermodynamically favorable ROP of a three membered ring *versus* larger rings. Substituents attached to the cycloalkanes decrease the thermodynamic feasibility for ROP due to substituent interactions in the linear polymer.

Table 2.1. Thermodynamics of the polymerization of various cycloalkanes at 25 °C.[2]

n	ΔH_{lc} (kJ mol^{-1})	ΔS_{lc} (J mol^{-1} K^{-1})	ΔG_{lc} (kJ mol^{-1})
3	-113.0	-69.1	-92.5
4	-105.1	-55.3	-90.0
5	-21.2	-42.7	-9.2
6	2.9	-10.5	5.9
7	-21.8	-15.9	-16.3
8	-34.8	-3.3	-34.3

Metal alkoxides, hydroxides, and amides typically initiate anionic ring-opening polymerization.[3] Most anionic ROP proceed as living polymerizations enabling block copolymer synthesis. Cationic polymerization of epoxides occurs via a tertiary oxonium ion formed through use of a Lewis acid. These are typically regioselective polymerizations, although in various polymerizations head-to-head and tail-to-tail structures can disrupt regioregularity.[4] Initiators for cationic polymerization of alkylene oxides include trifluoroacetic acid, fluorosulfonic acid, and triflic acid.[5] The counteranion (A^-) exhibits sufficient nucleophilicity to initiate anionic polymerization; therefore, the presence of a strong acid prevents the potential anionic polymerization. The presence of water inhibits ROP. Cationic photopolymerizations of alkylene oxides are also successful with use of diaryliodonium and triarylsulfonium salts.[6]

Since the 1950s, coordination initiators provide an additional method to ring-open alkylene oxides. This includes the Pruitt-Baggett initiator, a ferric chloride – propylene oxide adduct.[7] Other initiators include $Zn(OCH_3)_2$ and ($[Zn(OCH_3)_2]_2 \cdot [C_2H_5ZnOCH_3]_6$) adducts.[8,9] Metalloporphyrin derivatives containing zinc and aluminum to control the polymerization of ethylene oxide and ethylene oxide block copolymers resulting in narrow polydispersities.[10] In Figure 2.2, two different types of aluminum containing metalloporphyrin derivatives are shown. The polymerization rates accelerate through the use of a sterically-hindered Lewis acid, which weakens the C-O bond making the epoxide more susceptible to nucleophilic attack. Using a hindered acid prevents the acid from reacting with the propagating center of the porphyrin structure.[11] The metalloporphyrin coordinated polymerizations received the term "immortal polymerizations" because the polymerizations remain difficult to terminate due to exchange of once dead polymer chains with the coordination catalyst, therefore, re-initiating polymerization.

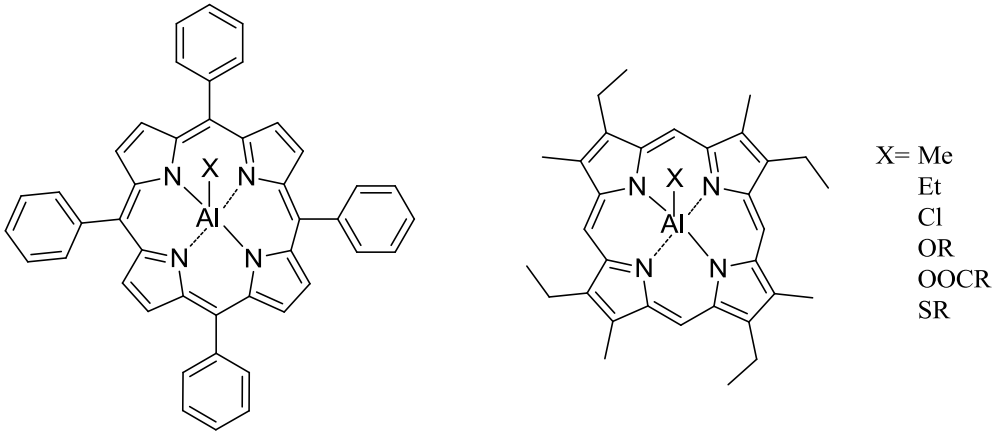

Figure 2.2. Structures of aluminum-containing metalloporphyrin coordination catalysts.[11]

Organotin phosphate condensate catalysts (Bu_2SnO-Bu_3PO_4) also perform ROP of oxirane monomers.[12,13]

Polymerization of PO and other substituted epoxides polymerize at a slower rate than ethylene oxide due to steric hindrance which arises from the additional substituent. Initially, industry began base-catalyzed polymerizations of PO utilizing a metal hydroxide initiator.[14] Abstraction of a proton from the methyl group attached to the epoxide ring resulted in chain transfer forming allyl and propenyl ether endgroups, lowering the degree of polymerization.[15,16] Crown ethers minimize chain transfer and accelerate anionic ring-opening polymerization of PO,[17] however high costs prevented industrial use.

This led to the development of double-metal cyanide (DMC) complex catalysts in the early 1960's for the polymerization of PO forming polyether polyols. Numerous improvements achieved narrow polydispersities, increased molecular weight control, and decreased chain transfer.[18-21] However, these DMC catalysts remained problematic, which required an activation source and long initiation times. Additionally, deactivation occurred when heated at temperatures greater than 100 °C.

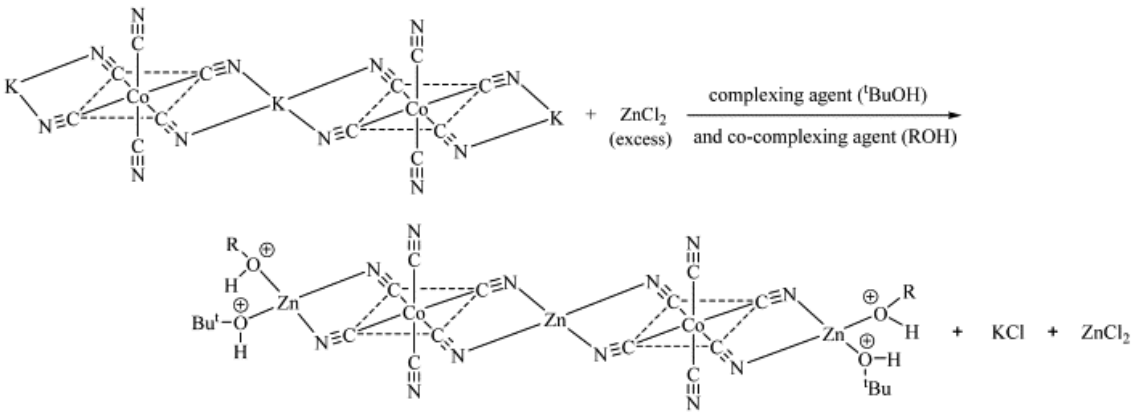

Figure 2.3. Proposed structure of DMC catalyst using ^{t}BuOH as a complexing agent along with a co-complexing agent.[22]

Kim et al. controlled the type and amount of complexing agent during catalyst synthesis as shown above in Figure 2.3 to address these problems.[22] These changes influenced catalytic activity, initiation time, and unsaturation of the endgroups. Qi et al. recently synthesized an improved DMC catalyst based on $Zn_3[Co(CN)_6]_2$, which polymerized PO under milder conditions.[23] The effect of zinc halides as the metal salt in the preparation of these catalysts provided another avenue to tune DMC catalysts for polyol synthesis.[24]

Recently, Moller et al. reported on the use of a phosphazene base (*t*-Bu-P_4, Figure 2.4) coupled with either *n*-butyllithium or an alcohol efficiently ring-opened ethylene oxide producing well-controlled, narrowly defined poly(ethylene oxide).[25-27] *t*-Bu-P_4 exhibited an extremely high basicity similar to alkyllithium reagents and a low nucleophilicity. The polymerizations remain advantageous due to the metal-free conditions, high solubility towards apolar solvents, mild reaction conditions, and stability towards water and oxygen. The phosphazene base effectively catalyzed the alkyllithium initiated polymerization of ethylene oxide through coordination of the Li^+ counterion, suppressing ion pair formation.

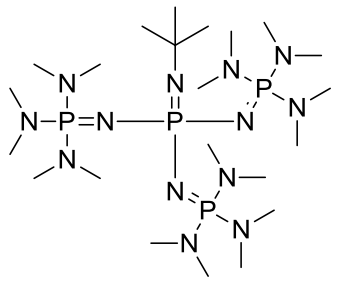

Figure 2.4. Structure of the phosphazene base utilized to ring-open ethylene oxide.

Controlling the stereochemistry of these polymerizations affects the physical properties of the synthesized polymers. Polymerization of the pure enantiomers of PO generates isotactic polymer structures when cleaved at the less sterically hindered carbon of PO. Ninety percent of anionic polymerization reactions show regioselectivity for attack on this carbon.[2] Selectivity at the unhindered carbon is minimal, unless a coordination catalyst is used. Coates and coworkers synthesized high molecular weight >99% isotactic poly(PO) utilizing a cobalt catalyst exclusive to PO.[28] Racemic PO polymerized anionically results in an atactic polymer structure. Cationic ring-opening demonstrated less regioselectivity. Numerous additional catalysts control the stereochemistry of PO and other substituted epoxides.[29]

Styrene oxide has undergone both cationic[30] and anionic[31] ring-opening polymerizations. The polymerizations typically generated oligomers despite high temperatures and long polymerization times. More recently, styrene oxide polymerizations occurred with dialkyl zinc initiators which produced slightly higher molecular weight polymers.[32-34] Another route to polymerization of styrene oxide was the use of a clay catalyst, protonated-montmorillonite, which provided a relatively environmentally benign route for the synthesis of poly(styrene oxide).[35] The use of an anionic organocatalyst, *t*-Bu-P_4, produced high molecular weight poly(styrene oxide) (5,200 - 21,800 g/mol) at room temperature with narrow polydispersities for the first time.[36]

2.3 *Glycidyl Ethers*

Glycidyl ethers are widely commercially available and inexpensive; therefore, the polymerization of these monomers occurs often. Figure 2.5 shows the structure of glycidyl ethers. The structure of glycidyl ethers creates a large amount of ring strain as shown previously in Table 2.1, which enables these monomers to undergo successful ROP utilizing anionic or cationic initiators. Furthermore, the non-oxiranic oxygen allows for ionic coordination polymerization as an additional route for macromolecular synthesis.[37]

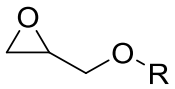

Figure 2.5. Structure of glycidyl ether monomers.

Glycidyl ethers remain popular monomers for cationic photoinitiated polymerizations.[38] Shown in Figure 2.6, Crivello proposed photoinitiated cationic ROP of cyclic ethers occurred as a four step mechanism. The photoinitiator first undergoes photolysis producing both radical and cationic products which will react further to produce a Bronstead acid (HMtXn). The following steps after photolysis are the same as acid-catalyzed cationic ring-opening polymerization of cyclic ethers. The acidic solution protonates the MtX_n^- anion forming HMtXn at the end of the reaction.

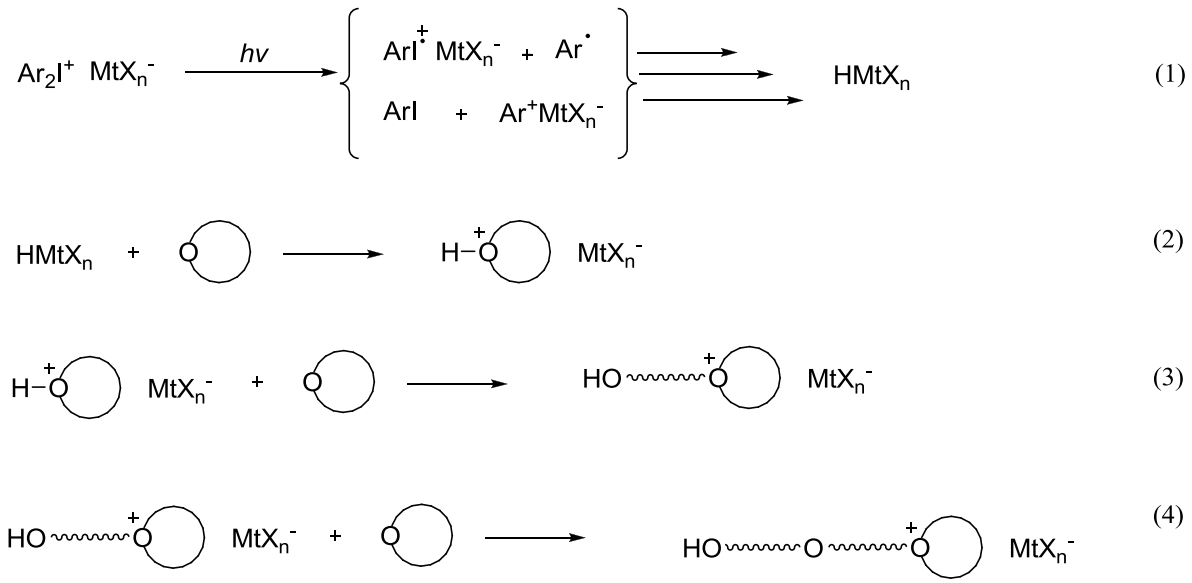

Figure 2.6. Proposed four step photoinitiated cationic ring-opening polymerization of cyclic ethers.[38]

Various alkyl glycidyl ether monomers were synthesized and photopolymerized cationically.[38] During the polymerization, a long induction period resulted due to the formation of a stable secondary oxonium ion. Minimal heat continued the polymerization of the activated monomer. The secondary oxonium ion for both mono- and multi-functional monomers underwent a frontal polymerization mechanism because hydrogen bonding from the ether oxygens stabilized the oxonium ion. After applying heat in an extremely localized fashion, a reaction front occurred emanating from the specific, heated area.

Deep UV microlens arrays contain glycidyl ethers because of their unique ability to photopolymerize easily.[39] A triarylsulfonium hexafluorophosphate salt photoinitiator cationically photopolymerized a copolymer consisting of 1,4-cyclohexandedimethanol diglycidyl ether and trimethylolpropane triglycidyl ether (TMTG). Successful photopolymerization occurred, and the high aliphatic content minimized UV absorption further proving the copolymers use for microlens arrays. Additionally, incorporating TMTG increased the thermal

stability of these arrays. The UV-transparency of these novel polymers produced lenses for AlInGaN light-emitting diodes operating at deep UV wavelengths.

Manufacturers commonly utilize glycidyl phenyl ether (GPE) as a dye or fiber modifier[40] as well as a diluent in epoxy resins.[41] GPE functions well as a model monomer in the study of thermo- and photo-latent initiators.[42] GPEs underwent cationic ring-opening polymerization with tropylium salts as newly synthesized thermal- and photo-latent initiators shown in Figure 2.7.[43]

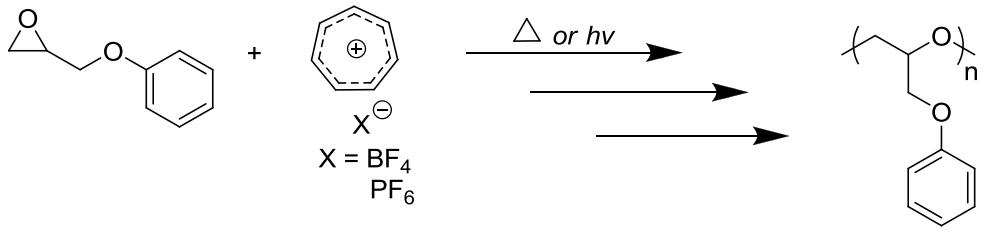

Figure 2.7. Polymerization of GPE using tropylium salts.[43]

GPE also experienced cationic ring-opening polymerization using xanthenyl phosphonium salts as a thermo-latent initiator.[44] Due to the greater reactivity of phosphonium salts, these initiators are preferred compared to other onium salt initiators. Other onium salt cationic ROP initiators of GPE include benzylammonium,[45] benzylsulfonium,[42] benzyl pyridinium,[46] and hydrazinium[47] salts.

Ortiz et al. recently developed activated monomers for the cationic photopolymerization of substituted epoxides.[48] These novel monomers contained substituted benzyl ether groups and those which contained electron-donating substituents exhibited faster rates of photopolymerization. The stabilization of the benzylic free radical and the benzyl carbocation intermediates resulted in the increased photopolymerization rate. Benzyl alcohol additives which contained an electron-donating substituent for the cationic photopolymerizations of epoxide monomers accelerated the polymerizations.[49]

Ronda and coworkers polymerized *p*-Substituted GPE containing electron-donating[50] and electron-withdrawing[51] substituents utilizing various aluminum-based coordinative initiators: $(C_2H_5)_3Al/H2O$ (Vandenberg catalyst), $(C_2H_5)_3Al/CH_3COCH_2COCH_3/H_2O$ (Vandenberg chelate catalyst), $[(CH_3)_2CHO]_2Al\text{-}O\text{-}Zn\text{-}O\text{-}Al[OCH(CH_3)_2]_2$ (Teyssié catalyst) and $[(CH_3)_2CHO]_3Al/ZnCl_2$ (Price catalyst). Although the substituents differed, the catalysts consistently produced polymers with high conversions and high regio- and stereo-selectivity. The results demonstrated non-bonding electrons (i.e. carbonyl oxygen) lowered the polymer conversion due to catalyst passivation.[52] These functionalized polyethers enabled the construction of polymeric supports similar to polystyrene resins.[35] Other coordination catalysts such as organotin phosphate ($Bu_2SnO\text{-}Bu_3PO_4$) selectively ring-opened di-substituted glycidyl ethers resulting in the formation of polyethers containing a side-chain epoxide ring.[53]

Enzymatic ring-opening polymerization has recently received attention as a new method for polymerizing glycidyl ethers. Epoxide hydrolases derived from various species ring-opening epoxides forming a diol.[54,55] The successful ring-opening created interest for enzyme use as a polymerization catalyst. Various lipases catalyzed enzymatic ring-opening polymerizations of dicarboxylic anhydrides with GPE and glycidyl methyl ether as shown in Figure 2.8.[56]

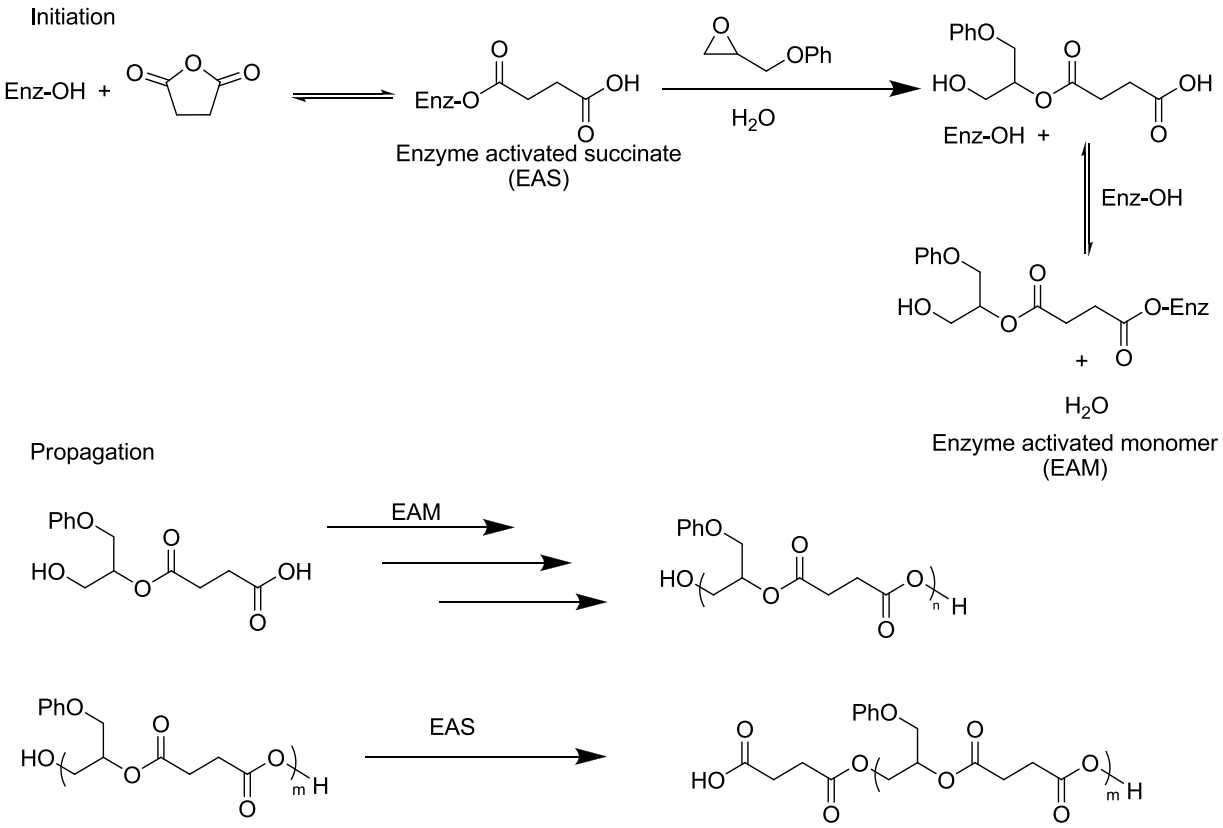

Figure 2.8. Proposed mechanism for the enzymatic ring-opening polymerization of GPE with succinic anhydride.[56]

Glycidyl ether copolymerization with a dicarboxylic anhydride utilized a stepwise reaction which produced weight-average molecular weight polymers (M_w) ranging from 1050-9800 g/mol. A nucleophilic initiator with a lipase catalyst successfully polymerized GPE. An epoxide hydrolase extracted from *Rhodococcus* sp. NCIMB 11216 and other lipases first enzymatically ring-opened glycidols producing water-soluble poly(glycidol).[57] Cationic ring-opening polymerizations which formed poly(glycidol)s exhibited two competing propagation mechanisms: monomer attacking the tertiary oxonium ion and the propagating polymer attacking the protonated monomer.[58,59] This competition resulted in both secondary and primary hydroxyl groups.

Anionic ring-opening polymerization methods polymerized two novel photoresponsive glycidyl-containing polymers, poly(4-glycidyloxyazobenzene) and poly(4-cyano-4'-glycidyloxyazobenzene) as shown in Figure 2.9.[60]

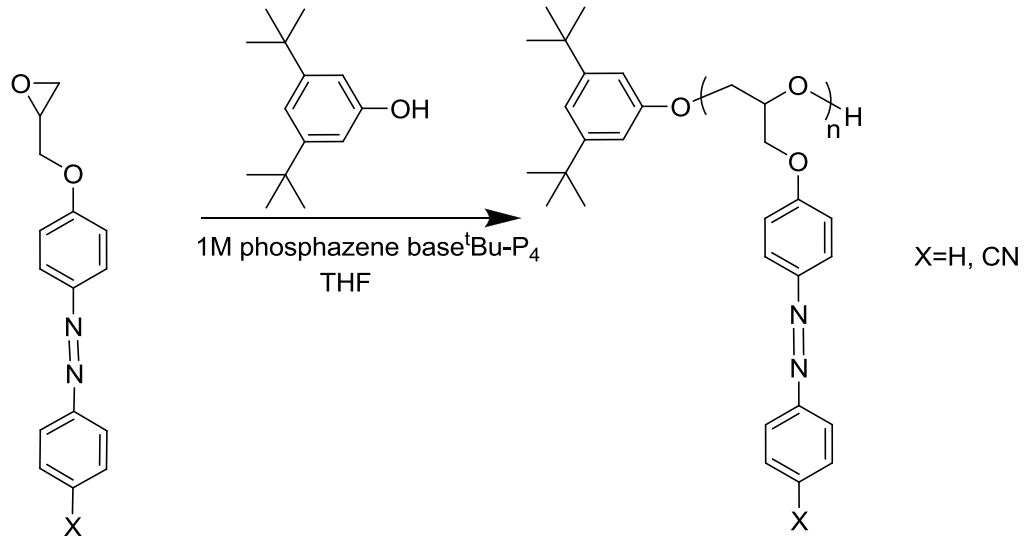

Figure 2.9. Polymerization of poly(4-glycidyl-oxyazobenzene) and poly(4-cyano-4'-glycidyl-oxyazobenzene).[60]

The glass transition temperatures (T_g) of the polymers were 58 °C and 88 °C respectively, with number-average molecular weights (M_n) of 4000 g/mol and polydispersities (PDIs) greater than 1.4 for both polymers. Poly(4-cyano-4'-glycidyloxyazobenzene) exhibited liquid crystalline behavior. Upon irradiation with UV light, both polymers underwent reversible E-Z isomerization. Liquid crystalline smectic behavior arose with the polymerization of benzyl glycidyl ethers substituted with 4-dodecyloxybenzyloxy groups.[61] Anionic ring-opening polymerization of this monomer produced low molecular weight polymers with low conversion; however, the Teyssié catalyst produced high molecular weight polymers with increased stereoregularity. Liquid crystalline behavior from the azobenzene substituents formed polyether structures capable of ion transport due to the weak metal coordinating ether oxygens.

Another novel diglycidyl ether monomer containing azomethine linkages also showed liquid crystalline behavior.[62] The monomers, seen in Figure 2.10, displayed nematic mesophases. Once cured with sulphanilamide, smectic organization occurred. Substituting the side chain with flexible linkages produced a mesophase change and lowered the melting point and T_g.

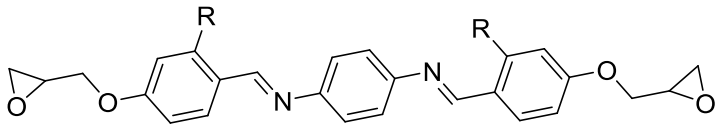

Figure 2.10. Novel azomethine-containing liquid crystalline epoxide (R = H, OCH_3).[62]

The cationic polymerization of allyl glycidyl ether in carbon tetrachloride and 1,2-dimethoxyethane used boron trifluoride tetrahydrofuranate as the initiator.[63] This selective polymerization prevented polymerization of the vinyl substituent. The potential exists to employ this reaction for the formation of multi-centered molecules such as various classes of biopolymers containing different functional substituents. Anionic ring-opening polymerization of ethoxyethyl glycidyl ether initiated with 3-phenyl-1-propanol, trimethylolpropane, di(trimethylolpropane), and dipentaerythrite produced 3-, 4-, and 6-armed star poly(glycidol acetal)s.[64] These polymers were post-functionalized to generate a multi-arm ATRP initiator core for grafting of acrylate monomers as shown in Figure 2.11.

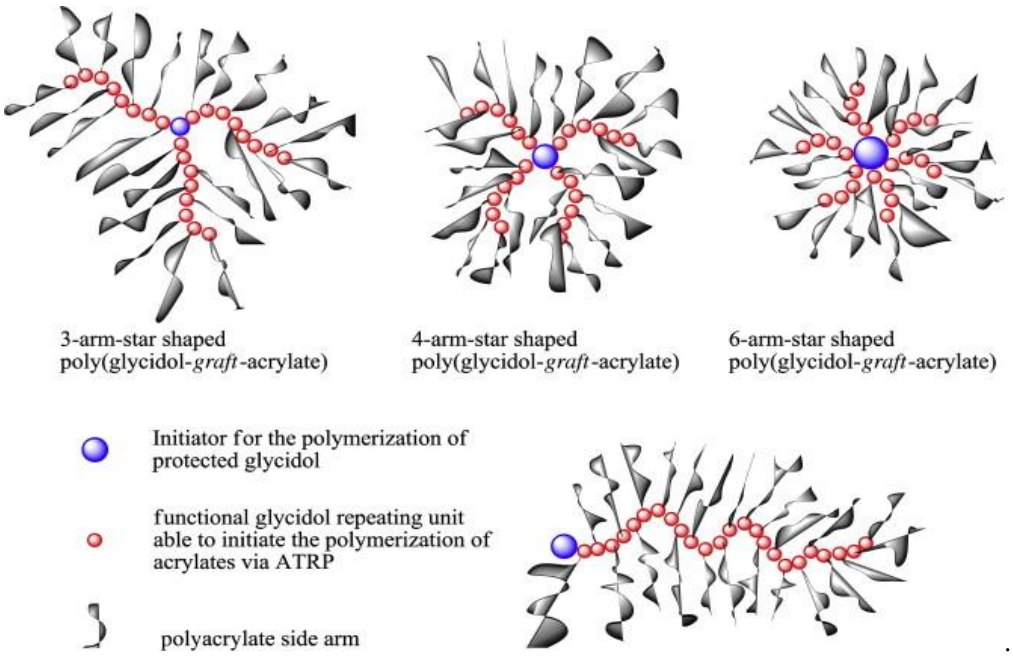

Figure 2.11. Formation of star shaped polymers using ethoxyethyl glycidyl ether.[64]

Poly(ethoxyethyl glycidyl ether) was also synthesized with phenothiazine endgroups using base catalyzed anionic ring-opening polymerization. This created a thermosensitive polymer, which underwent a reversible redox response for electrocatalytic reactions.[65] The incorporation of a cyclic acetal as a pendant group increased the polymer's biological activity. This novel glycidyl ether, 2-(1,3-dioxolan-2-yl)phenoxymethyloxirane, underwent successful anionic ring-opening polymerization using a potassium hydride/crown ether catalyst.[66]

Diglycidyl ethers are widely investigated for biological and electroactive applications. Various diglycidyl ethers underwent ring-opening polymerizations with numerous amines creating a library of eighty branched cationic polymers which delivered DNA for therapeutic applications.[67] The monomer combination of 1,4-cyclohexanedimethanol diglycidyl ether and 1,4-bis(3-aminopropyl) piperazine exhibited the highest transfection efficiency. The polymer transfected more effectively and was less cytotoxic than poly(ethyleneimine), a traditional positive control for nonviral DNA delivery. The curing of diglycidyl with various diamines and

glycidyltrimethylammonium bis(trifluoromethanesulfonyl)imide (GTMATFSI) formed an ion-conductive thermoset.[68] The different polymers displayed high thermal stabilities, low melting points and T_g's, and high ionic conductivities with various networked polymers reaching conductivities above 1.0 x 10^{-3} S/m. Figure 2.12 shows the various polymer compositions and the corresponding ionic conductivities associated with each polymer.

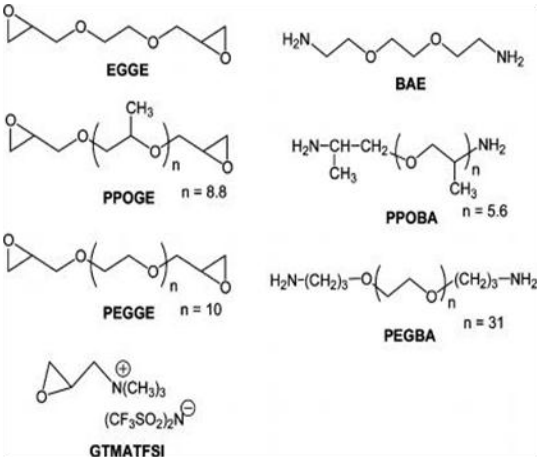

samples	GTMATFSI content (wt%)	ionic conductivity (S/m)
EGGE/GTMATFSI-0.5/BAE	43	$< 1.0 \times 10^{-5}$
EGGE/GTMATFSI-0.5/PPOBA	32	$< 1.0 \times 10^{-5}$
EGGE/GTMATFSI-0.5/PEGBA	15	1.5×10^{-3}
PPOGE/GTMATFSI-0.5/BAE	21	$< 1.0 \times 10^{-5}$
PPOGE/GTMATFSI-0.5/PPOBA	18	1.4×10^{-5}
PPOGE/GTMATFSI-0.5/PEGBA	11	1.2×10^{-3}
PEGGE/GTMATFSI-0.5/BAE	24	2.2×10^{-4}
PEGGE/GTMATFSI-0.5/PPOBA	20	2.3×10^{-4}

Figure 2.12. Various diglycidyl ethers and diamines cured with GTMATFSI with reported ionic conductivities.[68]

The polyether backbone promoted high ionic conductivity due to its extreme flexibility. This flexibility enhanced ionic transport, and the ether oxygens assisted in the dissociation of salts, which further increased polymer conductivity.[69]

Another polymer which could potentially assist in the dissociation of salts, is a novel ladder polymer which was synthesized using a two-step polymerization.[70] The novel glycidyl ether derivative, 3-ethyl-3-oxiranylmethoxymethyloxetane, formed a fused 15-crown-4 polymer. The first step of the polymerization opened the oxiranyl groups of the monomer using an anionic initiator and the second step involved cationic polymerization of the residual oxetanyl groups creating a ladder polymer. Due to the crown-ether like structure, the polymer bound cations effectively, especially Li^+, making it a potentially effective polymer for a lithium polymer

battery application.

2.4 *Carbazole-Containing Epoxides*

The carbazole moiety is a building block in numerous electroactive polymers because it is inexpensive, thermally stable, forms stable radical cations, and displays high charge carrier mobility.[71] Initially, various carbazolyl-substituted epoxide monomers shown in Figure 2.13 proved difficult to polymerize. Cationic initiators such as BF_3 and $SbCl_3$ produced oligomers with extremely low degrees of polymerization.[72] Anionic polymerization initiated with KOH in toluene produced larger oligomers, but the reaction remained heterogeneous. Crown ethers with this system produced a wide range of molecular weights.[73] Stolarzewicz and coworkers later studied the initiation of 2-(9-carbazolyl)ethyl glycidyl ether (CEGE) in K^-, K^+ with crown ether.[74] They found the epoxide ring opened at the un-substituted β-position, and potassium alkoxides formed during the reaction initiated the polymerization. Also, the formation of 9-vinylcarbazole was responsible for the wide range of molecular weights. Potassium *tert*-butoxide and potassium hydride initiators with crown ethers in THF achieved high degrees of polymerization.[75]

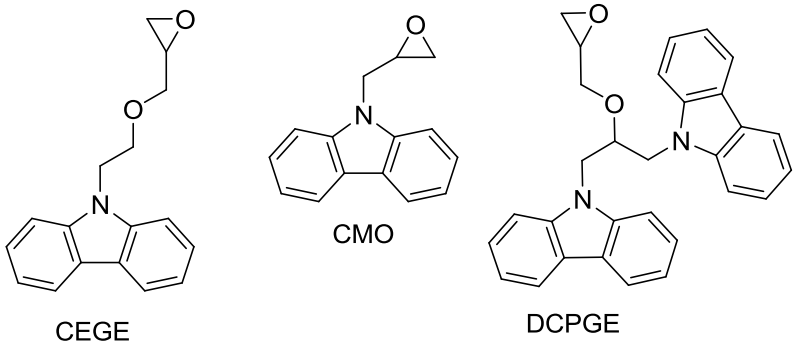

Figure 2.13. Various carbazolyl-substituted epoxide monomers.

Ring-opening *N*-epoxypropylcarbazole with a base successfully produced a high molecular weight (M_w = 440,000 g/mol) polymer. Radical chain inhibitors prevented radical polymerization from occurring. The main applications of this polymer include microfilm,

multicolor slides, and photothermoplastic printing because of its high hole drift mobility. [6,76,77] Another carbazole containing epoxide of interest is 1,3-di(9-carbazolyl)-2-propanol glycidyl ether (DCPGE).[78] This monomer underwent photoinitiated cationic polymerization as a potential application for electrophotographic photoreceptors and electroluminescent devices.[6] Oligomers with a number-average molecular weight (M_n) ranging from 1300-1600 g/mol were produced.

2.5 *Phosphorus-Containing Epoxides*

Poly(alkylene phosphate)s were synthesized in the late 1980s; however, these polymers were not derived from the ring-opening of an alkylene oxide ring.[79] Anionic ring-opening of a cyclic phosphate, followed with oxidation of the poly(alkylene phosphite) produced poly(alkylene phosphate)s as shown in Figure 2.14.

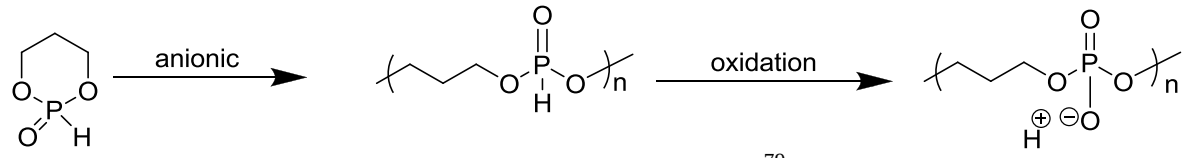

Figure 2.14. Two-step synthesis of poly(alkylene phosphate).[79]

Phosphorus-containing epoxides in which the phosphorus atom is attached directly to the α or β position on the epoxide ring remain unachievable due to the substitution reactions simultaneously opening the epoxide ring. As a result, indirect attachment of the phosphorous atom to the epoxide ring prevents epoxide ring opening as shown in Figure 2.15. These epoxides exhibit high thermal stabilities and typically reside in epoxy resin thermosets.

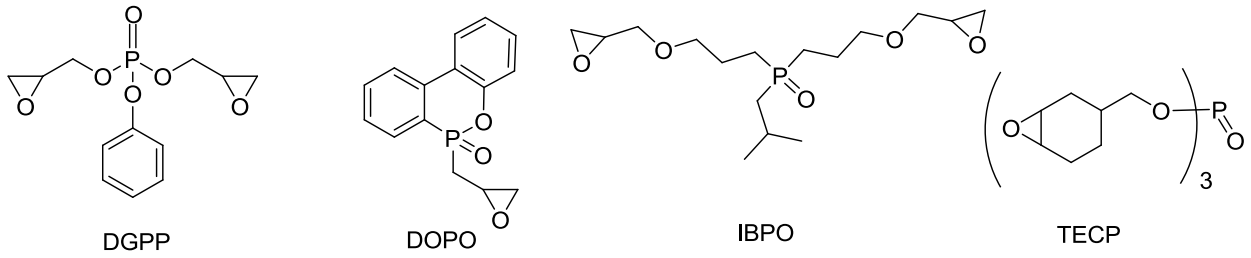

Figure 2.15. Structures of phosphorus-containing epoxide monomers.

Epoxy resin thermosets are industrially appealing because of low shrinkage, electrical insulation, excellent adhesive properties, and resistance to numerous chemicals.[80] Phosphorus-containing epoxy resins display high thermal stabilities and flame retardant characteristics.[81,82] Derouet et al. synthesized a phosphorus-containing epoxy resin through the reaction of 4,4'-diglycidylether of bisphenol A (DGEBA) with dialkyl phosphates which underwent curing with a sulfone-containing diamine.[83] Diphenylphosphate grafts improved the flame retardant nature of this resin. Bis-glycidyloxy phenylphosphate (DGPP) when cured with diamines showed high char yields and fire retardant behavior as seen in Figure 2.16.[84] They observed a two-step weight loss which indicated the phosphorus segments decomposed then formed a residue which prevented further decomposition resulting in a high char yield. High char yields remain important for flame retardant behavior because the minimized combustion prevents release of volatile and potentially harmful gases.

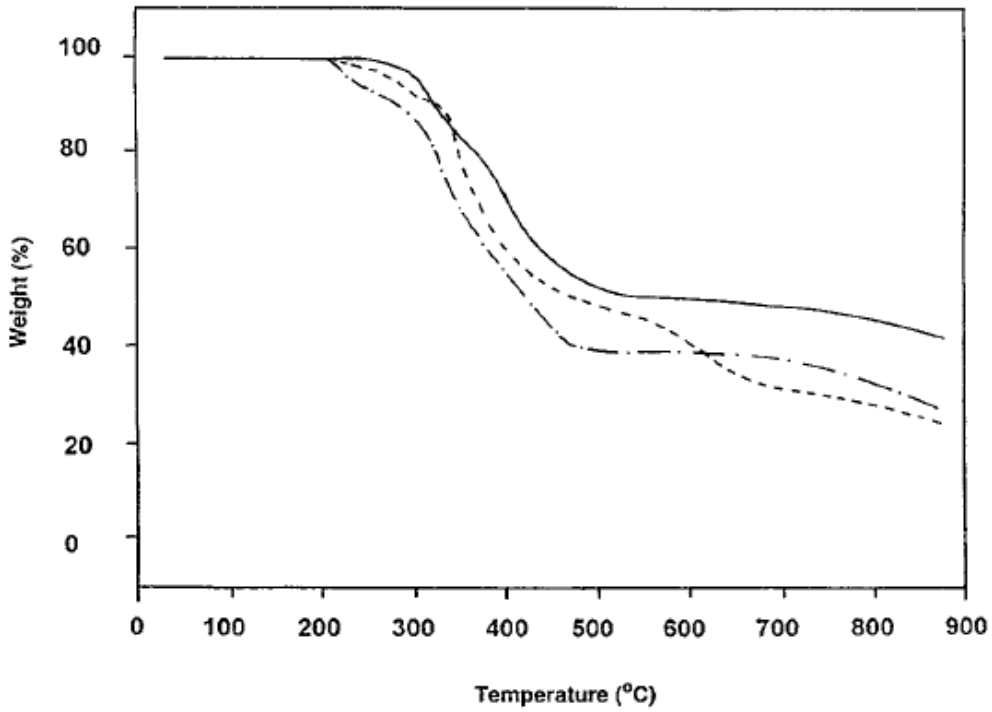

Figure 2.16. TGA thermogram of DGPP cured with various diamines.[85]

When blended with DGEBA, the mechanical properties of the polymer improved significantly. Also, DGPP cured with various aromatic diamines formed organophosphorus nematic liquid crystalline thermosets.[85]

A novel glycidyl compound, isobutylbis(glycidylpropylether) phosphine oxide (IBPO), was synthesized and polymerized to provide an environmentally friendly flame retardant material.[86] Previously, numerous phosphorus-containing diglycidyl ether compounds were synthesized containing the hydrolytically unstable P-O-C bond. This novel polymer contained P-C bonds which exhibited greater chemical stability. The anionic catalyst, 4-dimethylaminopyridine, successfully polymerized this monomer while cationic ring-opening failed to generate polymer. Cadiz et al. also synthesized another novel monomer, 9,10-dihydro-9-oxa-10-phosphaphenantrene-10-oxide (DOPO), where the glycidylic group attached directly to

the phosphorus atom.[87] This novel monomer polymerized cationically, but anionic polymerization and amine curing both failed.

Shi et al. synthesized a novel multi-functional monomer, tri(3,4-epoxycyclohexylmethyl) phosphate (TECP), which underwent cationic photopolymerization.[88] This monomer was of interest because most UV curable epoxy resins are flammable, but the incorporation of the phosphate group into this monomer imparted fire-retardant behavior. The flame retardancy of a cycloaliphatic epoxy resin showed an improvement from 21 to 27 on the limiting oxygen index scale, a measure of flame retardance, upon 50% incorporation of the TECP monomer. Tensile properties of the resin also improved.

2.6 *Fluorine-Containing Epoxides*

Fluorinated epoxide monomers have gained interest due to their low surface energy, excellent chemical and thermal stability, low refractive index, and low friction coefficient.[89-93] Gard et al. synthesized fluorinated aliphatic epoxides containing sulfonyl fluoride end groups which underwent a photocatalyzed copolymerization with a cycloaliphatic diepoxide as shown in Figure 2.17.[94-96] The sulfonyl fluoride groups coated the outer surface of the cross-linked film at the film-air interface. The polymerization advantageously created a thin film coating while using small quantities of expensive fluorinated monomer. These polymers have potential applications as ion-exchange resins or surfactants.

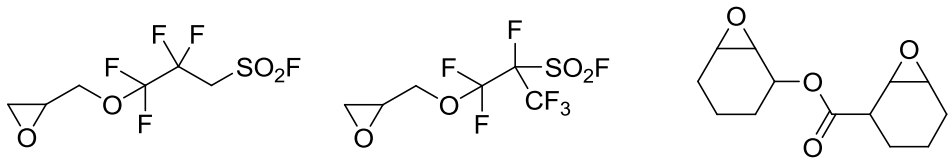

Figure 2.17. Two fluorinated epoxide monomers cured with a cycloaliphatic diepoxide.[94]

Priola et al. also photopolymerized novel difunctional fluorinated epoxide monomers.[97] These monomers were synthesized through allylation of a fluorinated diol followed with epoxidation as seen in Figure 2.18.

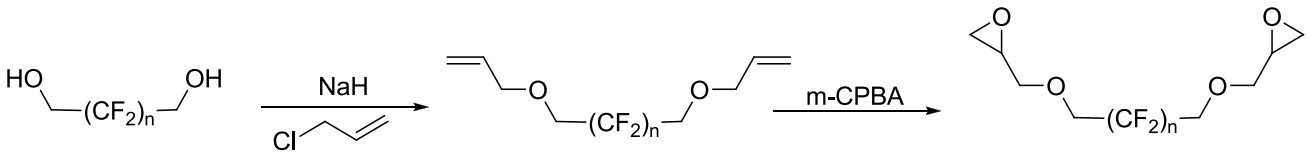

Figure 2.18. Synthetic of difunctional fluorinated epoxide monomers (n = 4, 8).[97]

The UV cured polymers and the fluorine-containing epoxides cured faster than hexanediol glycidyl ether as a result of the decreased nucleophilicity of the glycidyl oxygen due to the electronegativity of the fluorine atoms. The homopolymers formed glassy networks and the fluorinated monomer : HDGE comonomer (1:1 ratio) formed a homogeneous copolymer network which underwent post-curing polymerization. The surfaces of the fluorinated homopolymer films showed hydrophobic character as did the copolymer films due to the location of the fluorinated segments at the film-air interface as shown in Table 2.2. Gard and co-workers reported a similar photopolymerization surface coating phenomenon.[94]

Table 2.2. Contact angle measurements of various UV cured fluorine-containing epoxides.

UV cured sample	Θ (deg)
HDGE	70
F8	95
F16	110
HDGE:F8 1:1	98
HDGE:F16 1:1	112

Ring-opening polymerization of 1,2-epoxy-4,4,4-trifluoro-2-methylbutane was successfully reported using a bis(diisobutylaluminum oxide) catalyst.[98] Deprotonation of the methyl group limited the molecular weight of the polymer (M_n = 2,100 g/mol) due to the catalyst

binding to the least hindered face of the epoxide ring which placed the methyl group properly for regioselective deprotonation. Poly(3,3,3-trifluoropropylene oxide) was first polymerized using both cationic and anionic initiators with the use of successful endgroup determination.[99]

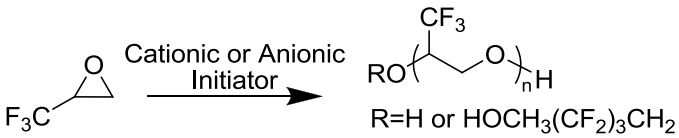

Figure 2.19. Polymerization of 3,3,3-trifluoropropylene oxide.[99,100]

Aluminum chloride or boron trifluoride successfully polymerized the fluorinated epoxide monomer cationically with hydroxyl endgroups as shown in Figure 2.19. However, BF_3 initiated polymers contained unsaturation as did polymers synthesized anionically utilizing potassium hydroxide, as a result of fluoride ion and proton abstraction respectively. Initiation with monosodium salt of hexafluoropentanediol afforded a monofunctional polymer containing only hydroxyl endgroups; ideal for incorporation into polyurethanes. The molecular weights obtained using these polymerizations ranged between 1000-4300 g/mol.

Fluorinated epoxides were also successfully polymerized with controlled regiochemistry. A zinc complex or KOH initiator generated poly(3,3,3-trifluoropropylene oxide) and its copolymers to control the polymerization regioselectivity.[100] Nozaki et al. developed an improved initiator/catalyst system using C_6F_6 as the solvent and $MePPh_3Br$ as the initiator.[101] This initiator produced more regioregular fluorine-rich epoxides due to better solubility of the epoxide as compared to zinc complex or KOH systems. They concluded the monosubstituted enantiopure epoxide monomers afforded optically active isotactic polyethers, and the corresponding racemic monomers produced atactic polyethers utilizing anionic polymerization.[102]

2.7 *Silicon-Containing Epoxides*

High reactivity and rapid cationic photopolymerization characterize silicon-containing epoxides. Applications including paper treatments and coatings for wood and plastics commonly utilize these monomers.[103] Addition of functional silanes to epoxides containing double bonds was the first reported synthesis of silicon-containing epoxides.[104,105] Crivello synthesized novel silicon-containing epoxide monomers with similar reactions.[6] Various derivatives included different amounts and placements of the epoxide rings. The epoxide rings attached to cycloaliphatic rings underwent cationic photoinitiated polymerization at a faster rate than conventional epoxides. Ortiz et al. synthesized novel highly reactive monomers for cationic photopolymerization through the modification of the silicon-epoxide monomer with substituted benzyl ether groups.[103] Monomers, shown in Figure 2.20, modified with methoxy groups exhibited faster rates of polymerization.

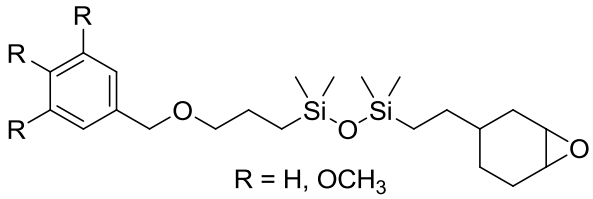

Figure 2.20. Modified silicon-epoxide monomer for cationic photopolymerization.

This was a result of stabilization of the carbocation formed during polymerization. The improved rate of polymerization proved suitable for potential photocurable applications which required a high speed, automated process.

Another application of silicon-containing epoxides is to improve holographic performance, specifically increasing the information packing density of optical storage data. The photopolymerization of original monomers resulted in volume shrinkage. It was found that ring-opening polymerization prevented volume shrinkage. Siloxane components targeted for this

application exhibit optical clarity and high thermal stability above 300 °C. The incorporation of the siloxane-containing bicyclic epoxide monomer improved diffraction efficiency and morphology of the holographic gratings.[106] Figure 2.21 shows SEM images of the original polymer and the newly synthesized polymer cured with the siloxane-containing bicyclic epoxide monomer. An increase in optical clarity and grating space is evident in the SEM images.

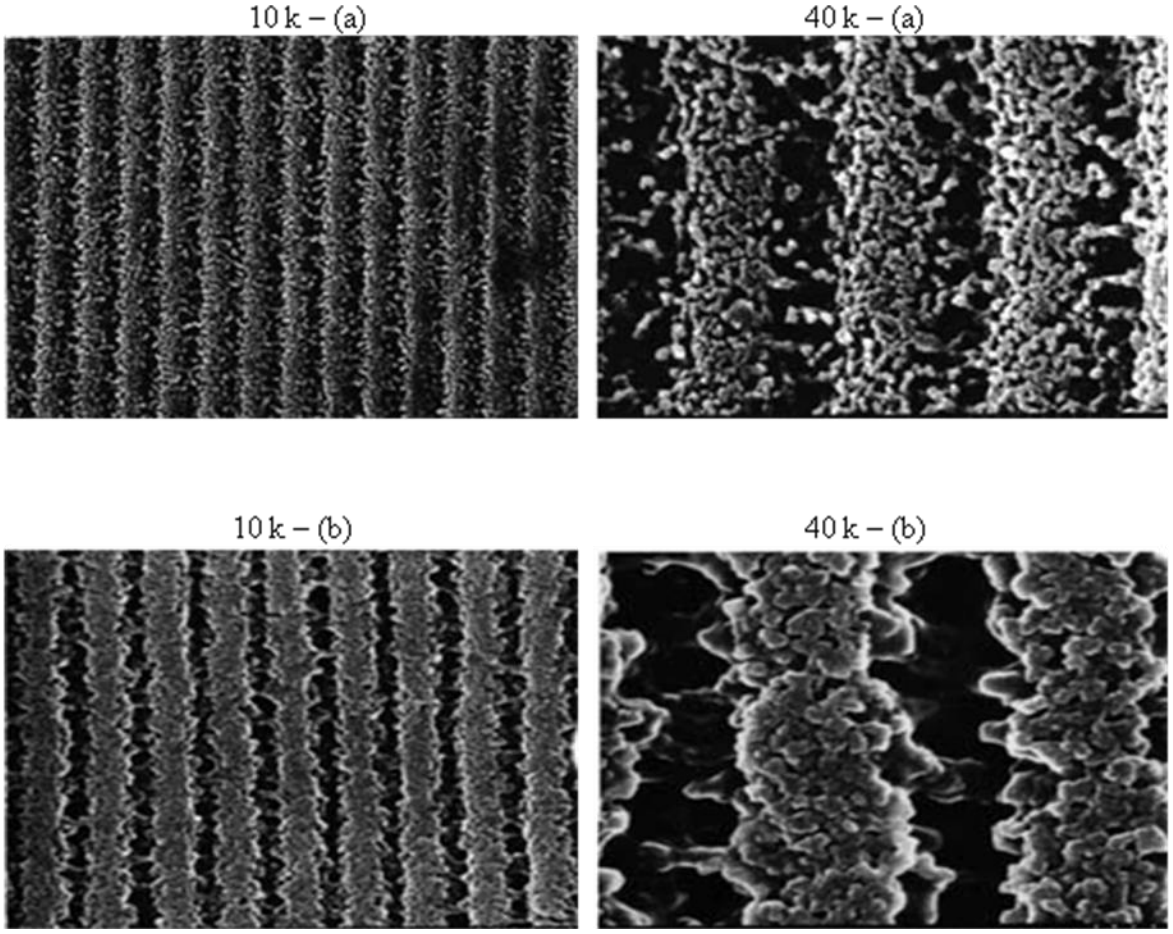

Figure 2.21. SEM images of original holographic polymer (a) and synthesized silicon-containing epoxide polymer (b).[106]

2.8 *Conclusions*

The ring-opening polymerization of substituted alkylene oxide monomers with various functionalities offers a variety of avenues to tailor polymer properties for emerging applications.

Propylene oxide and styrene oxide ROPs remain widely important for industrial applications; however, recent development of novel substituted alkylene oxide monomers has enabled the design of macromolecules for an assortment of biological and materials science applications. Numerous initiators and catalysts including anionic, cationic, coordination, and photoinitiators afford the synthesis of well-defined macromolecules with precise molecular weight control. Substituted alkylene oxide monomers which undergo ROP include glycidyl ether monomers, carbazolyl-containing epoxides, phosphorus-containing epoxides, fluorine-containing epoxides, and silicon-containing epoxides. ROP of glycidyl ether monomers and silicon-containing epoxides generate macromolecules for biological applications including nonviral gene delivery and optical device storage applications. Carbazolyl-containing epoxides are also commonly polymerized for electroactive membrane applications due their high thermal stability and inexpensive costs. Phosphorus-containing polymers also exhibit high thermal stabilities and flame retardant behavior. The use of fluorine-containing epoxides has become popular for numerous hydrophobic coatings due to the low surface energy and low coefficient of friction of these systems. The incorporation of a wide variety of these molecules into homopolymers and copolymers affords the design of novel polymer architectures for a wide array of future technologies.

2.9 *Acknowledgements*

This material is based upon work supported in part by the Macromolecular Interfaces with Life Sciences (MILES) Integrative Graduate Education and Research Traineeship (IGERT) of the National Science Foundation under Agreement No. DGE-0333378. This material is also based upon work supported in part by the US Army Research Office under Grant No. W911NF-07-1-0452 Ionic Liquids in Electro-Active Devices (ILEAD) MURI.

2.10 *References*

(1) Green, M.; Wittcoff, H. In *Organic Chemistry Principles and Industrial Practice*; Wiley-VCH: 2003, p 71-80.

(2) Odian, G. In *Principles of Polymerization: Fourth Edition*; John Wiley & Sons, Inc.: Hoboken, NJ, 2004.

(3) Boileau, S. In *Comprehensive Polymer Science*; Eastmond, G. C., Ledwith, A., Russo, S., Sigwalt, P., Eds.; Pergamon Press: London, 1989; Vol. 3, p 467-487.

(4) Worsfold, D. J.; Eastham, A. M. *J. Am. Chem. Soc.* **2002**, *79*, 900-902.

(5) Dreyfuss, P.; Dreyfuss, M. P. In *Comprehensive Polymer Science*; Eastmond, G. C., Ledwith, A., Russo, S., Sigwalt, P., Eds.; Pergamon Press: London, 1989; Vol. 3.

(6) Crivello, J. V. *Polymer Engineering & Science* **1992**, *32*, 1462-1465.

(7) Yilmaz, O.; Usanmaz, A.; Alyuruk, K. *Journal of Polymer Science, Part C: Polymer Letters* **1990**, *28*, 341-3.

(8) Hagiwara, T.; Ishimori, M.; Tsuruta, T. *Macromol. Chem. Phys.* **1981**, *182*, 501-11.

(9) Hasebe, Y.; Tsuruta, T. *Makromolekulare Chemie* **1988**, *189*, 1915-26.

(10) Aida, T.; Inoue, S. *Acc. Chem. Res.* **1996**, *29*, 39-48.

(11) Inoue, S. *J. Polym. Sci., Part A: Polym. Chem.* **2000**, *38*, 2861-2871.

(12) Miura, K.; Kitayama, T.; Hatada, K.; Nakata, T. *Polym. J.* **1993**, *25*, 685-696.

(13) Schütz, C.; Dwars, T.; Schnorpfeil, C.; Radnik, J.; Menzel, M.; Kragl, U. *J. Polym. Sci., Part A: Polym. Chem.* **2007**, *45*, 3032-3041.

(14) Simons, D. M.; Verbanc, J. J. *Journal of Polymer Science* **1960**, *44*, 303-311.

(15) Pierre, L. E. S.; Price, C. C. *J. Am. Chem. Soc.* **1956**, *78*, 3432-3436.

(16) Steiner, E. C.; Pelletier, R. R.; Trucks, R. O. *J. Am. Chem. Soc.* **1964**, *86*, 4678-4686.

(17) Becker, H.; Wagner, G. *Acta Polym.* **1984**, *35*, 28-32.

(18) Hinney, H. R.; Wardius, D. S. *Process for preparing metal cyanide complex catalyst*; (Arco Chemical Technology, L.P., USA). Application: US, 1992.

(19) Le-Khac, B. *Highly active double metal cyanide catalysts*; (ARCO Chemical Technology, L.P., USA). Application: US, 1997.

(20) McDaniel, K. G.; Perry, M. J.; Hayes, J. E. *Direct polyoxyalkylation of glycerin with double metal cyanide catalysis*; (Arco Chemical Technology, L.P., USA; Arco Chemie Technologie Nederland B.V.). Application: WO, 1999.

(21) Hofmann, J.; Gupta, P.; Pielartzik, H.; Ooms, P.; Schafer, W. *New zinc-metal-hexacyanocobaltate catalysts for the production of polyether polyols*; (Bayer A.-G., Germany). Application: EP, 1999.

(22) Kim, I.; Ahn, J.-T.; Ha, C. S.; Yang, C. S.; Park, I. *Polymer* **2003**, *44*, 3417-3428.

(23) Huang, Y.-J.; Qi, G.-R.; Wang, Y.-H. *J. Polym. Sci., Part A: Polym. Chem.* **2002**, *40*, 1142-1150.

(24) Kim, I.; Byun, S. H.; Ha, C.-S. *J. Polym. Sci., Part A: Polym. Chem.* **2005**, *43*, 4393-4404.

(25) Esswein, B.; Steidl, N. M.; Möller, M. *Macromol. Rapid Commun.* **1996**, *17*, 143-148.

(26) Esswein, B.; Möller, M. *Angew. Chem. Int. Ed.* **1996**, *35*, 623-625.

(27) Esswein, B.; Molenberg, A.; Möller, M. *Macromolecular Symposia* **1996**, *107*, 331-340.

(28) Peretti, K. L.; Ajiro, H.; Cohen, C. T.; Lobkovsky, E. B.; Coates, G. W. *J. Am. Chem. Soc.* **2005**, *127*, 11566-11567.

(29) *Stereoselective Polymerization with Single-Site Catalysts*; Baugh, L. S.; Canich, J. A. M., Eds.; CRC, 2007.

(30) Colclough, R. O.; Gee, G.; Higginson, W. C. E.; Jackson, J. B.; Litt, M. *Journal of Polymer Science* **1959**, *34*, 171-179.
(31) Jedli, Z.; nacute; ski; Kasperczyk, J.; Dworak, A.; Matuszewska, B. *Die Makromolekulare Chemie* **1982**, *183*, 587-591.
(32) Tsuruta, T.; Inoue, S.; Tsubaki, K. *Die Makromolekulare Chemie* **1968**, *111*, 236-246.
(33) Kasperczyk, J.; Jedli, Z. J.; nacute; ski *Die Makromolekulare Chemie* **1986**, *187*, 2215-2221.
(34) Sepulchre, M.; Kassamaly, A.; Moreau, M.; Spassky, N. *Die Makromolekulare Chemie* **1988**, *189*, 2485-2501.
(35) Yahiaoui, A.; Belbachir, M. *J. Appl. Polym. Sci.* **2006**, *100*, 1681-1687.
(36) Misaka, H.; Sakai, R.; Satoh, T.; Kakuchi, T. *Macromolecules* **2011**, *44*, 9099-9107.
(37) Shechter, L.; Wynstra, J. *Industrial & Engineering Chemistry* **1956**, *48*, 86-93.
(38) Crivello, J. V. *J. Polym. Sci., Part A: Polym. Chem.* **2006**, *44*, 6435-6448.
(39) Mackintosh, A. R.; Kuehne, A. J. C.; Pethrick, R. A.; Guilhabert, B.; Gu, E.; Lee, C. L.; Dawson, M. D.; Heliotis, G.; Bradley, D. D. C. *J. Phys. D: Appl. Phys.* **2008**, 094007.
(40) Kim, M.; Sanda, F.; Endo, T. *J. Appl. Polym. Sci.* **2001**, *81*, 2347-2351.
(41) Morikawa, H.; Sudo, A.; Nishida, H.; Endo, T. *J. Appl. Polym. Sci.* **2005**, *96*, 372-378.
(42) Shimomura, O.; Tomita, I.; Endo, T. *Macromol. Rapid Commun.* **1998**, *19*, 493-497.
(43) Hino, T.; Endo, T. *J. Polym. Sci., Part A: Polym. Chem.* **2004**, *42*, 2166-2170.
(44) Gupta, M.; Singh, R. *Polym. Bull.* **2008**, *60*, 755-763.
(45) Kirino, M.; Sanda, F.; Endo, T. *J. Polym. Sci., Part A: Polym. Chem.* **2000**, *38*, 3428-3433.
(46) Yagci, Y.; Endo, T. In *Polymer Synthesis/Polymer Catalysis* 1997, p 59-86.
(47) Kim, M. S.; Lee, S. B.; Lee, K. W.; Endo, T. *J. Appl. Polym. Sci.* **2005**, *95*, 1439-1442.
(48) Ortiz, R. A.; Herrera, L. E.; Crivello, J. V. In *Journal of Macromolecular Science: Pure & Applied Chemistry*; Taylor & Francis Ltd: 2004; Vol. 41, p 757-777.
(49) Crivello, J. V.; Ortiz, R. A. *J. Polym. Sci., Part A: Polym. Chem.* **2002**, *40*, 2298-2309.
(50) Ronda, J. C.; Serra, A.; Cádiz, V. *Macromol. Chem. Phys.* **1997**, *198*, 2917-2934.
(51) Ronda, J. C.; Serra, A.; Cádiz, V. *Macromol. Chem. Phys.* **1997**, *198*, 2935-2948.
(52) Ronda, J. C.; Serra, A.; Cádiz, V. *Macromol. Chem. Phys.* **1999**, *200*, 221-230.
(53) Iwasa, N.; Miura, K.; Kan, S.; Furukawa, Y. *Polym. Bull.* **2008**, *61*, 207-216.
(54) Archer, I. V. J. *Tetrahedron* **1997**, *53*, 15617-15662.
(55) Rink, R.; Kingma, J.; Lutje Spelberg, J. H.; Janssen, D. B. *Biochemistry* **2000**, *39*, 5600-5613.
(56) Soeda, Y.; Okamoto, T.; Toshima, K.; Matsumura, S. *Macromolecular Bioscience* **2002**, *2*, 429-436.
(57) Soeda, Y.; Toshima, K.; Matsumura, S. *Chem. Lett.* **2001**, *30*, 76-77.
(58) Tokar, R.; Kubisa, P.; Penczek, S.; Dworak, A. *Macromolecules* **2002**, *27*, 320-322.
(59) Dworak, A.; Walach, W.; Trzebicka, B. *Macromol. Chem. Phys.* **1995**, *196*, 1963-1970.
(60) Peris, S.; Tylkowski, B.; Ronda, J. C.; Garcia-Valls, R.; Reina, J. A.; Giamberini, M. *J. Polym. Sci., Part A: Polym. Chem.* **2009**, *47*, 5426-5436.
(61) Giamberini, M.; Reina, J. A.; Ronda, J. C. *J. Polym. Sci., Part A: Polym. Chem.* **2006**, *44*, 1722-1733.
(62) Lu, M.; Kim, S. *Korea Polymer Journal* **1999**, *7*, 304-309.
(63) Grinevich, T.; Belyakov, P.; Solov'yanov, A. *Polymer Science Series B* **2006**, *48*, 75-77.
(64) Schmitz, C.; Keul, H.; Möller, M. *Eur. Polym. J.* **2009**, *45*, 2529-2539.

(65) Nakadan, N.; Imabayashi, S.-i.; Watanabe, M. *Langmuir* **2004**, *20*, 8786-8791.
(66) Maślińska-Solich, J.; Sowa, M.; Neugebauer, D. *Polym. Int.* **2004**, *53*, 364-369.
(67) Barua, S.; Joshi, A.; Banerjee, A.; Matthews, D.; Sharfstein, S. T.; Cramer, S. M.; Kane, R. S.; Rege, K. *Molecular Pharmaceutics* **2008**, *6*, 86-97.
(68) Matsumoto, K.; Endo, T. *Macromolecules* **2009**, *42*, 4580-4584.
(69) Masuda, Y.; Seki, M.; Nakayama, M.; Wakihara, M.; Mita, H. *Solid State Ionics* **2006**, *177*, 843-846.
(70) Satoh, T.; Ishihara, H.; Sasaki, H.; Kaga, H.; Kakuchi, T. *Macromolecules* **2003**, *36*, 1522-1525.
(71) Grazulevicius, J. V.; Strohriegl, P.; Pielichowski, J.; Pielichowski, K. *Prog. Polym. Sci.* **2003**, *28*, 1297-1353.
(72) P. Bruzga, J. G., R. Kavalinas, Eur. Polym. J. 27, 707 (1991).
(73) J. Grauleviius, R. K., J. Urbonaviciené, Electronics of Organic Materials, Nauka, Moscow 1985, p. 362
(74) Grobelny, Z.; Stolarzewicz, A.; Morejko-Buz, B.; Buika, G.; Grazulevicius, J. V.; Maercker, A. *Eur. Polym. J.* **2002**, *38*, 2359-2363.
(75) Buika, G.; Gra, J. V.; zcaron; ulevi; ccaron; ius; Stolarzewicz, A.; Grobelny, Z. *Macromol. Chem. Phys.* **1995**, *196*, 1287-1293.
(76) Matsui, N.; Takano, S.; Vol. 462.
(77) Perepichka, D. F.; Perepichka, I. F.; Bryce, M. R.; Sokolov, N. I.; Moore, A. J. *J. Mater. Chem.* **2001**, *11*, 1772-1774.
(78) Lazauskaite, R.; Stanislovaityte, E.; Grazulevicius, J. V. *Monatshefte für Chemie / Chemical Monthly* **2008**, *139*, 887-893.
(79) Penczek, S.; Baran, J.; Biela, T.; Lapienis, G.; Nyk, A.; Klosinski, P.; Pretula, B. *British Polymer Journal* **1990**, *23*, 213-220.
(80) Lee, H. N., K. Hand Book of Epoxy Resin; McGraw-Hill: New York, 1967. .
(81) Mikroyannidis, J. A.; Kourtides, D. A. *J. Appl. Polym. Sci.* **1984**, *29*, 197-209.
(82) Wang, X.; Zhang, Q. *Eur. Polym. J.* **2004**, *40*, 385-395.
(83) Derouet, D.; Morvan, F.; Brosse, J. C. *J. Appl. Polym. Sci.* **1996**, *62*, 1855-1868.
(84) Liu, Y.-L.; Hsiue, G.-H.; Chiu, Y.-S.; Jeng, R.-J.; Perng, L.-H. *J. Appl. Polym. Sci.* **1996**, *61*, 613-621.
(85) Sudhakara, P.; Kannan, P. *Polym. Degrad. Stab.* **2009**, *94*, 610-616.
(86) José Alcón, M.; Ribera, G.; Galià, M.; Cádiz, V. *Polymer* **2003**, *44*, 7291-7298.
(87) Alcón, M. J.; Espinosa, M. A.; Galià, M.; Cádiz, V. *Macromol. Rapid Commun.* **2001**, *22*, 1265-1271.
(88) Wang, H.; Liu, J.; Xu, S.; Shi, W. *Prog. Org. Coat.* **2009**, *65*, 263-268.
(89) Uematsu, N.; Hoshi, N.; Koga, T.; Ikeda, M. *J. Fluorine Chem.* **2006**, *127*, 1087-1095.
(90) Extrand, C. W. *J. Fluorine Chem.* **2003**, *122*, 121-124.
(91) Persico, D. F.; Lagow, R. J. *Macromolecules* **2002**, *18*, 1383-1387.
(92) Reardon, J. P.; Zisman, W. A. *Macromolecules* **2002**, *7*, 920-923.
(93) Zhang, J.; Demas, N. G.; Polycarpou, A. A.; Economy, J. *Polym. Adv. Technol.* **2008**, *19*, 1105-1112.
(94) Schnurer, A. U.; Holcomb, N. R.; Gard, G. L.; Castner, D. G.; Grainger, D. W. *Chem. Mater.* **1996**, *8*, 1475-1481.
(95) Chen, L.-F.; Mohtasham, J.; Gard, G. L. *J. Fluorine Chem.* **1990**, *46*, 39-56.
(96) Hamel, N. N.; Russell, G. A.; Gard, G. L. *J. Fluorine Chem.* **1994**, *66*, 105-107.

(97) Montefusco, F.; Bongiovanni, R.; Sangermano, M.; Priola, A.; Harden, A.; Rehnberg, N. *Polymer* **2004**, *45*, 4663-4668.
(98) Nicholas, P. P. *J. Polym. Sci., Part A: Polym. Chem.* **1992**, *30*, 1123-1127.
(99) Trischler, F. D.; Hollander, J. *Journal of Polymer Science Part A-1: Polymer Chemistry* **1967**, *5*, 2343-2349.
(100) Hagiwara, T.; Terasaki, Y.; Hamana, H.; Narita, T.; Umezawa, J.; Furuhashi, K. *Die Makromolekulare Chemie, Rapid Communications* **1992**, *13*, 363-370.
(101) Sakakibara, K.; Nakano, K.; Nozaki, K. *Chem. Commun.* **2006**, 3334-3336.
(102) Sakakibara, K.; Nakano, K.; Nozaki, K. *Macromolecules* **2007**, *40*, 6136-6142.
(103) Acosta Ortiz, R.; Cisneros, M. d. L. G.; García, G. A. *Polymer* **2005**, *46*, 10663-10671.
(104) E. P. Plueddemann, C. E. D., 5, 59, (1960).
(105) E. P. Plueddemann and G. Fanger, J. A. C. S., 81, 2632, (1959).
(106) Cho, Y. H.; He, M.; Kim, B. K.; Kawakami, Y. *Science and Technology of Advanced Materials* **2004**, 319.

Chapter 3: Harnessing the Versatility of the Imidazole Ring: A Perspective on the Incorporation of Vinylimidazole Regioisomers into Macromolecules for Emerging Applications

Michael H. Allen, Jr., Sean T. Hemp, and Timothy E. Long

Macromolecules and Interfaces Institute, Department of Chemistry, Virginia Tech, Blacksburg, VA 24061

3.1 *Abstract*

The imidazole ring remains one of the premiere bioactive molecules utilized significantly for the design and synthesis of functional macromolecules. Found in the amino acid histidine, the imidazole substituent executes vital activities within the human body including oxygen capture, enzymatic catalysis, and metal ion complexation. The intense focus on the ubiquitous imidazole ring has propelled imidazole-containing polymers to the forefront of materials design due to their facile functionalization, biological relevance, and amphoteric nature. Researchers widely utilize the monomers, 1-, 2-, and 4-vinylimidazole regioisomers, which highlight imidazole as a focal point for synthetic macromolecular design. Additionally, free radical polymerization of these monomers allows for the development of novel polymer architectures. The propagating radical instability of 1-vinylimidazole limits the generation of precise polymer structures for future materials; whereas, the increased radical stability of 4-vinylimidazole generates polymers with well-defined molecular weights and precise architectures utilizing controlled radical polymerization strategies. These vinyl monomers inspired the generation of synthetic enzymes, water purification membranes, oxygen-transport materials, electroactive devices, nucleic acid therapeutics, and numerous additional applications. The synthetic versatility afforded through the incorporation of these vinylimidazole regioisomers into macromolecules remains integral as the drive towards a sustainable future continues.

3.2 *Introduction*

From delivering therapeutics for the treatment of chronic disease to the fabrication of membranes for electromechanical transducers, imidazole-containing macromolecules comprise an area of intense research focus. The planar, five membered imidazole ring, contained in the amino acid histidine, serves a variety of bioactive functions due to its amphoteric nature.[1] The acidic N1 and basic N3 nitrogens catalyze ester hydrolysis in the active site of enzymes,[2] participate as a coordinating ligand in metalloproteins,[3] and aid in protein folding.[4] The biologically relevant molecule histamine contains the imidazole ring to mediate inflammatory responses.[5] Additionally, the imidazole ring undergoes facile modification to generate ionic liquids.[6] The asymmetry associated with this organic cation and bulky counterion lowers the melting point of the ionic salt below 100 °C. Imidazolium ionic liquids exhibit high chemical and thermal stability, negligible vapor pressure, and high ionic conductivity. These properties have resulted in a wide variety of applications including batteries, fuel cells, and catalysis.

The sustained focus to derive fundamental polymer design parameters from nature and the high impact of ionic liquid research fueled the incorporation of the imidazole ring into numerous macromolecules (Figure 3.1). The amphoteric, heterocycle spans various research thrusts in polymer chemistry from components in electroactive devices to building blocks for nucleic acid therapeutics. Taking inspiration from histidine, researchers have designed imidazole-containing polymers for metal complexation to investigate new avenues for water purification,[7] and have begun to develop synthetic enzymes for industrial applications.[8,9] From water purification to CO_2 capturing membranes[10] to renewable feedstocks,[11,12] imidazole-containing macromolecules remain integral as the effort towards increased sustainability continues.

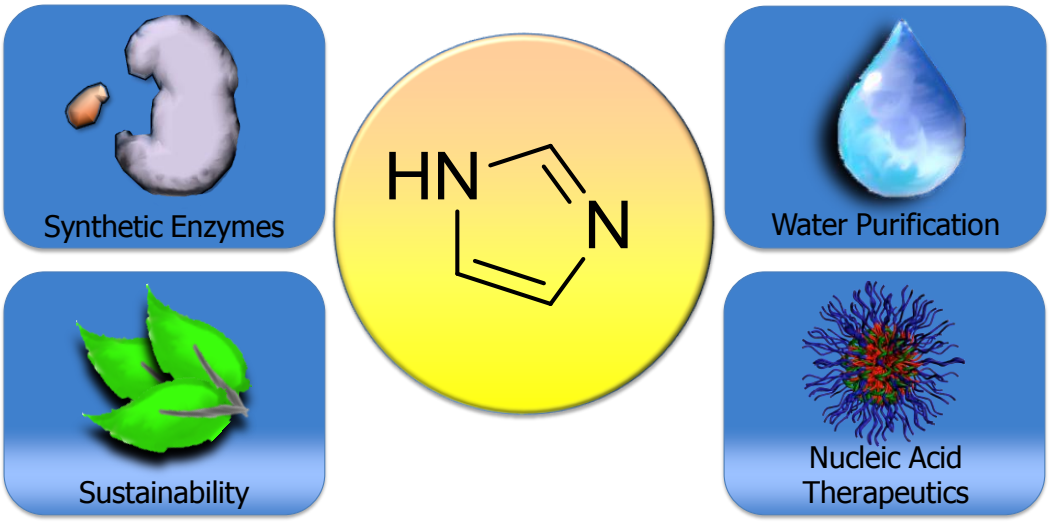

Figure 3.1. Incorporating the imidazole ring into a wide variety of applications.

A wide array of synthetic polymers incorporate the imidazole ring including polypeptides, polyesters, polyurethanes, ionenes, meth(acrylics), meth(acrylamides), and styrenics.[1,13,14] A unique class of chain growth monomers, vinylimidazoles, incorporates the imidazole ring attached directly to the polymer backbone without the influence of additional functional groups. Three regioisomers exist (Figure 3.2): *N*- or 1-vinylimidazole (1VIM), 2-vinylimidazole (2VIM), and 4-vinylimidazole (4VIM). The synthetic versatility afforded through the incorporation of these vinylimidazole regioisomers into macromolecules remains integral for the generation of novel materials. 1VIM remains the most heavily investigated monomer due to its inexpensive cost, commercial availability, and facile functionalization; the additional regioisomers currently remain unavailable through commercial resources. The synthesis of 4VIM requires the decarboxylation of urocanic acid,[15] whereas, the synthesis of 2VIM consists of a complex, multi-step procedure.[16]

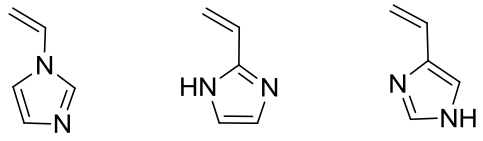

1VIM 2VIM 4VIM

Figure 3.2. Structures of vinylimidazole regioisomers.

The limited availability of these two regioisomers has prevented the integration of these monomers into an array of macromolecules. This review aims to focus on the polymerization of vinylimidazole monomers in materials science for emerging applications.

3.3 *1-Vinylimidazole*

1VIM remains the most commonly studied vinylimidazole regioisomer due to its widespread commercial availability. Unlike the amino acid histidine, the vinyl substituent at the 1-position eliminates intermolecular hydrogen bonding, lowering the monomer melting point below -50 °C.[17] Conventional free radical homopolymerization of 1VIM affords homopolymers with a number-average molecular weight (M_n) less than 100,000 g/mol with a glass transition temperature (T_g) around 180 °C. Poly(1VIM) remains thermally stable to 350 °C.

Copolymers incorporate 1VIM to impart various properties including metal binding affinity,[18] catalytic activity,[19] biocompatibility,[20] and polyelectrolyte behavior.[21] Petrak et al. utilized conventional free radical copolymerization and determined reactivity ratios of 1VIM with various monomers including styrene, vinyl acetate, and methyl methacrylate (MMA) (Table 3.1).[22]

Table 3.1. Copolymerization reactivity ratios of various monomers with 1VIM (M_1).

Comonomer (M_2)	Reactivity Ratios	Reference
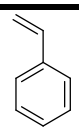	$r_1 = 0.10 \pm 0.02$ $r_2 = 10.0 \pm 0.2$	22
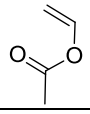	$r_1 = 1.50 \pm 0.02$ $r_2 = 0.2 \pm 0.02$	22

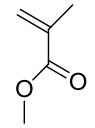	$r_1 = 0.03 \pm 0.01$ $r_2 = 4.10 \pm 0.02$	22
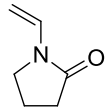	$r_1 = 0.95 \pm 0.01$ $r_2 = 0.17 \pm 0.01$	22
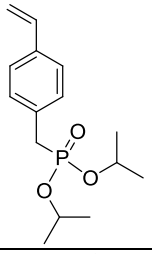	$r_1 = 0.10$ $r_2 = 3.10$	23
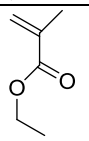	$r_1 = 0.35 \pm 0.02$ $r_2 = 3.47 \pm 0.2$	24
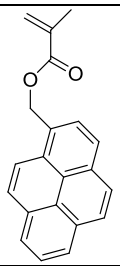	$r_1 = 0.28 \pm 0.04$ $r_2 = 1.32 \pm 0.12$	25
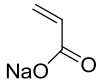	$r_1 = 0.54 \pm 0.06$ $r_2 = 1.3 \pm 0.3$	21
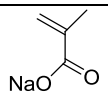	$r_1 = 0.23 \pm 0.01$ $r_2 = 2.6 \pm 0.2$	21
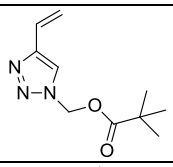	$r_1 = 0.30 \pm 0.02$ $r_2 = 0.51 \pm 0.03$	26
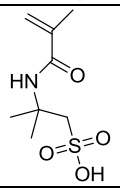	$r_1 = 0.13$ Acidic $r_2 = 0.30$ Acidic $r_1 = 0.10$ Basic $r_2 = 4.1$ Basic	27
	$r_1 = 0.24 \pm 0.01$ $r_2 = 0.12 \pm 0.2$	28

The copolymerization of 1VIM (r_1 = 0.10) and styrene (r_2 = 10.0) resulted in homopolymerization of each monomer. Conversely, copolymerization with MMA (r_{1VIM} = 0.03

and r_{MMA} = 4.1) produced copolymers with substantially more MMA in the copolymer than in the feed. Armes et al. copolymerized 1VIM with 4-aminostyrene to synthesize a steric stabilizer for polyaniline colloids; however, a lack of reactivity ratio determination and inadequate characterization failed to confirm the synthesis of a styrenic copolymer.[29] Copolymerizations of 1VIM with diisopropyl-*p*-vinylbenzyl phosphonate (DVBP) produced a proton-conducting copolymer through hydrolysis of the phosphonate group.[23] The obtained reactivity ratios (r_{1VIM} = 0.10; r_{DVBP} = 3.10) suggested the synthesis of copolymers with significantly higher incorporation of DVBP into the copolymer relative to the monomer feed.

Copolymerization kinetics determined 1VIM and ethyl methacrylate (EMA) copolymerized successfully with reactivity ratios of r_1 = 0.35 and r_2 = 3.47 respectively.[24] A complex formation between the carbonyl group on EMA and the imidazole residue on 1VIM produced a reactive EMA propagating radical. This resulted in substantially higher EMA incorporation into the copolymers compared to the monomer feed. A derivatized methacrylate monomer, 1-pyrene methyl methacrylate (PyMMA), copolymerized successfully with 1VIM to produce a fluorescent imidazole-containing copolymer (Figure 3.3).[25]

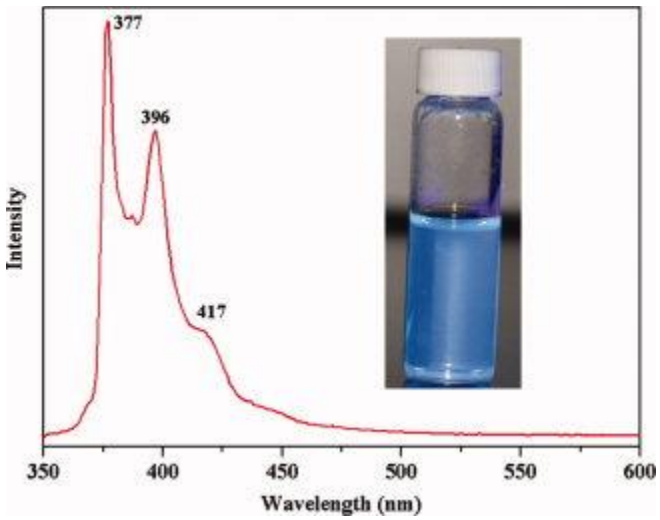

Figure 3.3. Fluorescence emission spectrum of poly(1VIM-*co*-PyMMA) in a DMF/water co-solvent. Reproduced with permission from reference [25].

The reactivity ratios (r_{1VIM} = 0.28; r_{PyMMA} = 1.22) suggested a copolymerization with preferential addition of the methacrylate monomer, which was in good agreement with various methacrylate polymerizations mentioned previously. The copolymerization of (meth)acrylic acid with 1VIM to synthesize hydrophilic polyampholytes resulted in copolymers contaminated with 1VIM due to coordination of the imidazole ring to the carboxylic acid groups. Annenkov et al. prevented the acid-base interaction through the conversion of the acids into the sodium salt forms and found similar reactivity ratios to 1VIM copolymerizations with methacrylic monomers.[21] 1VIM also copolymerized successfully with 4-vinyl-1,2,3-triazole.[26]

Free radical copolymerizations of 1VIM with acrylate, acrylamide, and methacrylamide monomers remain extremely limited. The copolymerization of 1VIM and *N*-isopropylacrylamide (NIPAM) generates stimuli-responsive copolymers for biomedical applications; however, no reports on the reactivity ratios of these monomers exist.[30-38] Schmidt-Naake et al. copolymerized a methacrylamide monomer, 2-acrylamido-2-methyl-1-propanesulfonic acid (AMPS) and its sodium salt with 1VIM to synthesize proton conducting polymer films.[27,39,40] The reactivity ratios in acidic solution varied from r_{AMPS} = 0.30 and r_{1VIM} = 0.13 to r_{AMPS} = 4.1 and r_{1VIM} = 0.10 in basic and neutral conditions.[27] Under acidic conditions, the monomers behaved as an electron donor/acceptor complex which produced copolymers with a more alternating comonomer sequence. NaAMPS reacted faster than AMPS complexed with the protonated imidazole monomer. The smaller sodium cation exhibited a tighter ionic bond with the sulfonate anion, thereby reducing electrostatic repulsion between anionic monomers, favoring NaAMPS incorporation. Copolymerization of 1VIM with acrylonitrile produced alternating copolymers due to donor-acceptor interactions between the imidazole ring and nitrile

groups on the monomers.[28] These copolymers formed a melt processable carbon fiber due to 1VIM's ability to disrupt PAN's crystallinity for wound healing applications (Figure 3.4).

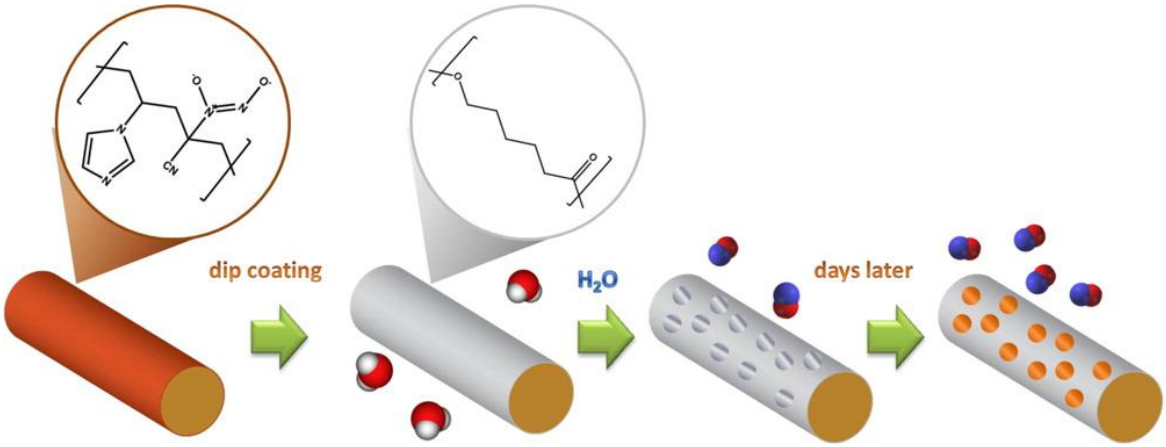

Figure 3.4. Poly(1VIM-*co*-AN) fibers coated with poly(caprolactone) to control the release of nitric oxide for wound healing. Reprinted with permission from reference [41].

Additionally, these copolymers effectively encapsulated metal nanoparticles for drug delivery and catalyst support appications.[41-43] Copolymerizations with maleic anhydride (MAH) failed to produce an alternating copolymer as the charge transfer complex between 1VIM and MAH did not participate in propagation.[44] The copolymerization proceeded spontaneously upon addition of MAH to 1VIM in dioxane and produced low molecular weight copolymers.

3.3.1 Metal chelation

Numerous researchers have investigated the ability of poly(1VIM) to chelate various metal ions. The interest began decades ago, when researchers discovered the binding sites of metal-binding proteins consisted of histidine residues.[45-47] Gurd and Goodman delved deeper into the proteins and attributed metal ion complexation to the imidazole ring.[48] They found four imidazole rings participated in the complexation of Zn^{2+} and Cu^{2+} ions. Gregor and co-workers previously investigated the binding of metallic ions with acrylic and methacrylic polymers and

applied this expertise to imidazole-containing macromolecules. They determined poly(1VIM) also displayed a preferred coordination number of four when complexing Cu^{2+} ions, similar to biological enzymes.[18,49] Poly(1VIM) coordinated additional ions including Ag^{+} (N = coordination number = 2) and Zn^{2+} (N = 4).[18,50] Pekel et al. studied the complex formation of poly(1VIM) hydrogels with trivalent metal ions in aqueous solution.[51] They found poly(1VIM) formed a N = 4 with V (III), Cr (III), and Fe (III). Annenkov et al. investigated the interaction of poly(1VIM) with an additional trivalent metal ion, Al^{3+}.[52] Through the titration of $AlCl_3$ and $Al(NO_3)_3$, they discovered unlike previous imidazole-metal complexes, the imidazole ring did not complex the Al^{3+} ions. Instead, cooperative hydrogen bonding of the imidazole ring to aluminum hydroxide promoted the formation of alumina particles.

These metal-binding properties of poly(1VIM) more recently generated interest in removal of heavy metals for water purification. Rivas et al. designed poly(1VIM) hydrogels crosslinked with *N,N'*-methylenebisacrylamide to chelate metal ions in aqueous solutions.[7] The hydrogels demonstrated effective binding of Cu^{2+}, Co^{2+}, Ni^{2+}, Zn^{2+}, Cd^{2+}, and Hg^{2+} ions. Subsequent elution of the metal ions with an acidic aqueous solution regenerated the hydrogel for further metal chelation. Crosslinked copolymers of poly(1VIM) with either acrylic acid or AMPS effectively bound similar ions.[53] The inclusion of the sulfonic acid comonomer increased metal binding affinity. These same copolymers bound uranyl ions with higher affinity than the respective homopolymers to demonstrate the recovery of uranium from contaminated water sources.[54] The resins underwent four cycles of loading and metal elution, but progressively lost metal ion affinity with each cycle. Tarley et al. synthesized poly(1VIM)-silica hybrid copolymers for Pb^{2+} ion removal, and the copolymers displayed selectivity for Pb(II) over Cu(II), Cd(II), and Zn(II).[55] Asayama and co-workers complexed Zn^{2+} ions with poly(1VIM) and

subsequently bound this complex with DNA for nonviral gene delivery.[56] The complexes displayed stimuli-responsive release of Zn^{2+} at acidic pH and significant transfection efficiency in HepG2 cells with minimal cytotoxicity. Additionally, the incorporation of poly(L-lysine) conjugated with lactose formed ternary complexes for nonviral gene delivery and exhibited higher transfection efficiency than PEI (Figure 3.5).[57]

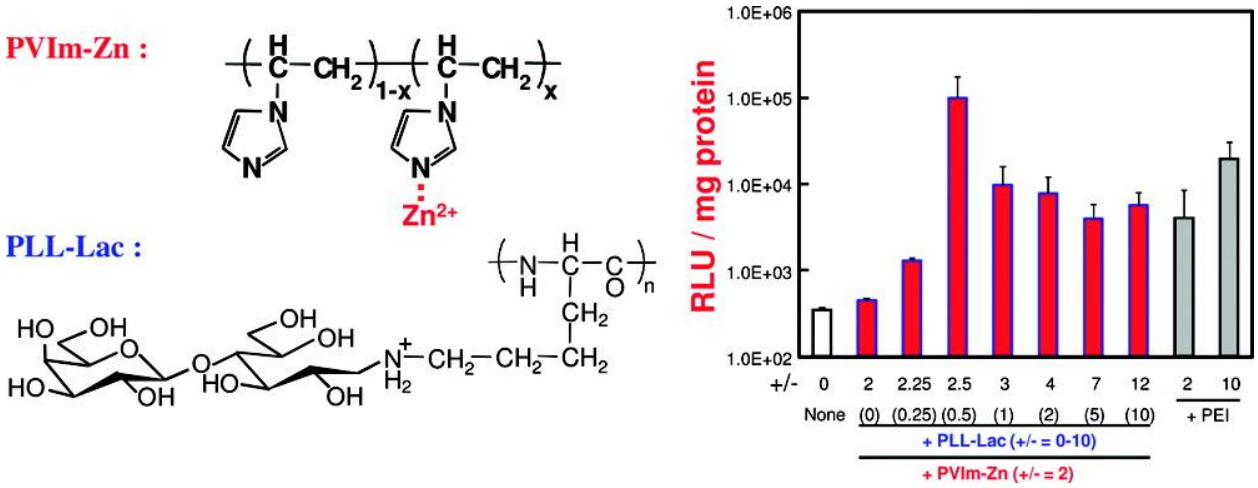

Figure 3.5. Diagram of poly(1VIM) complexed with Zn^{2+} ions and lactosylated poly(L-lysine) for nonviral gene delivery with subsequent transfection efficiencies. Reprinted with permission from reference [57].

Polymer-supported transition metal complexes continue to generate widespread attention amongst researchers. Ideally, these supports should immobilize the catalyst with high activity and selectivity. The most common polymer supports consist of polystyrene crosslinked with divinylbenzene; however, these supports are plagued with numerous problems including catalyst leaching, active site heterogeneity, and reactant inaccessibility. These difficulties have led to the investigation of ligands which form multidentate complexes with metal ions to resolve the aforementioned problems.

As mentioned previously, 1VIM complexes effectively with metal ions probing further investigation of this monomer into polymer-supported transition metal complexes. Terpolymers of styrene, divinylbenzene, and 1VIM complexed Rh(I) and catalyzed the hydrosilylation of cyclohexanone and acetone with triethylsilane and diphenylsilane.[58,59] These supports exhibited high activity and selectivity during five cycles which suggested high stability over prolonged use. Similar columns demonstrated Cu^{2+} ion complexation for the immobilization of proteins including α-amylase to hydrolyze polysaccharides such as starch.[60-62] The crosslinked spherical beads with rough surfaces are shown in Figure 3.6.

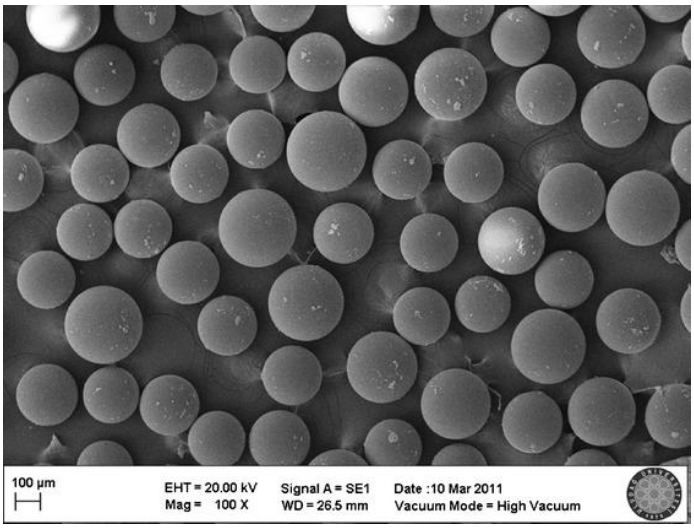

Figure 3.6. SEM image of poly(1VIM) microbeads crosslinked with divinylbenzene. Reprinted with permission from reference [60].

Kara et al. also showed these crosslinked materials effectively chelate Cr^{4+}.[63] Alginic acid/poly(1VIM) polyelectrolyte complexes immobilized tryosinase within the network, but the enzyme activity sharply decreased after use due to diffusional effects and structural instability.[64]

Free radical polymerization of a tri-functional 1VIM derivative *N,N',N''*-chelate ligand tris[2-(1-vinylimidazolyl)]phosphine produced a highly crosslinked polymers with a high density of binding sites for Cu(II) chelation to promote phosphoester hydrolysis.[65] Incorporation of

ethylene glycol dimethacrylate (EGDMA) lowered the binding site density allowing for isolated binding sites to catalyze phosphoester hydrolysis. Crosslinked poly(3-butyl-1-vinylimidazolium bromide) microspheres supported platinum nanoparticles and exhibited improved electrooxidation of methanol than pure platinum nanoparticles.[66] The recyclable catalysts also demonstrated selectivity for the oxidation of benzyl alcohol. A similar method functionalized these ionic liquid microspheres with gold and palladium nanoparticles to catalyze the hydrogenation of cyclohexene.[67]

Andersson et al. synthesized poly(1VIM-*co*-MMA) copolymers which incorporated 4 mol % and 44 mol % 1VIM for coordination to Cu^{2+} and Zn^{2+} ions.[68,69] Coordination to the metal ions formed crosslinked polymers which required strongly coordinating solvents such as DMSO or acetonitrile to redissolve the copolymers. The Cu^{2+} ions when bound to the imidazole units, crosslinked the copolymer chains inhibiting polymer chain segmental motion as depicted in Figure 3.7.[70]

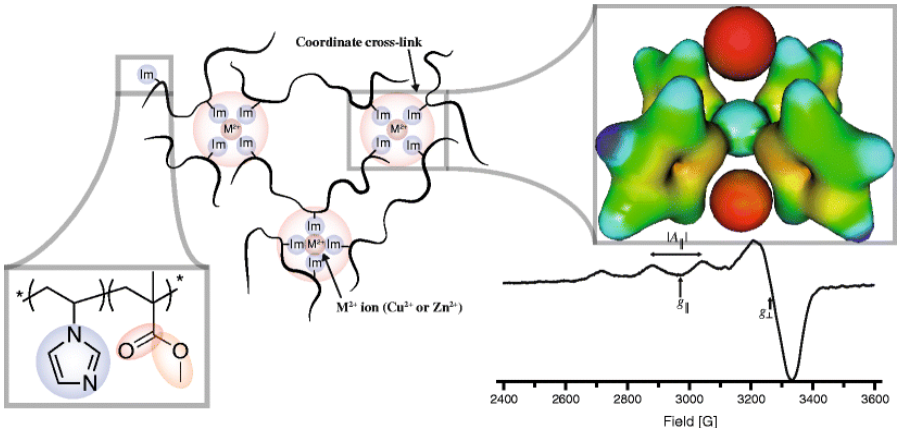

Figure 3.7. Schematic depicting crosslinked chains of poly(1VIM-*co*-MMA) due to the complexation of metal ions. EPR spectroscopy confirmed metal coordination occurred through the imidazole substituents. Reprinted with permission from reference [68].

Differential scanning calorimetry determined the T_g's of the copolymer increased when coordinated to Cu^{2+} ions. Furthermore, copolymers of poly(1VIM-*co*-MMA) functioned as a

polymeric support, binding Cu(II) to catalyze the oxidation of ethyl benzene to acetophenone with molecular oxygen.[71] A more hydrophilic copolymer poly(1VIM-*co*-acrylic acid) effectively sequestered Cu^{2+} ions.[72] The copolymer chelated the metal ions through the carboxylate groups of the acrylic acid repeat units and not the imidazole rings; however, the combination of repeat units strengthened complexation through intramolecular interactions of 1VIM and AA. Additionally, the homopolymers of each respective monomer were mixed together with Cu^{2+} ions which acted as a bridging ion between the interpolymer complexes. Poly(4-vinylpyridine-*co*-1VIM) treated with various bromoalkanes complexed Cu(II) to generate a Cu(0) metal nanocatalyst for the reduction of 4-nitrophenol.[73] The copolymers also removed arsenic from aqueous solution and demonstrated efficiency as a drug delivery vehicle for naproxene sodium salt.

Vos et al. first coordinated poly(1VIM) with hydrated bis(2,2'-bipyridyl)ruthenium(II) dichloride to form ruthenium-poly(VIM) complexes.[74] This spurred investigations into photoinduced electron transfer reactions involving these complexes to potentially design a synthetic photosynthesis complex. To achieve an artificial photosynthetic complex, the design of a highly efficient oxidation-reduction complex is required. Suzuki and co-workers thoroughly investigated various photosensitive reactions with a poly(1VIM) terpolymer (QPIM) containing repeat units complexed with $Rh(II)(bpy)_2$, quaternized repeat units with a long alkyl chain, and unfunctionalized repeat units as shown in Figure 3.8.[75-95] Scheme 3.1 shows the investigated photosensitized oxidation-reduction reaction.

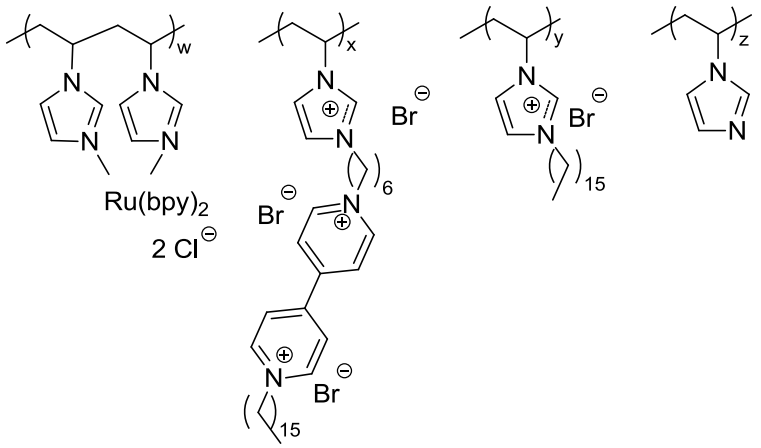

Figure 3.8. Structures of imidazolium copolymers investigated in photosensitized oxidation-reduction reactions. QPIM terpolymers lack the viologen repeat unit.

$$\text{Ru(II)QPIM} \xrightarrow{h\nu} \text{*Ru(II)QPIM}$$

$$\text{*Ru(II)QPIM} \longrightarrow \text{Ru(II)QPIM} + h\nu' + \Delta$$

$$\text{*Ru(II)QPIM} + \text{R-V}^{2+} \longrightarrow \text{Ru(III)QPIM} + \text{R-V}^{+\bullet}$$

$$\text{Ru(III)QPIM} + \text{R-V}^{+\bullet} \longrightarrow \text{*Ru(II)QPIM} + \text{R-V}^{2+}$$

$$\text{Ru(III)QPIM} + \text{TEOA} \longrightarrow \text{Ru(II)QPIM} + \text{TEOAox}$$

Scheme 3.1. Photosensitized oxidation-reduction reaction involving QPIM and a ruthenium-based complex to design an artificial photosynthesis mimic. Reproduced with permission from reference [89].

The Ru(II)QPIM terpolymer acts as a photosensitizer, the alkylated viologen ($R\text{-}V^{2+}$; 1,1'-Dialkyl-4,4'-bipyridinium dications) acts as an electron acceptor, and triethanolamine (TEOA) undergoes oxidation (TEOAox) acting as a sacrificial donor to regenerate the Ru(II)QPIM complex. They found the rate of viologen radical formation increased as the alkyl chain length increased on the polymer, but decreased with the incorporation of higher charge densities. Electrostatic repulsions, sterics, and π-π interactions between the terpolymer and the viologen were identified as three possible factors impacting the rate of the oxidation-reduction reaction.[95] The terpolymers generated hydrogen gas when irradiated in aqueous solution for 25 light cycles after which the platinum catalyst became inactivated; however, the films maintained their

photosensitizing ability over 200 cycles.[89,91,93] Covalent attachment of the viologen to the terpolymer produced an orange to blue color change in the polymer film in response to irradiation and temperature.[94] The polymer chains contained at least four Ru(II) complexes per polymer chain.[90] Suzuki and co-workers also studied the effect of L-tyrosine esters on the photosensitized oxidation-reduction reactions involving these polymer systems.[76,77,82,88] In photosynthesis, photoinduced electron transfer occurs through tyrosine residues in polypeptides. The incorporation of L-tyrosine into a methanol solution enhanced viologen radical formation aiding in photoinduced electron transfer from the ruthenium complex to the viologen.

In the 1970s and 1980's, interest in designing artificial oxygen carriers developed. It became necessary to design polymers to interact with the heme group or other porphinatoiron complexes to prevent irreversible oxidation. Isolation from myoglobin or hemoglobin resulted in iron's immediate oxidation to its ferric (III) state preventing its use as an oxygen carrier. The iron-porphyrin complexes when attached to a polymer chain or modified to incorporate bulky groups to sterically functionalize the complexes prevented oxidation in aprotic solvents; however, aqueous media caused irreversible oxidation. Pratt and others attempted to understand the coordination chemistry that occurred in the active site of hemoproteins and discovered imidazole and subsequently poly(1VIM) coordinated to Fe(III) protoporphyrin IX (hemin) in organic solvents.[96-98] Tushida et al. showed for the first time the interaction of the heme (reduced form of hemin) group with imidazole on poly(2-methyl-1VIM) formed the five coordinate heme complex and prevented irreversible oxygen binding in aqueous solution.[99] Picket fence cobaltporphyrin also complexed to poly(1VIM) to improve oxygen-binding specificity and reversibility as shown in Figure 3.9.[100,101] The copolymerization of octyl methacrylate with 1VIM resulted in an oxygen-sensitive polymer for optical sensors.[102-104] Copolymerization with

fluoroalkyl methacrylates extended the operational life time of these sensors to over one month and displayed a selective and reversible response to oxygen in an aqueous environment.[105,106]

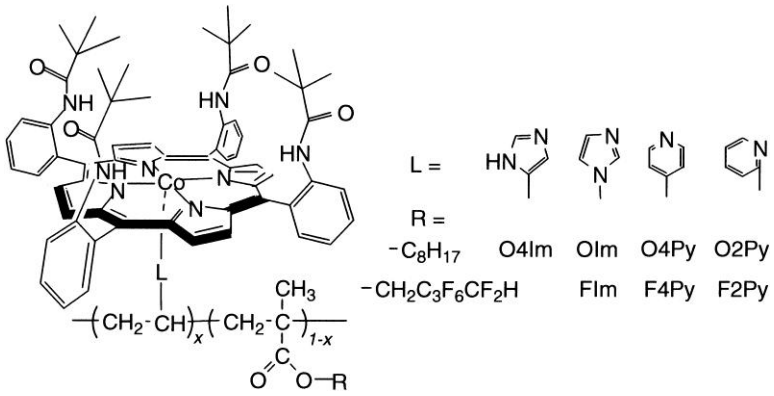

Figure 3.9. Interactions of heterocyclic-containing polymers with picket fence cobalt-porphyrin. Reprinted with permission from reference [105].

Molecular imprinted thermosensitive copolymers containing trifluoromethacrylic acid demonstrated catalytic activity towards *p*-nitrophenyl acetate (PNPA) above 40 °C (temperature required to dissociate the copolymer intermolecular interactions).[107] Additionally, Co(II) chelation prepared a molecularly imprinted polymer for an enhanced rate of hydrolysis of PNPA with high specificity.[108,109]

Researchers have employed enzyme-based electrodes for biosensors, bioreactors, and biofuel cells due to their high substrate selectivity, low cost, and mild operation conditions.[110] The electron transfer between the enzyme and the solid conducting support however limits performance. The electrodes require the wiring of an enzyme to the electrode to transport the discharged electrons from the enzyme to the electrode. The wiring (a redox polymer) must bind to the protein without modifying or denaturing the macromolecule, connect the protein to the electrode, and subsequently establish the electrical connection between the enzyme and electrode.[111] The ability for poly(1VIM) to bind to protein and complex metals established the polymer as a potential wiring agent to tether a protein to an electrode. Heller et al. determined a

redox polymer hydrogel consisting of poly(1VIM) complexed to osmium-(4,4'-dimethylbpy)$_2$Cl adequately conducted electrons from the redox site of glucose oxidase (GOX) to the electrodes.[112] These hydrogels when immobilizing either GOX or lactate oxidase served as glucose or lactate sensing electrodes.[113] Other researchers explored poly(1VIM)-osmium redox polymers to wire gram-positive and gram-negative bacteria to electrodes without penetrating the inner cytoplasmic membrane as shown in Figure 3.10.[114-117]

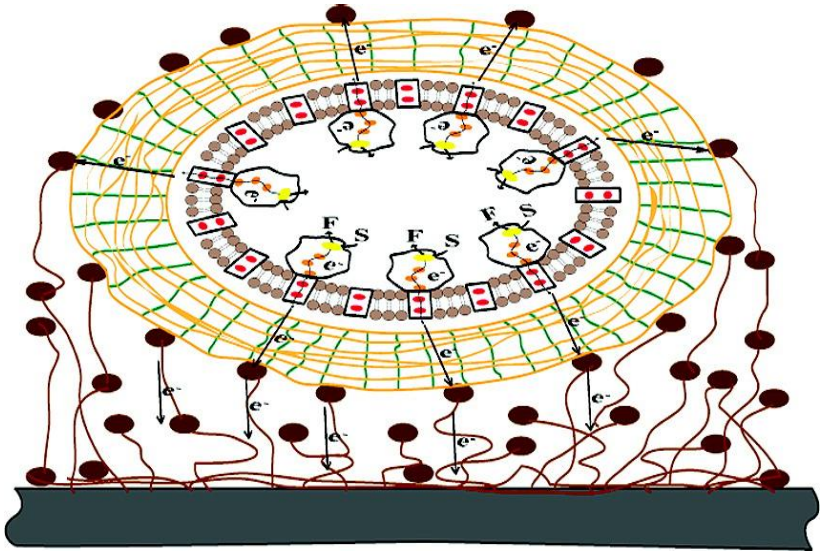

Figure 3.10. Diagram of *Bacillus subtilis* wired to an electrode with poly(1VIM)-osmium redox polymers to transport electrons from the gram-positive bacteria cell to the electrode. Reprinted with permission from reference [114].

Additional articles focus on electrode fabrication and enzyme selection through the incorporation of poly(1VIM)-osmium redox polymers.[118-126] Vansco et al. designed a new redox-responsive organometallic hydrogel which contained 1VIM grafted onto a poly(ferrocenylsilane) backbone with subsequent crosslinking of 1VIM.[127]

3.3.2 Synthetic Enzymes

The design of synthetic enzymes to replace natural proteins for catalytic production of small molecules on an industrial scale with selectivity and specificity remains popular. Enzymes

exhibit a high selectivity and efficiency toward structurally similar substrates typically depending on a concerted action between various functional groups in the active site of the enzyme. This includes hydrophobic and electrostatic interactions which promote the binding of a substrate into the active site in an enzyme. Deriving their inspiration from nature, numerous researchers have investigated incorporating the imidazole ring into synthetic macromolecules to mimic the active site of numerous natural enzymes. Poly(2-ethyl-1VIM) quaternized with ethyl bromide and lauryl bromide catalyzed the flavin oxidation of thiols due to the activation of the thiolate anion.[128] Similar copolymers catalyzed the decarboxylation of 6-nitrobenzisoxazole-3-carboxylate.[129] The balance of the hydrophobic lauryl domains with the cationic imidazolium rings enabled the tuning of the polymer's catalytic activity.[130] These copolymers also served as apoenzymes binding various thiol-containing coenzymes including coenzyme A and glutathione to catalyze the hydrolysis of PNPA.[131] The coenzymes required binding to an apoenzyme to exhibit high enzymatic reactivities. The lauryl substituents established a hydrophobic environment necessary to bind the thiolate anions on the coenzymes. Additionally, the cationic polyelectrolyte poly(1-butyl-3-vinylimidazolium chloride) strongly bound proteins including lysozyme and anion exchange tuned the polymer morphology and thermal properties; however, enzymatic studies were not performed.[132]

Salamone et al. fully quaternized poly(1VIM) with methyl and hexadecyl substituents to study the effect of the polymer side chains on the alkaline hydrolysis of PNPA and *p*-nitrophenyl laurate (PNPL).[133] The quaternization failed to influence the hydrolysis of PNPA; however, the hexadecyl-functionalized polymer exhibited an enhanced rate of hydrolysis due to the increased hydrophobicity of the polyelectrolyte. Brembilla confirmed poly(3-alkyl-1-vinylimidazolium)s formed hydrophobic microdomains in aqueous solution with fluorescent probes and viscosity

measurements.[134] A highly crosslinked, quaternized imidazolium homopolymer facilitated the one-step synthesis of cyclic carbonates through the catalysis of the coupling of CO_2 with epoxides.[135] As shown in Figure 3.11, the catalyst retained 100% selectivity over a period of five cycles, but lost approximately 20% of its activity over the same period.

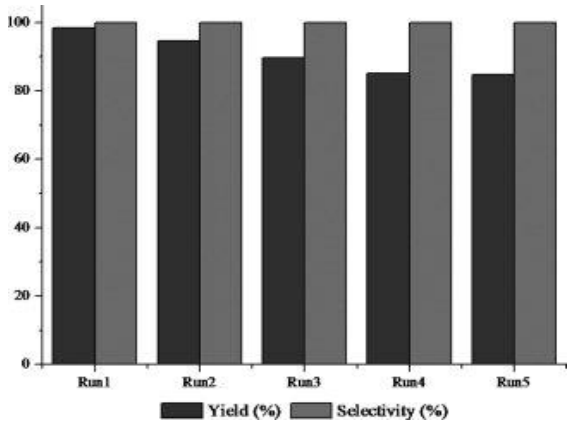

Figure 3.11. Stability and recyclability of a crosslinked, quaternized imidazolium homopolymer catalyst for cyclic carbonate synthesis. Reprinted with permission from reference [135].

Additionally, Pourjavadi et al. coated magnetic nanoparticles with a quaternized vinylimidazolium homopolymer which created a recoverable and recyclable heterogeneous catalyst for organic synthesis as shown in Figure 3.12.[136]

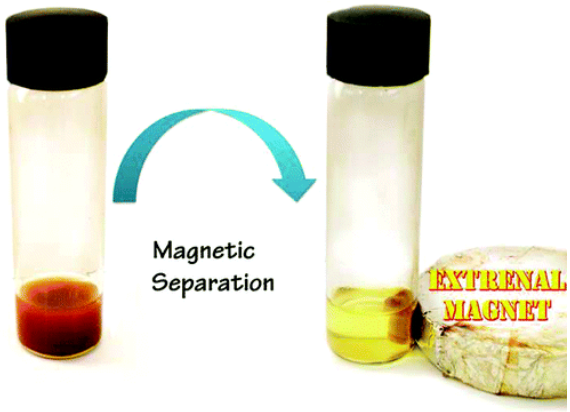

Figure 3.12. Separation of heterogeneous nanoparticles catalysts from reaction solution through application of an external magnet. Reprinted with permission from reference [136].

Poly(1VIM) and poly(4-vinylpyridine) effectively catalyzed the ester hydrolysis of nitrophenyl esters containing an anionic charge including 4-acetoxy-3-nitrobenzenesulfonate, but the polymers failed to complex with structurally similar, neutral substrates suggesting an electrostatic interaction between substrate and catalyst.[137] Poly(1VIM) promoted the ester hydrolysis of acrylic acid-2,4-dinitrophenyl *p*-vinylbenzoate copolymeric substrates through the electrostatic complex of the carboxylate anion to the protonated imidazole ring.[138] Neither imidazole nor methylimidazole exhibited similar reactivity towards the polymeric substrate. Additionally, structurally similar substrates (e.g. 2,4-dinitrophenyl *p*-isopropylbenzoate) failed to complex with poly(1VIM) due to the lack of electrostatic interactions demonstrating the importance of electrostatic charge in nucleophilic catalysis in synthetic macromolecular systems. Letsinger et al. also found poly(1VIM) catalyzed the hydrolysis of the nitrophenyl ester derivative of poly(uridylic acid) due to the anionic charges present in the sugar-phosphate backbone.[139] Interestingly, poly(L-histidine) catalyzed the hydrolysis more rapidly than poly(1VIM).

Khokhlov and co-workers approached the design of synthetic enzymes with inspiration from computer-aided biomimetic design of functional copolymers.[140] They realized two important parameters that were not discussed previously: proteins are globular and soluble in aqueous medium. To mimic these attributes a synthetic polymer requires a hydrophobic core with a hydrophilic shell. *N*-vinylcaprolactam copolymerized with 1VIM in a 10% aqueous DMSO solution which produced a copolymer that behaved similar to a protein in aqueous media. The copolymers which contained 10-15 mol % 1VIM when heated to 70 °C did not precipitate and at 35 °C underwent a conformation transition from a coil to globule. These copolymers along with poly(NIPAM-*co*-1VIM) exhibited a coil-to-globule transition upon heating in water

or water-isopropanol solutions due to the LCST behavior of the hydrophobic monomers. The transition to a globule resulted in enhanced catalytic activity attributed to the existence of numerous hydrophobic polymer/solvent interfaces for the binding of PNPA as shown in Figure 3.13.[141]

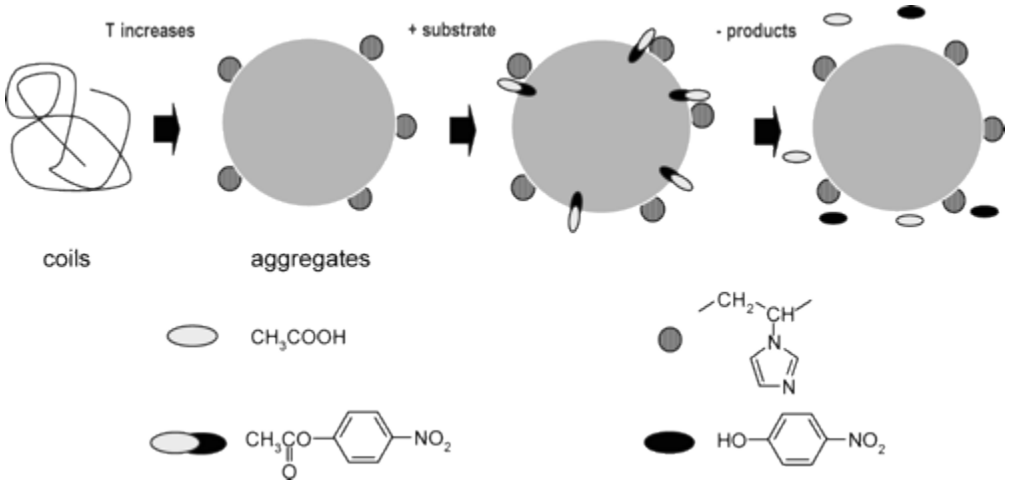

Figure 3.13. Diagram demonstrating poly(NIPAM-*co*-1VIM) coil to globule transition with subsequent hydrolysis of PNPA at the aggregate surface. Reprinted with permission from reference [141].

The hydrophilic 1VIM appeared in a high concentration at the water/polymer interface; therefore, a high concentration of the active species (catalyst and substrate) were localized in close proximity to each other enabling a faster rate of catalysis compared to poly(1VIM). At high temperatures however, the polymers rate of catalysis decreased due to the formation of an unstable globule attributed to the random structure of the copolymer.

To overcome this problem, Liu et al. successfully synthesized NIPAM-1VIM block copolymers with xanthate RAFT agents.[142] These were the first 1VIM block copolymers synthesized to catalyze esterolytic reactions. The block copolymers behaved similarly to the random copolymers (Figure 3.14) and exhibited enhanced catalytic activity above the LCST of NIPAM.

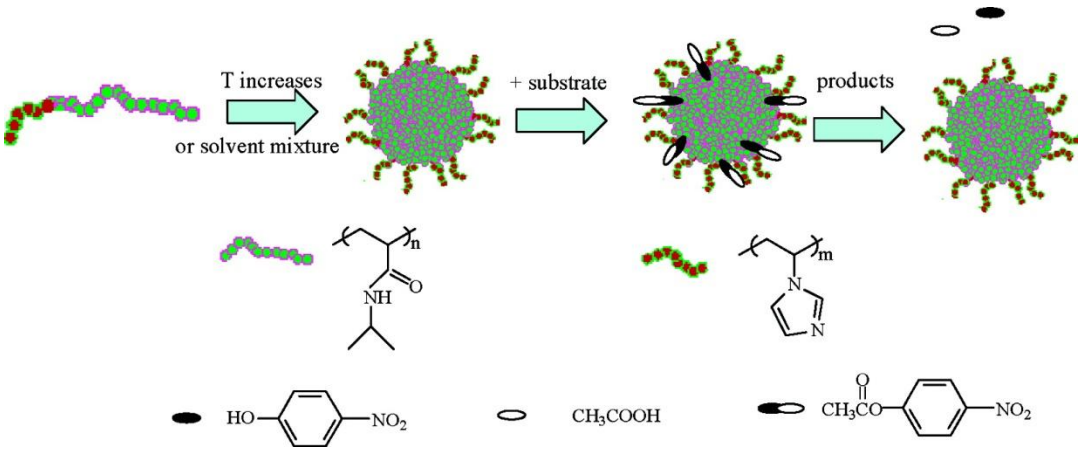

Figure 3.14. Illustration of NIPAM-1VIM block copolymer nanoreactors for the hydrolysis of PNPA. Reprinted with permission from reference [142].

The blocky nature of the copolymers maintained micellization to high temperatures (> 45 °C) unlike the random copolymers. Yuan et al. utilized a similar copolymer system, poly(NIPAM-*co*-1-ethyl-3-vinylimidazolium bromide (EVIM-Br)), to stabilize multi-walled carbon nanotubes in aqueous solution through temperature and ionic strength.[143]

3.3.3 Polymerized Ionic Liquids for Conductive Applications

Organic salts with a melting point below 100 °C compose ionic liquids. These designer molecules enable facile control of chemical properties including polarity, solubility, thermal stability through cation and anion selection. The imidazolium cation remains an area of intense focus in the ionic liquid literature due to its high chemical and thermal stability, high ionic conductivity, and negligible vapor pressure. Numerous reviews provide a comprehensive evaluation on polymerized ionic liquids and their applications.[13,14,144,145] Quaternization of 1VIM and post-polymerization functionalization with alkyl halides produced ionic liquid monomers and polymers. Salamone et al. synthesized, characterized, and polymerized the first quaternized 1-vinylimidazole and 2-methyl-1-vinylimidazole monomers.[146] Previously, researchers synthesized poly(1VIM) and through post-polymerization reactions functionalized

poly(1VIM) with difficulty obtaining 100% functionalization.[147] Various *n*-alkyl iodides (n = 1 – 16) quaternized the 3-position of the imidazole ring producing the respective *n*-alkyl-vinylimidazolium iodide monomers. The free radical initiator, 4,4'-azobiscyanovaleric acid, successfully homopolymerized all respective monomers.

Almost thirty years later, the interest in these quaternized systems was reignited as research in the field of ionic liquids accelerated. Mecerreyes et al. synthesized and homopolymerized *n*-ethyl-3-vinylimidazolium bromide and *n*-butyl-3-vinylimidazolium bromide.[148] After polymerization, the homopolymers underwent anion exchange from the bromide counterion to various hydrophobic counterions to investigate the impact of anion exchange on polymer solubility. Additionally, methyl, propyl, and perfluorodecyl-substituted monomers were synthesized and characterized for use in dye sensitized solar cells.[149] When doped with ionic liquid, the polymers exhibited room temperature conductivities between 10^{-3}-10^{-7} S/cm. Microwave irradiation of these homopolymers in DMF dealkylated the homopolymer resulting in mainly poly(1VIM) with minor amine, formamide, and alkene side products.[150] 1VIM functionalized with *t*-butylbromoacetate produced foamable polymerized ionic liquids through microwave irradiation due to isobutylene release (Figure 15).[151]

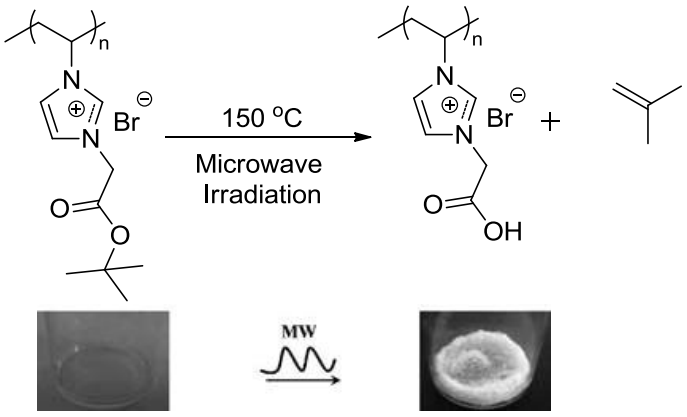

Figure 3.15. Microwave accelerated isobutylene release forming foamable polymerized ionic liquids. Reprinted with permission from reference [151].

Salamone and others functionalized 1VIM with sulfobetaine substituents to generate zwitterionic imidazolium monomers,[152] nitrile substituents,[153] and vinylsulfonic acid and 3-sulfopropyl acrylate.[154] Copolymerizations of 1VIM and the ionic liquid derivatives with styrene determined the reactivity ratios of those systems (r_{1VIM} = 0.10, $r_{styrene}$ = 10.0) which suggested the polymers failed to copolymerize and resulted in homopolymer formation.[22] The imidazole-containing monomers successfully copolymerized with vinyl acetate and methyl methacrylate.

Long et al. additionally characterized the influence of anion and alkyl substituent length on the thermal and conductivity properties of similar systems.[155] An increase in alkyl chain length decreased the T_g and the normalized ionic conductivity of these samples decreased due to an increase in polymer backbone-to-backbone spacing as shown in Figure 3.16.[156]

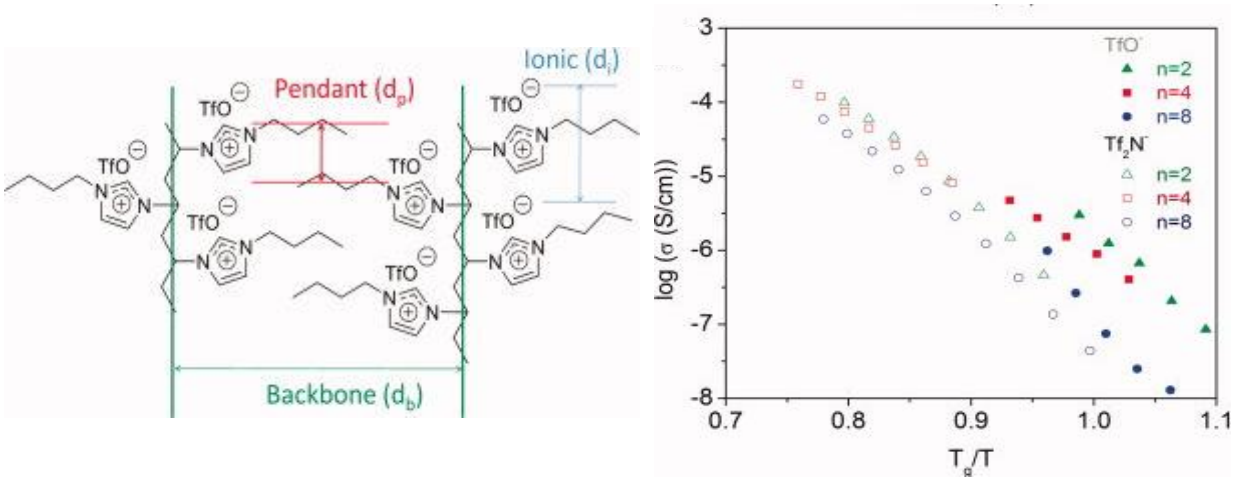

Figure 3.16. Schematic depicting the spacing observed in X-ray scattering and the T_g-independent ionic conductivities. Reprinted with permission from reference [156].

A decrease in T_g and an increase in thermal stability occurred as the anion exchanged to a bulkier, less basic anion (i. e. bis(trifluoromethanesulfonyl)imide (Tf_2N^-)). Nakamura et al. investigated the dielectric relaxation of poly(EVIM) and poly(BVIM) to further investigate the effect of polymer structure on ionic conductivity.[157-159] The T_g influenced polymer segmental motion, side chain motion remained independent of T_g and counterion structure, and anion size controlled

ion-pair life times. These observations led to the conclusion that counterion translational diffusion above T_g and counterion transportation due to dynamic ion-pair formation and dissociation above and below T_g contributed significantly to ionic conductivity values.

Wan et al. synthesized 1VIM monomers functionalized with anthraquinone imide pendant groups to generate near-infrared electrochromic polyelectrolytes.[160] This novel monomer underwent copolymerization with 3-butyl-1-vinylimidazolium bromide to improve polymer solubility. The polymer film without electrolyte additives exhibited color change at a wavelength of 810 nm with a response time of 1 s. Electropolymerization of a vinylimidazolium monomer with a thiophene substituent produced a crosslinked polymer film that also exhibited electrochromism.[161] Electrical conductivity achieved 2.36 S/cm when doped with iodine and 0.53 S/cm in the neutral form. The films formed a lamellar structure with thiophene sheets perpendicular to the polymerized vinylimidazolium substituents as shown in Figure 3.17.

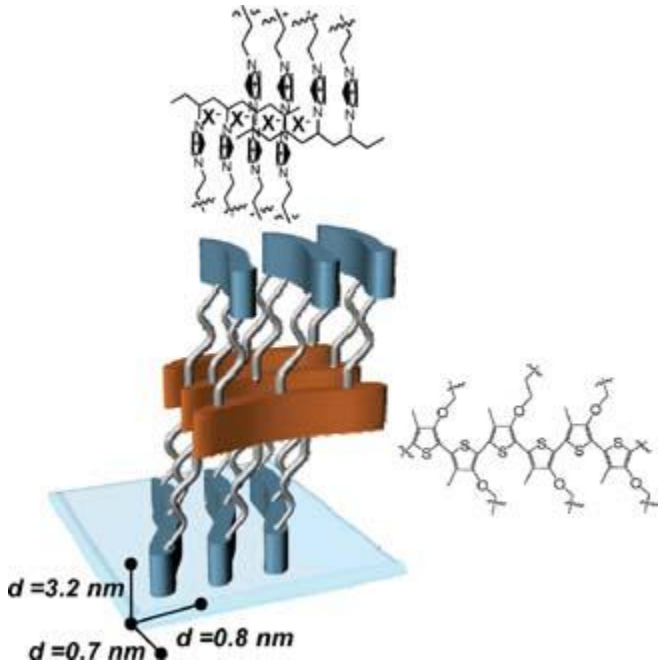

Figure 3.17. Schematic of the proposed structure of the polymerized ionic liquid according to X-ray scattering results. Orange units represent the thiophene sheets and blue units represent the imidazolium rings. Reprinted with permission from reference [161].

Antonetti et al. first determined the thermolysis of ionic liquids containing dicyanamide anions produced nitrogen-doped graphite-like precursors.[162] Extending the process to macromolecules, pyrolysis of various vinylimidazolium homopolymers doped with $FeCl_2 \cdot 4H_2O$ produced mesoporous graphitic carbon materials.[163] Yuan and co-workers generated nitrogen-doped carbon fibers through the electrospinning and subsequent crosslinking and carbonization of poly(3-allyl-1-vinylimidazolium dicyanamide).[164] The resulting materials exhibited ionic conductivities of 200 S/cm.

3.3.4 Biological Applications

Polymer nanoparticles which self-assemble into various compartments enable the design of advanced drug delivery vehicles. Yuan and co-workers have focused extensively on the self-assembly of vinylimidazolium homopolymers into highly ordered nanoparticles.[165] The dispersion polymerization of 3-dodecyl-1-vinylimidazolium bromide and the corresponding C14 - C18 derivatives afforded colloidally stable polymer nanoparticles (20-40 nm in diameter) in water with concentric multi- and uni-lamellar inner structures as shown in Figure 3.18.[166]

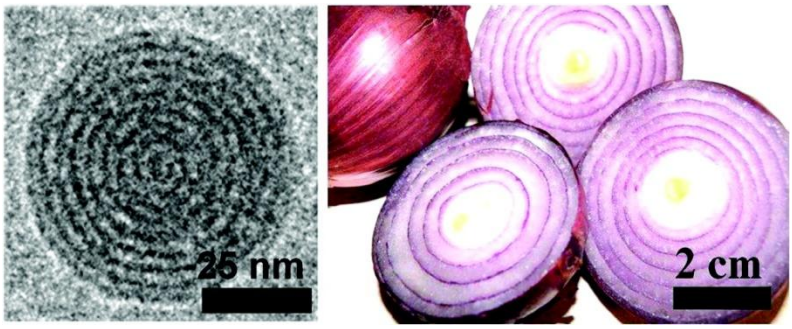

Figure 3.18. Cryo-TEM image of polymerized ionic liquid nanoparticles in aqueous solution. Reprinted with permission from reference [166].

The dispersion polymerization did not require the addition of a dispersing agent or stabilizers due to the monomer and oligomers behaving as effective stabilizers.[167] The C12 and larger substituents monomers formed smectic A mesophases.[168] Varying alkyl chain length and

counter ion size ($Br^- < I^- < BF_4^- < PF_6^-$) enabled tuning of the phase transition temperature. A zwitterionic monomer, sulfobetaine 1-vinylimidazole (SBVIM), underwent free radical homopolymerization with the addition of a crosslinker to form a nonfouling hydrogel.[169] The hydrogels resisted protein adsorption similarly to a zwitterionic methacrylate monomer, and advantageously showed improved tensile and compressive mechanical properties for potential tissue engineering scaffolds.

Midoux and co-workers recently published a review on nucleic acid delivery vehicles containing histidine.[170] Polymers containing the amino acid histidine or imidazole commonly improve nonviral gene delivery compared to unmodified macromolecules due to imidazole's buffering capacity (pKa ~ 6) near endosomal pH. Midoux and co-workers functionalized poly(L-lysine) with histidine residues and found a 3-4 order of magnitude increase in transfection efficiency compared to the unfunctionalized homopolymer.[171]

Asayama and coworkers have explored numerous derivatives of poly(1VIM) for nonviral DNA delivery. Unfunctionalized poly(1VIM) does not complex DNA in aqueous solutions at physiological pH, therefore, requiring quaternization to impart a permanent positive charge. Initially, lactosylated poly(L-lysine) (PLL) grafted onto poly(1VIM) produced a comb-like copolymer which bound DNA effectively, but these systems were not delivered to cells.[172] As discussed previously, poly(1VIM) complexed with Zn^{2+} ions and PLL delivered DNA more effectively than PEI to HepG2 cells.[57] Additionally, Asayama and co-workers functionalized poly(1VIM) with amine and alkyl groups for nucleic acid delivery.[173,174] Amine functionalization produced a minimal effect on gene transfection due to 2.5 mol % quaternization on poly(1VIM). Oligomerization of bromoethylamine hydrobromide prevented higher functionalization percentages on the homopolymer. Functionalization with alkyl groups (ethyl,

butyl, octyl) generated imidazolium copolymers containing a maximum of 50% cationic charge. The butyl-functionalized imidazolium copolymers displayed the highest luciferase expression in HepG2 cells as shown in Figure 3.19. The copolymers remained nontoxic due to the low amount of charge density in these systems.

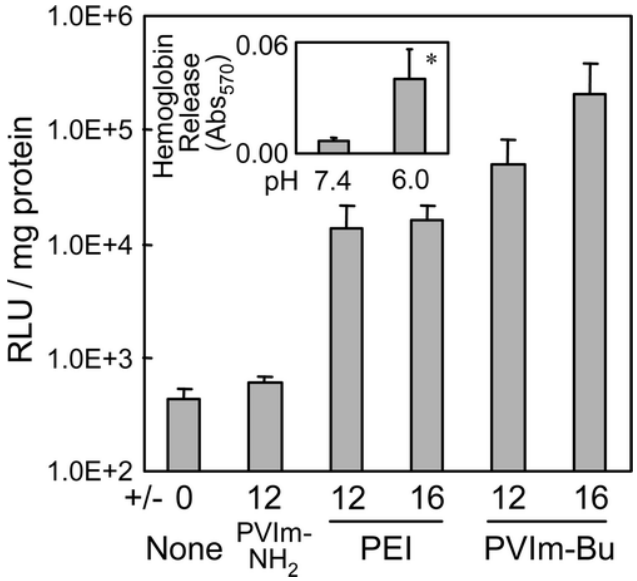

Figure 3.19. Luciferase expression of HepG2 as a function of various nonviral gene delivery vectors. Reprinted with permission from reference [173].

Long et al. later functionalized poly(1VIM) with hydrogen bonding substituents to investigate the effects of charge density and hydrogen bonding on nucleic acid delivery.[20] As charge density and hydrogen bonding increased, the polymer-DNA binding affinity increased. However, increased charge density increased copolymer cytotoxicity; whereas, copolymers containing increased hydrogen bonding remained nontoxic. Copolymers which displayed an intermediate polymer-DNA binding affinity through controlling charge density and hydrogen bonding exhibited the highest transfection efficiencies as shown in Figure 20.

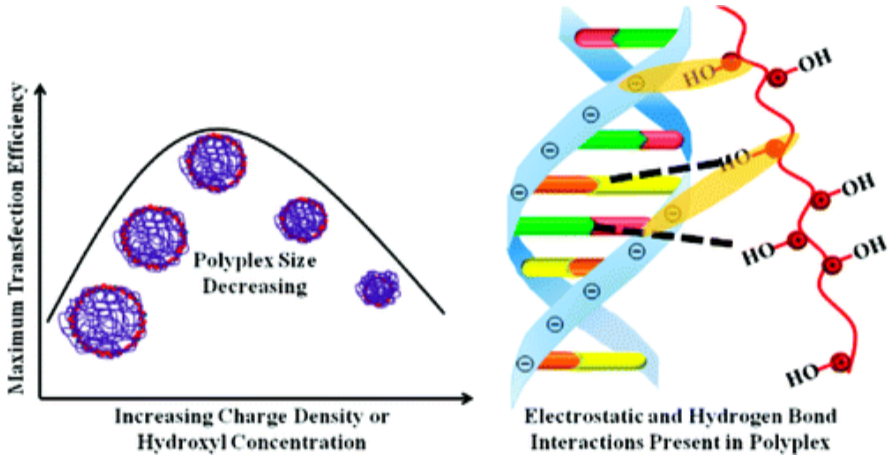

Figure 3.20. Diagram depicting the importance of controlling polymer-DNA binding affinity for optimized DNA delivery through electrostatic or hydrogen bonding interactions. Reprinted with permission from reference [20].

3.3.5 Controlled Radical Polymerization

N-vinyl monomers including 1VIM form an unstable propagating radical during polymerization. The lack of resonance stabilization produces an increased likelihood of chain transfer and chain termination events, limiting polymer molecular weight. The controlled radical polymerization of these monomers is often difficult due to the decreased stability of the propagating radical. Numerous *N*-vinyl monomers including *N*-vinylcarbazole, *N*-vinylindole, *N*-vinylpyrrolidone, *N*-vinylphthalimide were polymerized in a controlled fashion with various controlled radical polymerization processes.[17] Bamford et al. studied the conventional free radical polymerization of 1VIM in the early 1980s and determined a degradative addition reaction between monomer and the propagating polymer radical occurred.[175] The propagating polymer chain added to the 2-position on the 1VIM monomer forming a resonance stabilized radical on the 3-position. When the 2-position contained a methyl group (2-methyl-1-vinylimidazole) the degradative addition was significantly reduced. They also determined polymerization of 1VIM in an acidic aqueous solution, protonated the monomer and increased

the polymer molecular weight due to resonance stabilization of the cationic charge. Dambatta and Ebdon further confirmed these observations and determined 1VIM polymerizations initiated with benzoyl peroxide (BPO) induced decomposition of the initiator.[176]

The difficulties mentioned above have resulted in limited success to control the polymerization of 1VIM and its quaternized analogs. Nakamura et al. synthesized 1VIM homopolymers in a controlled fashion (PDIs < 1.2) utilizing UV irradiation and a tellurium-based chain transfer agent.[177] Endo et al. employed MADIX (macromolecular design via interchange of xanthate) polymerization, a more common polymerization strategy previously applied to various *N*-vinyl monomers.[178] This class of reversible addition-fragmentation chain transfer (RAFT) polymerizations used active xanthate chain transfer agents (CTAs) to attempt to control the polymerization of three quaternized 1VIM monomers. The molecular weights varied significantly from theoretical values; however, kinetics studies and subsequent chain extension/blocking experiments to synthesize block copolymers confirmed controlled behavior. These monomers also successfully produced diblock copolymers when reacted with a poly(NIPAM) macroCTA. Yuan et al. employed this synthetic strategy to produce poly(NIPAM) and poly(*N*,*N*-dimethylacrylamide) macroCTAs which were subsequently copolymerized with vinylimidazolium monomers.[179] These dually-responsive diblock copolymers to temperature and ionic strength were employed as carbon precursors for the generation of graphitic nanostructures.

Recently, cobalt-mediated polymerization controlled the homopolymerization of 3-ethyl-1-vinylimidazolium bromide with controlled molecular weight growth and narrow PDIs in methanol.[180] The metal-mediated polymerizations (i.e. ATRP) of uncharged 1VIM proved unsuccessful due to the coordination of 1VIM to the metal catalyst. Jiang et al. attempted ATRP of a zwitterionic sulfonated vinylimidazolium monomer, but failed to characterize the resulting

polymer.[169] Previously, our group attempted the control of 1VIM utilizing nitroxide-mediated polymerization (NMP); however, size exclusion chromatography and blocking experiments indicated a lack of control.[17] These few reports on the controlled radical polymerization of 1VIM and its quaternized analogs indicated difficulties which continue to impede the progress of designing 1VIM-containing block copolymers. A more radically stable monomer is required to overcome these obstacles to generate polymers that contain imidazole connected directly to the polymer backbone. As shown previously in Figure 3.2, 4VIM and 2VIM present potential solutions to this issue.

3.4 *4-Vinylimidazole*

Overberger and coworkers first synthesized 4VIM, a crystalline solid with a melting point of 86-88 °C, from histidine, but later developed a more direct synthesis involving a one-step decarboxylation of urocanic acid.[15] Others investigated different routes to synthesize 4VIM in gram scale quantities with few synthetic steps; however, the reactions proved unsuccessful or more complex than a one-step decarboxylation reaction.[181,182] Overberger et al. performed heterogeneous homopolymerizations in benzene and copolymerized 4VIM with a variety of comonomers including vinyl acetate, methyl acrylate, and acrylic acid.

One of the main research thrusts involving the polymerization of 4VIM was for the design of synthetic enzymes. As discussed previously, the histidine residue is widely found in the active site of numerous natural enzymes. The development of synthetic enzyme mimics remains important industrially and academically. Natural enzymes for industrial applications denature easily in harsh conditions and are impractical due to the high costs associated with these systems. A synthetic replacement would reduce cost, provide increased stability, and allow for catalyst reusability. Overberger and co-workers synthesized a variety of 4VIM copolymers to investigate the esterolytic activity of these systems.[183-189] Various properties studied, included

the effect of copolymer functional groups,[184] charge density,[187] and alkyl groups attached to 4VIM repeat units on the rate of catalysis.[189-192] Trityl-protection on the 1-position failed to produce poly(4VIM) with different stereochemistries to investigate the effect of tacticity on catalysis.[193] The amphoteric nature of poly(4VIM) resulted in a more active catalysis of PNPA hydrolysis compared to poly(1VIM). Kunitake et al. prepared a bifunctional catalyst through free radical copolymerization of 4VIM with *N*-methyl-*N*-hydroxyacrylamide to hydrolyze PNPA similar to serine proteases.[194] The copolymerization of 4VIM with itaconic acid and a crosslinking agent produced microspheres for the catalysis of transesterification reactions.[195] Song et al. copolymerized 4VIM with acrylamide to investigate the interaction of polymer chains containing reactive substituents with catalytic polymers. The 4VIM copolymers failed to catalyze the hydrolysis of poly(acrylamide-*co*-*p*-nitrophenyl acrylate) which was attributed to steric hindrance preventing the groups from interacting.[196] Placement of the imidazole ring further from the polymer backbone successfully promoted hydrolysis of the *p*-nitrophenyl acrylate repeat unit.

4VIM resembles imidazole compounds which occur in biology (i.e. histidine, histamine) as both are connected to their respective functionalities at the 4-position on the imidazole ring. Alvarez-Lorenzo et al. prepared biomimetic hydroxyethyl methacrylate and *N*,*N*-dimethylacrylamide hydrogels to optimize ocular delivery of carbonic anhydrase inhibitor drugs.[197,198] They incorporated 1VIM and 4VIM into the hydrogels to coordinate Zn^{2+} ions to mimic the cone-shaped cavity of carbonic anhydrase (Figure 3.21) and found 4VIM containing-hydrogels more effectively hosted the Zn^{2+} ions and antiglaucoma drugs for the development of medicated soft contact lenses. Oner et al. utilized poly(4VIM-*co*-vinylphosphonic acid) copolymers to study the biomimetic mineralization of hydroxyapatite crystals on the copolymer

surface.[199] The rates of hydroxyapatite crystal growth depended on the phosphate content of the copolymer.

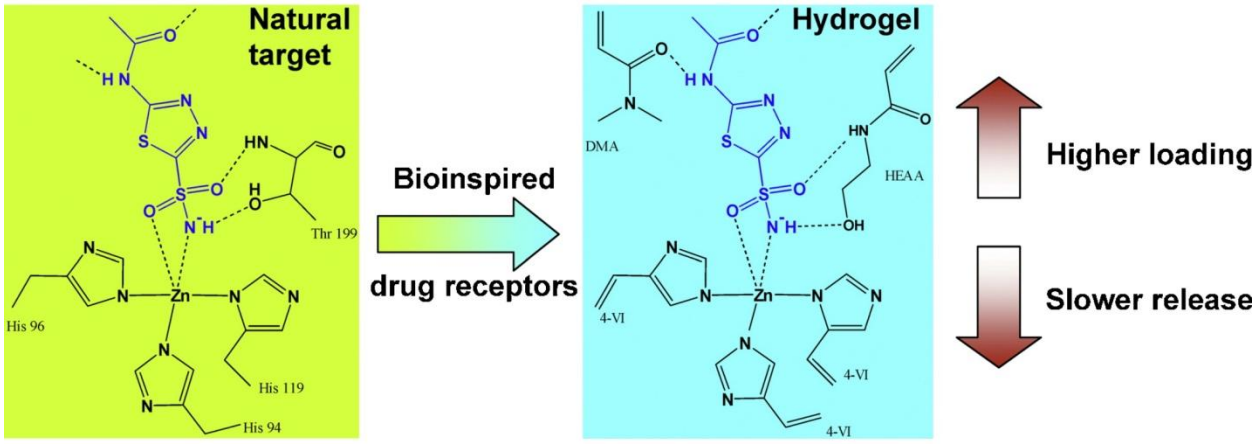

Figure 3.21. Bioinspired design of hydrogels for ocular drug delivery. Reprinted with permission from reference [198].

Cho et al. explored poly(4VIM) as a nonviral delivery vehicle.[200,201] The polymer bound DNA at a pH of 7.4 due to approximately 25% protonation of the imidazole repeat units. Poly(4VIM) transfected HeLa cells about 50% less effectively than PEI, but PEI exhibited greater cytotoxicity. Figure 3.22 shows the successful transfection of HeLa and MC3T3-E1 cells with both poly(4VIM) and PEI. Qualitatively, the cell morphology also suggested the high toxicity of PEI and the low toxicity of poly(4VIM).

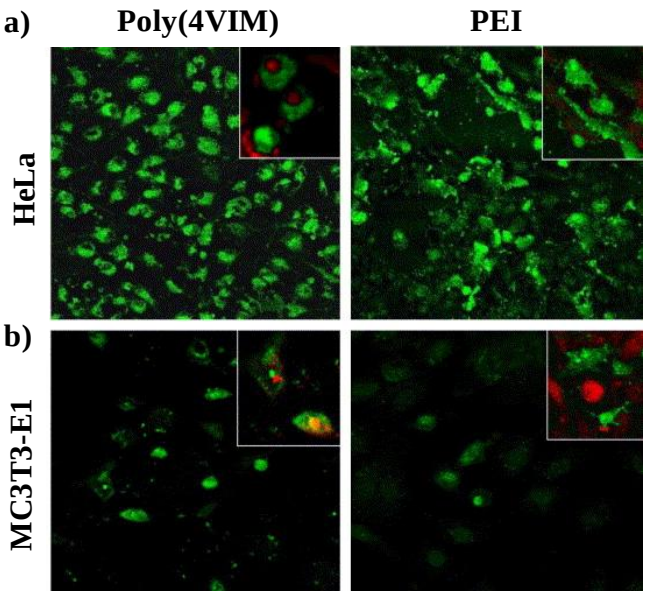

Figure 3.22. In vitro transfection of a) HeLa and b) MC3T3-E1 cells with poly(4VIM) and PEI with GFP. Nuclei were stained red with propidium iodide. Reprinted with permission from reference [200].

Bozkurt and co-workers copolymerized 4VIM with numerous comonomers for the development of proton conducting polymer films. Imidazole presents an attractive alternative to replace water as a proton conducting species enabling the design of anhydrous conducting membranes. Initially blends of poly(4VIM) with phosphoric acid and sulfuric acid were characterized to generate an anhydrous proton conducting film that exhibited thermal stability above 100 °C.[202,203] Proton hopping and polymer segmental motion influenced proton transport in the membranes. Vinylphosphonic acid and vinylbenzylboronic acid copolymerized with 4VIM produced novel proton conducting polymers with low conductivities in the dry state, but proton conductivity reached 2.7×10^{-3} S/cm when doped with acid.[204,205] Unexpectedly, the polymers remained thermally stable above 200 °C with 50 mol % vinylphosphonic acid comonomer. Copolymerizations with ethylene glycol methacrylate phosphate (EGMAP) produced alternating copolymers with poor proton conductivity due to ionic crosslinking in the polymers which restricted segmental motion.[206]

Despite the limited amount of publications incorporating 4VIM into macromolecules compared to 1VIM, 4VIM remains a better mimic of biological imidazole-containing systems. As mentioned previously, 1VIM's propagating radical instability limited its incorporation into a variety of macromolecules with advanced architectures. Recently, we reported on the unprecedented controlled radical polymerization of 4VIM utilizing RAFT polymerization strategies.[207] The polymerizations in acetic acid displayed linear pseudo-first order kinetics and linear molecular weight growth with monomer conversion through systematic variation of polymerization parameters as shown in Figure 3.23.

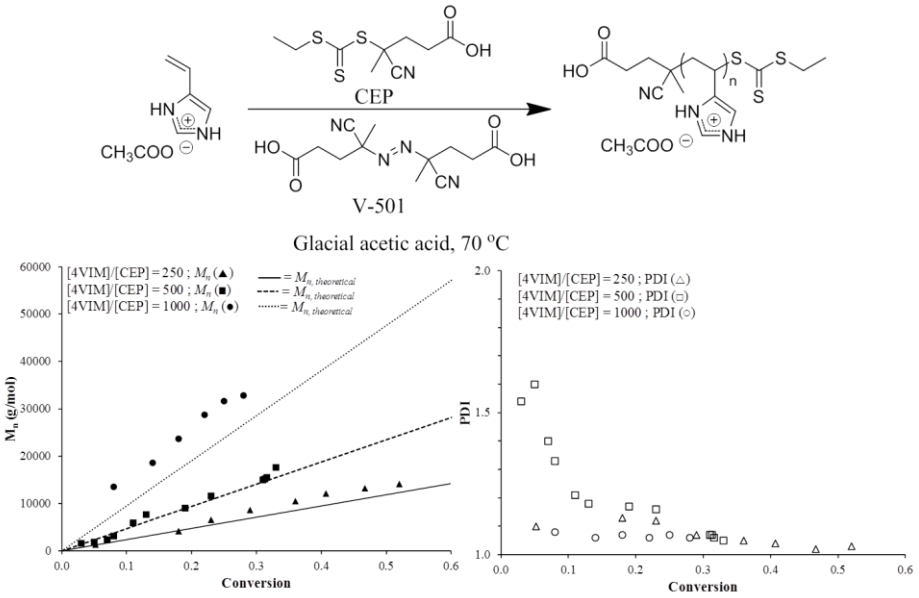

Figure 3.23. RAFT polymerization of 4VIM in glacial acetic acid with well-defined molecular weight and narrow polydispersities. Reprinted with permission from reference [207].

Effectively controlling 4VIM homopolymerizations enables the future design of block copolymers for numerous emerging applications including synthetic enzymes, gene delivery vehicles, and anti-corrosive agents.

3.5 *2-Vinylimidazole*

2VIM publications remain extremely limited due to its difficult synthesis. Although 2VIM exhibits increased radical stability compared to 4VIM and 1VIM due to its additional

resonance contributors, no publications on the controlled radical polymerization of 2VIM exist. Lawson first synthesized 2VIM (melting point = 128-129 °C) through the dehydration of 2-hydroxyethylimidazole.[208] The synthesis of 2-hydroxyethylimidazole proved complicated and the difficult purifications limited yields (< 15%). 2VIM successfully copolymerized with acrylonitrile, styrene, and methyl methacrylate; however, the copolymer properties were not determined. Overberger et al. improved the yield of 2VIM through a dehydrohalogenation of 2-bromoethylimidazole; however, the procedure still required the complicated synthesis of 2-hydroxyethylimidazole.[16] Shimko et al. polymerized 2VIM using cobalt 60 gamma irradiation and found the hydrogen bonding of the solvent impacted the tacticity of the resulting polymer.[209] A more facile synthesis would enable the design of numerous polymers incorporating 2VIM as these three publications remain the only reports on 2VIM. The increased radical stability of 2VIM opens a variety of possibilities for the design of amphoteric macromolecules utilizing both conventional and controlled radical polymerization strategies.

3.6 *Conclusions*

The intense focus on the ubiquitous imidazole ring has propelled imidazole-containing polymers to the forefront of materials design. Researchers widely utilize the monomers, 1-, 2-, and 4-vinylimidazole regioisomers, and free radical polymerization of these monomers allows for the development of novel polymer architectures. Polymers based on 1VIM are utilized in a wide variety of applications including metal chelation, catalysis, and nonviral gene delivery. The commercial availability of 1VIM has spurred copolymerizations with numerous comonomers and novel derivatives of 1VIM through its facile functionalization which affords the tailoring of polymer properties for numerous technologies. The propagating radical stability of 1VIM limits the generation of novel architectures with controlled radical polymerization strategies. 4VIM a better synthetic mimic to biological molecules containing imidazole rings, exhibits an increased

radical stability enabling controlled radical polymerization. Although, a lack of commercial production limits the use of 2VIM and 4VIM, the recent success utilizing RAFT polymerization strategies to produce well-defined polymers facilitates the future generation of novel polymer architectures for emerging applications.

3.7 *Acknowledgements*

This material is based upon work supported in part by the Macromolecular Interfaces with Life Sciences (MILES) Integrative Graduate Education and Research Traineeship (IGERT) of the National Science Foundation under Agreement No. DGE-0333378. This material is also based upon work supported in part by the US Army Research Office under Grant No. W911NF-07-1-0452 Ionic Liquids in Electro-Active Devices (ILEAD) MURI.

3.8 *References*

(1) Anderson, E. B.; Long, T. E. *Polymer* **2010**, *51*, 2447-2454.
(2) Bachovchin, W. W. *Biochemistry* **1986**, *25*, 7751-7759.
(3) Vallee, B. L.; Auld, D. S. *Proceedings of the National Academy of Sciences* **1990**, *87*, 220-224.
(4) Chan, C. K.; Hu, Y.; Takahashi, S.; Rousseau, D. L.; Eaton, W. A.; Hofrichter, J. *Proceedings of the National Academy of Sciences* **1997**, *94*, 1779-1784.
(5) Akdis, C. A.; Blaser, K. *Journal of allergy and clinical immunology* **2003**, *112*, 15-22.
(6) Rogers, R. D.; Seddon, K. R. *Science* **2003**, *302*, 792-793.
(7) Rivas, B. L.; Maturana, H. A.; Molina, M. J.; Gómez-Aantón, M. R.; Piérola, I. F. *J. Appl. Polym. Sci.* **1998**, *67*, 1109-1118.
(8) Skouta, R.; Wei, S.; Breslow, R. *J. Am. Chem. Soc.* **2009**, *131*, 15604-15605.
(9) Piacham, T.; Ayudhya, C. I. N.; Prachayasittikul, V.; Buelow, L.; Ye, L. *Chem. Commun.* **2003**, 1254-1255.
(10) Tang, J.; Tang, H.; Sun, W.; Radosz, M.; Shen, Y. *J. Polym. Sci., Part A: Polym. Chem.* **2005**, *43*, 5477-5489.
(11) Fürmeier, S.; Metzger, Jürgen O. *Eur. J. Org. Chem.* **2003**, *2003*, 885-893.
(12) Sanders, J. P. M.; Clark, J. H.; Harmsen, G. J.; Heeres, H. J.; Heijnen, J. J.; Kersten, S. R. A.; van Swaaij, W. P. M.; Moulijn, J. A. *Chemical Engineering and Processing: Process Intensification* **2012**, *51*, 117-136.
(13) Green, M. D.; Long, T. E. *Polymer Reviews* **2009**, *49*, 291 - 314.
(14) Mecerreyes, D. *Prog. Polym. Sci.* **2011**, *36*, 1629-1648.
(15) Overberger, C. G.; Vorchheimer, N. *J. Am. Chem. Soc.* **1963**, *85*, 951-955.
(16) Overberger, C. G.; Gerberding, K. *Journal of Polymer Science: Polymer Letters Edition* **1973**, *11*, 465-469.
(17) Green, M. D.; Allen Jr, M. H.; Dennis, J. M.; Cruz, D. S.-d. l.; Gao, R.; Winey, K. I.; Long, T. E. *Eur. Polym. J.* **2011**, *47*, 486-496.
(18) Liu, K.-J.; Gregor, H. P. *J. Phys. Chem.* **1965**, *69*, 1252-9.
(19) Gregor, H. P.; Liu, K.-J. *J. Am. Chem. Soc.* **1965**, *87*, 1678-81.
(20) Allen, M. H.; Green, M. D.; Getaneh, H. K.; Miller, K. M.; Long, T. E. *Biomacromolecules* **2011**, *12*, 2243-2250.
(21) Annenkov, V. V.; Danilovtseva, E. N.; Tenhu, H.; Aseyev, V.; Hirvonen, S. P.; Mikhaleva, A. I. *Eur. Polym. J.* **2004**, *40*, 1027-1032.
(22) Petrak, K. L. *J. Polym. Sci., Polym. Lett. Ed.* **1978**, *16*, 393-9.
(23) Pu, H.; Qin, Y.; Wan, D.; Yang, Z. *Macromolecules* **2009**, *42*, 3000-3004.
(24) Pekel, N.; Şahiner, N.; Güven, O.; Rzaev, Z. M. O. *Eur. Polym. J.* **2001**, *37*, 2443-2451.
(25) Yan, Y.; Lu, N.; Cui, J.; Zhang, J. *J. Appl. Polym. Sci.* **2012**, *125*, 2867-2873.
(26) Danilovtseva, E. N.; Chafeev, M. A.; Annenkov, V. V. *J. Polym. Sci., Part A: Polym. Chem.* **2012**, *50*, 1539-1546.
(27) Schaeffner, F.; Drache, M.; Schmidt-Naake, G. *Macromol. Mater. Eng.* **2011**, *296*, 535-543.
(28) Pekel, N.; Rzaev, Z. M. O.; Güven, O. *Macromol. Chem. Phys.* **2004**, *205*, 1088-1095.
(29) Bay, R. F. C.; Armes, S. P.; Pickett, C. J.; Ryder, K. S. *Polymer* **1991**, *32*, 2456-2460.
(30) Uzum, O. B.; Karadag, E. *Polym. Adv. Technol.* **2007**, *18*, 483-489.
(31) Bisht, H. S.; Wan, L.; Mao, G.; Oupicky, D. *Polymer* **2005**, *46*, 7945-7952.
(32) Yi, J. W.; Na, K.; Bae, Y. H. *Macromolecular Symposia* **2004**, *207*, 131-138.

(33) Kumar, A.; Kamihira, M.; Galaev, I. Y.; Iijima, S.; Mattiasson, B. *Langmuir* **2003**, *19*, 865-871.
(34) Kazakov, S.; Kaholek, M.; Kudasheva, D.; Teraoka, I.; Cowman, M. K.; Levon, K. *Langmuir* **2003**, *19*, 8086-8093.
(35) Hyeong Kwon, O.; Kikuchi, A.; Yamato, M.; Okano, T. *Biomaterials* **2003**, *24*, 1223-1232.
(36) Ito, S.; Ogawa, K.; Suzuki, H.; Wang, B.; Yoshida, R.; Kokufuta, E. *Langmuir* **1999**, *15*, 4289-4294.
(37) Galaev, I. Y.; Kumar, A.; Mattiasson, B. *J. Macromol. Sci., Pure Appl. Chem.* **1999**, *A36*, 1093-1105.
(38) Park, K.-H.; Park, W.; Na, K. *J. Biosci. Bioeng.* **2009**, *108*, 168-173.
(39) Wiechers, S.; Schmidt-Naake, G. *Macromol. Symp.* **2009**, *281*, 47-53.
(40) Schmidt, C.; Merz, F.; Jiang, S.; Drache, M.; Schmidt-Naake, G. *Macromol. Mater. Eng.* **2007**, *292*, 428-436.
(41) Lowe, A.; Deng, W.; Smith, D. W.; Balkus, K. J. *Macromolecules* **2012**, *45*, 5894-5900.
(42) Deng, W.; Lobovsky, A.; Iacono, S. T.; Wu, T.; Tomar, N.; Budy, S. M.; Long, T.; Hoffman, W. P.; Smith, D. W., Jr. *Polymer* **2011**, *52*, 622-628.
(43) Sahiner, N.; Butun, S.; Ilgin, P. *Colloids Surf., A* **2011**, *381*, 74-84.
(44) Göksel, C.; Hacioğlu, B.; Akbulut, U. *J. Polym. Sci., Part A: Polym. Chem.* **1997**, *35*, 3735-3743.
(45) Tanford, C.; Wagner, M. L. *J. Am. Chem. Soc.* **1953**, *75*, 434-5.
(46) Tanford, C. *J. Am. Chem. Soc.* **1952**, *74*, 211-15.
(47) Gurd, F. R. N.; Goodman, D. S. *J. Am. Chem. Soc.* **1952**, *74*, 670-5.
(48) Edsall, J. T.; Felsenfeld, G.; Goodman, D. S.; Gurd, F. R. N. *J. Am. Chem. Soc.* **1954**, *76*, 3054-3061.
(49) Gold, D. H.; Gregor, H. P. *The Journal of Physical Chemistry* **1960**, *64*, 1464-1467.
(50) Gold, D. H.; Gregor, H. P. *The Journal of Physical Chemistry* **1960**, *64*, 1461-1463.
(51) Pekel, N.; Savaş, H.; Güven, O. *Colloid & Polymer Science* **2002**, *280*, 46-51.
(52) Annenkov, V. V.; Filina, E. A.; Danilovtseva, E. N.; Zinchenko, S. V.; Mikhaleva, A. I. *J. Sol-Gel Sci. Technol.* **2003**, *27*, 163-166.
(53) Rivas, B. L.; Jara, M.; Pereira, E. D. *J. Appl. Polym. Sci.* **2003**, *89*, 2852-2856.
(54) Rivas, B. L.; Pereira, E.; Jara, M.; Esparza, C. *J. Appl. Polym. Sci.* **2006**, *99*, 706-711.
(55) Tarley, C. R. T.; Andrade, F. N.; de, S. H.; Zaia, D. A. M.; Beijo, L. A.; Segatelli, M. G. *React. Funct. Polym.* **2012**, *72*, 83-91.
(56) Asayama, S.; Nishinohara, S.; Kawakami, H. *Metallomics* **2011**, *3*, 680-682.
(57) Asayama, S.; Nishinohara, S.; Kawakami, H. *Bioconjugate Chem.* **2011**, *22*, 1864-1868.
(58) Strzelec, K.; Wasikowska, K.; Cypryk, M.; Pospiech, P. *J. Appl. Polym. Sci.* **2012**, *124*, 3538-3546.
(59) Zhao, C.; Wang, H.-Z.; Yan, N.; Xiao, C.-X.; Mu, X.-D.; Dyson, P. J.; Kou, Y. *J. Catal.* **2007**, *250*, 33-40.
(60) Osman, B.; Kara, A.; Demirbel, E.; Kok, S.; Besirli, N. *Appl Biochem Biotechnol* **2012**.
(61) Kara, A.; Demirbel, E. *Sep. Sci. Technol.* **2012**, *47*, 709-722.
(62) Osman, B.; Kara, A.; Besirli, N. *J. Macromol. Sci., Part A: Pure Appl. Chem.* **2011**, *48*, 387-399.
(63) Kara, A.; Demirbel, E. *Water, Air, Soil Pollut.* **2012**, *223*, 2387-2403.

(64) Kartal, M.; Kayahan, S. K.; Bozkurt, A.; Toppare, L. *Polym. J. (Tokyo, Jpn.)* **2009**, *41*, 46-50.
(65) Schiller, A.; Scopelliti, R.; Benmelouka, M.; Severin, K. *Inorg. Chem.* **2005**, *44*, 6482-6492.
(66) Yang, J.; Qiu, L.; Liu, B.; Peng, Y.; Yan, F.; Shang, S. *J. Polym. Sci., Part A: Polym. Chem.* **2011**, *49*, 4531-4538.
(67) Hu, B.; Wu, T.; Ding, K.; Zhou, X.; Jiang, T.; Han, B. *J. Phys. Chem. C* **2010**, *114*, 3396-3400.
(68) Andersson, M.; Hansson, O.; Oehrstroem, L.; Idstroem, A.; Nyden, M. *Colloid Polym. Sci.* **2011**, *289*, 1361-1372.
(69) Andersson, T. M.; Maartensson, A.; Nyden, M. *Vib. Spectrosc.* **2012**, *61*, 38-42.
(70) Wu, K. H.; Chang, T. C.; Wang, Y. T.; Hong, Y. S.; Wu, T. S. *Eur. Polym. J.* **2002**, *39*, 239-245.
(71) Li, G.; Li, J.; Han, C.; Zhang, J.; Liang, L.; Zhou, H.; Liang, J. *Adv. Mater. Res. (Durnten-Zurich, Switz.)* **2012**, *393-395*, 1143-1148.
(72) Annenkov, V. V.; Danilovtseva, E. N.; Saraev, V. V.; Mikhaleva, A. I. *J. Polym. Sci., Part A: Polym. Chem.* **2003**, *41*, 2256-2263.
(73) Sahiner, N.; Ozay, O. *React. Funct. Polym.* **2011**, *71*, 607-615.
(74) Geraty, S. M.; Vos, J. G. *J. Chem. Soc., Dalton Trans.* **1987**, 3073-3078.
(75) Suzuki, M.; Mori, Y.; Kimura, M.; Hanabusa, K.; Shirai, H. *J. Chem. Soc., Faraday Trans.* **1996**, *92*, 3599-3604.
(76) Suzuki, M.; Kimura, M.; Hanabusa, K.; Shirai, H. *Polymer* **2001**, *42*, 9235-9241.
(77) Suzuki, M.; Kimura, M.; Hanabusa, K.; Shirai, H. *Macromol. Chem. Phys.* **2001**, *202*, 3506-3512.
(78) Suzuki, M.; Bartels, O.; Gerdes, R.; Schneider, G.; Wohrle, D.; Schulz-Ekloff, G.; Kimura, M.; Hanabusa, K.; Shirai, H. *PCCP* **2000**, *2*, 109-114.
(79) Suzuki, M.; Yokoyama, N.; Kimura, M.; Hanabusa, K.; Shirai, H. *React. Funct. Polym.* **1999**, *40*, 97-105.
(80) Suzuki, M.; Yokoyama, N.; Kimura, M.; Hanabusa, K.; Shirai, H. *React. Funct. Polym.* **1999**, *40*, 241-248.
(81) Suzuki, M.; Yokoyama, M.; Kimura, M.; Hanabusa, K.; Shirai, H. *Eur. Polym. J.* **1999**, *35*, 1057-1063.
(82) Suzuki, M.; Sano, M.; Kimura, M.; Hanabusa, K.; Shirai, H. *J. Polym. Sci., Part A: Polym. Chem.* **1999**, *37*, 4360-4367.
(83) Suzuki, M.; Kimura, M.; Hanabusa, K.; Shirai, H. *Acta Polym.* **1999**, *50*, 45-50.
(84) Suzuki, M.; Kimura, M.; Hanabusa, K.; Shirai, H. *Polymer* **1999**, *40*, 3971-3978.
(85) Suzuki, M.; Kimura, M.; Hanabusa, K.; Shirai, H. *Eur. Polym. J.* **1999**, *35*, 977-983.
(86) Suzuki, M.; Bartels, O.; Gerdes, R.; Schneider, G.; Wohrle, D.; Schulz-Ekloff, G.; Kimura, M.; Hanabusa, K.; Shirai, H. *Chem. Lett.* **1999**, 579-580.
(87) Suzuki, M.; Yokohama, N.; Kimura, M.; Hanabusa, K.; Shirai, H. *Macromol. Chem. Phys.* **1998**, *199*, 2267-2274.
(88) Suzuki, M.; Sano, M.; Kimura, M.; Hanabusa, K.; Shirai, H. *New J. Chem.* **1998**, *22*, 1431-1436.
(89) Suzuki, M.; Kobayashi, S.; Uchida, S.; Kimura, M.; Hanabusa, K.; Shirai, H. *Polymer* **1998**, *39*, 1539-1543.

(90) Suzuki, M.; Kobayashi, S.; Uchida, S.; Kimura, M.; Hanabusa, K.; Shirai, H. *Macromol. Chem. Phys.* **1998**, *199*, 937-943.
(91) Suzuki, M.; Kimura, M.; Hanabusa, K.; Shirai, H. *Macromol. Chem. Phys.* **1998**, *199*, 945-948.
(92) Suzuki, M.; Mori, Y.; Yokoyama, N.; Kimura, M.; Hanabusa, K.; Shirai, H. *Macromol. Chem. Phys.* **1997**, *198*, 959-967.
(93) Suzuki, M.; Kobayashi, S.; Kimura, M.; Hanabusa, K.; Shirai, H. *Chem. Commun.* **1997**, 227-228.
(94) Suzuki, M.; Kimura, M.; Shirai, H. *Chem. Commun.* **1997**, 2061-2062.
(95) Suzuki, M.; Kimura, M.; Hanabusa, K.; Shirai, H. *J. Chem. Soc., Faraday Trans.* **1997**, *93*, 4137-4143.
(96) Baldwin, D. A.; Hepner, C. E.; Pratt, J. M. *J. Inorg. Biochem.* **1979**, *10*, 159-67.
(97) Adams, P. A.; Baldwin, D. A.; Hepner, C. E.; Pratt, J. M. *Bioinorganic Chemistry* **1978**, *9*, 479-494.
(98) Scheler, W.; Mohr, P.; Pommerening, K.; Behlke, J. *Eur. J. Biochem.* **1970**, *13*, 77-85.
(99) Tsuchida, E.; Nishide, H.; Vögtle, F.; Weber, E.; Springer Berlin / Heidelberg: 1986; Vol. 132, p 63-99.
(100) Nishide, H.; Kawakami, H.; Suzuki, T.; Azechi, Y.; Soejima, Y.; Tsuchida, E. *Macromolecules* **1991**, *24*, 6306-9.
(101) Fuhrhop, J. H.; Besecke, S.; Vogt, W.; Ernst, J.; Subramanian, J. *Makromolekulare Chemie* **1977**, *178*, 1621-31.
(102) Suzuki, T.; Yasuda, H.; Nishide, H.; Chen, X.-s.; Tsuchida, E. *J. Membr. Sci.* **1996**, *112*, 155-60.
(103) Suzuki, T.; Soejima, Y.; Nishide, H.; Tsuchida, E. *Bull. Chem. Soc. Jpn.* **1995**, *68*, 1036-41.
(104) Suzuki, T.; Nishide, H.; Itakura, K.; Tsuchida, E. *Polym. Adv. Technol.* **1994**, *5*, 253-6.
(105) Suzuki, Y.; Nishide, H.; Tsuchida, E. *Macromolecules* **2000**, *33*, 2530-2534.
(106) Shentu, B.; Shinohara, H.; Nishide, H. *Polym. J. (Tokyo, Jpn.)* **2001**, *33*, 807-811.
(107) Li, S.; Ge, Y.; Turner, A. P. F. *Adv. Funct. Mater.* **2011**, *21*, 1194-1200.
(108) Li, S.; Tong, K.; Zhang, D.; Huang, X. *J. Inorg. Organomet. Polym. Mater.* **2008**, *18*, 264-271.
(109) Zhang, D.; Li, S.; Li, W.; Chen, Y. *Catal. Lett.* **2007**, *115*, 169-175.
(110) Marko-Varga, G.; Emnéus, J.; Gorton, L.; Ruzgas, T. *TrAC, Trends Anal. Chem.* **1995**, *14*, 319-328.
(111) Heller, A. *The Journal of Physical Chemistry* **1992**, *96*, 3579-3587.
(112) Ohara, T. J.; Rajagopalan, R.; Heller, A. *Polym. Mater. Sci. Eng.* **1993**, *70*, 182-3.
(113) Ohara, T. J.; Rajagopalan, R.; Heller, A. *Anal. Chem.* **1994**, *66*, 2451-7.
(114) Coman, V.; Gustavsson, T.; Finkelsteinas, A.; von, W. C.; Haegerhaell, C.; Gorton, L. *J. Am. Chem. Soc.* **2009**, *131*, 16171-16176.
(115) Timur, S.; Haghighi, B.; Tkac, J.; Pazarlioglu, N.; Telefoncu, A.; Gorton, L. *Bioelectrochemistry* **2007**, *71*, 38-45.
(116) Timur, S.; Anik, U.; Odaci, D.; Gorton, L. *Electrochem. Commun.* **2007**, *9*, 1810-1815.
(117) Vostiar, I.; Ferapontova, E. E.; Gorton, L. *Electrochem. Commun.* **2004**, *6*, 621-626.
(118) Gallaway, J. W.; Calabrese, B. S. A. *J. Electroanal. Chem.* **2009**, *626*, 149-155.
(119) Yamada, R.; Fujieda, N.; Tsutsumi, M.; Tsujimura, S.; Shirai, O.; Kano, K. *Electrochemistry (Tokyo, Jpn.)* **2008**, *76*, 600-602.

(120) Tasca, F.; Timur, S.; Ludwig, R.; Haltrich, D.; Volc, J.; Antiochia, R.; Gorton, L. *Electroanalysis* **2007**, *19*, 294-302.
(121) Tsujimura, S.; Kano, K.; Ikeda, T. *Chem. Lett.* **2002**, 1022-1023.
(122) Tessema, M.; Csoeregi, E.; Ruzgas, T.; Kenausis, G.; Solomon, T.; Gorton, L. *Anal. Chem.* **1997**, *69*, 4039-4044.
(123) Ruzgas, T.; Csoregi, E.; Katakis, I.; Kenausis, G.; Gorton, L. *J Mol Recognit* **1996**, *9*, 480-4.
(124) Csoeregi, E.; Schmidtke, D. W.; Heller, A. *Anal. Chem.* **1995**, *67*, 1240-4.
(125) Ohara, T. J.; Rajagopalan, R.; Heller, A. *Anal. Chem.* **1993**, *65*, 3512-17.
(126) Antiochia, R.; Gorton, L. *Biosens. Bioelectron.* **2007**, *22*, 2611-2617.
(127) Sui, X.; Hempenius, M. A.; Vancso, G. J. *J. Am. Chem. Soc.* **2012**, *134*, 4023-4025.
(128) Shinkai, S.; Ando, R.; Kunitake, T. *J. Chem. Soc., Perkin Trans. 2* **1978**, 1271-7.
(129) Kunitake, T.; Shinkai, S.; Hirotsu, S. *J. Org. Chem.* **1977**, *42*, 306-12.
(130) Shinkai, S.; Kunitake, T. *Polym. J.* **1977**, *9*, 423-8.
(131) Shinkai, S.; Kunitake, T. *Biopolymers* **1977**, *16*, 2393-405.
(132) Yuan, S.; Deng, Q.; Fang, G.; Pan, M.; Zhai, X.; Wang, S. *J. Mater. Chem.* **2012**, *22*, 3965-3972.
(133) Papathomas, K. I.; Israel, S. C.; Salamone, J. C. *J. Appl. Polym. Sci.* **1989**, *38*, 1077-89.
(134) Damas, C.; Brembilla, A.; Baros, F.; Viriot, M.-L.; Lochon, P. *Eur. Polym. J.* **1994**, *30*, 1215-22.
(135) Xiong, Y.; Wang, Y.; Wang, H.; Wang, R.; Cui, Z. *J. Appl. Polym. Sci.* **2012**, *123*, 1486-1493.
(136) Pourjavadi, A.; Hosseini, S. H.; Doulabi, M.; Fakoorpoor, S. M.; Seidi, F. *ACS Catal.* **2012**, *2*, 1259-1266.
(137) Letsinger, R. L.; Savereide, T. J. *J. Am. Chem. Soc.* **1962**, *84*, 3122-3127.
(138) Letsinger, R. L.; Klaus, I. S. *J. Am. Chem. Soc.* **1965**, *87*, 3380-6.
(139) Letsinger, R. L.; Wagner, T. E. *J. Am. Chem. Soc.* **1966**, *88*, 2062-3.
(140) Lozinsky, V. I.; Simenel, I. A.; Kulakova, V. K.; Kurskaya, E. A.; Babushkina, T. A.; Klimova, T. P.; Burova, T. V.; Dubovik, A. S.; Galaev, I. Y.; Mattiasson, B.; Khokhlov, A. R. *Macromolecules* **2003**, *36*, 7308-7323.
(141) Okhapkin, I. M.; Bronstein, L. M.; Makhaeva, E. E.; Matveeva, V. G.; Sulman, E. M.; Sulman, M. G.; Khokhlov, A. R. *Macromolecules* **2004**, *37*, 7879-7883.
(142) Ge, Z.; Xie, D.; Chen, D.; Jiang, X.; Zhang, Y.; Liu, H.; Liu, S. *Macromolecules* **2007**, *40*, 3538-3546.
(143) Soll, S.; Antonietti, M.; Yuan, J. *ACS Macro Lett.* **2012**, *1*, 84-87.
(144) Lu, J.; Yan, F.; Texter, J. *Prog. Polym. Sci.* **2009**, *34*, 431-448.
(145) Armand, M.; Endres, F.; MacFarlane, D. R.; Ohno, H.; Scrosati, B. *Nat Mater* **2009**, *8*, 621-629.
(146) Salamone, J. C.; Israel, S. C.; Taylor, P.; Snider, B. *Polymer* **1973**, *14*, 639-44.
(147) Hoover, M. F. *Journal of Macromolecular Science: Part A - Chemistry* **1970**, *4*, 1327-1418.
(148) Marcilla, R.; Blazquez, J. A.; Rodriguez, J.; Pomposo, J. A.; Mecerreyes, D. *J. Polym. Sci., Part A: Polym. Chem.* **2003**, *42*, 208-212.
(149) Azaceta, E.; Marcilla, R.; Sanchez-Diaz, A.; Palomares, E.; Mecerreyes, D. *Electrochim. Acta* **2010**, *56*, 42-46.
(150) Dickmeis, M.; Ritter, H. *Macromol. Chem. Phys.* **2009**, *210*, 776-782.

(151) Amajjahe, S.; Ritter, H. *Macromol. Rapid Commun.* **2009**, *30*, 94-98.
(152) Salamone, J. C.; Volksen, W.; Israel, S. C.; Olson, A. P.; Raia, D. C. *Polymer* **1977**, *18*, 1058-62.
(153) Evsyukov, S. E.; Gautheron, F.; Hoffken, H. W.; Bohn, K. *J. Appl. Polym. Sci.* **2001**, *82*, 499-509.
(154) Yoshizawa, M.; Ogihara, W.; Ohno, H. *Polym. Adv. Technol.* **2002**, *13*, 589-594.
(155) Green, M. D.; Salas-de, l. C. D.; Ye, Y.; Layman, J. M.; Elabd, Y. A.; Winey, K. I.; Long, T. E. *Macromol. Chem. Phys.* **2011**, *212*, 2522-2528.
(156) Salas-de, l. C. D.; Green, M. D.; Ye, Y.; Elabd, Y. A.; Long, T. E.; Winey, K. I. *J. Polym. Sci., Part B: Polym. Phys.* **2012**, *50*, 338-346.
(157) Nakamura, K.; Fukao, K.; Inoue, T. *Macromolecules (Washington, DC, U. S.)* **2012**, *45*, 3850-3858.
(158) Nakamura, K.; Saiwaki, T.; Fukao, K.; Inoue, T. *Macromolecules* **2011**, *44*, 7719-7726.
(159) Nakamura, K.; Saiwaki, T.; Fukao, K. *Macromolecules (Washington, DC, U. S.)* **2010**, *43*, 6092-6098.
(160) Zheng, Y.; Zheng, J.; Dou, L.; Qiao, W.; Wan, X. *J. Mater. Chem.* **2009**, *19*, 8470-8477.
(161) Lee, S.; Becht, G. A.; Lee, B.; Burns, C. T.; Firestone, M. A. *Adv. Funct. Mater.* **2010**, *20*, 2063-2070.
(162) Paraknowitsch, J. P.; Zhang, J.; Su, D.; Thomas, A.; Antonietti, M. *Adv. Mater.* **2010**, *22*, 87-92.
(163) Yuan, J.; Giordano, C.; Antonietti, M. *Chem. Mater.* **2010**, *22*, 5003-5012.
(164) Yuan, J.; MÃ¡rquez, A. G.; Reinacher, J.; Giordano, C.; Janek, J.; Antonietti, M. *Polymer Chemistry* **2011**.
(165) Koebe, M.; Drechsler, M.; Weber, J.; Yuan, J. *Macromol. Rapid Commun.* **2012**, *33*, 646-651.
(166) Yuan, J.; Soll, S.; Drechsler, M.; Müller, A. H. E.; Antonietti, M. *J. Am. Chem. Soc.* **2011**, *133*, 17556-17559.
(167) Yuan, J.; Antonietti, M. *Macromolecules (Washington, DC, U. S.)* **2011**, *44*, 744-750.
(168) Luo, S.-C.; Sun, S.; Deorukhkar, A. R.; Lu, J.-T.; Bhattacharyya, A.; Lin, I. J. B. *J. Mater. Chem.* **2011**, *21*, 1866-1873.
(169) Carr, L.; Cheng, G.; Xue, H.; Jiang, S. *Langmuir* **2010**, *26*, 14793-14798.
(170) Midoux, P.; Pichon, C.; Yaouanc, J.-J.; Jaffrès, P.-A. *British Journal of Pharmacology* **2009**, *157*, 166-178.
(171) Midoux, P.; Monsigny, M. *Bioconjugate Chem.* **1999**, *10*, 406-411.
(172) Asayama, S.; Akaike, T.; Maruyama, A. *Colloids Surf., B* **2001**, *22*, 183-191.
(173) Asayama, S.; Hakamatani, T.; Kawakami, H. *Bioconjugate Chem.* **2010**, *21*, 646-652.
(174) Asayama, S.; Sekine, T.; Kawakami, H.; Nagaoka, S. *Bioconjugate Chem.* **2007**, *18*, 1662-1667.
(175) Bamford, C. H.; Schofield, E. *Polymer* **1981**, *22*, 1227-35.
(176) Dambatta, B. B.; Ebdon, J. R. *Eur. Polym. J.* **1986**, *22*, 783-6.
(177) Yamago, S.; Ukai, Y.; Matsumoto, A.; Nakamura, Y. *J. Am. Chem. Soc.* **2009**, *131*, 2100-2101.
(178) Mori, H.; Yahagi, M.; Endo, T. *Macromolecules* **2009**, *42*, 8082-8092.
(179) Yuan, J.; Schlaad, H.; Giordano, C.; Antonietti, M. *Eur. Polym. J.* **2011**, *47*, 772-781.
(180) Detrembleur, C.; Debuigne, A.; Hurtgen, M.; Jérôme, C.; Pinaud, J.; Fèvre, M. v.; Coupillaud, P.; Vignolle, J.; Taton, D. *Macromolecules* **2011**, *44*, 6397-6404.

(181) Hirsch, A.; Richardson, K. *Journal of Applied Chemistry* **1969**, *19*, 83-85.
(182) Kokosa, J. M.; Szafasz, R. A.; Tagupa, E. *The Journal of Organic Chemistry* **1983**, *48*, 3605-3607.
(183) Overberger, C. G.; Pierre, T. S.; Vorchheimer, N.; Yaroslavsky, S. *J. Am. Chem. Soc.* **1963**, *85*, 3513-3515.
(184) Overberger, C. G.; Salamone, J. C.; Yaroslavsky, S. *J. Am. Chem. Soc.* **1967**, *89*, 6231-6236.
(185) Overberger, C. G.; Salamone, J. C. *Acc. Chem. Res.* **1969**, *2*, 217-224.
(186) Overberger, C. G.; Maki, H. *Macromolecules* **1970**, *3*, 220-223.
(187) Overberger, C. G.; Maki, H. *Macromolecules* **1970**, *3*, 214-220.
(188) Okamoto, Y.; Overberger, C. *Journal of Polymer Science Part Aâ€•1: Polymer Chemistry* **1972**, *10*, 3387-3395.
(189) Overberger, C. G.; Kawakami, Y. *Journal of Polymer Science: Polymer Chemistry Edition* **1978**, *16*, 1237-1248.
(190) Overberger, C. G.; Smith, T. W. *Macromolecules* **1975**, *8*, 416-424.
(191) Overberger, C. G.; Smith, T. W. *Macromolecules* **1975**, *8*, 401-406.
(192) Overberger, C. G.; Smith, T. W. *Macromolecules* **1975**, *8*, 407-415.
(193) Schiavone, R.; Overberger, C. *J. Polym. Sci., Part A: Polym. Chem.* **1988**, *26*, 107-115.
(194) Kunitake, T.; Okahata, Y. *J. Am. Chem. Soc.* **1976**, *98*, 7793-7799.
(195) Meng, Z.; Sode, K. *Journal of Molecular Recognition* **2005**, *18*, 262-266.
(196) Morawetz, H.; Song, W. *J. Am. Chem. Soc.* **1966**, *88*, 5714-5718.
(197) Ribeiro, A.; Veiga, F.; Santos, D.; Torres-Labandeira, J. J.; Concheiro, A.; Alvarez-Lorenzo, C. *Biomacromolecules* **2011**, *12*, 701-709.
(198) Ribeiro, A.; Veiga, F.; Santos, D.; Torres-Labandeira, J. J.; Concheiro, A.; Alvarez-Lorenzo, C. *J. Membr. Sci.* **2011**, *383*, 60-69.
(199) Doğan, Ö.; Öner, M. *Langmuir* **2006**, *22*, 9671-9675.
(200) Ihm, J. E.; Han, K.-O.; Hwang, C. S.; Kang, J. H.; Ahn, K.-D.; Han, I.-K.; Han, D. K.; Hubbell, J. A.; Cho, C.-S. *Acta Biomaterialia* **2005**, *1*, 165-172.
(201) Ihm, J.-E.; Han, K.-O.; Han, I.-K.; Ahn, K.-D.; Han, D.-K.; Cho, C.-S. *Bioconjugate Chem.* **2003**, *14*, 707-708.
(202) Pu, H.; Meyer, W. H.; Wegner, G. *Macromol. Chem. Phys.* **2001**, *202*, 1478-1482.
(203) Bozkurt, A.; Meyer, W. H. *Solid State Ionics* **2001**, *138*, 259-265.
(204) Bozkurt, A.; Meyer, W. H.; Gutmann, J.; Wegner, G. *Solid State Ionics* **2003**, *164*, 169-176.
(205) Sezgin, A.; Akbey, Ü.; Graf, R.; Bozkurt, A.; Baykal, A. *J. Polym. Sci., Part B: Polym. Phys.* **2009**, *47*, 1267-1274.
(206) Bozkurt, A.; Karadedeli, B. *React. Funct. Polym.* **2007**, *67*, 348-354.
(207) Allen, M. H.; Hemp, S. T.; Smith, A. E.; Long, T. E. *Macromolecules* **2012**, *45*, 3669-3676.
(208) Lawson Jr, J. K. *J. Am. Chem. Soc.* **1953**, *75*, 3398-3400.
(209) Lando, J.; Litt, M.; Shimko, T.; Kumar, N. *Polymer Engineering & Science* **1976**, *16*, 361-364.

Chapter 4: Tailoring Charge Density and Hydrogen Bonding of Imidazolium Copolymers for Efficient Gene Delivery

(Published in *Biomacromolecules* **2011**, *12*, 2243-2250.)

Michael H. Allen, Jr., Matthew D. Green,[‡] Hiwote K. Getaneh,[§] Kevin M. Miller,[⊥] and Timothy E. Long

Departments of Chemistry and Macromolecules and Interfaces Institute, Chemical Engineering,[‡] and Biochemistry,[§] Virginia Tech, Blacksburg, VA 24061

[⊥]Department of Chemistry, Murray State University, Murray, KY 42071

4.1 *Abstract*

Conventional free radical polymerization with subsequent post-polymerization modification afforded imidazolium copolymers with controlled charge density and side chain hydroxyl number. Novel imidazolium-containing copolymers where each permanent cation contained one or two adjacent hydroxyls allowed precise structure-transfection efficiency studies. The degree of polymerization was identical for all copolymers to eliminate the influence of molecular weight on transfection efficiency. DNA binding, cytotoxicity, and *in vitro* gene transfection in African green monkey COS-7 cells revealed structure-property-transfection relationships for the copolymers. DNA gel shift assays indicated that higher charge densities and hydroxyl concentrations increased DNA binding. As the charge density of the copolymers increased, toxicity of the copolymers also increased; however, as hydroxyl concentration increased, cytotoxicity remained constant. Changing both charge density and hydroxyl levels in a systematic fashion revealed a dramatic influence on transfection efficiency. Dynamic light scattering of the polyplexes, which were composed of copolymer concentrations required for the highest luciferase expression, showed an intermediate DNA-copolymer binding affinity. Our studies supported the conclusion that cationic copolymer binding affinity significantly impacts overall transfection efficiency of DNA delivery vehicles, and the incorporation of hydroxyl sites offers a less toxic and effective alternative to more conventional highly charged copolymers.

4.2 *Introduction*

Nonviral gene therapy is currently an area of intense research focus due to its growth as a potential treatment for numerous human diseases.[1,2] Although viral gene therapies are highly effective, deleterious immunogenic response and limited DNA loading capacity are common.[3,4] Nonviral delivery agents such as cationic polyelectrolytes offer a suppressed immunogenic risk and the opportunity to tailor macromolecular design.[5,6] Controlled free radical polymerization techniques afford strategies for the design of various macromolecular architectures with precise molecular weights and narrow polydispersity.[7] However, nonviral delivery agents need to overcome many obstacles that limit the efficiency of these therapeutics, including cellular uptake, endosomal escape, and delivery of the genetic cargo into the nucleus.[8,9] The cationic polymer must also sufficiently compact DNA to effectively inhibit cellular, enzymatic degradation. Long et al.[10] found that increasing poly(2-(dimethylamino)ethyl methacrylate) (PDMAEMA) molecular weight increased plasmid DNA (pDNA) binding affinity, leading to reduced enzymatic degradation and consequently increased luciferase reporter expression. Additional cationic polyelectrolytes for nonviral gene therapy include poly(L-lysine),[11,12] poly(ethyleneimine) (PEI),[13,14] poly(amido amine) dendrimers,[15-17] and step-growth polymers such as cationic polysaccharides[18-20] and ionenes.[21]

Cationic polymers electrostatically bind and condense anionic pDNA forming a polyplex. Various factors including molecular weight,[10,22] charge density,[23] and hydrogen bonding[24] impact polyplex stability. Rungsardthong et al.[25] observed a greater polyplex binding affinity and smaller more compact polyplexes as the degree of ionization in PDMAEMA samples increased with varying pH; however, the authors did not report the impact on transfection efficiency. Anderson et al.[26] later reported that polymers with tightly bound or encapsulated pDNA prevented pDNA release, and loosely bound pDNA degraded. They concluded that both factors

lowered transfection efficiency. Lauffenburger et al.[27] showed as molecular weight of poly(L-lysine) increased above a critical value, the transfection efficiency decreased due to limited pDNA-vector unpacking. This is in contrast to Long et al.,[10] but points to the importance of composition on the transfection efficiency as a function of molecular weight.

Polymers containing histidine or imidazole are known to enhance gene expression compared to unmodified polymers.[23,28-30] Histidine-rich peptide antibiotics also enable efficient DNA delivery properties in mammalian cells.[31,32] Peptides including LAH4 and Tat peptides functionalized with histidine units displayed high pDNA delivery efficiencies.[33,34] Midoux and coworkers[35] prepared histidylated poly(L-lysine) and found the incorporation of histidine residues increased transfection 3-4 orders-of-magnitude compared to poly(L-lysine). In contrast, Benns et al.[36] incorporated histidine onto poly(L-lysine) using a grafting approach. They also found an increase of transfection compared to the poly(L-lysine) homopolymer. Poly(L-lysine) dendrimers showed increased transfection when substituted with histidine-rich residues at the terminal sites of the dendrimer.[37] Langer et al.[38] employed a high-throughput technique to synthesize a library of poly(β-amino esters) to study the influence of polymer structure on transfection efficiency. They found that polymeric composition with alcohol or imidazole functionalities resulted in the highest luciferase expression. Langer invoked the proton sponge hypothesis to explain the improvement in DNA delivery. The pKa of the conjugate acid of the imidazole tertiary nitrogen is ~6, suggesting a buffering capacity near endosomal pH.[39] According to the proton sponge hypothesis, the polyelectrolyte is further protonatable inside the acidic endosome leading to endosomal swelling and rupture.

We report herein novel, pH-sensitive, imidazolium copolymers and our studies demonstrate the potential synergy of charge density and hydrogen bonding on transfection

efficiency. 1-vinylimidazole homopolymers require subsequent alkylation to create a water-soluble, cationic polyelectrolyte capable of binding anionic pDNA. Imidazoles upon functionalization provide the permanent cationic imidazolium site; however, the ring loses the ability to hydrogen bond.[40] Alkylation with hydroxyl-containing groups ensures adjacent hydrogen bonding sites in a controlled fashion. Reineke et al.[24] showed a combination of electrostatic interactions and hydrogen bonding enhanced the association between the polymer and DNA. They suggested that the incorporation of hydrogen bonding sites allowed for the design of less-toxic polymers due to a reduction in cytotoxic cationic charge that is necessary to effectively interact with pDNA. However, Reineke studied low molecular weight polymers (degree of polymerization $\leq$ 15) and they concluded that pDNA-polymer interactions increased in the presence of hydroxyl groups and binding was *independent* of hydroxyl concentration. Reineke and co-workers[41,42] also showed the addition of hydroxyl groups improved transfection efficiency, but they did not report a systematic change in pDNA delivery with increasing hydroxyl concentration. Reineke further determined hydroxyl stereochemistry effectively controlled pDNA–polymer binding affinity in their carbohydrate-based polymers.

In this work, we tailored charge density and hydroxyl concentration through functionalization of 1-vinylimidazole homopolymers of relatively high molecular weight. All polymeric precursors had an equivalent degree of polymerization to eliminate molecular weight influences on transfection efficiency. Hydroxyl incorporation precisely ranged between zero to two per cationic charge to reveal the influence of hydroxyl incorporation in the absence of significant molecular weight differences. We evaluated the influence of charge density and hydroxyl incorporation on DNA binding, cytotoxicity, and *in vitro* DNA delivery.

4.3 *Experimental Section*

4.3.1 General Methods and Materials

1-vinylimidazole was distilled under reduced pressure (VIM, 99%, Aldrich). 2,2'-Azobisisobutyronitrile (AIBN, 99%, Sigma-Aldrich) was recrystallized from methanol. Bromoethane (99%, Sigma-Alrich), 2-bromoethanol (95%, Aldrich), and 3-bromo-1,2-propanediol (97%, Aldrich) were used as received. Deuterium oxide (D_2O, 99.9% Cambridge Isotope Laboratories) was used as received for ^1H NMR spectroscopy. A Millipore Direct-Q5 purification system produced ultrapure water having a resistivity of 18.2 MΩ·cm. All other solvents and reagents were used as received from commercial sources without further purification unless specifically noted elsewhere. ^1H NMR spectra were obtained using a Varian Unity 400 MHz spectrometer.

4.3.2 Synthesis of Poly(1-Vinylimidazole) and Imidazolium Copolymers

In a typical polymerization, VIM was charged with 0.5 mol % AIBN in DMF at 20 wt % solids in a 100- mL round-bottomed flask with a magnetic stir bar. The reaction mixture was sparged with nitrogen for 30 min and submerged in a preheated oil bath at 65 °C. After 24 h, the polymer was precipitated into ethyl acetate, redissolved in methanol, and precipitated a second time into ethyl acetate to remove any residual DMF. The polymer was dried under vacuum at 40 °C for 24 h to constant weight. The molecular weight of the homopolymer was measured using size exclusion chromatography (SEC) (flow rate of 0.8 mL/min through 2x Waters Ultrahydrogel Linear and 1x Waters Ultrahydrogel 250 columns, solvent: 28.5 / 71.5 EtOH/H_2O (v/v %) 0.017 M Tris / 0.05 M HCl pH = 2; standards: PEO).

Upon drying, various extents of quaternization of poly(1-hydroxyethyl-3-vinylimidazolium bromide-*co*-1-vinylimidazole) (PHEVIM) were synthesized. In a typical reaction, various equivalents of 2-bromoethanol were charged into a 25 mL, round-bottomed,

flask containing poly(1-vinylimidazole) (PVIM) (0.500 g) dissolved in methanol at 25 wt % solids. The reaction was refluxed at 75 °C for 24 h to obtain different quaternization percentages. The copolymer was precipitated into ethyl acetate and dried under reduced pressure at 40 °C for 24 h. The synthesis of poly(1-ethyl-3-vinylimidazolium bromide-*co*-1-vinylimidazole) (PEVIM) and poly(1-(1,2-propanediol)-3-vinylimidazolium bromide-*co*-1-vinylimidazole) (PDHVIM) followed the procedure described above (**Error! Reference source not found.**, Table 4.1).

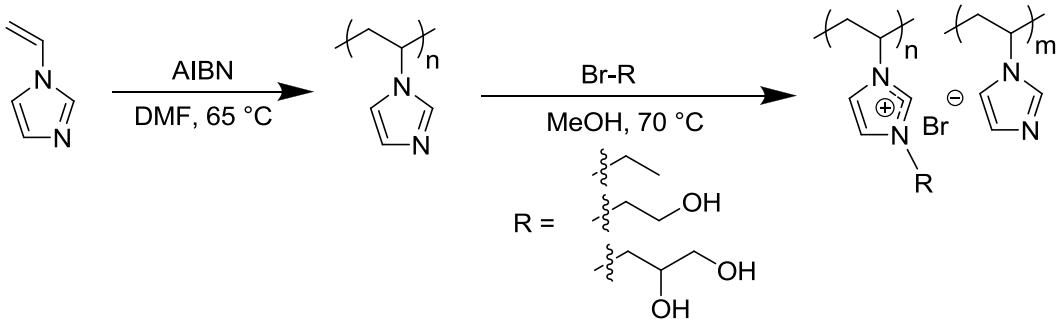

Scheme 4.1. Post-polymerization quaternization of poly(1-vinylimidazole) for the synthesis of imidazolium-containing copolymers.

Table 4.1. Polymers discussed in this paper.

Abbreviation	Substituent	Quaternization (%)
PVIM	None	0
$PHEVIM_{13}$		13
$PHEVIM_{25}$		25
$PHEVIM_{50}$	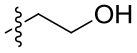	50
$PHEVIM_{65}$		65
$PHEVIM_{100}$		100
$PEVIM_{25}$		25
$PDHVIM_{25}$	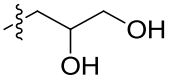	25

The degree of quaternization was determined using ^{1}H NMR. All samples were dialyzed against ultrapure water for 48 h using Spectra/Por® dialysis tubing (MWCO 3500 g/mol). Lyophilization was used to recover samples prior to characterization.

4.3.3 Acid-Base Titration

Copolymer samples were dissolved in dH_2O at a concentration of 0.010 M. The solutions were brought to an initial pH of 11.0 using a concentrated NaOH solution with a negligible change to the copolymer solution volume. The samples were then titrated with a standardized 2.0 M HCl solution until the solution reached a pH of 3.0, and the pH of the solution recorded using an Orion 3-Star plus pH portable meter (Thermo).

4.3.4 DNA Gel Shift Assay

Polyplexes were prepared using 0.20 μL of gWiz-Luc plasmid (1 μg/μL in H_2O, Aldevron) in ~28 μL of 1X Tris-acetate-EDTA (TAE, Sigma) buffer. Various amounts of copolymer were added to the DNA solutions targeting nitrogen/phosphorous (N/P) ratios from 1-14. Upon addition of copolymer to the DNA solutions, the solutions were incubated at room temperature for 30 min to allow for polyplex formation. After 30 min, 7 μL of gel loading buffer (Sigma) was added to each solution. The solutions were added to a 0.9 wt % agarose gel containing SYBR Green I (Sigma). Gel electrophoresis occurred at 70 V for 90 min in 1X TAE buffer. The gels were imaged using a MultiDoc-it™ Digital Imaging System (UVP).

4.3.5 Heparin Competitive Binding Assay

Polyplexes were prepared using 0.20 μL of gWiz-Luc plasmid (1 μg/μL in H_2O) in ~28 μL of 1X Tris-acetate-EDTA (TAE, Sigma) buffer. Copolymer was added to the DNA solutions targeting an N/P ratio of 20. After a 30 min incubation at room temperature, the polyplexes were challenged with 0.01 – 0.40 (U) of heparin which corresponded to 0.05-2.0 U/μg of DNA. The polyplex-heparin solution was incubated for 30 min at room temperature and 7 μL of gel loading buffer was subsequently added to each solution. The solutions were added to a 0.9 wt % agarose gel containing SYBR Green I. Gel electrophoresis occurred at 70 V for 90 min in 1X TAE buffer. The gels were imaged using a MultiDoc-it™ Digital Imaging System (UVP).

4.3.6 Cell Culture

African green monkey COS-7 cells were cultured in Dulbecco's modified Eagle's medium (DMEM) containing 10% fetal bovine serum (FBS), 100 U/mL of penicillin and 100 μg/mL of streptomycin (all reagents from Mediatech). Cells were incubated at 37 °C with 5% CO_2 in a 95% humid atmosphere.

4.3.7 Cell Viability Assay

Copolymer cytotoxicity was determined using the 3-[4,5-dimethylthiazol-2-yl]2,5-diphenyltetrazolium bromide (MTT, Sigma-Aldrich) conversion assay. Copolymer samples were dissolved in ultrapure water at a concentration of 1 mg/mL. The copolymer stock solution was diluted with DMEM to obtain copolymer solutions ranging in concentration from 1-200 μg/mL. The samples were added to a 96-well plate containing COS-7 cells seeded at a density of 5000 cells/well. COS-7 cells were plated 24 h prior to the experiment. After the 24 h incubation, the cells were rinsed with 100 μL of DMEM followed by the addition of 100 μL of the diluted copolymer solutions. After 24 h, the solutions were aspirated and cells were rinsed with 100 μL of 1X Hank's buffered salt solution (HBSS). For 4 h at 37 °C, the cells were treated with 100 μL of a 0.5 mg/mL MTT solution in DMEM, and the media was subsequently aspirated and the formazan product dissolved with DMSO. A SPECTRAmax M2 microplate reader (Molecular Devices Corp.) was used to measure the absorbance at 570 nm for each well.

4.3.8 Luciferase Expression Assay

To prepare the polyplex solutions, gWiz-Luc plasmid (1 μg/μL in H_2O) was diluted in DMEM and serum-containing DMEM to a concentration of 1.2 μg/mL and concurrently copolymer solutions were diluted at various concentrations in DMEM and serum-containing DMEM corresponding to the targeted N/P ratios. Upon 10 min of incubation, equal volumes of the solutions were combined (final gWiz-Luc concentration of 0.6 μg/mL) and incubated for 30

min at room temperature. COS-7 cells were plated on 24-well plates at a density of 1.0 X 10^5 cells/well 24 h prior to the experiment. The cells were then rinsed with 1X HBSS and treated with 500 μL of the transfection solution. After a 4 h incubation at 37 °C with 5% CO_2, the transfection solution was aspirated and replaced with complete DMEM and incubated for 48 h at 37 °C with 5% CO_2 to allow for protein expression. Cells were rinsed with 500 μL of PBS and 125 μL of lysis buffer was added to each well. The cells were scraped and after a 30 min incubation at room temperature the lysate was subjected to a -80 °C/37 °C freeze-thaw cycle. Luciferase activity was measured following the instructions for the SPECTRAmax L luminometer (Molecular Devices Corp.) and the luciferase assay kit (Promega). Protein concentration was determined using a DC protein assay kit (Bio-Rad Laboratories). Gene expression was reported as relative light units per milligram of cell protein lysate (RLU/mg). Experiments were repeated twice with samples collected in quadruplicate.

4.3.9 Wide-Field Fluorescence Optical Microscopy

Polyplexes were prepared for cellular uptake experiments with Cy5-labeled gWiz-Luc plasmid (0.1 μg/μL in H_2O). The pDNA solution was diluted with DMEM to a concentration of 2.0 μg/mL and combined with a corresponding copolymer-DMEM solution to produce polyplexes with an N/P ratio corresponding to the highest transfection efficiency as determined with the luciferase expression assay. After a 30 min incubation, the solutions were applied to COS-7 cells plated at a concentration of 1.0 X 10^5 cells/well on a 24 well plate and subsequently incubated for an additional 30 min at 37 °C, 5% CO_2. 1 μL of 4',6-diamidino-2-phenylindole (DAPI, 1 μg/μL in PBS) was added to the transfection media, and the cells were incubated for an additional 30 min at 37 °C, 5% CO_2. The cells were then rinsed twice with PBS and fixed with paraformaldehyde (2 wt % in PBS, Sigma). In addition, membranes were permeabilized with

TritonX-100 (0.1 vol % in PBS, Sigma), washed with PBS, and F-actin filaments were stained with Alexa Fluor phalloidin 488 (5 U/mL in PBS, Invitrogen). The fixed cells were imaged using a Nikon Eclipse TE2000-U inverted microscope with a Nikon C-HGFI Intensilight epifluorescence system and Nikon DS-Qi,Mc BW CCD digital camera. The multichannel fluorescence images were acquired using UV-2EC, Cy5, and F/EGFP filters.

4.3.10 Dynamic Light Scattering (DLS)

Copolymer and gWiz-Luc plasmid were diluted in separate DMEM solutions. After 10 min, the copolymer solution was added to the gWiz-Luc plasmid solution and allowed to incubate for 30 min at 25 °C. Varying copolymer concentrations produced a range of N/P ratios (final DNA concentration of 1 μg/mL), and all experiments were performed in triplicate at 25 °C. Size and zeta-potential of the polyplexes were determined with a Zetasizer Nano Series Nano-ZS (Malvern) instrument equipped with a 4.0 mW He-Ne laser at a scattering angle of 173° producing a wavelength of 633 nm. All polyplexes displayed monomodal hydrodynamic diameters, and data was analyzed using Dispersion Technology Software (DTS) version 6.12.

4.4 *Results and Discussion*

Free radical polymerization afforded PVIM with a number-average molecular weight (M_n) of 23,000 g/mol with a PDI of 1.89 relative to poly(ethylene oxide) standards using size exclusion chromatography. DLS confirmed that the aqueous mobile phase eliminated the presence of large scale aggregates. The synthesis of a PVIM homopolymer precursor eliminated the influence of the degree of polymerization on subsequent transfection experiments.[10,43] Controlled stoichiometries of 2-bromoethanol provided a series of quaternized copolymers ($PHEVIM_x$; x = mol % charge) with varying amounts of charge. ^{1}H NMR spectroscopy verified the chemical structure of the copolymers and determined the extent of quaternization. Acid-base

titration also qualitatively verified the extent of quaternization of the PHEVIM copolymers and found a pKa of approximately 5.5 for PVIM (Figure 4.1).

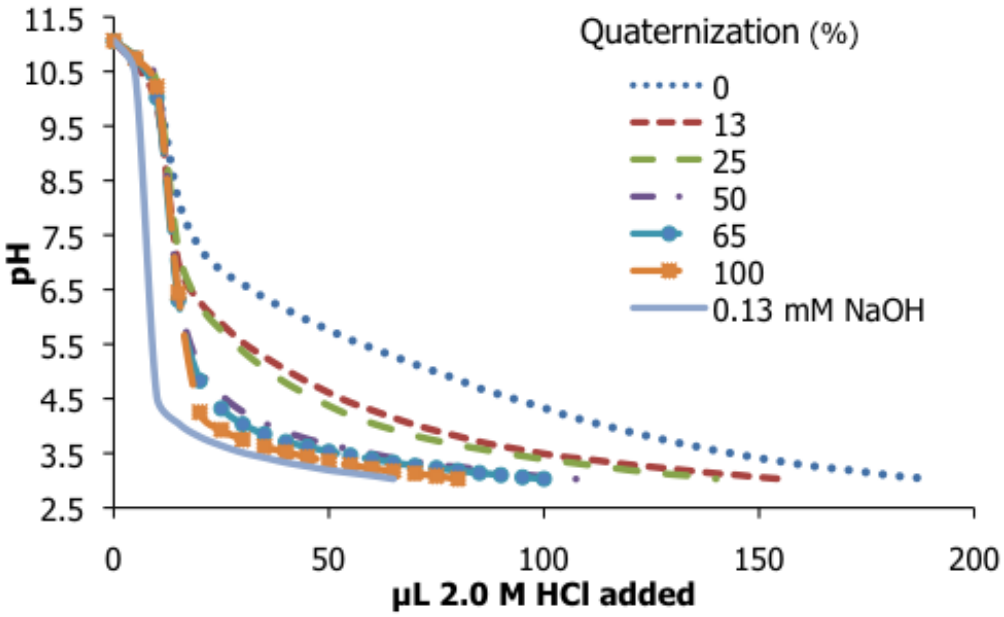

Figure 4.1. Acid-base titration to determine buffering capacity of PHEVIM copolymers.

As quaternization increased in the copolymer, fewer sites were available for protonation, and upon titration from basic to acidic solutions, the buffering capacity of the copolymer decreased. As expected, the fully quaternized copolymer did not buffer an aqueous solution and behaved similar to a strong acid / strong base titration.

DNA binding assays further confirmed quaternization differences between PHEVIM copolymers, and these assays also determined the molar ratio of copolymer necessary to effectively bind pDNA. As shown in Figure 4.2, as the quaternization level increased, the N/P ratio for $PHEVIM_x$ copolymer-pDNA complexation decreased. Water-soluble PVIM did not bind pDNA at a physiological pH due to the absence of charge. The results clearly showed that

an increase in the charge density of the copolymer required less copolymer to bind the negatively charged pDNA.

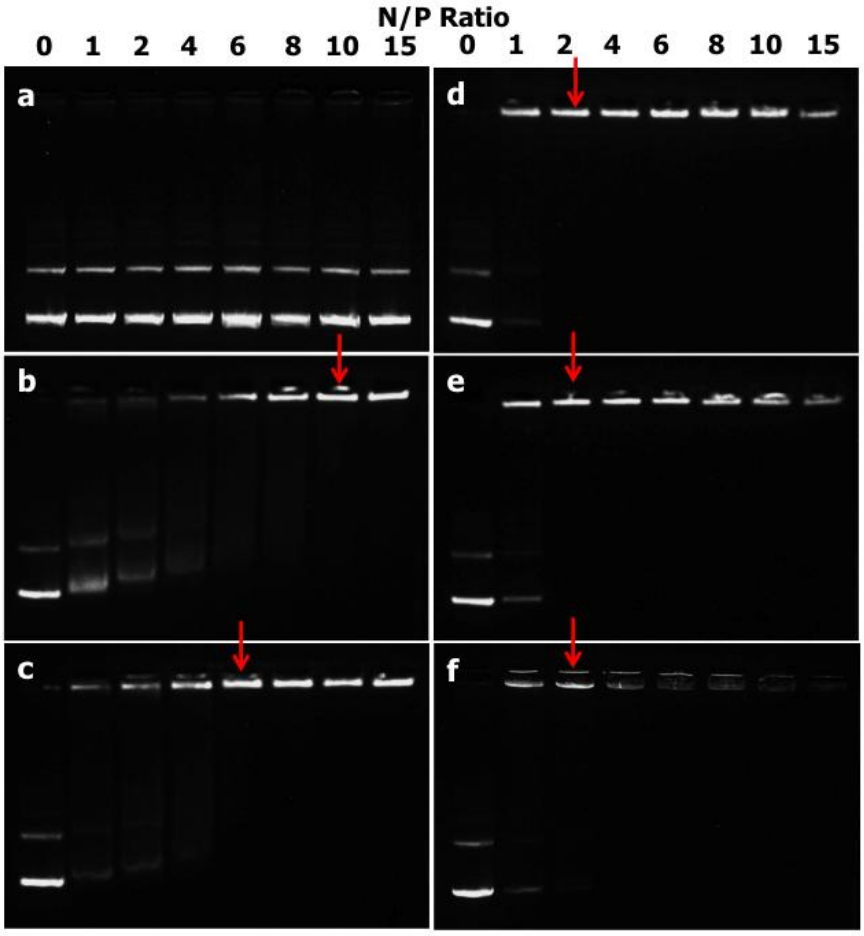

Figure 4.2. Electrophoretic gel shift assay of PHEVIM copolymers at various quaternization percentages to determine copolymer-pDNA complexation: a (0%), b (13%) c (25%), d (50%), e (65%), f (100%). Arrows indicate N/P ratio necessary for complete DNA binding.

The MTT conversion assay determined cytotoxicity of the PHEVIM copolymers. Figure 4.3a shows the influence of quaternization percentage and copolymer concentration on COS-7 cell viability. As the extent of quaternization of the copolymer increased, the cytotoxicity of the copolymer sample increased. $PHEVIM_{25}$ and $PHEVIM_{13}$ did not display cytotoxicity even at high copolymer concentrations (~200 μg/mL). Kissel et al.[44] determined that a higher

concentration of cationic charge on a polymer leads to greater cytotoxicity. Figure 4.3b shows the effect of polyplexes on COS-7 cell viability.

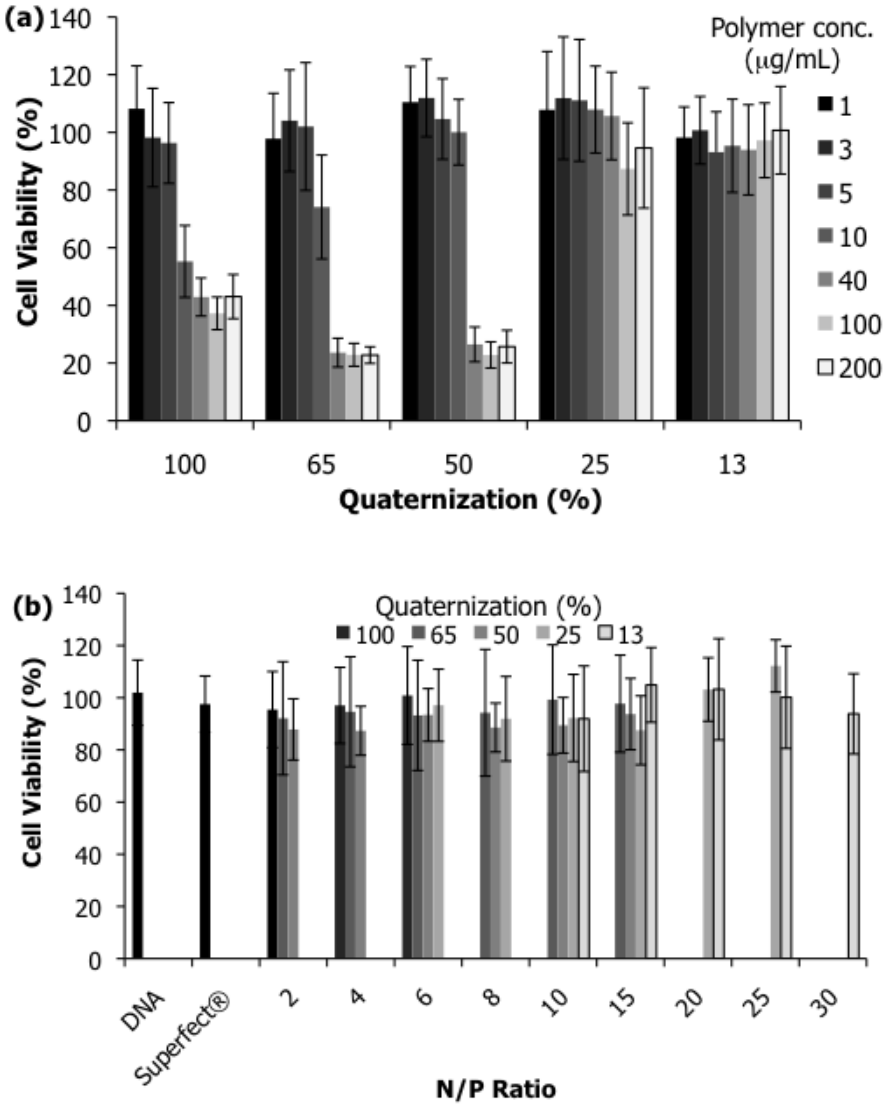

Figure 4.3. COS-7 cell viability as a function of (a) quaternization percentage at various copolymer concentrations and (b) polyplex N/P ratios. Values represent mean ± SD (n = 8).

The selected N/P ratios were optimized according to the transfection experiments. All N/P ratios of the copolymers and Superfect® concentration evaluated were non-toxic. This ensured that the polyplexes for our *in vitro* luciferase expression assay were at non-toxic concentrations.

The luciferase expression assay evaluated the influence of charge density of PHEVIM$_x$ copolymers on *in vitro* pDNA delivery. Factors that influence gene expression include the stability of the copolymer-pDNA complex,[45] and if the complex is not stable, premature dissociation will occur in the transfection process resulting in minimal transgene expression. In addition, highly stable complexes will not release pDNA also resulting in low expression.[46] Thus, it is necessary to balance the copolymer-pDNA binding affinity to achieve maximum transfection efficiency. We investigated various quaternization percentages over a range of N/P ratios, and the initial N/P ratios for each quaternization percentage corresponded to the onset of stable polyplex formation as determined using the DNA gel shift assay. MTT cytotoxicity results determined the non-toxic N/P ratios used for the luciferase expression assay. Figure 4.4 shows luciferase expression as a function of charge density and N/P ratio in (a) serum-free media and (b) serum-containing media in comparison to Superfect®.

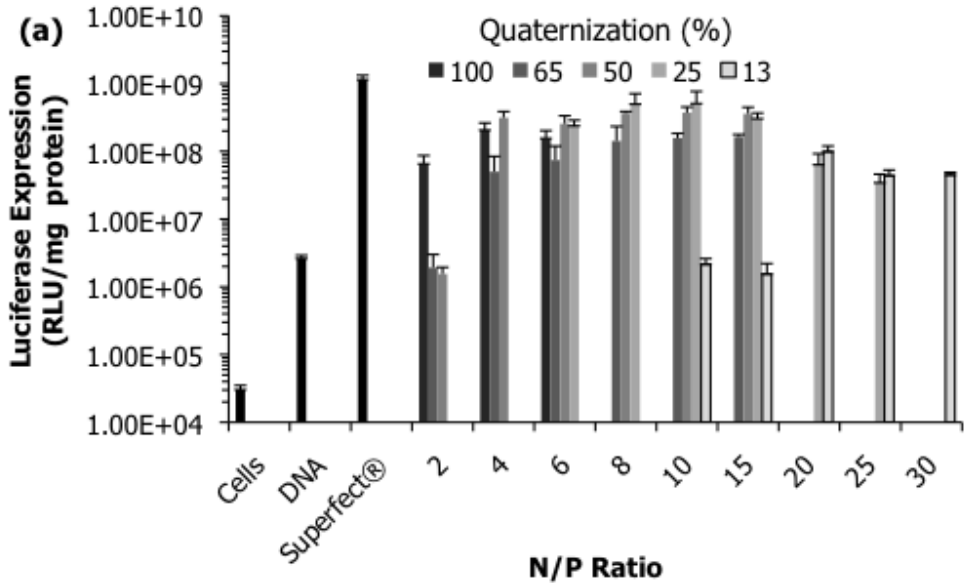

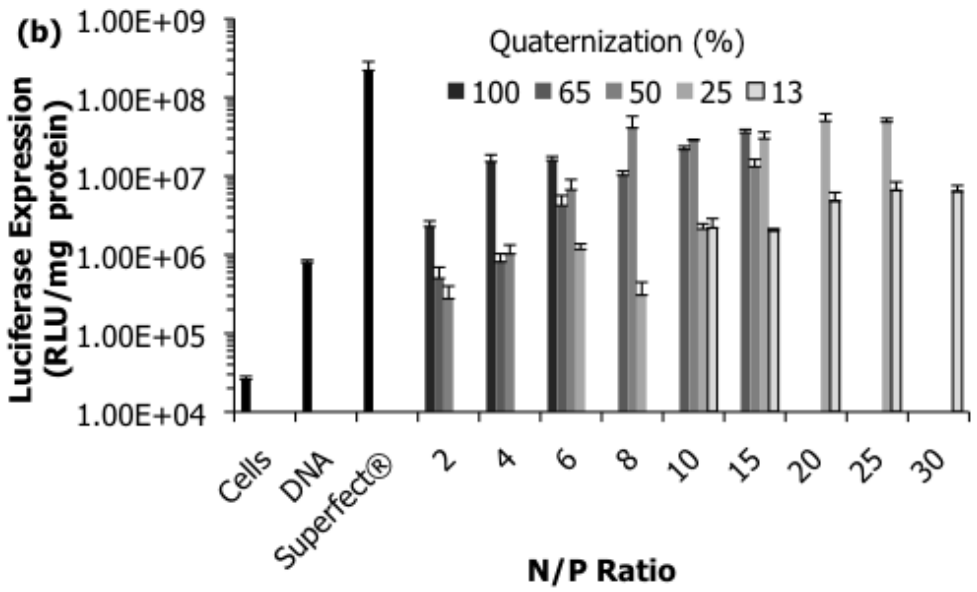

Figure 4.4. In vitro gene transfection efficiency as a function of N/P ratio at various charge densities in COS-7 cells in (a) serum-free and (b) serum-containing media. Non-toxic N/P ratios chosen for luciferase transfection. Values represent mean $\pm$ SD (n = 4).

The optimal N/P ratios for DNA delivery in serum-free (or serum) for $PHEVIM_{13}$, $PHEVIM_{25}$, $PHEVIM_{50}$, $PHEVIM_{65}$, and $PHEVIM_{100}$ were 20 (or 30), 8 (or 20), 8 (or 10-15), 8 (or 10-15), and 4 (or 4-6) respectively. Increased polyplex stability, as a result of increased positive charge on the copolymer, decreased the optimal N/P ratio for DNA delivery. For transfection in serum-free media, all charged copolymers were less than an order-of-magnitude lower than Superfect® and two-orders-of-magnitude higher than naked DNA, which we attributed to protein aggregation with the copolymers.[47] We observed a five-fold increase in maximum luciferase expression as the charge density of the PHEVIM copolymer increased from 13% to 25% attributed to increased polyplex stability. As charge density increased further, the maximum transfection efficiency, which we defined as the maximum RLU/mg for each quaternization percentage regardless of N/P ratio, decreased slightly since the complexes did not release DNA effectively. Our findings agreed well with previously published work by Zhou et

al.[43] Zhou et al. synthesized various percentages of quaternized cellulose with the same degree of polymerization and concluded an intermediate quaternization percentage transfected the most efficiently due to intermediate binding stability. Figure 4.4b shows the results for luciferase expression in serum-containing media. The luciferase expression of all samples including Superfect®, decreased approximately one-order-of-magnitude and shifted the optimal transfection efficiency for each quaternized copolymer to a higher N/P ratio as a result of serum aggregation. The overall trend remained the same, and $PHEVIM_{25}$ exhibited a maximum transfection efficiency, larger than any other quaternized samples. Figure 4.5 supports that polyplexes entered the cell and gained entry into the nucleus.

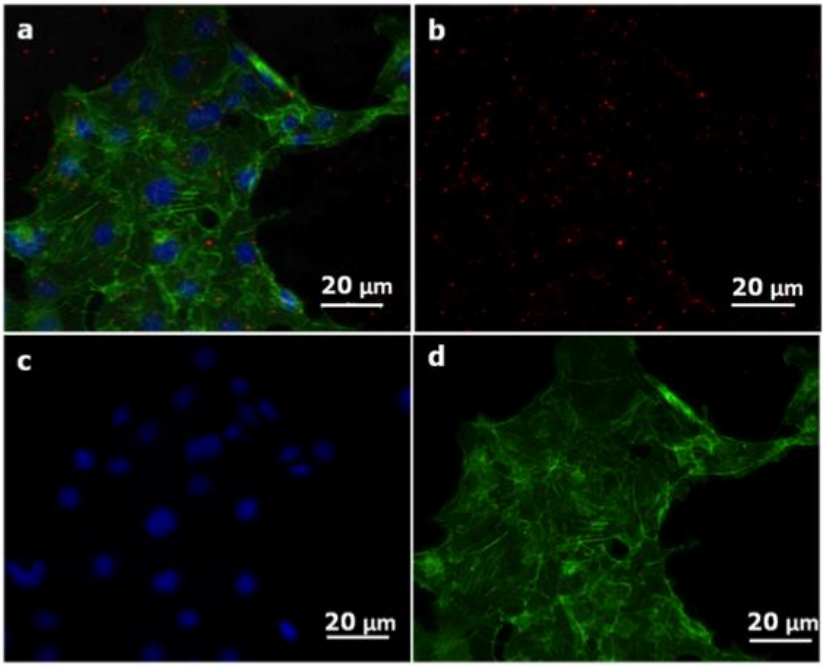

Figure 4.5. Fluorescence optical micrographs of COS-7 cells transfected with Cy5-labeled PHEVIM (50% quaternized)/pDNA polyplexes. 1 μg DNA per 100,000 cells, N/P = 8 were fixed and stained 1 h after treatment with polyplexes. (a) Multichannel composite image, (b) Cy5 channel showing polyplexes, (c) DAPI channel showing cellular nuclei, (d) AlexaFluor 488-Phollodin channel showing F-actin.

Figure 4.6 summarizes the polyplex hydrodynamic diameter and ζ-potential as a function of charge density.

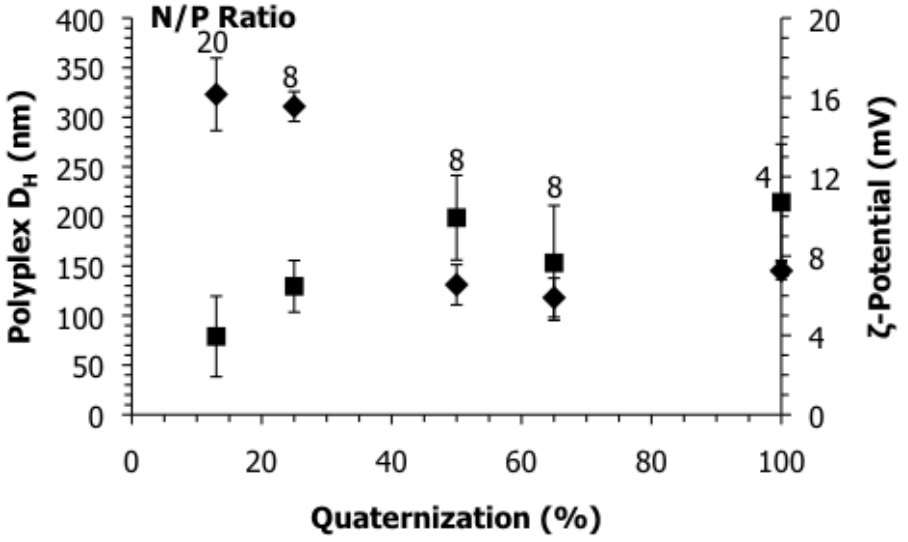

Figure 4.6. Polyplex hydrodynamic diameter (♦) and ζ-potential (■) as a function of charge density. The N/P ratios chosen exhibited the greatest transfection efficiency for each quaternization percentage investigated. Values represent mean ± SD (n = 3).

The analyzed N/P ratios corresponded to the maximum transfection efficiency of each copolymer sample in serum-free media. The hydrodynamic diameter decreased from ~300 nm to ~150 while ζ-potential increased slightly as quaternization percentage increased. The decrease in polyplex size with an increase in quaternization percentage suggested tighter binding between the polymer and pDNA, further supporting the decrease in luciferase expression above 25% quaternization.

We synthesized two additional 25% quaternized copolymers to study the effects of adjacent hydroxyl number on transfection efficiency. $PEVIM_{25}$ did not contain hydroxyl groups (n = 0), $PHEVIM_{25}$ contained on average one hydroxyl group for every four repeat units (n = 1), and $PDHVIM_{25}$ contained 2 hydroxyl groups for every four repeat units (n = 2). These copolymers revealed the influence of a pendant hydroxyl substituent on pDNA transfection.

Reineke et al.[24] found the incorporation of hydroxyl groups further enhanced the binding of polymer to pDNA through hydrogen bonding and concluded hydrogen bond formation between polymer and pDNA would serve as a less toxic alternative to high charge density polyelectrolytes. DNA gel shift and heparin competitive binding assays, shown in Figure 4.7, revealed the influence of hydroxyl concentration on pDNA binding and polyplex stability.

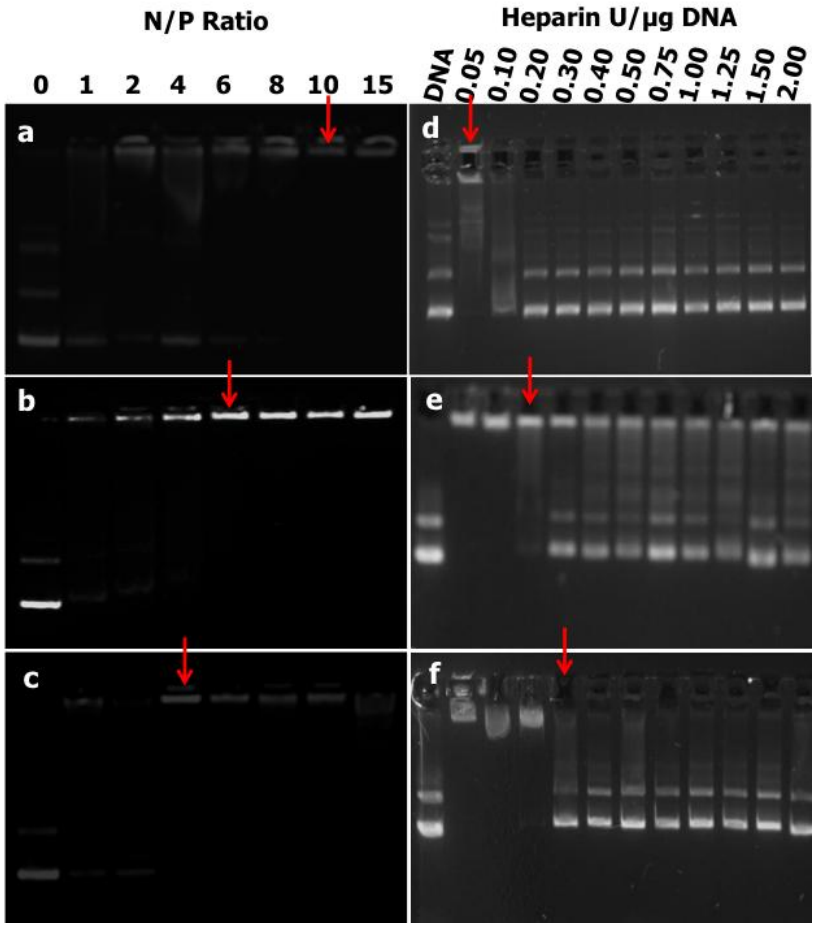

Figure 4.7. Electrophoretic gel shift assay of imidazolium copolymers of various hydroxyl content to determine copolymer-pDNA complexation: a (PEVIM), b (PHEVIM), c (PDHVIM). Arrows indicate N/P ratio necessary for complete DNA binding. Heparin competitive binding assay to determine polyplex stability as a function of increasing: d (PEVIM), e (PHEVIM), f (PDHVIM). Arrows indicate onset of polyplex disassembly.

As hydroxyl number increased from n = 0 to n = 2, the initial N/P ratio required for polyplex formation decreased from 10 to 6 to 4 respectively, suggesting hydrogen bond formation

between the copolymer and pDNA. A heparin competitive binding assay further probed this copolymer-pDNA binding stability. The assay challenged the copolymer-pDNA complexes with various concentrations of heparin to cause polyplex dissociation. The greater the amount of heparin required to cause polyplex dissociation, the greater the copolymer-pDNA binding affinity. Figure 4.7 e-g shows that the heparin concentration required to cause full polyplex dissociation at an N/P of 20 increased as the hydroxyl number increased; $PEVIM_{25}$ dissociated at a concentration of 0.05 U/μg DNA, $PHEVIM_{25}$ at 0.20 U/μg, and $PDHVIM_{25}$ at 0.30 U/μg. These results supported the presence of stronger interactions between the copolymer and pDNA as hydroxyl number increased.

An MTT cytotoxicity assay determined the effect of increasing hydroxyl number on cell viability of COS-7 cells. Shown in Figure 4.8a, all copolymer formulations were non-toxic at concentrations to 150 μg/mL. Figure 4.8b, confirmed polyplex formulations containing copolymer concentrations between 1-150 μg/mL were also non-toxic.

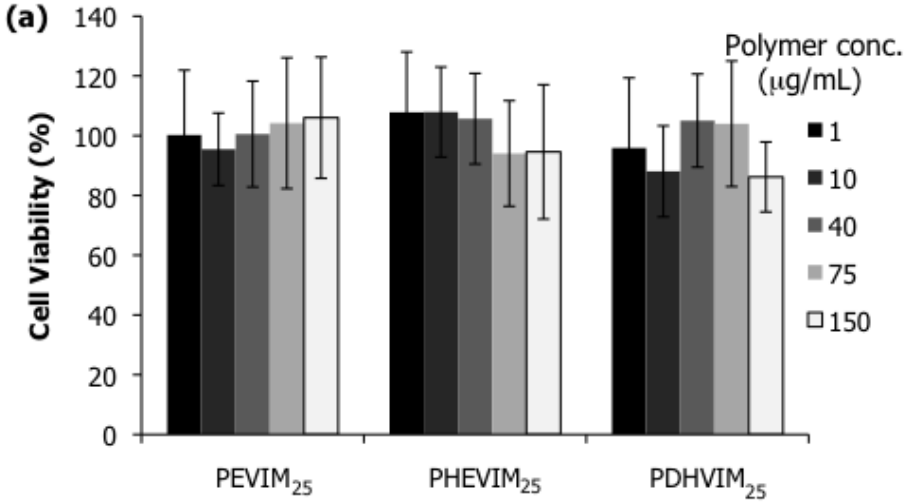

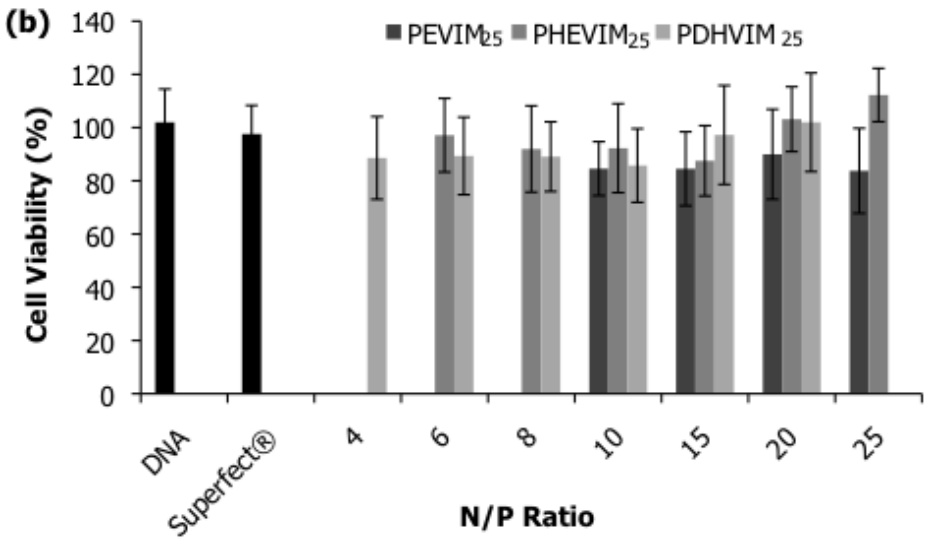

Figure 4.8. COS-7 cell viability as a function of (a) copolymer hydroxyl composition at various copolymer concentrations and (b) polyplex N/P ratios. Values represent mean ± SD (n = 8).

The MTT assay and electrophoretic experiments collectively demonstrated control over copolymer-pDNA binding affinity. Cell viabilities remained >90% with functional substituent variation, thus avoiding the expected toxicity associated with increased charge density on polymer vehicles.

An *in vitro* luciferase assay determined the transfection efficiency of the imidazolium copolymers as a vehicle for delivery of pDNA. The N/P ratios were chosen according to the same method described above in the charge density discussion. The optimal N/P ratios for pDNA delivery (Figure 4.9) in serum-free (serum) for $PEVIM_{25}$ were 25 (25), 8 (20) for $PHEVIM_{25}$, and 8 (20) for $PDHVIM_{25}$.

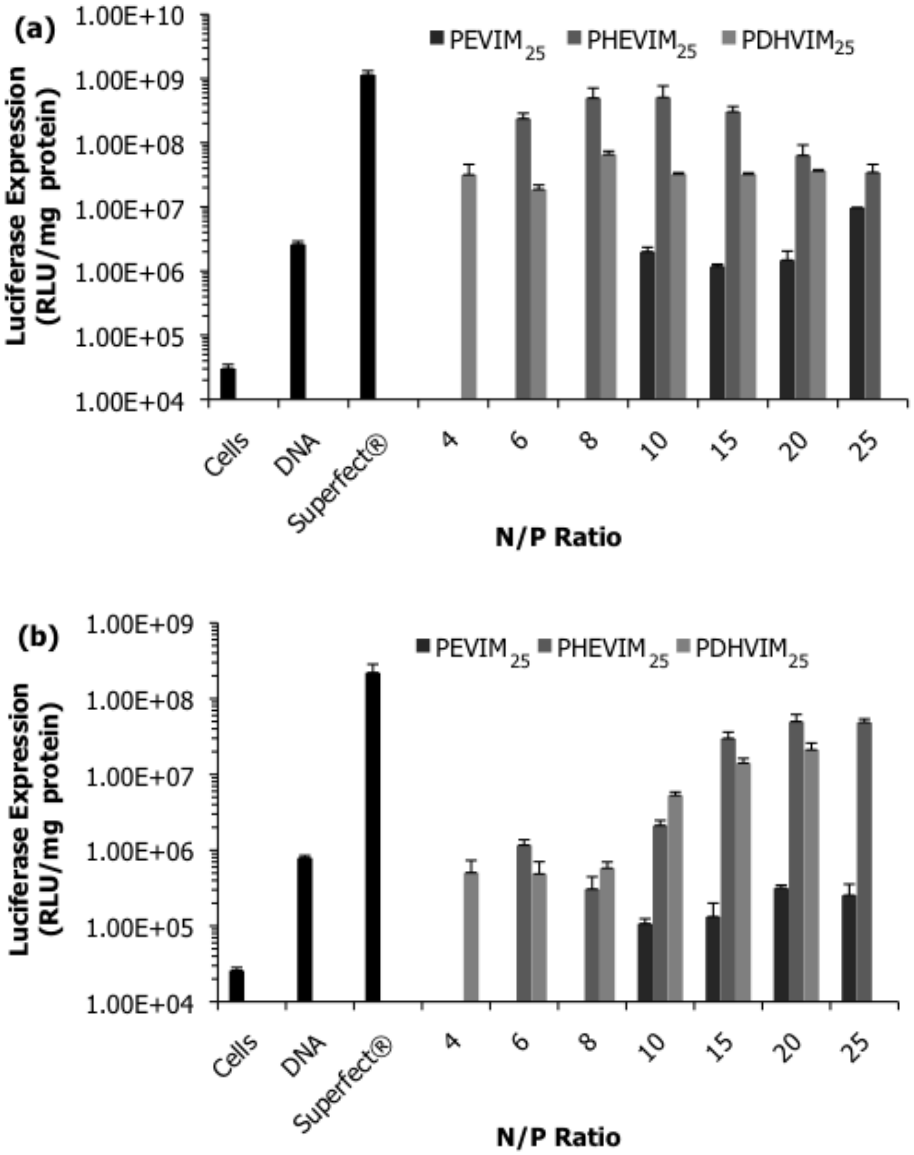

Figure 4.9. In vitro gene transfection efficiency in COS-7 cells as a function of N/P ratio with various copolymer hydroxyl compositions in (a) serum-free and (b) serum-containing media. Non-toxic N/P ratios chosen for luciferase transfection. Values represent mean ± SD (n = 4).

$PEVIM_{25}$ luciferase expression in serum-free media was two-orders-of-magnitude lower than Superfect®, whereas $PHEVIM_{25}$ was of similar magnitude to Superfect® through the addition of a hydroxyethyl group instead of an ethyl group attached to the imidazolium ring. Therefore, the addition of the hydroxyl group, which presumably forms hydrogen bonds with DNA, dramatically increased the transfection efficiency of the imidazolium copolymers. When two

hydroxyl groups were present in the repeating unit, further increasing hydrogen bonding substituents, $PDHVIM_{25}$ displayed an order-of-magnitude decrease compared to $PHEVIM_{25}$. In addition, $PDHVIM_{25}$ exhibited an order-of-magnitude greater luciferase expression than $PEVIM_{25}$. These results confirm the results found in the charge density experiments, i.e. the copolymer with intermediate binding with pDNA was most effective for pDNA delivery.

The serum transfection results, shown in Figure 4.9b, illustrate a decrease in luciferase expression in all samples. Superfect® luciferase expression decreased 81%. $PEVIM_{25}$ luciferase expression decreased 97%; $PHEVIM_{25}$ and $PDHVIM_{25}$ decreased 90% and 67% respectively. The hydroxyl-containing imidazolium copolymers exhibited a smaller decrease in luciferase expression than $PEVIM_{25}$. $PDHVIM_{25}$ decreased in luciferase expression dramatically less compared to all samples including Superfect®. These results agreed with Xu et al.[48] and Ma et al.[49] who found the addition of hydroxyl groups to a cationic polymer shielded the positive surface charge reducing protein aggregation. This charge screening increased transfection efficiency compared to polymers without a hydroxyl group.

DLS determined polyplex hydrodynamic diameter and ζ-potential of the imidazolium copolymers. DLS revealed the greater amount of hydroxyl groups present on the repeating unit, the tighter the binding of copolymer to pDNA as evidenced with the decrease in polyplex hydrodynamic diameter (Figure 4.10).

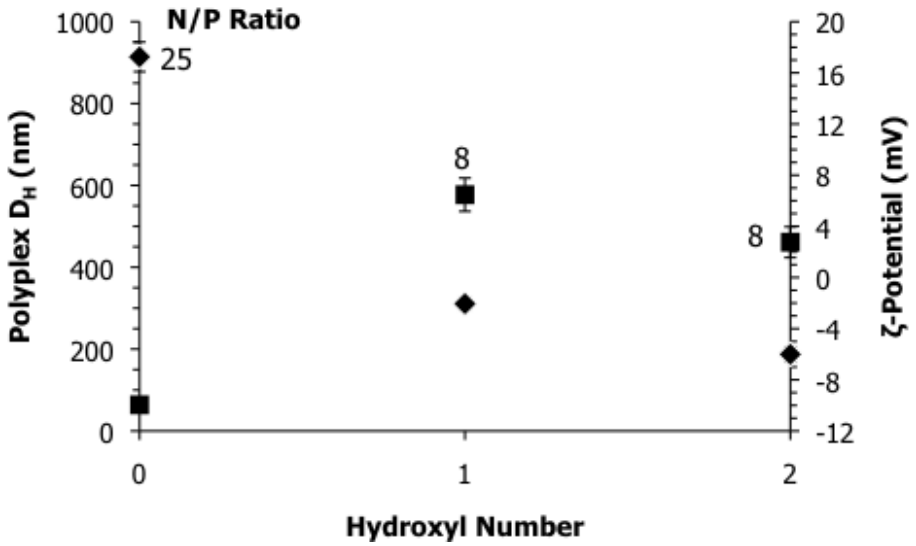

Figure 4.10. Polyplex hydrodynamic diameter (♦) and ζ-potential (■) as a function of hydroxyl number. The N/P ratios chosen exhibited the greatest transfection efficiency for each quaternization percentage investigated. Values represent mean ± SD (n = 3).

This data further confirmed that copolymers with an intermediate binding affinity for pDNA were the most effective for transfection. $PEVIM_{25}$ polyplex large hydrodynamic size and negative ζ-potential suggested the polyplexes form aggregates in solution limiting the transfection efficiency of this copolymer.

4.5 *Conclusions*

Copolymer binding affinity significantly influenced overall transfection efficiency of DNA delivery vehicles, and the incorporation of hydroxyl sites offers a safe and effective alternative to more highly charged copolymers for nonviral gene delivery. An intermediate binding affinity between polymer and pDNA was ideal for obtaining high transfection efficiency through the variation of functional substituents. Conventional free radical polymerization afforded PVIM for subsequent post-polymerization modification to produce novel imidazolium copolymers of various charge densities and hydroxyl concentrations, which allowed for precise structure-transfection efficiency studies. MTT assays revealed imidazolium copolymers with

quaternization values above 25 mol % exhibited significant toxicity; however, copolymers containing 25 mol % cationic charge or less, displayed negligible toxicity. DNA binding and heparin competitive binding assays indicated higher charge density and hydroxyl incorporation resulted in increased binding affinity between polymer and pDNA. Luciferase expression assays found 25 mol % cationic charge as the ideal charge density for the cationic polyelectrolyte. In addition, a repeating unit containing one hydroxyl group was unexpectedly more effective than zero or two hydroxyl groups for pDNA delivery. DLS confirmed that 25 mol % charge and the presence of one hydroxyl group resulted in an intermediate DNA binding affinity was ideal for effective DNA delivery.

4.6 *Acknowledgments*

This material is based upon work supported in part by the Macromolecular Interfaces with Life Sciences (MILES) Integrative Graduate Education and Research Traineeship (IGERT) of the National Science Foundation under Agreement No. DGE-0333378. This material is also based upon work supported in part by the US Army Research Office under Grant No. W911NF-07-1-0452 Ionic Liquids in Electro-Active Devices (ILEAD) MURI.

4.7 *References*

(1) Li, S. D.; Huang, L. *Gene Ther* **2006**, *13*, 1313-1319.
(2) Gao, X.; Kim, K.-S.; Liu, D. *The AAPS Journal* **2007**, *9*, E92-E104.
(3) Thomas, C. E.; Ehrhardt, A.; Kay, M. A. *Nat Rev Genet* **2003**, *4*, 346-358.
(4) Kay, M. A.; Glorioso, J. C.; Naldini, L. *Nat Med* **2001**, *7*, 33-40.
(5) Thomas, M.; Klibanov, A. M. *Appl. Microbiol. Biotechnol.* **2003**, *62*, 27-34.
(6) Mintzer, M. A.; Simanek, E. E. *Chem. Rev.* **2008**, *109*, 259-302.
(7) Heath, W. H.; Senyurt, A. F.; Layman, J.; Long, T. E. *Macromol. Chem. Phys.* **2007**, *208*, 1243-1249.
(8) Wong, S. Y.; Pelet, J. M.; Putnam, D. *Prog. Polym. Sci.* **2007**, *32*, 799-837.
(9) Nishikawa, M.; Huang, L. *Human Gene Therapy* **2001**, *12*, 861-870.
(10) Layman, J. M.; Ramirez, S. M.; Green, M. D.; Long, T. E. *Biomacromolecules* **2009**, *10*, 1244-1252.
(11) Kwoh, D. Y.; Coffin, C. C.; Lollo, C. P.; Jovenal, J.; Banaszczyk, M. G.; Mullen, P.; Phillips, A.; Amini, A.; Fabrycki, J.; Bartholomew, R. M.; Brostoff, S. W.; Carlo, D. J.

Biochimica et Biophysica Acta (BBA) - Gene Structure and Expression **1999**, *1444*, 171-190.
(12) Farrell, L.-L.; Pepin, J.; Kucharski, C.; Lin, X.; Xu, Z.; Uludag, H. *European Journal of Pharmaceutics and Biopharmaceutics* **2007**, *65*, 388-397.
(13) Godbey, W. T.; Wu, K. K.; Mikos, A. G. *J. Controlled Release* **1999**, *60*, 149-160.
(14) Demeneix, B.; Behr, J.; Leaf Huang, M.-C. H.; Ernst, W. In *Advances in Genetics*; Academic Press: **2005**, *53*, 215-230.
(15) Majoros, I. J.; Myc, A.; Thomas, T.; Mehta, C. B.; Baker, J. R. *Biomacromolecules* **2006**, *7*, 572-579.
(16) Luo, D.; Haverstick, K.; Belcheva, N.; Han, E.; Saltzman, W. M. *Macromolecules* **2002**, *35*, 3456-3462.
(17) Jevprasesphant, R.; Penny, J.; Jalal, R.; Attwood, D.; McKeown, N. B.; D'Emanuele, A. *Int. J. Pharm.* **2003**, *252*, 263-266.
(18) Dang, J. M.; Leong, K. W. *Advanced Drug Delivery Reviews* **2006**, *58*, 487-499.
(19) De Smedt, S. C.; Demeester, J.; Hennink, W. E. *Pharm. Res.* **2000**, *17*, 113-126.
(20) Xu, F. J.; Ping, Y.; Ma, J.; Tang, G. P.; Yang, W. T.; Li, J.; Kang, E. T.; Neoh, K. G. *Bioconjugate Chem.* **2009**, *20*, 1449-1458.
(21) Ramirez, S. M.; Layman, J. M.; Long, T. E. *Macromolecular Bioscience* **2009**, *9*, 1127-1134.
(22) Georgiou, T. K.; Vamvakaki, M.; Patrickios, C. S.; Yamasaki, E. N.; Phylactou, L. A. *Biomacromolecules* **2004**, *5*, 2221-2229.
(23) Asayama, S.; Hakamatani, T.; Kawakami, H. *Bioconjugate Chem.* **2010**, *21*, 646-652.
(24) Prevette, L. E.; Kodger, T. E.; Reineke, T. M.; Lynch, M. L. *Langmuir* **2007**, *23*, 9773-9784.
(25) Rungsardthong, U.; Ehtezazi, T.; Bailey, L.; Armes, S. P.; Garnett, M. C.; Stolnik, S. *Biomacromolecules* **2003**, *4*, 683-690.
(26) Green, J. J.; Langer, R.; Anderson, D. G. *Acc. Chem. Res.* **2008**, *41*, 749-759.
(27) Schaffer, D. V.; Fidelman, N. A.; Dan, N.; Lauffenburger, D. A. *Biotechnol. Bioeng.* **2000**, *67*, 598-606.
(28) Kim, T. H.; Ihm, J. E.; Choi, Y. J.; Nah, J. W.; Cho, C. S. *J. Controlled Release* **2003**, *93*, 389-402.
(29) Swami, A.; Aggarwal, A.; Pathak, A.; Patnaik, S.; Kumar, P.; Singh, Y.; Gupta, K. C. *Int. J. Pharm.* **2007**, *335*, 180-192.
(30) Mishra, S.; Heidel, J. D.; Webster, P.; Davis, M. E. *J. Controlled Release* **2006**, *116*, 179-191.
(31) Kichler, A.; Leborgne, C.; MÃ¤rz, J.; Danos, O.; Bechinger, B. *Proceedings of the National Academy of Sciences of the United States of America* **2003**, *100*, 1564-1568.
(32) Mason, A. J.; Leborgne, C.; Moulay, G.; Martinez, A.; Danos, O.; Bechinger, B.; Kichler, A. *J. Controlled Release* **2007**, *118*, 95-104.
(33) McKenzie, D. L.; Smiley, E.; Kwok, K. Y.; Rice, K. G. *Bioconjugate Chem.* **2000**, *11*, 901-909.
(34) Brooks, H.; Lebleu, B.; Vivès, E. *Advanced Drug Delivery Reviews* **2005**, *57*, 559-577.
(35) Midoux, P.; Monsigny, M. *Bioconjugate Chem.* **1999**, *10*, 406-411.
(36) Benns, J. M.; Choi, J.S.; Mahato, R. I.; Park, J.S.; Kim, S. W. *Bioconjugate Chem.* **2000**, *11*, 637-645.
(37) Okuda, T.; Sugiyama, A.; Niidome, T.; Aoyagi, H. *Biomaterials* **2004**, *25*, 537-544.

(38) Anderson, D. G.; Akinc, A.; Hossain, N.; Langer, R. *Mol Ther* **2005**, *11*, 426-434.
(39) Midoux, P.; Pichon, C.; Yaouanc, J.-J.; Jaffrès, P.-A. *British Journal of Pharmacology* **2009**, *157*, 166-178.
(40) Anderson, E. B.; Long, T. E. *Polymer* **2010**, *51*, 2447-2454.
(41) Liu, Y.; Reineke, T. M. *Bioconjugate Chem.* **2005**, *17*, 101-108.
(42) Liu, Y.; Reineke, T. M. *Biomacromolecules* **2010**, *11*, 316-325.
(43) Song, Y.; Wang, H.; Zeng, X.; Sun, Y.; Zhang, X.; Zhou, J.; Zhang, L. *Bioconjugate Chem.* **2010**, *21*, 1271-1279.
(44) Fischer, D.; Li, Y.; Ahlemeyer, B.; Krieglstein, J.; Kissel, T. *Biomaterials* **2003**, *24*, 1121-1131.
(45) Lavertu, M.; Méthot, S.; Tran-Khanh, N.; Buschmann, M. D. *Biomaterials* **2006**, *27*, 4815-4824.
(46) MacLaughlin, F. C.; Mumper, R. J.; Wang, J.; Tagliaferri, J. M.; Gill, I.; Hinchcliffe, M.; Rolland, A. P. *J. Controlled Release* **1998**, *56*, 259-272.
(47) Ogris, M.; Brunner, S.; Schüller, S.; Kircheis., R.; Wagner, E. *Gene Ther* **1999**, *6*, 595-605.
(48) Xu, F. J.; Chai, M. Y.; Li, W. B.; Ping, Y.; Tang, G. P.; Yang, W. T.; Ma, J.; Liu, F. S. *Biomacromolecules* **2010**, *11*, 1437-1442.
(49) Ma, M.; Li, F.; Yuan, Z.F.; Zhuo, R.X. *Acta Biomaterialia* **2010**, *6*, 2658-2665.

Chapter 5: Synthesis of Folic Acid-Containing Imidazolium Copolymers for Potential Gene Delivery Applications

(Submitted to *Macromolecular Chemistry and Physics*)

Michael H. Allen, Jr., Kelsea N. Day, Sean T. Hemp, and Timothy E. Long

Macromolecules and Interfaces Institute, Department of Chemistry, Virginia Tech, Blacksburg, VA 24061

5.1 *Abstract*

Folic acid conjugation onto poly(1-vinylimidazole) (PVIM) generated imidazolium copolymers for potential receptor-mediated nonviral gene delivery. Conventional free radical polymerization afforded high molecular weight PVIM (M_n = 23,000 g/mol) for post-polymerization modification. The degree of polymerization for all copolymers remained identical to eliminate molecular weight effects on gene delivery. Homopolymer quaternization with various *t*Boc-protected bromoalkylamines imparted a permanent, cationic charge for nucleic acid complexation. Incorporation of primary amine groups provided a site for folic acid conjugation onto imidazolium copolymers. DNA binding, cytotoxicity, and *in vitro* gene transfection in a cervical cancer cell line, HeLa cells, established structure-property-transfection relationships for the imidazolium copolymers. As charge density of the imidazolium copolymers increased, the toxicity of the copolymers also increased. Folic acid incorporation did not impact cytotoxicity or DNA binding affinity. Luciferase expression assays revealed that primary amine conjugation onto imidazolium copolymers up to 30 mol % failed to improve transfection efficiency. In sharp contrast, incorporation of folic acid onto the copolymers improved transfection efficiency 250-fold. Our studies supported the conclusion that folic acid conjugation onto copolymers for gene delivery substantially improves transfection efficiency.

5.2 *Introduction*

Nonviral gene delivery remains a promising area of research for the treatment of numerous chronic diseases including cancer,[1-3] and successful clinical applications require the development of efficacious gene delivery vehicles. Deleterious immunogenic response and limited DNA loading capacity plague the development of viral gene therapies despite high gene delivery efficiencies.[4,5] Tailoring macromolecular design of nonviral delivery vehicles through synthetic variation enables the development of efficient transfection agents with a suppressed immunogenic risk.[6,7] These designer macromolecules must overcome numerous obstacles that limit transfection including cellular uptake, endosomal escape, and delivery of the genetic cargo into the nucleus.[8,9] Cationic polyelectrolytes must also sufficiently bind and compact DNA to prevent nucleic acid degradation. A wide array of cationic polyelectrolytes employed for nonviral gene therapy include chitosan,[10-12] poly(2-(dimethylamino)ethyl methacrylate) (PDMAEMA),[13-15] poly(L-lysine),[16,17] poly(ethyleneimine) (PEI),[18,19] poly(amido amine) dendrimers,[20,21] phosphonium-containing polymers,[22-24] and imidazole-containing polymers.[25-27] Modification through charge density,[28] hydrogen bonding substituents,[27,29] or polyethylene glycol (PEG)[22,30] affords fine tuning of macromolecular properties to reduce cytotoxicity, impact DNA binding affinity, and increase colloidal stability.

These cationic delivery vehicles primarily facilitate cellular internalization through interaction with negatively charged proteoglycans on the cell surface.[31] The lack of cellular specificity limits transfection efficiency and targeted delivery to a cell population in vivo. Cancer cell lines and tumors commonly over-express folate receptors on the cell surface, providing a biological handle for receptor-mediated gene delivery.[32,33] The folate receptor exhibits a high affinity for folate molecules (K_D ~ 100 pM) and preferentially mediates uptake. The two-step internalization process consists of initial folate binding to the complementary

receptor, and subsequent receptor-mediated endocytosis through the caveolar pathway in HeLa cells.[33] Pack et al. demonstrated that caveolae-mediated cellular uptake primarily contributed to high transfection efficiency for PEI.[34] This pathway avoided rapid and direct trafficking of the caveosomes to the lysosome while the clathrin-mediated pathway in HeLa cells shuttled the endosome directly to the lysosome, limiting transfection efficiency. Numerous researchers have shown folic acid conjugation improved cellular uptake and transfection of various macromolecules including chitosan,[10,35,36] PDMAEMA,[37] poly(L-lysine),[38,39] and PEI.[40]

Macromolecular delivery vehicles, which display a buffering capacity near endosomal pH, typically escape the endosome through the proton sponge mechanism.[41,42] Polymer protonation in the endosome leads to a cascade of events involving endosomal swelling and rupture, which result in improved gene delivery. Polymers containing the amino acid histidine or imidazole commonly improve nonviral gene delivery compared to unmodified macromolecules due to the buffering capacity of imidazole (pKa ~ 6) near endosomal pH.[43] Midoux and co-workers functionalized poly(L-lysine) with histidine residues and found a 3-4 order of magnitude increase in transfection efficiency compared to the unfunctionalized homopolymer.[44] Benns et al. grafted histidine onto poly(L-lysine) and observed a similar increase in transfection.[45] Additionally, Davis et al. functionalized linear, cyclodextrin-containing polyelectrolytes with imidazole-containing substituents and reported increased transfection efficiency.[46] Polyphosphazenes containing imidazole groups also displayed higher luciferase expression compared to the unfunctionalized analogs.[47]

Imidazole-containing homopolymers require subsequent functionalization to impart a cationic charge on the polymer.[48,49] The establishment of a permanent, positive charge affords electrostatic complexation with anionic macromolecules including plasmid DNA. Previously,

Asayama et al. functionalized poly(1-vinylimidazole) (PVIM) with various alkyl groups tuning the charge density and hydrophobicity of the copolymers for nonviral gene delivery in HepG2 cells.[26] In addition, we developed novel imidazolium copolymers with tailored charge density and hydrogen bonding through post-polymerization functionalization with hydroxyalkyl groups.[27] Tuning hydrogen bonding substituent concentration provided a unique, nontoxic method to control polymer-DNA binding affinity. Additionally, Asayama et al. also functionalized PVIM with hydrogen bonding substituents, primary amino groups, but only obtained 2.5 mol % quaternization.[50] These copolymers required high polymer concentrations to bind DNA due to the low quaternization percentages and failed to achieve high luciferase expression.

We report herein novel imidazolium copolymers functionalized with folic acid to target cancer cells for potential receptor-mediated delivery of DNA therapeutics. Our studies demonstrate the potential synergy of polyplexes functionalized with targeting ligands and the impact on transfection efficiency. In this work, protection chemistry yielded primary amino groups onto PVIM utilizing protection chemistry with quaternization percentages $\leq$ 30 mol %. Additionally, functionalization with folic acid onto these imidazolium copolymers promoted receptor-mediated endocytosis to mimic cancer cell targeting for potential *in vivo* applications. To our knowledge, these are the first imidazolium copolymers that are functionalized with folic acid for receptor-mediated gene delivery. All polymeric precursors had an equivalent degree of polymerization to eliminate molecular weight influences on nonviral gene delivery. This report describes the influence of primary amino incorporation and folic acid functionalization on DNA binding, cytotoxicity, and *in vitro* DNA delivery.

5.3 *Experimental Section*

5.3.1 Materials

1-Vinylimidazole was distilled under reduced pressure (VIM, 99%, Aldrich). 2,2'-Azobisisobutyronitrile (AIBN, 99%, Sigma-Aldrich) was recrystallized from methanol. 2-Bromoethanamine hydrobromide (99%, Aldrich), 3-bromopropylamine hydrobromide (98%, Aldrich), di-*t*-butyl dicarbonate (99%, Aldrich), *N*-hydroxysuccinimide (NHS, 98%, Aldrich), *N*,*N*′-dicyclohexylcarbodiimide (DCC, 99%, Aldrich), triethylamine (TEA, ≥99%, Sigma-Aldrich), boric acid (≥99.5%, Sigma), sodium phosphate dibasic (>98.5%, Sigma), and folic acid (FA, 97%, Aldrich) were used as received. Deuterated dimethyl sulfoxide (d_6-DMSO, 99.9% Cambridge Isotope Laboratories), dimethylformamide (DMF, ≥99%, Fisher), and dichloromethane (DCM, ≥99%, Fisher) were used as received.

5.3.2 Analytical Techniques

^{1}H NMR spectroscopy (Varian Inova, 400 MHz, CD_3OD) confirmed monomer and polymer structures. TA Instruments thermogravimetric analyzer (TGA) Hi-Res 2950 with a heating rate of 10 °C/min from 23 °C to 600 °C under a nitrogen atmosphere determined copolymer thermal stability. Aqueous size exclusive chromatography (SEC, flow rate of 0.8 mL/min through two Waters Ultrahydrogel Linear and one Waters Ultrahydrogel 250 columns, solvent: 54/23/23 H_2O/MeOH/acetic acid (v/v/v %), 0.1 M $NaNO_3$) equipped with a Waters 1515 isocratic HPLC pump, a Waters 717plus autosampler, a Wyatt miniDAWN multiangle laser light scattering (MALLS, wavelength = 690 nm), and a Waters 2414 differential refractive index detector determined polymer molecular weights relative to poly(ethylene oxide) standards. Prior to SEC, polymer samples were screened with dynamic light scattering (DLS, Malvern Zetasizer NanoZS) to confirm the absence of polymer aggregates in the SEC mobile phase. UV-Visible spectroscopy determined folic acid concentration at λ = 340 nm. A standard curve was

prepared with various concentrations of folic acid dissolved in 0.1 M NaOH. Spectra were obtained utilizing an Analytical Instrument Systems Inc. spectrophotometer containing fiber-optic light guides, a DT1000CE light source, and an Ocean Optics USB2000 UV-Vis detector.

5.3.3 *t*Boc Protection

In a representative reaction, 2-bromoethanamine hydrobromide (16.3 g, 79.6 mmol) and di-*t*-butyl dicarbonate (19.8 g, 90.7 mmol) were added to a 250-mL, round-bottomed flask equipped with a stir bar and dissolved in 100 mL CH_2Cl_2 at 0 °C. Triethylamine (12.6 mL, 90.4 mmol) was added dropwise to the solution for 30 min, after which, the mixture was stirred for 1 h at 0 °C and an additional 16 h at 23 °C. The organic phase was washed three times with a 1M HCl (100 mL), three times with a saturated $NaHCO_3$ solution (100 mL), and a final three times with a saturated brine solution (100 mL). The organic layer was then dried over $MgSO_4$ and dried under reduced pressure to yield a colorless oil. The oil was recrystallized in hexanes to form a white crystalline solid which was dried under reduced pressure (8.91 g, 50 % yield). ^{1}H NMR (d_6-DMSO):δ 1.38 (s, 9H), 3.39 (m, 2H), 3.47 (t, 2H), 4.90 (s, 1H). The synthesis of a *t*Boc-protected bromopropylamine followed a similar procedure (7.09 g, 40% yield). ^{1}H NMR (d_6-DMSO):δ 1.37 (s, 9H), 1.98 (m, 2H), 3.20 (t, 2H), 3.37 (t, 2H), 4.61 (s, 1H).

5.3.4 Synthesis of Poly(1-Vinylimidazole)

In a typical polymerization, VIM was charged with 1.0 mol % AIBN in DMF at 20 wt % solids in a 100- mL, round-bottomed flask with a magnetic stir bar. The reaction mixture was sparged with nitrogen for 30 min and submerged in a thermostated oil bath at 65 °C. After 24 h, the polymer was precipitated into ethyl acetate, redissolved in methanol, and precipitated a second time into ethyl acetate to remove residual DMF. The polymer was dried under vacuum at 40 °C for 24 h to constant weight. The molecular weight of the homopolymer was measured using size exclusion chromatography (SEC, M_n = 23,000 g/mol, PDI = 1.89).

5.3.5 Synthesis of Imidazolium Copolymers

In a typical reaction, various equivalents of *t*-butyl *N*-(1-bromoethyl)carbamate were charged into a 50-mL, round-bottomed, flask containing PVIM (0.500 g) dissolved in DMF at 50 wt % solids. The reaction was heated at 65 °C for 24 h to obtain different quaternization percentages. The copolymer was precipitated into ethyl acetate and dried under reduced pressure at 40 °C for 24 h. Upon drying, a copolymer with 30 % quaternization was obtained. The process was repeated with *t*-butyl *N*-(1-bromopropyl)carbamate to produce a 15% quaternized copolymer. Acid catalysis (2 M HCl, 2 h) removed the *t*Boc protecting group. The reaction was dialyzed against water to remove small molecule impurities and residual acid. The copolymers were lyophilized to obtain a white powder generating poly(1-ethylamine-3-vinylimidazolium bromide-*co*-1-vinylimidazole) and poly(1-propylamine-3-vinylimidazolium bromide-*co*-1-vinylimidazole).

5.3.6 Folic Acid Conjugation onto Imidazolium Copolymers

In a dry 250-mL, round-bottomed flask equipped with stir bar, FA (5.00 g, 11.3 mmol) and NHS (2.50 g, 21.7 mmol) were dissolved in 100 mL of anhydrous DMSO and 2.50 mL TEA at 40 °C. The flask was sparged with nitrogen for 30 min. DCC (4.70 g, 22.7 mmol) was added to the solution, and the reaction was stirred for 24 h in the absence of light. The reaction mixture was filtered to remove the urea byproduct, concentrated in vacuo, and then precipitated into a 30/70 acetone/diethyl ether (v/v %) mixture. The orange solid was filtered and dried under reduced pressure (5.50 g, 90% yield). ^{1}H NMR (d_6-DMSO):δ 2.04 (m, 2H), 2.30 (s, 2H), 2.89 (m, 4H), 4.31 (d, 1H), 4.48 (m, 2H), 6.61 (d, 2H), 6.90 (t, 3H), 7.63 (d, 2H), 8.10 (d, 1H), 8.63 (d, 1H), 11.42 (s, 1H).

The activated folate (20 mg) was dissolved in 10 mL DMSO and added dropwise to a stirring aqueous solution (0.1 M Na_2HPO_4, 0.1 M boric acid, pH = 8.5) of an aminated

imidazolium copolymer (30 mg). The solution stirred overnight and was passed through a Zeba™ spin desalting column (7000 g/mol MWCO) to remove excess folic acid. The collected liquid was lyophilized to obtain folic acid functionalized imidazolium copolymers (Table 5.1).

Table 5.1. Polymer acronyms.

Abbreviation	Substituent	Quaternization (%)
PVIM	None	0
$PAEVIM_{30}$	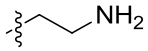	30
$PAEVIM_{30}$-FA	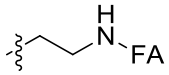	30
$PAPVIM_{15}$	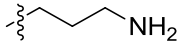	15
$PAPVIM_{15}$-FA	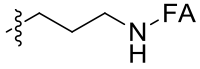	15

FA = Folic Acid

5.3.7 DNA Gel Shift Assay

DNA-polymer complexes (polyplexes) were prepared with 0.20 μL of gWiz-Luc plasmid (1 μg/μL in H_2O, Aldevron) in ~28 μL of 1X Tris-acetate-EDTA (TAE, Sigma) buffer. Various concentrations of copolymer were titrated into the DNA solutions to produced a variety of nitrogen/phosphorus (N/P) ratios from 1-14. After copolymer addition to the plasmid DNA solutions, the polyplexes were incubated at 23 °C for 30 min to promote DNA complexation. The solutions were added to a 0.9 wt % agarose gel stained with SYBR Green I (Sigma). The solutions were metered for 60 min at 70 V in 1X TAE buffer and then imaged under UV-irradiation with a MultiDoc-it™ Digital Imaging System (UVP).

5.3.8 Cell Culture

Cervical cancer HeLa cells were cultured in Dulbecco's modified Eagle's medium (DMEM) containing 10% fetal bovine serum (FBS), 100 U/mL of penicillin and 100 μg/mL of streptomycin (all reagents from Mediatech). The cells were maintained in an incubator operating at 37 °C with 5% CO_2 in a 95% humid atmosphere.

5.3.9 Cell Viability Assay

A 3-[4,5-dimethylthiazol-2-yl]2,5-diphenyltetrazolium bromide (MTT, Sigma-Aldrich) conversion assay determined copolymer cytotoxicity. All copolymer samples dissolved in ultrapure water (1 mg/mL) were diluted with DMEM to obtain copolymer solutions ranging in concentration from 1-200 μg/mL. HeLa cells were plated onto a 96-well plate 24 h prior to addition of the copolymer solutions to promote cell attachment. The cells were rinsed with 100 μL of DMEM and 100 μL copolymer solutions were added to each well. After 24 h, the polymer solutions were aspirated from the wells, and the wells were rinsed with 100 μL of 1X Hank's buffered salt solution (HBSS) to remove any residual polymer. The cells were treated with 100 μL of a 0.5 mg/mL MTT solution in DMEM for 4 h. The media was aspirated and DMSO was added to dissolve the formazan product. A SPECTRAmax M2 microplate reader (Molecular Devices Corp.) measured the absorbance at 570 nm for each well. Cell viability was determined from sample absorbance relative to the cells only control.

5.3.10 Luciferase Expression Assay

HeLa cells were plated on 24-well plates at a density of 1.0 X 10^5 cells/well 24 h prior to transfection to allow for cell attachment and equilibration. The cells were rinsed with HBSS and treated with 500 μL of the polyplex transfection solution. To prepare the polyplex solutions, gWiz-Luc plasmid (1 μg/μL in H_2O) was diluted in DMEM to a concentration of 1 μg DNA/well and concurrently copolymer solutions were diluted at various concentrations in DMEM and serum-containing DMEM corresponding to the targeted N/P ratios. The solutions of equal volume were mixed and incubated for 30 min at room temperature. The polyplexes remained on the cells for 4 h at 37 °C with 5% CO_2 and were subsequently removed from the cells. DMEM with serum was added to the cells and incubated (37 °C with 5% CO_2) for an additional 48 h to promote protein expression. The HeLa cells were rinsed with 500 μL of PBS and 125 μL of lysis

buffer was added to each well. The cells were subjected to -80 °C/37 °C freeze-thaw cycle three times to promote cell lysis. The lysate was collected and luciferase activity was measured following the instructions for the SPECTRAmax L luminometer (Molecular Devices Corp.) and the luciferase assay kit (Promega). Protein concentration was determined using a Pierce BCA Protein Assay kit according to the enclosed directions. Gene expression was reported as relative light units per milligram of cell protein lysate (RLU/mg). Experiments were repeated twice in quadruplicate.

5.3.11 GFP Expression Wide-Field Fluorescence Optical Microscopy

Polyplexes were prepared for GFP expression experiments with gWiz-GFP plasmid according to the luciferase procedure. The evaluated N/P ratios corresponded to the highest transfection efficiency as determined with the luciferase expression assay. The polyplexes were applied to the HeLa cells for 4 h. The HeLa cells were rinsed with PBS and imaged using a Nikon Eclipse TE2000-U inverted microscope with a Nikon C-HGFI Intensilight epifluorescence system and Nikon DS-Qi,Mc BW CCD digital camera. The multichannel fluorescence images were acquired using UV-2EC, Cy5, and F/EGFP filters.

5.4 *Results and Discussion*

Conventional free radical polymerization of VIM afforded a homopolymer with a number-average molecular weight (M_n) of 23,000 g/mol with a PDI of 1.89. PVIM failed to complex DNA in physiological buffer, and quaternization imparted a necessary, permanent cationic charge onto the polymer.[27] Primary amines on PVIM permitted DCC coupling of folic acid onto the imidazolium copolymer. Functionalization of PVIM with a primary amine required amine protection to suppress oligomerization. Busetto et al. showed the functionalization of 1-methylimidazole with unprotected 2-bromoethylamine hydrobromide produced a wide distribution of products including protonated 1-methylimidazole in 70% yield.[51] Scheme 5.1

depicts the synthesis *t*Boc-protected amines to generate both *t*Boc-bromoethylamine and *t*Boc-bromopropylamine. The alkylene spacer tailored the distance the primary amine from the polymer backbone.

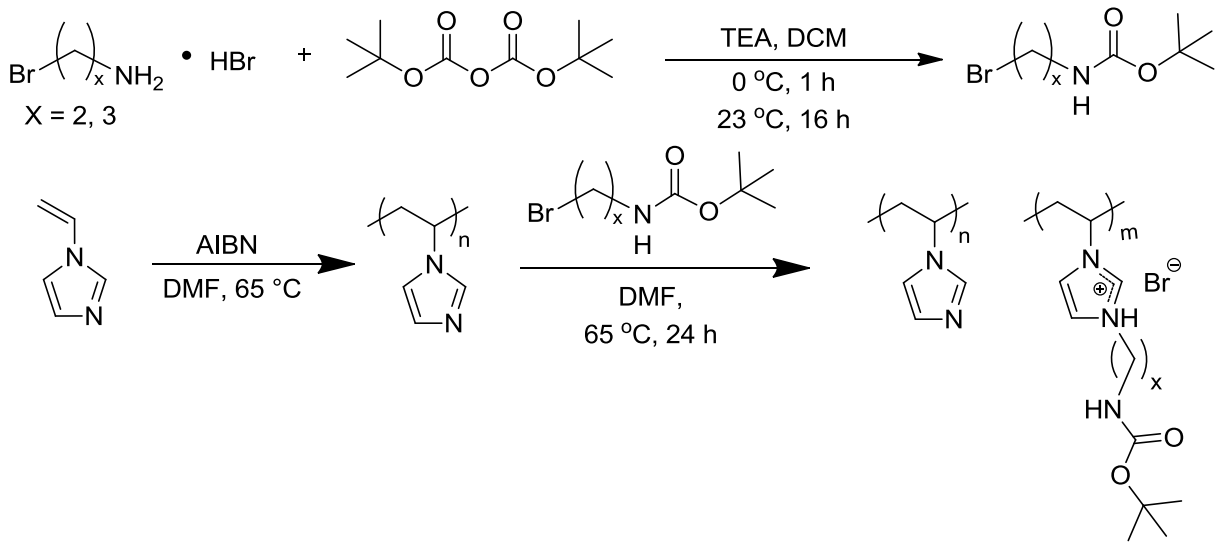

Scheme 5.1. Synthesis of *t*Boc-protected amines and subsequent quaternization of PVIM.

The protected amines readily reacted with PVIM and led to partial quaternization of the homopolymer. Seven equivalents of amine to polymer afforded the ethylamine and propylamine modified copolymers with 30 mol % quaternization and 15 mol % quaternization, respectively. Reactions with higher concentrations of protected amines failed to achieve larger quaternization percentages. ^{1}H NMR spectroscopy and TGA confirmed quaternization percentages as shown in Figure 5.1a and 1b.

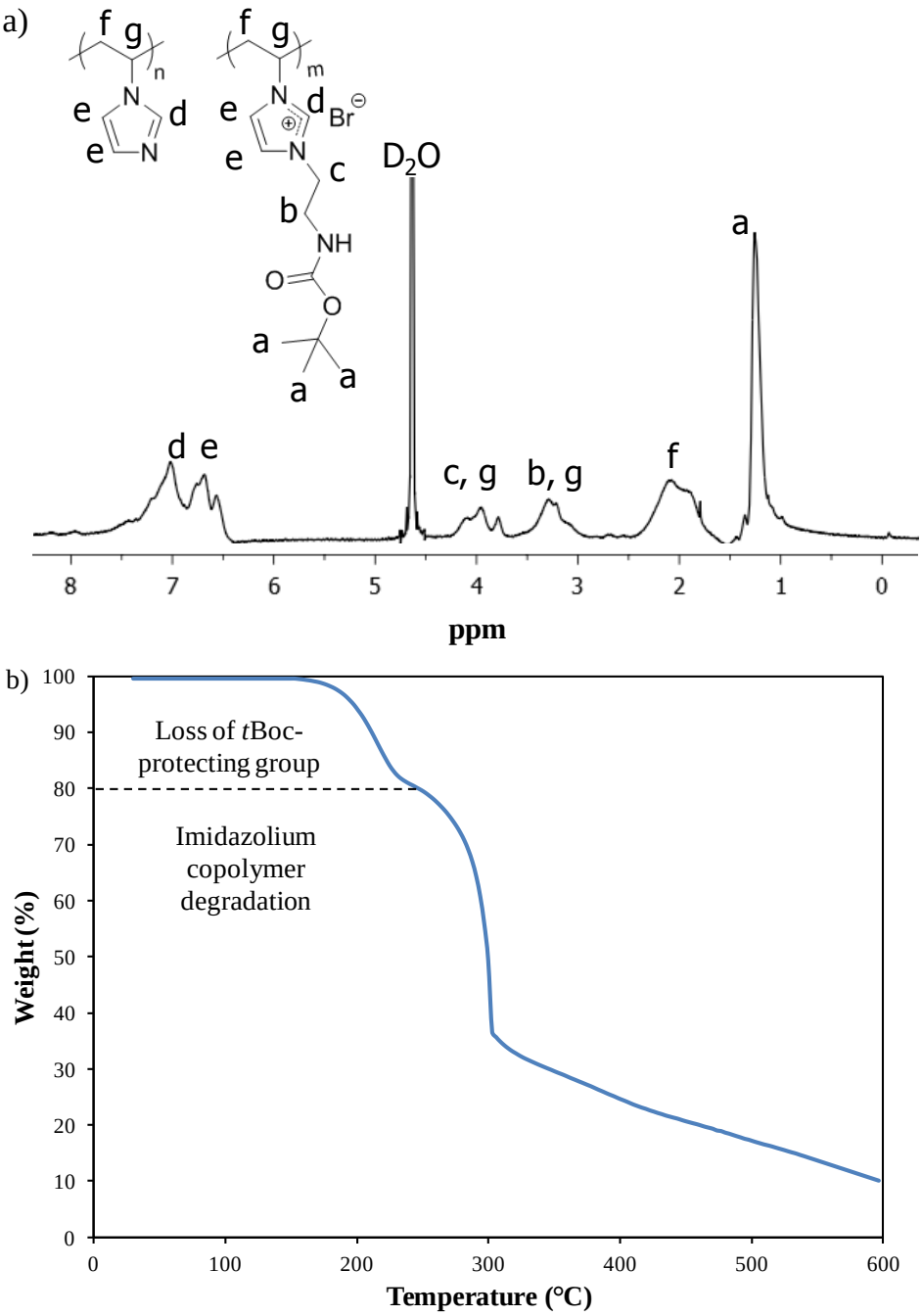

Figure 5.1. a) ^{1}H NMR of PAEVIM$_{30}$ confirmed successful quaternization of PVIM. b) TGA at a ramp rate of 10 °C/min under nitrogen further confirmed quaternization percentage determined with ^{1}H NMR. Initial weight loss of *t*Boc-protecting group corresponded to 30 mol % quaternization of PAEVIM$_{30}$.

The quaternizations utilized significantly less quaternizing agent and time to obtain charge densities that were 10-fold higher than previous studies. Asayama et al. functionalized PVIM

with 70 molar equivalents of unprotected, 2-bromoethylamine hydrobromide to obtain only 2.5% quaternization; our studies confirmed the necessity for protection chemistry to achieve high quaternization percentages.[50] The quaternized copolymers required an N/P ratio of 40 to electrostatically complex DNA and failed to transfect various cell lines. The low level of quaternization severely reduced the efficacy of these gene delivery vehicles due to their limited ability to complex DNA.

Functionalization of the protected-amine imidazolium copolymers with folic acid required deprotection of the primary amine. Two common methods utilized from the earlier literature include acid and thermal deprotection. Isothermal TGA determined thermal deprotection occurred at 150 °C. Initial efforts involved thermal deprotection of the copolymers to limit further purification steps; however, the copolymers crosslinked and remained insoluble in water. Acid deprotection in a 2 M HCl solution generated quantitative deprotection of the primary amine, and TGA confirmed complete removal of the *t*Boc group (Figure 5.2). Dialysis against water purified the deprotected-copolymer.

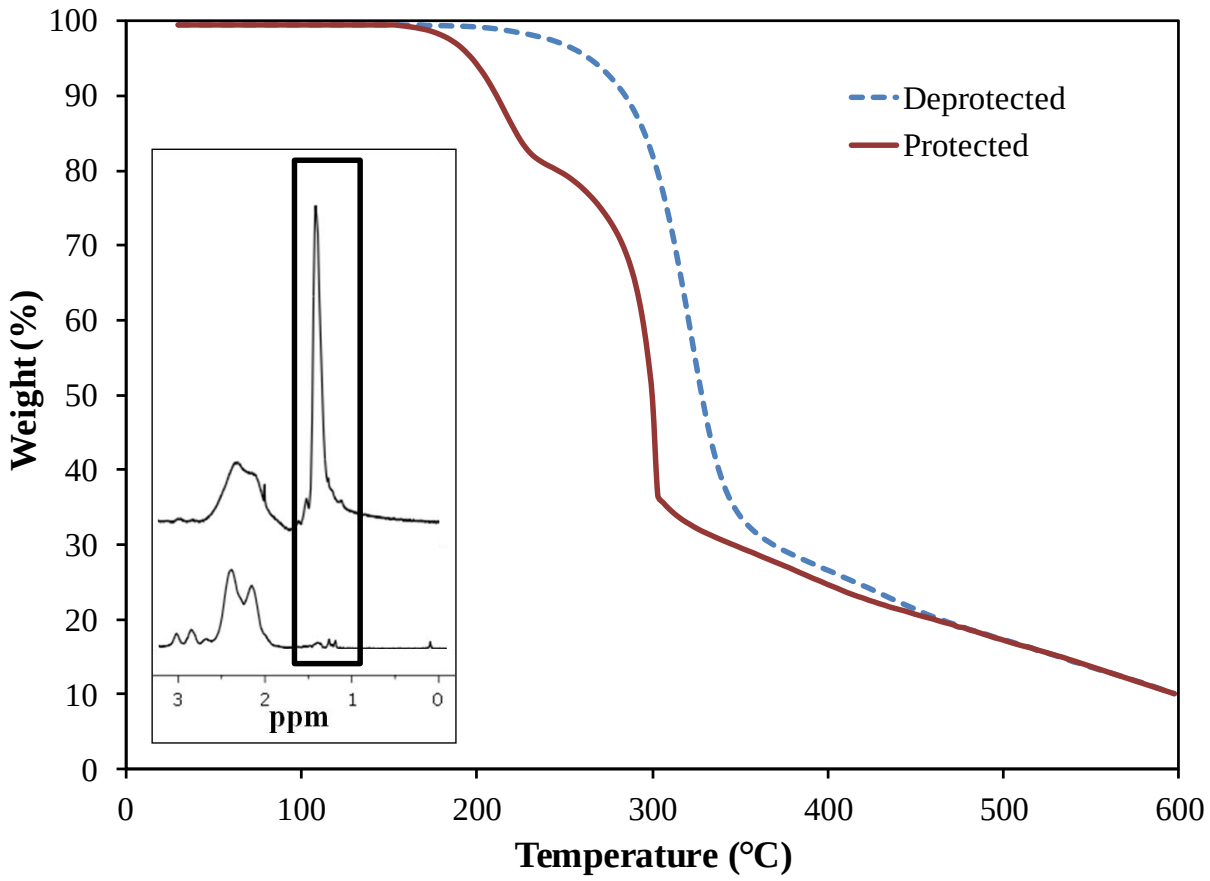

Figure 5.2. TGA of $PAEVIM_{30}$ at a ramp rate of 10 °C/min under nitrogen confirmed successful acid deprotection. ^{1}H NMR insert confirmed disappearance of *t*Boc protecting group.

PVIM required post-polymerization functionalization to conjugate folic acid onto the polymer for potential receptor-mediated gene delivery, and DCC coupling executed effective and efficient conjugation of folic acid onto polymers quantitatively.[52,53] Prior to conjugation onto PVIM, folic acid was reacted with NHS at the γ-carboxylic acid to activate the folic acid ester for nucleophilic attack as shown in Scheme 5.2. NHS-folate reacted with the deprotected copolymer to generate a novel folic acid-functionalized imidazolium copolymer as shown in Scheme 5.3.

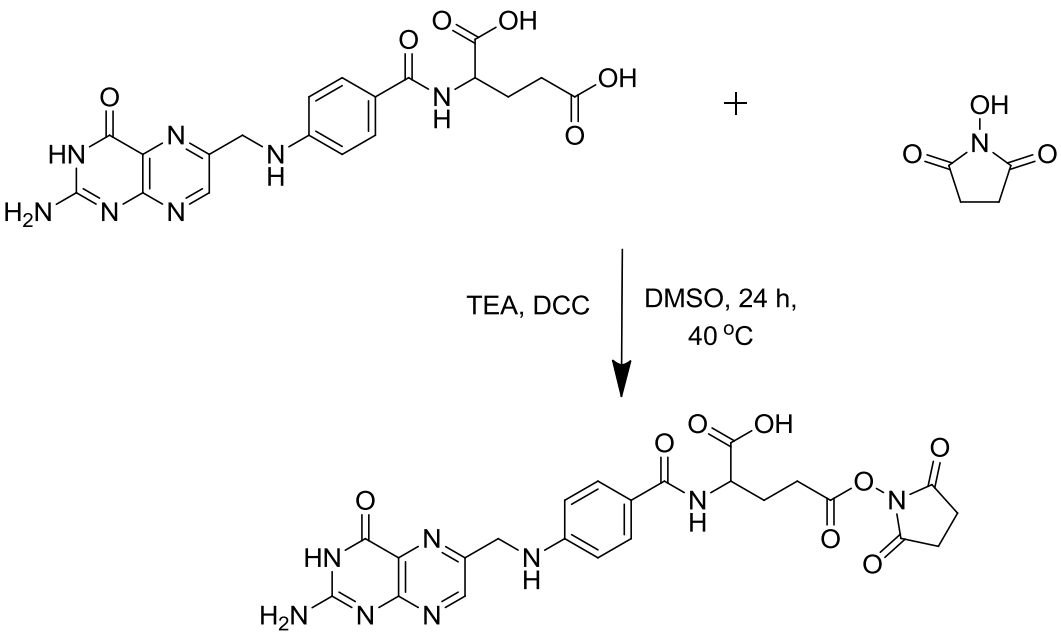

Scheme 5.2. DCC coupling of folic acid with *N*-hydroxysuccinimide (NHS) to generate an activated folate for nucleophilic attack. ^{1}H NMR spectroscopy confirmed successful NHS activation of the γ-carboxylic acid.

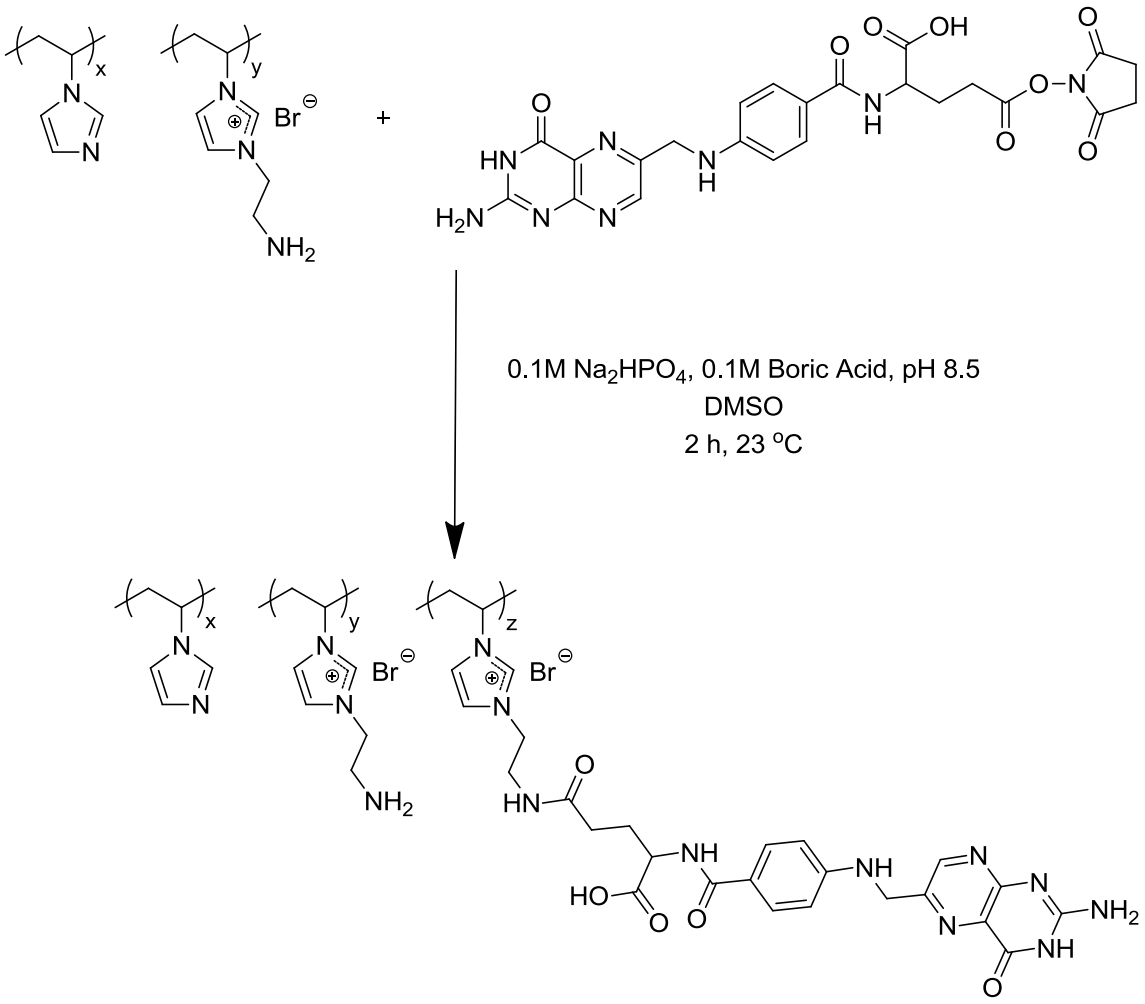

Scheme 5.3. Folic acid conjugation onto an imidazolium copolymer for receptor-mediated nonviral gene delivery.

After removal of excess folic acid, ^{1}H NMR spectroscopy confirmed the presence of folic acid conjugated onto the imidazolium copolymers. Controlling the concentration of folic acid conjugated onto the copolymers proved difficult. Previous studies determined the concentration of folic acid molecules per polymer chain required optimization to produce the high transfection efficiencies for poly(ethylene glycol) (PEG) delivery vehicles.[54] Low folic acid concentrations fail to complex with folate receptors on the cell membrane surface, while higher folic acid concentrations limit polymer solubility in water. Two equivalents of folic acid for copolymer conjugation resulted in < 1 folic acid molecule per polymer chain, while 65 equivalents produced

water-insoluble copolymers. Targeting a concentration of 30 equivalents of folic acid produced water-soluble copolymers with sufficient folic acid functionalization. UV-Vis spectroscopy indicated successful folic acid conjugation onto $PAEVIM_{30}$ and $PAPVIM_{15}$ with an average of 8 and 4 molecules of folic acid per polymer chain, respectively.

DNA gel shift assays determined the amount of copolymer required to effectively bind DNA for luciferase transfection assays. As shown in Figure 5.3, all imidazolium copolymers bound DNA at N/P ratios of 4, compared to previous literature which described N/P ratios above 40 to effectively complex plasmid DNA. Folic acid conjugation did not influence the DNA binding affinity of the copolymers. These quaternized copolymers bound DNA at lower polymer concentrations than hydroxyalkyl analogs due to protonation of the primary amines at physiological pH.[27]

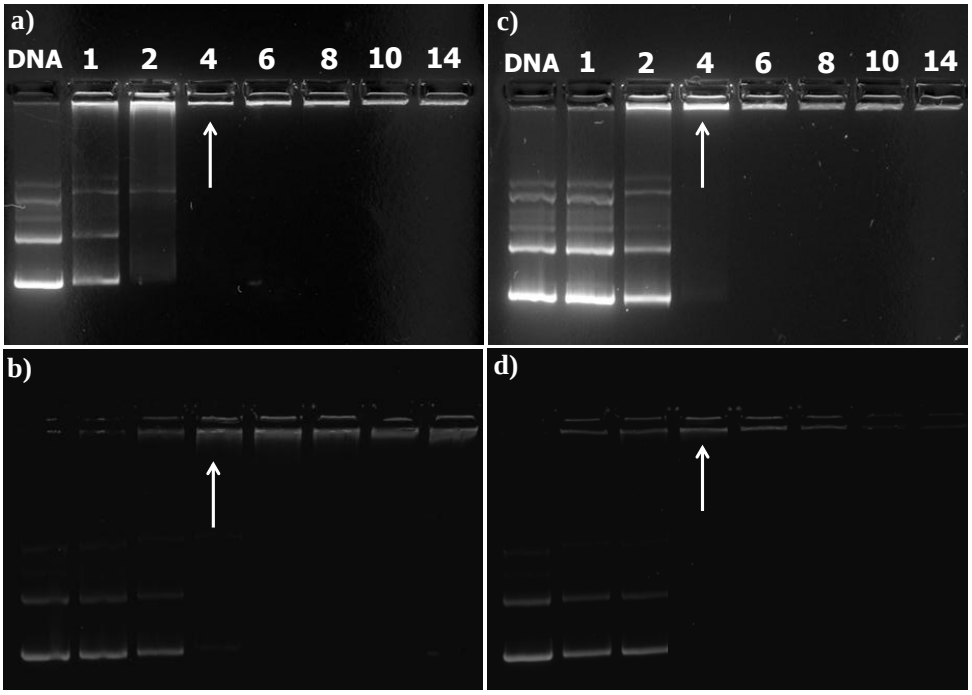

Figure 5.3. Electrophoretic gel shift assay of imidazolium copolymers to determine copolymer–pDNA complexation: a) $PAEVIM_{30}$; b) $PAEVIM_{30}$-FA; c) $PAPVIM_{15}$; d) $PAPVIM_{15}$-FA. Arrows indicate N/P ratio necessary for complete DNA binding.

The MTT conversion assay determined the cytotoxicity as a function of concentration for the copolymers (Figure 5.4).

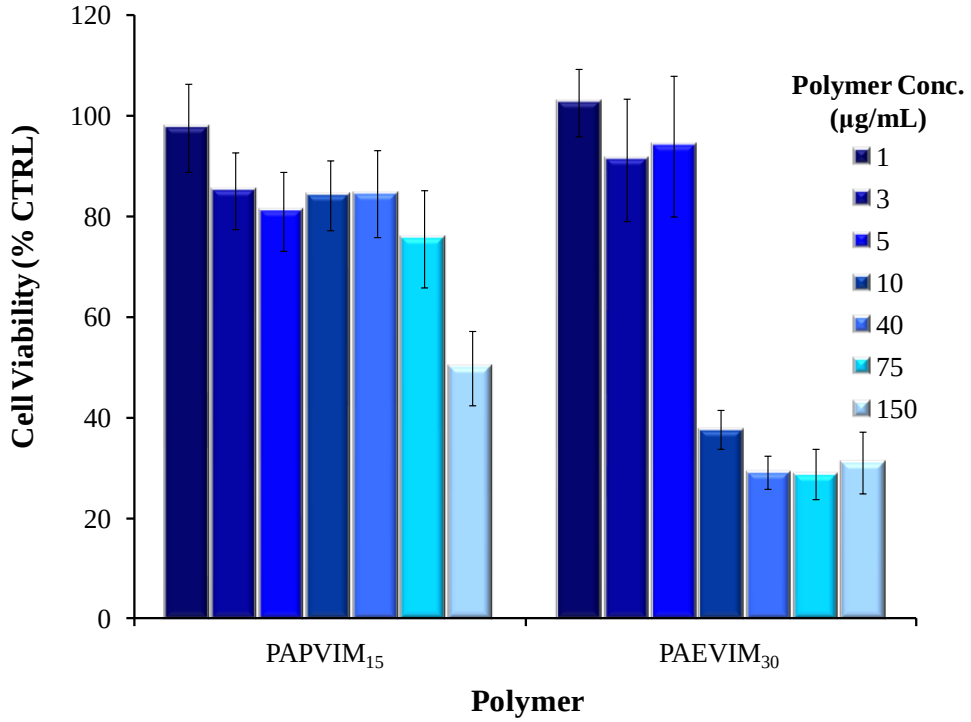

Figure 5.4. HeLa cell viability at various imidazolium copolymer concentrations. Values represent mean ± SD (n = 8).

$PAEVIM_{30}$ exhibited significant cytotoxicity above a polymer concentration of 5 µg/mL and $PAPVIM_{15}$ exhibited toxicity above 75 µg/mL. As expected, cytotoxicity increased with a higher charge density in the copolymer. Kissel et al. determined that a higher concentrations of cationic charge in the copolymer led to greater cytotoxicity.[55] Folic acid functionalization insignificantly impacted the cytotoxicity of the copolymers. Transfection experiments examined the delivery efficiency of the aminated and folic acid-conjugated imidazolium copolymers utilizing N/P ratios that corresponded to nontoxic polymer concentrations.

The luciferase expression assay evaluated the influence of the alkylene spacer and folic acid functionalization on *in vitro* gene delivery. Nucleic acid delivery to HeLa provided a high

concentration of folate receptors on their cell membrane surface compared to non-cancerous cell lines.[56] The unfunctionalized imidazolium copolymers delivered gWiz-Luc inefficiently as shown in Figure 5.5.

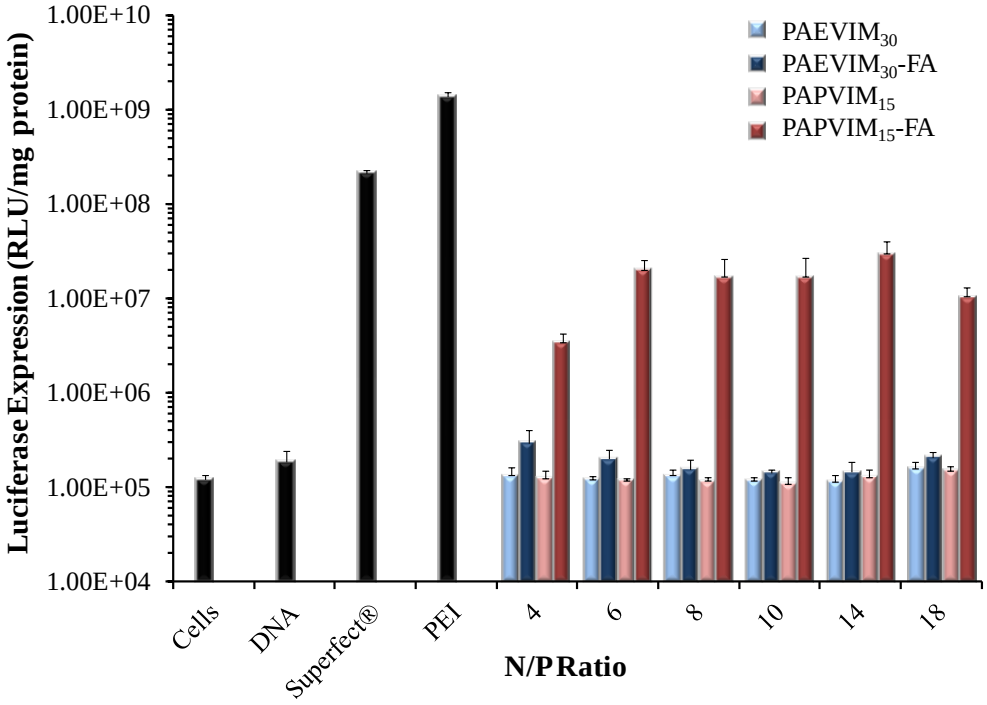

Figure 5.5. In vitro gene transfection efficiency of various imidazolium copolymers as a function of N/P ratio in serum-free media. Nontoxic N/P ratios chosen for luciferase transfection. Values represent mean ± SD (n = 4).

When functionalized with folic acid, $PAEVIM_{30}$-FA exhibited a slight increase in delivery efficiency, but $PAPVIM_{15}$-FA exhibited a dramatic increase in transfection efficiency. $PEVIM_{30}$-FA displayed a 2.5-fold increase in luciferase expression while $PAPVIM_{15}$-FA showed a 250-fold increase in luciferase expression. All copolymers failed to achieve values similar to Superfect or PEI; however, further optimization these copolymers may result in higher transfection values. The mechanism of imidazolium copolymer nonviral delivery and the influence of folic acid on the uptake of the copolymers will be discussed in a future article.

GFP expression experiments complemented the luciferase expression assay. As shown in Figure 5.6, HeLa cells transfected with Superfect™ displayed GFP expression, while cells transfected with PAPVIM$_{30}$-FA transfected significantly more HeLa cells.

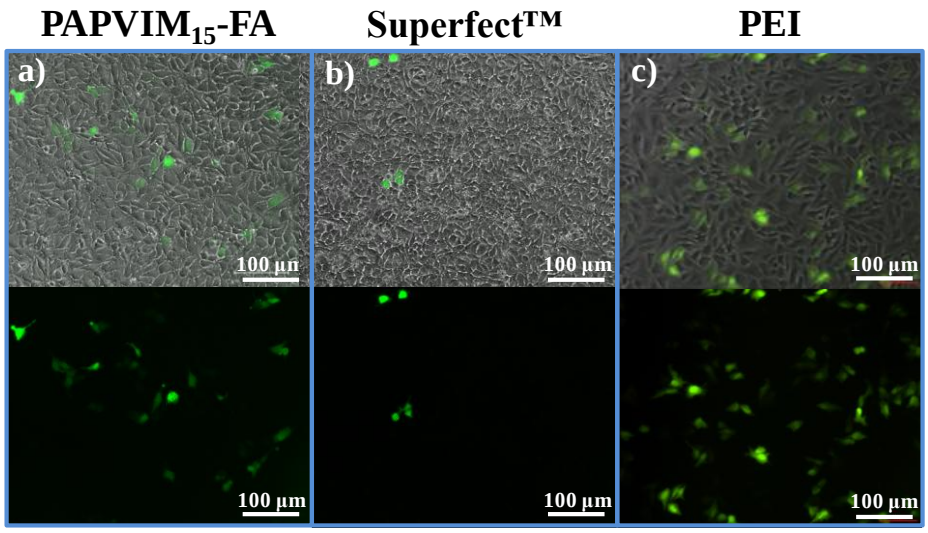

Figure 5.6. Fluorescence microscopy of HeLa cells transfected with gWiz-GFP. The top image is a composite image of HeLa cells with transfected cells and bottom image highlights only cells producing GFP.

Fluorescence microscopy revealed that cells transfected with PAPVIM$_{30}$-FA had substantially less fluorescence intensity compared to cells transfected with Superfect™. This discrepancy is consistent with the difference between the luciferase and GFP expression assays. The cells transfected with Superfect™, despite a lower percentage, produced more luciferase protein than PAPVIM$_{30}$-FA, resulting in higher luciferase expression. Cells transfected with PAPVIM$_{30}$-FA also qualitatively displayed a healthier cell morphology compared to the rounded cell morphology exhibited in HeLa cells transfected with Superfect™.

5.5 *Conclusions*

Synthesis of amine-containing imidazolium copolymers afforded folic acid conjugation onto these macromolecules for the first time and significantly influenced the overall transfection efficiency of DNA delivery vehicles. Conventional free radical polymerization afforded high

molecular weight PVIM for subsequent post-polymerization modification. The synthesis of various *t*Boc-protected amines afforded partial homopolymer quaternization ($\leq$ 30 mol %) with significantly less quaternizing agent and reaction time to obtain charge densities 10-fold higher than previous studies. TGA confirmed acid deprotection generated quantitative removal of the *t*Boc group. DCC coupling executed effective and efficient folic acid conjugation onto the imidazolium copolymers. Low incorporations of folic acid onto the copolymers remained ideal for nonviral gene delivery as large concentrations produced water-insoluble copolymers. The incorporation of folic acid offers a safe and effective avenue to tailor imidazolium copolymer gene delivery in HeLa cells.

5.6 *Acknowledgements*

This material is based upon work supported in part by the Macromolecular Interfaces with Life Sciences (MILES) Integrative Graduate Education and Research Traineeship (IGERT) of the National Science Foundation under Agreement No. DGE-0333378. This material is also based upon work supported in part by the US Army Research Office under Grant No. W911NF-07-1-0452 Ionic Liquids in Electro-Active Devices (ILEAD) MURI. This material is based on work partially supported by the U.S. Army Research Laboratory and the U.S. Army Research Office under the Army Materials Center of Excellence Program, contract W911NF-06-2-0014. This material is based on work supported by the Army Research Office (ARO) under Award No. W911NF-10-1-0307 (DURIP).

5.7 *References*

(1) Ledley, F. D. *Human Gene Therapy* **1995**, *6*, 1129-1144.
(2) Gao, X.; Kim, K.-S.; Liu, D. *The AAPS Journal* **2007**, *9*, E92-E104.
(3) Kamimura, K.; Suda, T.; Zhang, G.; Liu, D. *Pharmaceutical Medicine* **2011**, *25*, 293-306.
(4) Bessis, N.; GarciaCozar, F.; Boissier, M. *Gene Therapy* **2004**, *11*, S10-S17.
(5) Thomas, C. E.; Ehrhardt, A.; Kay, M. A. *Nat. Rev. Genet.* **2003**, *4*, 346-358.
(6) Mintzer, M. A.; Simanek, E. E. *Chem. Rev.* **2008**, *109*, 259-302.
(7) Nguyen, J.; Szoka, F. C. *Acc. Chem. Res.* **2012**, *45*, 1153-1162.

(8) Wong, S. Y.; Pelet, J. M.; Putnam, D. *Prog. Polym. Sci.* **2007**, *32*, 799-837.
(9) Wiethoff, C. M.; Middaugh, C. R. *J. Pharm. Sci.* **2003**, *92*, 203-217.
(10) Yang, S. J.; Lin, F. H.; Tsai, K. C.; Wei, M. F.; Tsai, H. M.; Wong, J. M.; Shieh, M. J. *Bioconjugate Chem.* **2010**, *21*, 679-689.
(11) Thibault, M.; Nimesh, S.; Lavertu, M.; Buschmann, M. D. *Mol. Ther.* **2010**, *18*, 1787-1795.
(12) MacLaughlin, F. C.; Mumper, R. J.; Wang, J.; Tagliaferri, J. M.; Gill, I.; Hinchcliffe, M.; Rolland, A. P. *J. Controlled Release* **1998**, *56*, 259-272.
(13) Schallon, A.; Jérôme, V.; Walther, A.; Synatschke, C. V.; Müller, A. H. E.; Freitag, R. *React. Funct. Polym.* **2010**, *70*, 1-10.
(14) Layman, J. M.; Ramirez, S. M.; Green, M. D.; Long, T. E. *Biomacromolecules* **2009**, *10*, 1244-1252.
(15) Georgiou, T. K.; Vamvakaki, M.; Patrickios, C. S.; Yamasaki, E. N.; Phylactou, L. A. *Biomacromolecules* **2004**, *5*, 2221-2229.
(16) Farrell, L.-L.; Pepin, J.; Kucharski, C.; Lin, X.; Xu, Z.; Uludag, H. *Eur. J. Pharm. Biopharm.* **2007**, *65*, 388-397.
(17) Kwoh, D. Y.; Coffin, C. C.; Lollo, C. P.; Jovenal, J.; Banaszczyk, M. G.; Mullen, P.; Phillips, A.; Amini, A.; Fabrycki, J.; Bartholomew, R. M.; Brostoff, S. W.; Carlo, D. J. *BBA-Gene Struct. Expr.* **1999**, *1444*, 171-190.
(18) Demeneix, B.; Behr, J.; Leaf Huang, M.-C. H.; Ernst, W. In *Advances in Genetics*; Academic Press: 2005; Vol. Volume 53, p 215-230.
(19) Godbey, W. T.; Wu, K. K.; Mikos, A. G. *J. Controlled Release* **1999**, *60*, 149-160.
(20) Wan, L.; You, Y.; Zou, Y.; OupickyÌ • , D.; Mao, G. *J. Phys. Chem. B* **2009**, *113*, 13735-13741.
(21) Lin, C.; Engbersen, J. F. J. *J. Controlled Release* **2008**, *132*, 267-272.
(22) Hemp, S. T.; Smith, A. E.; Bryson, J. M.; Allen, M. H.; Long, T. E. *Biomacromolecules* **2012**, *13*, 2439-2445.
(23) Hemp, S. T.; Allen, M. H.; Green, M. D.; Long, T. E. *Biomacromolecules* **2011**, *13*, 231-238.
(24) Ornelas-Megiatto, C.; Wich, P. R.; Frechet, J. M. J. *J. Am. Chem. Soc.* **2012**.
(25) Asayama, S.; Nishinohara, S.; Kawakami, H. *Bioconjugate Chem.* **2011**, *22*, 1864-1868.
(26) Asayama, S.; Hakamatani, T.; Kawakami, H. *Bioconjugate Chem.* **2010**, *21*, 646-652.
(27) Allen, M. H.; Green, M. D.; Getaneh, H. K.; Miller, K. M.; Long, T. E. *Biomacromolecules* **2011**, *12*, 2243-2250.
(28) Grigsby, C. L.; Leong, K. W. *Journal of The Royal Society Interface* **2010**, *7*, S67-S82.
(29) Prevette, L. E.; Kodger, T. E.; Reineke, T. M.; Lynch, M. L. *Langmuir* **2007**, *23*, 9773-9784.
(30) Yue, X.; Qiao, Y.; Qiao, N.; Guo, S.; Xing, J.; Deng, L.; Xu, J.; Dong, A. *Biomacromolecules* **2010**, *11*, 2306-2312.
(31) Kopatz, I.; Remy, J.-S.; Behr, J.-P. *The Journal of Gene Medicine* **2004**, *6*, 769-776.
(32) Khalil, I. A.; Kogure, K.; Akita, H.; Harashima, H. *Pharmacological reviews* **2006**, *58*, 32-45.
(33) Leamon, C. P.; Low, P. S. *Drug Discovery Today* **2001**, *6*, 44-51.
(34) Gabrielson, N. P.; Pack, D. W. *J. Controlled Release* **2009**, *136*, 54-61.
(35) Mansouri, S.; Cuie, Y.; Winnik, F.; Shi, Q.; Lavigne, P.; Benderdour, M.; Beaumont, E.; Fernandes, J. C. *Biomaterials* **2006**, *27*, 2060-2065.

(36) Chan, P.; Kurisawa, M.; Chung, J. E.; Yang, Y. Y. *Biomaterials* **2007**, *28*, 540-549.
(37) Benoit, D. S. W.; Srinivasan, S.; Shubin, A. D.; Stayton, P. S. *Biomacromolecules* **2011**, *12*, 2708-2714.
(38) Lee, R. J.; Huang, L. *J. Biol. Chem.* **1996**, *271*, 8481-8487.
(39) Sulistio, A.; Lowenthal, J.; Blencowe, A.; Bongiovanni, M. L.; Ong, L.; Gras, S. L.; Zhang, X.; Qiao, G. G. *Biomacromolecules* **2011**.
(40) Guo, W.; Lee, R. *The AAPS Journal* **1999**, *1*, 20-26.
(41) Behr, J. P. *CHIMIA International Journal for Chemistry* **1997**, *51*, 1-2.
(42) Akinc, A.; Thomas, M.; Klibanov, A. M.; Langer, R. *The Journal of Gene Medicine* **2004**, *7*, 657-663.
(43) Midoux, P.; Pichon, C.; Yaouanc, J.-J.; Jaffrès, P.-A. *British Journal of Pharmacology* **2009**, *157*, 166-178.
(44) Midoux, P.; Monsigny, M. *Bioconjugate Chem.* **1999**, *10*, 406-411.
(45) Benns, J. M.; Choi, J.-S.; Mahato, R. I.; Park, J.-S.; Kim, S. W. *Bioconjugate Chem.* **2000**, *11*, 637-645.
(46) Mishra, S.; Heidel, J. D.; Webster, P.; Davis, M. E. *J. Controlled Release* **2006**, *116*, 179-191.
(47) Yang, Y.; Xu, Z.; Jiang, J.; Gao, Y.; Gu, W.; Chen, L.; Tang, X.; Li, Y. *J. Controlled Release* **2008**, *127*, 273-279.
(48) Green, M. D.; Long, T. E. *Polym. Rev.* **2009**, *49*, 291-314.
(49) Bara, J. E.; Noble, R. D.; Gin, D. L. *Ind. Eng. Chem. Res.* **2009**, *48*, 4607-4610.
(50) Asayama, S.; Sekine, T.; Kawakami, H.; Nagaoka, S. *Bioconjugate Chem.* **2007**, *18*, 1662-1667.
(51) Busetto, L.; Cristina Cassani, M.; Femoni, C.; Macchioni, A.; Mazzoni, R.; Zuccaccia, D. *J. Organomet. Chem.* **2008**, *693*, 2579-2591.
(52) Stella, B.; Arpicco, S.; Peracchia, M. T.; Desmaële, D.; Hoebeke, J.; Renoir, M.; D'Angelo, J.; Cattel, L.; Couvreur, P. *J. Pharm. Sci.* **2000**, *89*, 1452-1464.
(53) Liu, M.; Fréchet, J. M. J. *Pharmaceutical science & technology today* **1999**, *2*, 393-401.
(54) Canal, F.; Vicent, M. J.; Pasut, G.; Schiavon, O. *J. Controlled Release* **2010**, *146*, 388-399.
(55) Fischer, D.; Li, Y.; Ahlemeyer, B.; Krieglstein, J.; Kissel, T. *Biomaterials* **2003**, *24*, 1121-1131.
(56) Lee, R. J.; Low, P. S. *BBA-Biomembranes* **1995**, *1233*, 134-144.

Chapter 6: Hydroxyalkyl-Containing Imidazolium Homopolymers: Correlation of Structure with Conductivity

(In preparation for *Macromolecules*)

Michael H. Allen, Jr., Sharon Wang,[‡] Sean T. Hemp, Karen I. Winey,[‡] and Timothy E. Long

Macromolecules and Interfaces Institute, Department of Chemistry, Virginia Tech, Blacksburg, VA 24061

[‡]*Department of Material Science and Engineering, University of Pennsylvania, Philadelphia, PA 19104*

6.1 *Abstract*

Conventional free radical polymerization of (hydroxy)alkyl-containing vinylimidazolium ionic liquid monomers generated high molecular weight polymers to relate chemical composition to macromolecular properties. Varying substituent chain length and functionality of the imidazolium polymerized ionic liquids (PILs) significantly influenced numerous polymer properties. Incorporation of a hydroxyl group at the terminus of the alkyl substituent lowered the glass transition temperature (T_g) of the PILs approximately 50 °C and increased the homopolymer thermal stability compared to the respective alkyl analog. Anion exchange provided a further avenue to further tailor homopolymer transition temperatures; counterion exchange from a bromide (Br^-) anion to a bis(trifluoromethanesulfonyl)imide (Tf_2N^-) anion lowered the T_g's and improved the thermal stabilities of the PILs. X-ray scattering demonstrated that the (hydroxy)alkyl chain length influenced backbone-to-backbone spacing, and more importantly, showed hydroxyl incorporation diminished the nanophase-separated morphology present in the alkyl analogs. Ionic conductivity of the imidazolium homopolymers increased over an order of magnitude upon hydroxyl group incorporation due to the polarity of the hydroxyl groups solvating the homopolymer electrostatic interactions. Effectively controlling the homopolymer chemical composition enabled the tuning of thermal properties and polymer morphology for improved ionic conductivity.

6.2 *Introduction*

Imidazolium ionic liquid monomers, defined as organic salts with a melting point below 100 °C, remain an area of intense focus.[1-4] These monomers display advantageous properties including high chemical and thermal stability, negligible volatility, and high ionic conductivity.[5-8] The diversity of ionic liquid compositions enables the synthesis of "designer" molecules with tailored physical properties through judicious anion and cation selection. Alkyl-functionalized imidazolium ionic liquids have received widespread interest,[9-14] and recent attention has focused on the development of hydroxyl- and ether-functionalized ionic liquids.[15,16] Afonso et al. reported that ether-containing imidazolium ionic liquids displayed reduced viscosities compared to alkylated analogs.[17] Molecular dynamics simulations and X-ray crystallography determined ether chains and hydroxyl-containing substituents formed intra- and inter-molecular hydrogen bonds with the acidic hydrogen on the C2 position of the imidazolium cation.[18-21] This interaction weakened the specific cation-anion interactions, which reduced viscosity and increased conductivity. Furthermore, Russina and Triolo demonstrated that the incorporation of polar substituents in room-temperature imidazolium ionic liquids disrupted the nanophase-separated morphology for alkylated analogs.[19,22,23] Density functional theory calculations of hydroxyl-containing imidazolium ionic liquids also supported the observations of Russina and Triolo, and these calculations suggested that the polarity of hydroxyl substituents reduces cation-anion electrostatic interactions.[24,25]

Polymerization of ionic liquid monomers enables the design of conductive membranes suitable for electroactive devices,[26,27] gas separation,[28,29] and microwave-absorbing materials.[30] In polymerized ionic liquids (PILs), the cation or anion remains covalently bound to the macromolecule, thus restricting its mobility. The mobility restriction advantageously prevents leakage of liquid electrolytes in electrochemical devices; however, the reduction in ionic

conductivity proves problematic. Anion selection remains a highly researched component of cationic PILs to improve macromolecular ionic conductivity.[1,31-37] Elabd et al. examined various counterions in a methacrylate-based imidazolium PIL from a tetrafluoroborate (BF_4^-) anion to a bis(trifluoromethanesulfonyl)imide (Tf_2N^-) anion.[32] The bulkier Tf_2N^- anion significantly reduced the glass transition temperature (T_g) and increased ionic conductivity. Long et al. also observed a similar impact on T_g and demonstrated enhanced thermal stability through exchangeable anion selection in alkyl-substituted 1-vinylimidazolium (AVIM) PILs.[38] Further studies confirmed that counterion exchange also influenced ionic conductivity due to anion size and symmetry as well as ion pair dissociation energy.[39]

Imidazolium cation structure also affects the ionic conductivity of cationic polyelectrolytes. Various imidazolium-containing ionic liquid monomers include 1--vinylimidazoliums,[37,38,40] styrenics,[31,41] and (meth)acrylics.[27,42,43] Ohno et al. synthesized and polymerized substituted VIM monomers for electroactive materials.[37] Spacing the imidazolium cation further from the polymer backbone with an oligo(ethylene oxide) chain improved homopolymer ionic conductivity 300-fold. Gibson et al. polymerized acrylate-functionalized imidazolium ionic liquids containing a diethyleneoxy or butyl substituent on the imidazolium cation.[42] The diethyleneoxy substituent displayed higher ionic conductivities than the butyl substituent due to a lower binding energy between the imidazolium ring and the counterion. Previously, our research group examined functionalized VIM with various alkyl substituents (ethyl, butyl, and octyl chains) and found increased alkyl chain length increased the backbone-to-backbone distance. This increased spacing resulted in a reduced, T_g-independent, ionic conductivity. Modifying the imidazolium macromolecules through functional substituent selection enabled the tuning of polymer thermal properties and ionic conductivity without the

addition of low molar mass plasticizers. Although effective in reducing T_g and subsequently increasing ionic conductivity, evaporation, leaching, and degradation commonly plague the use of low molar mass plasticizers for advanced electroactive membranes.[44]

In this article, we synthesized for the first time VIM ionic liquid monomers functionalized with various hydroxyalkyl groups to investigate the impact of functional substituents on PVIM thermal properties, morphology, and ionic conductivity. Conventional free radical polymerization of AVIM and hydroxyalkyl-substituted 1-vinylimidazolium (HAVIM) monomers with variable substituent length afforded a series of homopolymers for structure-property characterization. As expected, anion exchange from a bromide counterion (Br^-) to a Tf_2N^- counterion lowered homopolymer T_g and increased thermal stability. X-ray scattering investigated the relationship between chemical structure and morphology on ionic conductivity. Facile modification of imidazolium macromolecules enables the future design of improved ionically conductive polyelectrolytes for advanced applications including electroactive devices and gas separation membranes.

6.3 *Experimental Section*

6.3.1 Materials

Bromoethane (98%, Sigma-Aldrich), 1-bromopropane (99%, Aldrich), 1-bromohexane (98%, Aldrich), (99%, Aldrich), 2-bromoethanol (95%, Aldrich), 3-bromo-1-propanol (97%, Aldrich), 6-bromo-1-hexanol (97%, Aldrich), and 8-bromo-1-octanol (95%, Aldrich) were used as received. 1-Vinylimidazole (VIM, 99%, Aldrich) was distilled under reduced pressure. 2,2'-Azobisisobutryonitrile (AIBN, 99%, Sigma-Aldrich) was recrystallized from methanol. Lithium bis(trifluoromethane)sulfonimide ($LiTf_2N$, $\geq$ 99%, Aldrich) and lithium bromide ($\geq$ 99%, Aldrich) were used as received. All solvents were obtained from Fisher Scientific and used as received.

6.3.2 Analytical Techniques

^{1}H NMR spectroscopy (Varian Inova, 400 MHz, CD_3OD) confirmed monomer and polymer structure. Thermal analysis of the various imidazolium polymers was performed on a TA Instruments thermogravimetric analyzer (TGA) Hi-Res 2950 with a heating rate of 10 °C/min from 23 °C to 600 °C under a nitrogen atmosphere. Differential scanning calorimetry (DSC, TA instruments, Q1000, 10 °C/min) utilizing a heat/cool/heat method to erase polymer thermal history determined thermal transitions. Aqueous size exclusion chromatography (SEC, flow rate of 0.8 mL/min through two Waters Ultrahydrogel Linear and one Waters Ultrahydrogel 250 columns, solvent: 54/23/23 H_2O/MeOH/acetic acid (v/v/v %), 0.1 M $NaNO_3$) equipped with a Waters 1515 isocratic HPLC pump, a Waters 717plus autosampler, a Wyatt miniDAWN multiangle laser light scattering (MALLS, wavelength = 690 nm), and a Waters 2414 differential refractive index detector determined polymer molecular weights relative to poly(ethylene oxide) standards. Prior to SEC analysis, polymer samples were screened with dynamic light scattering (DLS, Malvern Zetasizer NanoZS) to confirm the absence of polymer aggregates in the SEC mobile phase.

In-plane conductivities were measured using a four-electrode method with a Metrohm Autolab 302N impedance analyzer equipped with a custom-made Teflon-coated stainless steel cell over a frequency range of 10^{-1} Hz to 10^6 Hz at 200 mV. An ESPEC BTL-433 environmental chamber controlled temperature up to 135 °C and relative humidity (10% RH below 95 °C, <10% RH above 95 °C). Samples were equilibrated for 2 h prior to each measurement. Polymer films were cast from a 30 wt % solution (acetone or methanol) onto a Mylar® substrate and dried under ambient conditions for 48 h followed with drying under reduced pressure for an additional 48 h. The films were annealed for 24 h at 135 °C immediately prior to impedance measurements. The impedance or resistance, *R*, was measured between the two inner reference electrodes while

the alternating current was applied to the outer two electrodes. The x-intercept of the semicircle of the Nyquist plot in the Autolab Nova software suite determined the resistance to calculate the conductivity of the polymer film. The equation, $\sigma = L/AR$, where L is the distance between the inner electrodes, and A is the cross-sectional area of the polymer film calculated ionic conductivity. Five measurements were performed at each temperature (10 °C/step) and the values reported were an average of these steady-state measurements.

Utilizing the Origin Lab 7 software suite, the temperature-dependent ionic conductivities of the imidazolium homopolymers were fit with the Vogel-Fulcher-Tammann (VFT) equation:

$$\sigma(T) = \sigma_0 \exp\left(\frac{-B}{T - T_0}\right) \quad (1)$$

In the VFT equation, σ_0 (S cm^{-1}) is the infinite temperature conductivity, B (K) is a fitting parameter related to the Arrhenius activation energy, and T_0 is the Vogel temperature; therefore, the VFT equation requires three fitting parameters. To confirm the accuracy of the fitting parameters, Elabd et al.[39] reduced the number of fitting parameters in Eq. (1) converting the equation into the following:

$$\sigma(T) = \sigma(T_r) \exp\left(-B\left(\frac{1}{T - T_0} - \frac{1}{T_r - T_0}\right)\right) \quad (2)$$

where $\sigma(T_r)$ is the ionic conductivity at a determined reference temperature (135 °C). The replacement of σ_0 with $\sigma(T_r)$ reduced the number of fitting parameters from three to two. Additionally, researchers utilize the Williams-Landel-Ferry (WLF) equation to fit temperature-dependent ionic conductivities of polyelectrolytes.

$$\log\left(\frac{\sigma(T)}{\sigma(T_g)}\right) = \frac{C_1^g (T - T_g)}{C_2^g + (T - T_g)} \quad (3)$$

In the WLF equation, $\sigma(T)$ and $\sigma(T_g)$ are the conductivities at a temperature *T*, and at the glass transition temperature (T_g) respectively. The fitting parameters C_1^g and C_2^g (K) were determined utilizing Elabd et al. previously published method.[39] The WLF and VFT are mathematically equivalent where $B = 2.303\, C_1^g\, C_2^g$ and $T_0 = T_g - C_2^g$.

6.3.3 Synthesis of Imidazolium Monomers

The 1-alkyl-3-vinylimidazolium bromide (AVIM-Br) monomers were synthesized according to previous literature.[38,45,46] The 1-hydroxyalky-3-vinylimidazolium (HAVIM) monomer synthesis required a modified procedure. In a typical reaction, VIM (1.00 g, 10.6 mmol), 2-bromoethanol (1.46 g, 11.7 mmol) and acetonitrile (2.46 g, 61.4 mmol) were charged to a 25-mL, round-bottomed flask equipped with a stir bar and stirred for 48 h at 40 °C. Acetonitrile and excess 2-bromoethanol were removed under reduced pressure and a yellow oil was precipitated into ethyl acetate. After three washings with ethyl acetate, the yellow oil was dried under reduced pressure overnight (1.40 g, 70% yield). The monomer was redissolved in deionized water (5.00 g, 278 mmol H_2O) and slowly added dropwise to an aqueous solution of $LiTf_2N$ (3.06 g, 10.7 mmol $LiTf_2N$ in 5.00 g, 278 mmol H_2O). The monomer 1-hydroxyethyl-3-vinylimidazolium bis(trifluoromethane)sulfonimide precipitated as a colorless oil (HEVIM-Tf_2N) and was washed with deionized water five times to remove residual salt (2.44 g, 91% yield). ^{1}H NMR (CD_3OD):δ 9.23 (t, 1H), 7.99 (d, 1H), 7.73 (d, 1H), 7.25 (dd, 1H), 5.91 (dd, 1H), 5.44 (dd, 1H), 4.33 (t, 2H), 3.89 (t, 2H). ^{13}C NMR (CD_3OD):δ 135.4 (s), 128.3 (s), 123.4 (s), 119.0 (s), 108.5 (s), 59.4 (s), 52.2 (s). ^{19}F NMR (CD_3OD):δ -80.7 (s). ESI-mass spectra for $C_8H_{13}N_2O$: Calculated: 139.0866 g/mol; Found: 139.0858 g/mol.

1-Hydroxyproply-3-vinylimidazolium Tf_2N (HPVIM-Tf_2N). ^{1}H NMR (CD_3OD):δ 7.98 (d, 1H), 7.74 (d, 1H), 7.22 (dd, 1H), 5.90 (dd, 1H), 5.44 (dd, 1H), 4.37 (t, 2H), 3.61 (t, 2H), 2.10 (tt, 2H). ^{13}C NMR (CD_3OD):δ 128.3 (s), 123.1(s), 119.3(s), 108.4 (s), 57.5(s), 47.0 (s), 31.8 (s). ^{19}F NMR (CD_3OD):δ -80.1 (s). ESI-mass spectra for $C_8H_{13}N_2O$: Calculated: 153.1028 g/mol; Found: 153.1020 g/mol.

1-Hydroxyhexyl-3-vinylimidazolium Tf_2N (HHVIM-Tf_2N). ^{1}H NMR (CD_3OD):δ 9.21(s, 1H), 7.96 (s, 1H), 7.73 (s, 1H), 7.21 (dd, 2H), 5.89 (dd, 1H), 5.43 (dd, 1H), 4.25 (t, 2H), 3.55 (t, 2H), 1.93 (t, 2H), 1.55 (m, 2H), 1.40 (dd, 4H). ^{13}C NMR (CD_3OD):δ 134.9 (s), 128.4 (s), 123.0 (s), 119.3 (s), 108.5 (s), 61.3 (s), 49.8 (s), 31.8 (s), 29.4 (s), 25.2 (s). ^{19}F NMR (CD_3OD):δ -80.7 (s). ESI-mass spectra for $C_{11}H_{19}N_2O$: Calculated: 195.1497 g/mol; Found: 195.1485 g/mol.

1-Hydroxyoctyl-3-vinylimidazolium Tf_2N (HOVIM-Tf_2N). ^{1}H NMR (CD_3OD):δ 9.20 (d, 1H), 7.95 (d, 1H), 7.72 (d, 1H), 7.21 (dd, 1H), 5.89 (dd, 1H), 5.42 (dd, 1H), 4.24 (m, 2H), 3.53 (t, 2H), 1.93 (d, 2H), 1.51 (d, 2H), 1.36 (dt, 8H). ^{13}C NMR (CD_3OD):δ 134.8 (s), 128.3 (s), 123.0 (s), 119.3 (s), 108.5 (s), 61.5 (s), 49.8 (s), 32.1 (s), 29.4 (s), 28.8 (s), 28.6 (s), 25.7 (s), 25.4 (s). ^{19}F NMR (CD_3OD):δ -80.6 (s). ESI-mass spectra for $C_{13}H_{23}N_2O$: Calculated: 223.1810 g/mol; Found: 223.1798 g/mol.

6.3.4 Synthesis of Imidazolium Polymers and Anion Exchange

The AVIM-Br monomers were polymerized and underwent anion exchange according to previous literature.[38,45,46] The HAVIM-Tf_2N monomers were polymerized with a modified procedure. In a representative conventional free radical polymerization, HEVIM-Tf_2N (0.500 g, 11.9 mmol), AIBN (1.98 mg, 11.9 μmol), and DMSO (2.00 g, 25.6 mmol) were charged to a 25-mL, round bottomed-flask equipped with stir bar. The reaction was sparged with argon at room temperature for 30 min. and immersed in a 65 °C thermostated oil bath for 24 h. The polymer was precipitated into ethyl acetate, redissolved in methanol, and dialyzed against methanol

(MWCO = 3500 g/mol) for 48 h to remove residual monomer. The polymer was dried under reduced pressure for 24 h (340 mg, 68 % yield).

Poly(HEVIM-Tf_2N) (340 mg, 0.811 μmol) was dissolved in methanol (5.00 g, 156 mmol) with lithium bromide (5.00 g, 57.6 mmol) and dialyzed against a 1 M LiBr-methanol solution for five days. The polymer was then dialyzed against deionized water for 48 h to remove excess LiBr. The polymer was freeze dried to remove water for 48 h. Silver nitrate titrations confirmed the absence of excess salt and XPS analysis determined less than 0.2% Tf_2N remained. ^{1}H NMR confirmed polymer structures. Polymer molecular weights relative to poly(ethylene oxide) standards were determined utilizing aqueous SEC.

6.3.5 X-ray scattering

X-ray scattering was performed using a multi-angle X-ray scattering (MAXS) system. The MAXS system generates Cu-Kα X-rays, λ = 0.154 nm, from a Nonius FR 591 rotating anode operated at 40 kV and 85 mA. The bright, highly collimated beam was obtained via Osmic Max-Flux optics and pinhole collimation in an integral vacuum system. The scattering data were collected using a Bruker Hi-Star two-dimensional detector with a sample-to-detector distance of 11 cm and analyzed using Datasqueeze software. The intensities were corrected for primary beam intensity, and background scattering was subtracted. The isotropic 2-D scattering patterns were then azimuthally integrated to yield intensity versus scattering angle (q) profiles. The intensities are reported in arbitrary units (a.u.).

Samples were prepared for room temperature X-ray scattering utilizing the casting conditions described above for impedance spectroscopy. Room-temperature data were collected on bare samples. For elevated temperature X-ray scattering experiments, thin strips of cast poly(HAVIM-Tf_2N) samples were cut and inserted into 1 mm glass capillaries, which were then flame sealed. Variable temperature data were collected *in situ* using a Linkham HFS91

temperature controller, which has a temperature resolution of ±0.1 °C. Data were collected at temperatures ranging from 10 °C to 125 °C, with an additional scan at 25 °C to assess sample recovery, at heating and cooling rates of 10 °C/min. Samples were equilibrated at desired temperatures for 15 min before collecting X-ray data for 30 min.

6.4 *Results and Discussion*

The quaternization reaction of VIM with various bromoalcohols afforded a series of HAVIM-Br monomers shown in Scheme 6.1.

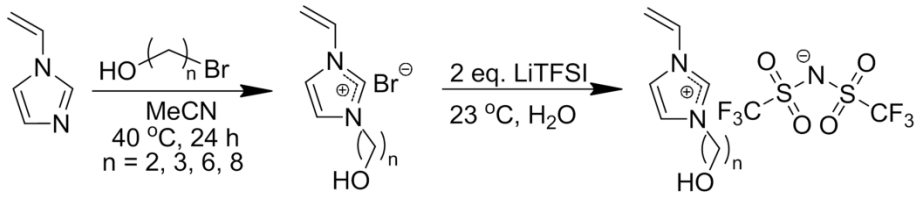

Scheme 6.1. Synthesis of HAVIM ionic liquid monomers with subsequent anion exchange.

Functionalization of VIM with 4-bromo-1-butanol resulted in THF formation which prevented quaternization of the imidazole ring with a hydroxybutyl substituent.[47] The HAVIM-Br monomers were further modified through with anion exchange of a Br^- counterion to a less basic, more hydrophobic Tf_2N^- counterion to tune thermal properties and ionic conductivity. DSC detected the thermal transitions of the HAVIM-Br monomers (Table 6.1; the ionic liquids exhibited T_g's between -58 °C through -42 °C and melting points below 60 °C. Exchange of the Br^- anion to Tf_2N^- lowered T_g's approximately 30 °C. Widespread research on AVIM-Br monomers determined the melting points of shorter chain substituents remained above 100 °C (ethyl, propyl) while anion exchange to Tf_2N^- lowered the T_g's to similar temperatures as the HAVIM-Tf_2N monomers.[37,48]

Table 6.1. Thermal analysis of vinylimidazolium monomers.

Abbreviation	Hydroxyalkyl Substituent	Anion	T_g (°C)	T_m (°C)
HEVIM-Br	Ethyl	Bromide	-42	25
HEVIM-Tf_2N	Ethyl	Tf_2N	-73	ND
HPVIM-Br	Propyl	Bromide	-43	55
HPVIM-Tf_2N	Propyl	Tf_2N	-73	ND
HHVIM-Br	Hexyl	Bromide	-58	37
HHVIM-Tf_2N	Hexyl	Tf_2N	-74	ND
HOVIM-Br	Octyl	Bromide	-53	41
HOVIM-Tf_2N	Octyl	Tf_2N	-84	ND

ND = Not Detected Utilizing DSC Thermal Analysis (-150 °C – 200 °C)

Conventional free radical polymerization of the vinylimidazolium monomers (Scheme 6.2a and b) afforded homopolymers with various alkyl and hydroxyalkyl substituents.

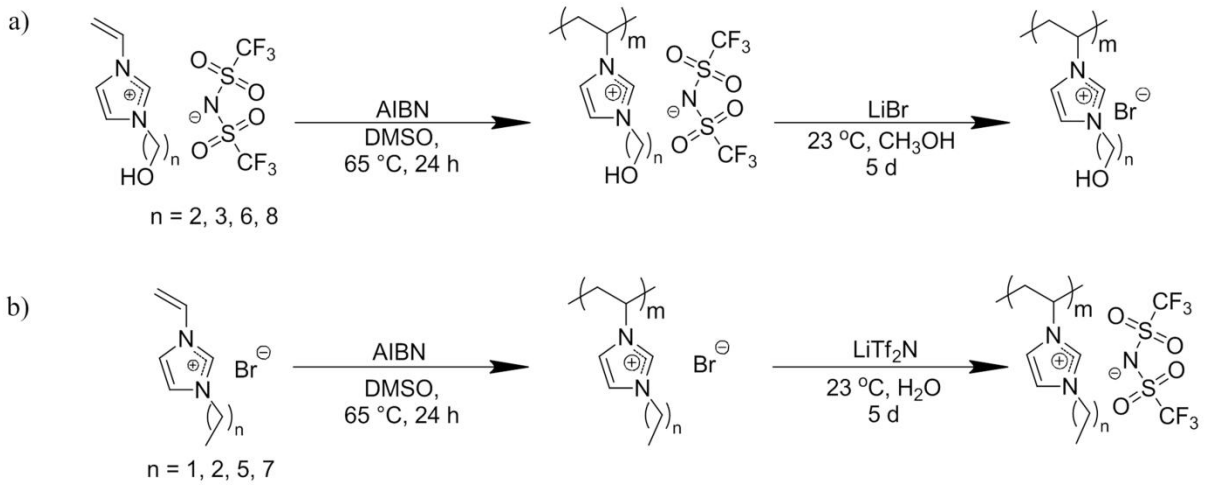

Scheme 6.2. Conventional free radical homopolymerization of a) HAVIM and b) AVIM ionic liquid monomers with subsequent anion exchange.

The AVIM-Br monomers homopolymerized according to previous literature procedures, and the polymeric precursor was susceptible to anion exchange with $LiTf_2N$ to generate AVIM-Tf_2N homopolymers.[38] Free radical homopolymerization of HAVIM-Br monomers produced an insoluble, covalently crosslinked network. Heating poly(HAVIM-Br) to 65 °C in DMSO

(homopolymerization conditions) failed to produce an insoluble, crosslinked polymer. Thermoset generation during free radical polymerization suggested a counterion- and substituent-dependent reaction mechanism; however, the exact mechanism remains undetermined. Anion exchange to HAVIM-Tf_2N and subsequent polymerization prevented network formation. We propose an acid impurity in DMSO catalyzes an elimination reaction which generates a difunctional imidazolium monomer which would presumably promote crosslinking (Supporting Information). Post-polymerization anion exchange from Tf_2N^- to Br^- provided an alternative synthetic route to generate poly(HAVIM-Br) thermoplastics.

Aqueous SEC determined imidazolium homopolymer molecular weights relative to poly(ethylene oxide) standards. Previously, we reported that column interactions and polymer aggregation in SEC mobile phases prevented molecular weight analysis of various imidazole- and imidazolium-containing polymers. The AVIM-Br homopolymers remained difficult to analyze with SEC due to either homopolymer aggregation in various aqueous media or column interactions in organic solvents (DMF, THF) that prevented homopolymer elution. Conversely, HAVIM-Br homopolymers exhibited an absence of polymer aggregates in a 54/23/23 (v/v/v %) water/methanol/acetic acid co-solvent with 0.1 M $NaNO_3$ and successfully eluted from the SEC columns as shown in Figure 6.1

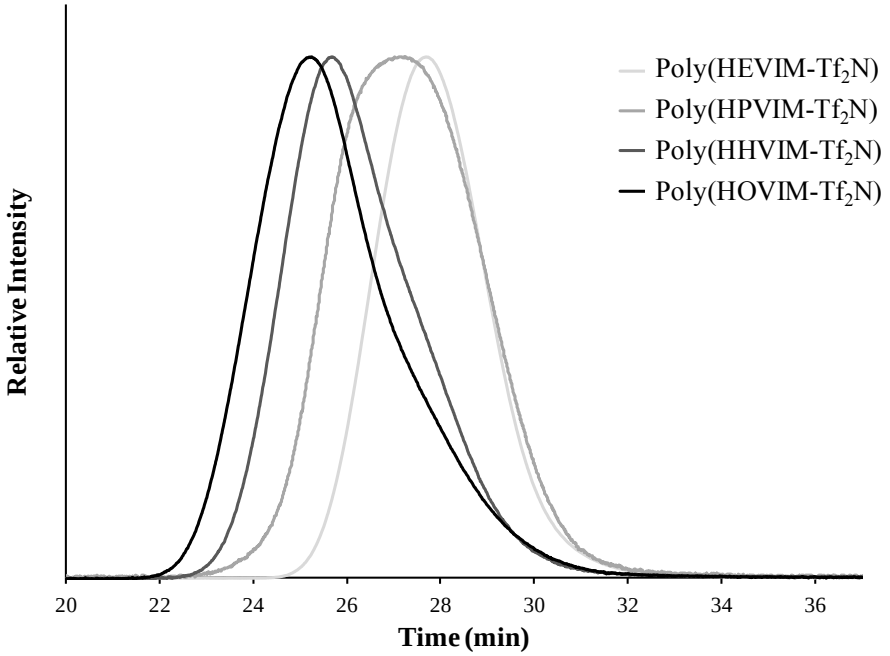

Figure 6.1. Aqueous SEC dRI chromatograms of HAVIM-Tf_2N homopolymers.

The number-average molecular weights (M_n) increased with increasing substituent chain length and all polydispersity indices (PDI) were consistent with a conventional free radical polymerization (Table 6.2). Despite obtaining only HAVIM-Br homopolymer molecular weights, identical polymerization conditions for AVIM-Br homopolymerizations presumably afforded similar polymer molecular weights.

Table 6.2. Relative molecular weights of HAVIM-Tf_2N homopolymers.

Polymer	M_n (g/mol)	M_w (g/mol)	PDI
Poly(HEVIM-Tf_2N)	26,000	37,200	1.43
Poly(HPVIM-Tf_2N)	24,000	38,600	1.61
Poly(HHVIM-Tf_2N)	50,000	75,500	1.51
Poly(HOVIM-Tf_2N)	57,000	123,700	2.17

SEC Conditions: 54/23/23 H_2O/MeOH/acetic acid (v/v/v %), 0.1 M $NaNO_3$

Counterion selection significantly impacts the thermal properties of cationic polyelectrolytes.[31,32,35] TGA determined the influence of counterion selection and functional substituent composition on PIL weight loss as a function of temperature (Figure 6.2).

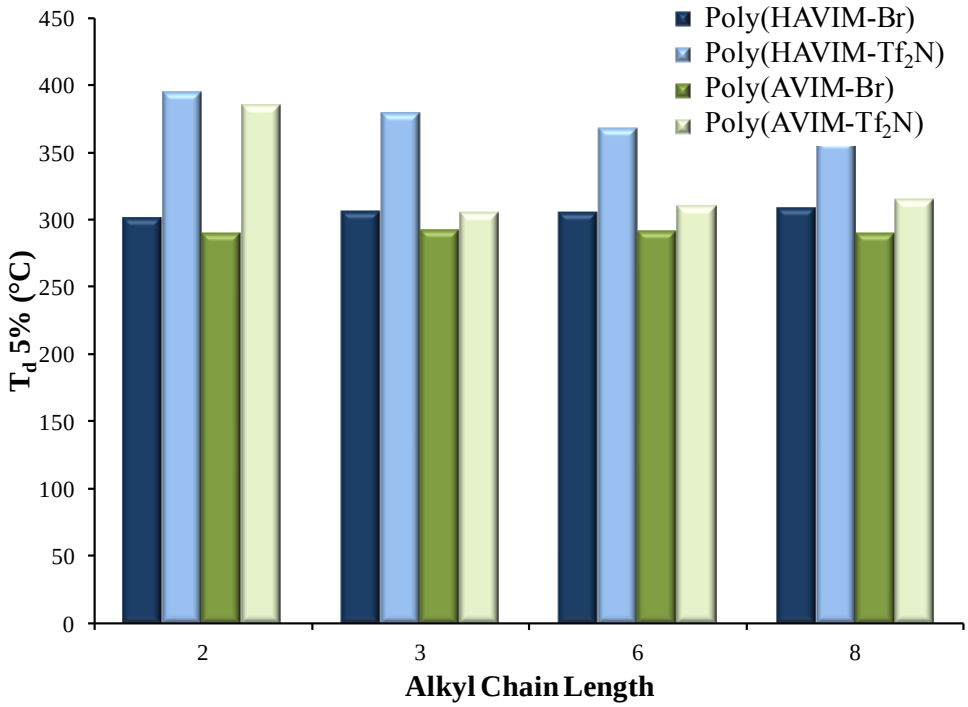

Figure 6.2. $T_{d,5\%}$ for poly(HAVIM-X) and poly(AVIM-X) varying alkyl chain length and counterion (X = Br^-, Tf_2N^-). TGA performed at 10 °C/min under N_2 atmosphere.

As expected, the thermal stability of the imidazolium homopolymers increased upon anion exchange to the less basic Tf_2N^- counterion regardless of substituent chain length. As alkyl chain length increased, the thermal stability of the polymers decreased similar to previous observations.[38] Interestingly, the HAVIM-X homopolymers exhibited significantly increased thermal stabilities (≥50 °C) compared to the corresponding AVIM-X homopolymers. The room temperature ionic liquids [EMIM][Tf_2N] and [HEMIM][Tf_2N] also exhibited ~ 50 °C increase in thermal stability upon addition of a hydroxyl substituent to the ionic liquid monomers.[15,49]

Thermal characterization demonstrated counterion selection and alkyl substituent composition dramatically influenced the T_g's of the various cationic polyelectrolytes. As

expected, the anion exchange from Br^- to the larger Tf_2N^- counterion significantly reduced the T_g of AVIM PILs.[38,45] Anion exchange to the Tf_2N^- counterion reduced polymer T_g's approximately 100-150 °C while increased substituent length on the imidazolium ring also decreased T_g (Figure 6.3).

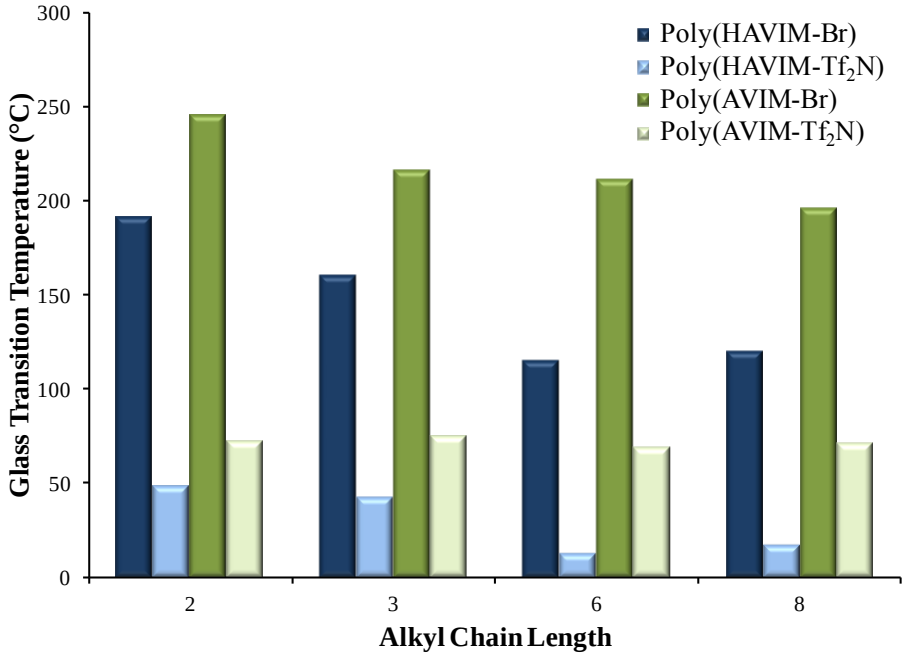

Figure 6.3. T_g's of poly(HAVIM-X) and poly(AVIM-X) varying alkyl chain length and counteranion. DSC heat/cool/heat performed at 10 °C/min under N_2 atmosphere.

Interestingly, the HAVIM homopolymers exhibited lower T_g's (30-50 °C) than their AVIM analogs. The increased polarity of the hydroxyl group presumably facilitated solvation of the electrostatic interactions in the cationic polyelectrolyte resulting in a reduction of the T_g.[18,19]

Room temperature WAXS probed the impact of substituent chain length and hydroxyl incorporation on imidazolium homopolymer morphology. Winey et al. previously investigated similar AVIM homopolymers with WAXS and found that the substituent chain length influenced the homopolymer backbone-to-backbone spacing.[40] Figure 6.4a and b show three peaks in the X-ray scattered intensity *versus* scattering vector (q) plots.

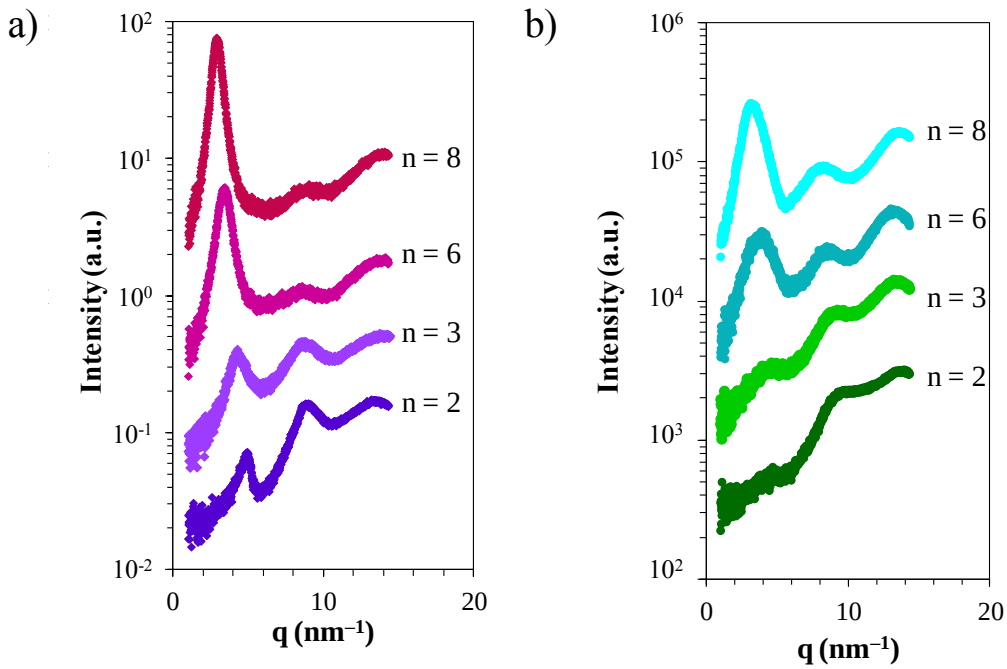

Figure 6.4.WAXS profiles of (a) poly(AVIM-Tf_2N) and (b) poly(HAVIM-Tf_2N) homopolymers with varying alkyl chain lengths. The X-ray scattering data is shifted vertically for clarity.

The lower angle peak at 3-5 nm^{-1} corresponded to the backbone-to-backbone correlation distance (q_b), and the higher angle peak at 12-14 nm^{-1} corresponded to the pendant-to-pendant spacing (q_p, distance between side chains). The middle angle peak at 6-10 nm^{-1} correlated to anion-to-anion distance (q_i). These peak assignments agreed favorably with previous literature.[50]

The q_i and q_p peaks remained unchanged for the imidazolium homopolymers as n (n = number of carbon atoms in (hydroxy)alkyl chain) varied from 2-8 (ethyl-octyl substituent length). As the substituent length n increased, q_b shifted to lower q values. The q_b peak intensity also increased noticeably due to increased electron density contrast between functional groups. The incorporation of longer (hydroxy)alkyl chains increased the phase separation between the polar and nonpolar phases. This observation agreed with numerous molecular dynamics simulation studies of AVIM room-temperature ionic liquids.[51-54] Alkyl side chains ($n \geq 4$) spurred the

formation of polar and nonpolar nanoscale phases due to side chain aggregation. Increasing the alkyl chain length produced larger, more interconnected nonpolar domains.

Triolo et al. provided the first experimental evidence of nanoscale heterogeneities present in imidazolium ionic liquids and determined the domain size varied proportionally to alkyl chain length.[55] In Figure 6.4a, q_b exhibited a sharp, intense peak for the AVIM-Tf_2N homopolymers. Conversely, a broader, less intense q_b peak was observed for the hydroxyl analogs (Figure 6.4b), which suggested the presence of hydroxyl groups induced phase mixing of the polar and nonpolar nanodomains. The less defined nanodomains of the HAVIM-Tf_2N homopolymers resulted in weakened scattering compared to the nanophase-separated AVIM-Tf_2N homopolymers. Consequently for the shorter substituents (n = 2, 3), the q_i and q_p peaks exhibited less resolution, and the q_b peak remained minimally detectable for the HAVIM-Tf_2N homopolymers compared to the AVIM-Tf_2N homopolymers. As the substituent length increased for poly(HAVIM-Tf_2N) (n = 6, 8), the q_b peak became more discernible but remained broader and less intense than the alkyl analogs. Russina and Triolo demonstrated for room-temperature imidazolium ionic liquids that the replacement of the alkyl functionality with an ether- or hydroxyl-containing substituent disrupted the mesoscopic order due to increased side chain polarity producing a more homogeneous morphology.[22,23]

Increased side chain polarity enabled a potential interaction with the imidazolium group through either intra- or inter-molecular hydrogen bonding as described previously.[18,19,24] WAXS observed the q_b peak at comparable spacings for the hydroxyalkyl- and alkyl-containing imidazolium homopolymers, despite the addition of a hydroxyl group to the terminus of the substituent chain. Figure 5 depicts the average backbone-to-backbone distance $<d_b>$ between the two homopolymer analogs as a function of alkyl chain length. This analysis further demonstrated

the similar backbone spacing for the HAVIM-Tf_2N and AVIM-Tf_2N imidazolium homopolymers, suggesting the hydroxyl group interacts with the imidazolium cation or Tf_2N^- anion. The average pendant-to-pendant correlation distance $<d_p>$ and average anion-to-anion distance $<d_i>$ remained constant as a function of alkyl chain length for all homopolymers at ~0.46 nm and ~0.72 nm respectively and agreed with previous literature.[40,50,51] Figure 6.5 also showed $<d_b>$ increased linearly at an average rate of ~0.13 nm/CH_2 as *n* increased HAVIM-Tf_2N and AVIM-TF_2N homopolymers, which indicated the side chains are less than fully interdigitated.

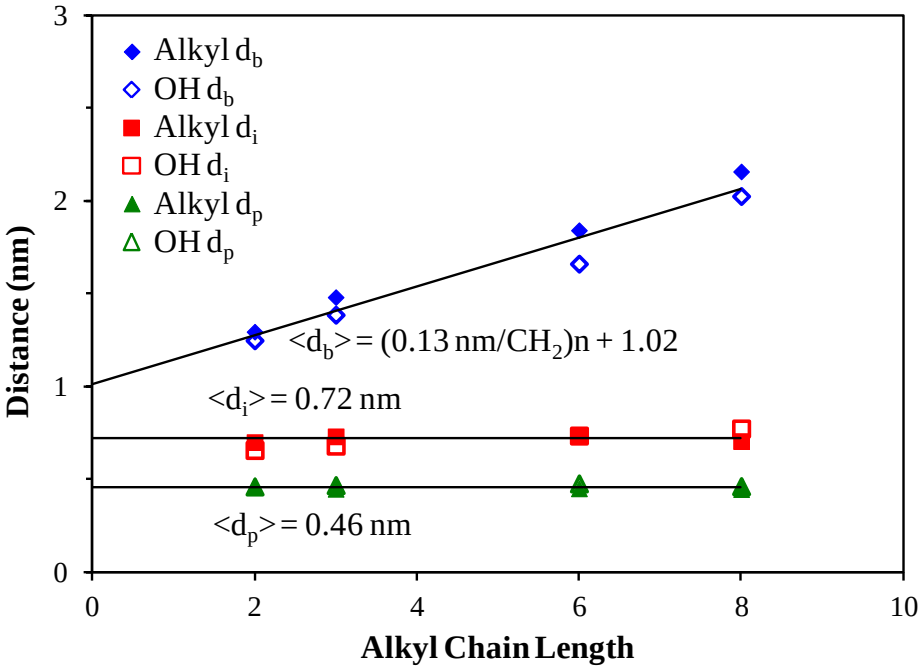

Figure 6.5. Correlation length for d_b (diamonds), d_i (squares), and d_p (triangles) obtained from $d = 2\pi/q$, as a function of alkyl chain length for poly(AVIM-Tf_2N) and poly(HAVIM-Tf_2N) homopolymers (filled and unfilled, respectively).

Winey et al. reported previously $<d_b>$ as a function of *n* for poly(AVIM-X) with various counterions (Br^-, BF_4^-, TfO^-, Tf_2N^-) increased ~0.20 nm/CH_2;[40] however, the current study investigated one counterion type eliminating the influence of counterion size to more accurately establish the trend of d_b versus *n* in HAVIM-Tf_2N and AVIM-Tf_2N homopolymers.

WAXS also probed the morphologies of HAVIM-Tf_2N homopolymers at elevated temperatures to investigate the homopolymer morphology under conditions similar to ionic conductivity experiments. The temperature-dependent X-ray scattering data for poly(HPVIM-Tf_2N) and poly(HOVIM-Tf_2N) determined negligible morphological variation for the homopolymers at increased temperatures. Winey et al. previously showed the AVIM-Tf_2N homopolymers failed to exhibit morphological changes at elevated temperatures.

Solid-state NMR (SSNMR) remains a powerful technique to understand polymer structure and dynamics at the molecular level.[56-58] SSNMR investigated the molecular associations and the local morphology present in these novel polymer systems. Figure 6.6a shows standard ^{13}C CP-MAS spectra of poly(EVIM-Tf_2N), poly(HEVIM-Tf_2N), poly(HVIM-Tf_2N) and poly(HHVIM-Tf_2N).

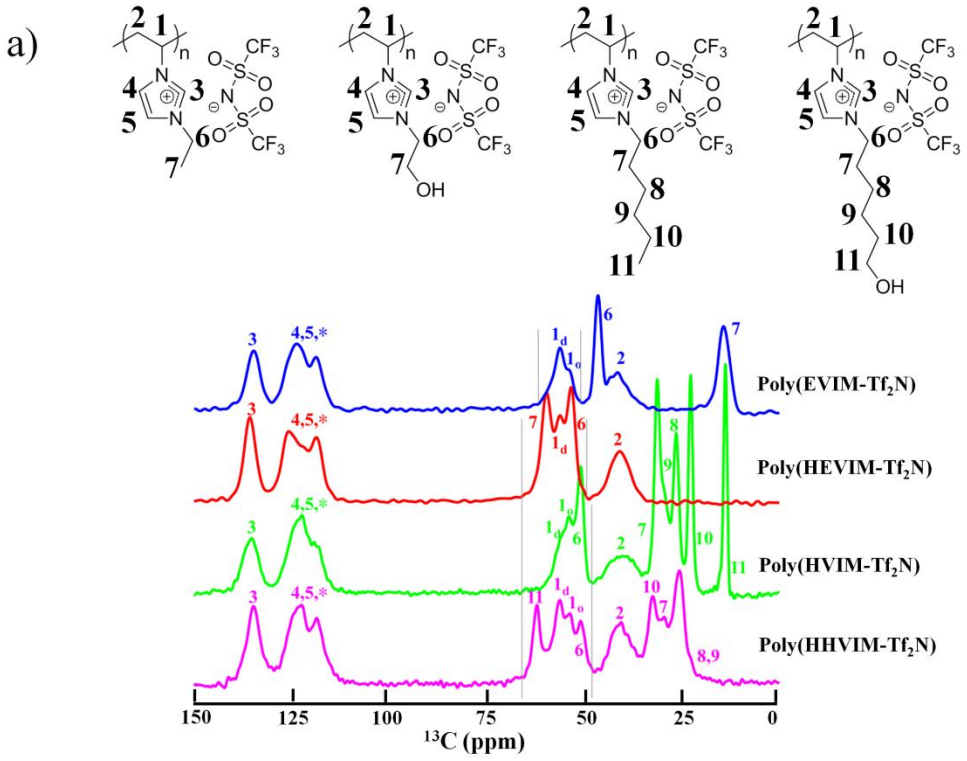

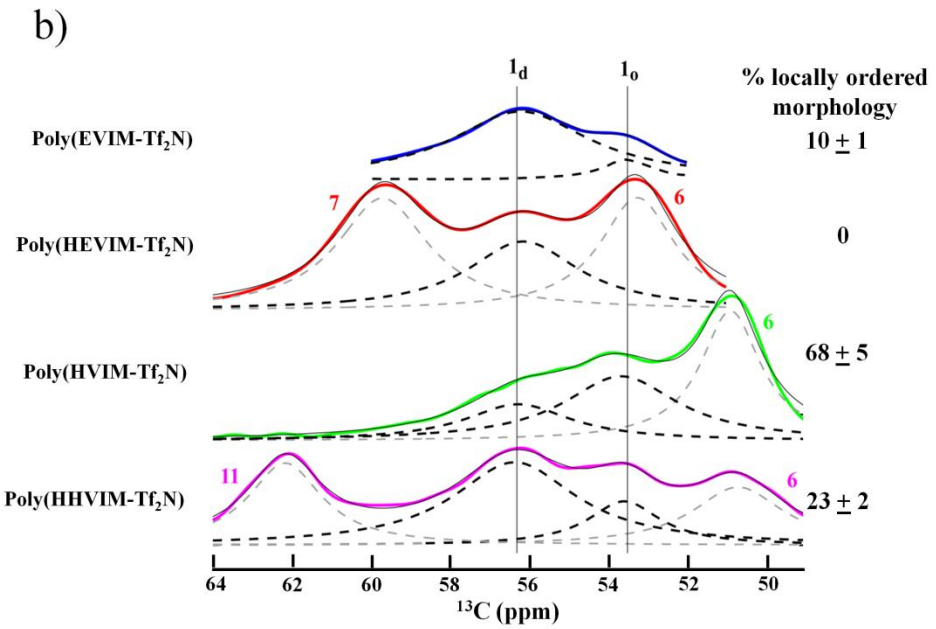

Figure 6.6. (a) ^{13}C CP-MAS spectra of poly(EVIM-Tf_2N), poly(HEVIM-Tf_2N), poly(HVIM-Tf_2N) and poly(HHVIM-Tf_2N). Assignments of peaks and their linewidths provide information about local polymer molecular associations and dynamics. (b) Deconvolution of resonances between 64 - 49 ppm where 1_d and 1_o represent the backbone methine carbons in homogenously disordered and locally ordered morphologies, respectively. Thus, SSNMR enables the determination of the percent locally ordered morphology in each sample through spectral deconvolution (shown at right of each spectrum).

The resonances from the backbone carbons consisted of the methylene (C2) centered at 40.7 ppm as well as the methine (C1) at 56.2 and 53.6 ppm. Upon changing alkyl chain length or hydroxyl group incorporation to the terminus of the substituent chain, no significant changes were observed in the chemical shifts of methylene carbons. However, the resonance line became relatively sharper for poly(HEVIM-Tf_2N) and poly(HHVIM-Tf_2N) compared to poly(EVIM-Tf_2N) and poly(HVIM-Tf_2N). This indicated a faster motion for the main-chain carbon with a more polar side chain.

Unlike methylene carbons, methine carbon resonances exhibit remarkable differences (Figure 6.6b). For all samples the methine carbons correspond to the resonances at 56.2 ppm and 53.6 ppm, except for poly(HEVIM-Tf_2N) where the 53.6 ppm peak remains absent. These two

resonances for the methine carbons provide strong evidence of two distinct chemical environments. In a nanophase separated morphology, the Tf_2N^- anions reside away from nonpolar side chain aggregates and closely bind to imidazolium cations. Consequently, the backbone methine carbons experience a more negative chemical environment compared to a phase-mixed morphology where anions are more homogeneously distributed in the polymer matrix. Therefore, the upfield resonance at 53.6 ppm was assigned to the nanophase-separated, locally ordered region, and the downfield 56.2ppm to a more disordered region. Assuming similar cross-polarization efficiencies in the two morphologies, the amount of phase separation can be quantified through deconvolution of the peaks between 64-49 ppm (Figure 6.6b). The locally ordered fraction increased from 10% to 68% with increasing alkyl chain length from n = 2 to n = 6; addition of the hydroxyl group to the side chain terminus decreased the locally ordered fraction from 10% to 0% for n = 2 and from 68% to 23% for n = 6. This ordering trend strongly agrees with and amplifies results from WAXS where the q_b peak becomes less intense and broader with hydroxyl group incorporation (Figure 6.4).

Impedance spectroscopy at 10% RH below 95 °C and < 10% RH above 95 °C revealed bulk ionic conductivities of the imidazolium homopolymers containing the Tf_2N^- counterion. The Br^- containing polymers failed to form intimate contact with the electrodes due to their high T_g's resulting in unreliable data. The temperature dependent ionic conductivities of the imidazolium homopolymers varied as a function of counterion and substituent composition (Figure 6.7a).

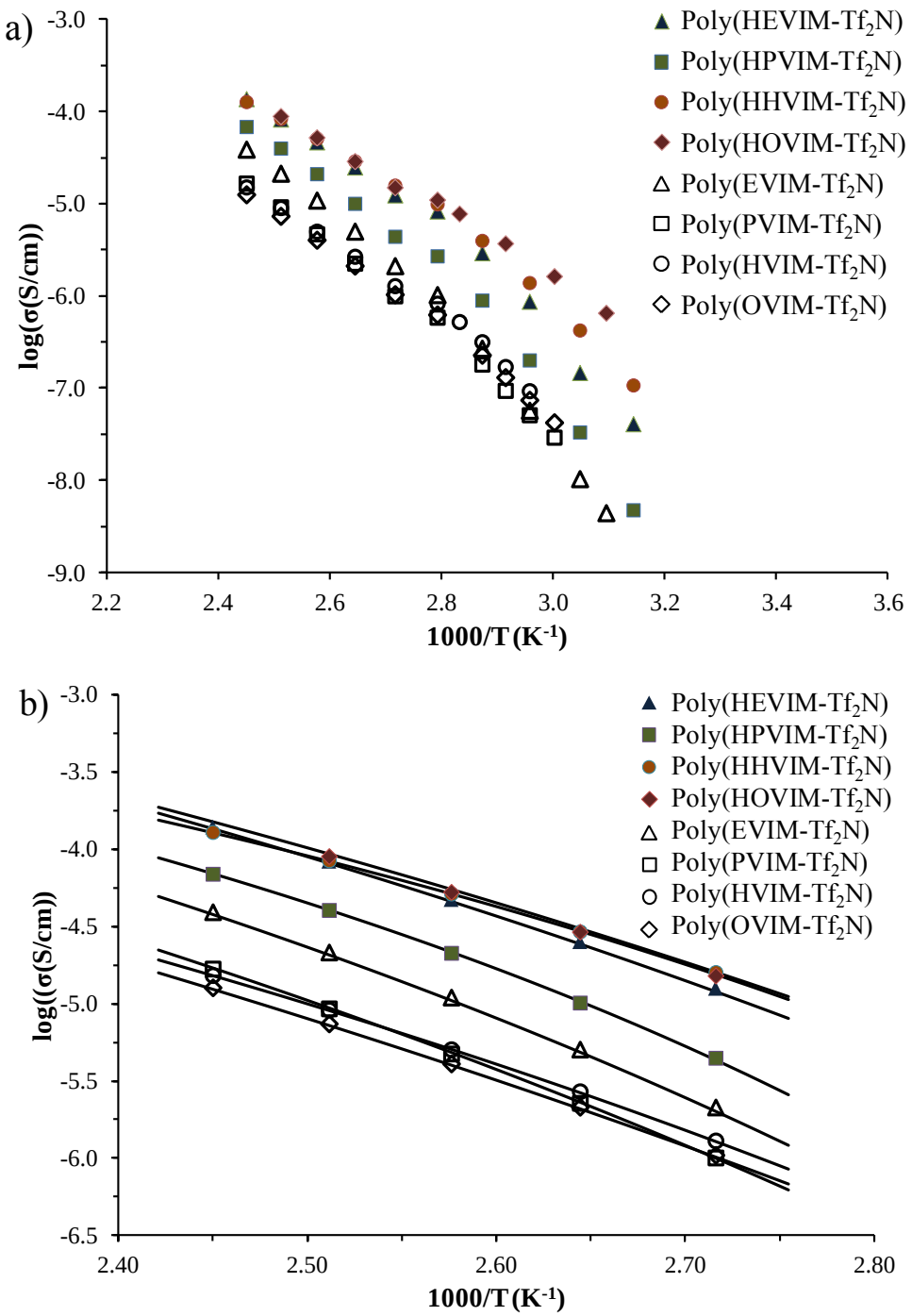

Figure 6.7. (a) Temperature-dependent ionic conductivities of poly(HAVIM-Tf_2N) and poly(AVIM-Tf_2N) and (b) the respective VFT fits at <10% relative humidity from 95 °C – 135 °C.

The shift in the curve at 1000/T equal to 2.7 corresponded to the change in RH from 10% to < 10% due to limitations of the wick-based ESPEC BTL-433 environmental chamber. TGA-SA

confirmed that the polymers at 10% RH absorbed approximately 0.30 wt. % water under the impedance spectroscopy conditions. In Figure 6.7a, the HAVIM-Tf_2N polymers exhibited ionic conductivities an order of magnitude greater than the respective AVIM-Tf_2N polymers over the studied temperature range. The plasticization effect of the hydroxyl group in the HAVIM-Tf_2N homopolymers suggested hydroxyl incorporation improved homopolymer ionic conductivity and weakened the nanoscale phase-separated morphology observed in the AVIM-Tf_2N homopolymers. Figure 6.7b shows quality fitting utilizing the VFT equation. All values determined utilizing these equations are reported in Table 6.3. These values determined with the WLF equation agree favorably with the values determined utilizing the 2- and 3- parameter VFT equations.

Table 6.3. VFT and WLF fitting of temperature dependent ionic conductivities at < 10% RH (95 °C – 135 °C).

Polymer	VFT 3-Parameter (VFT 2-Parameter)				WLF			
	σ_{inf} (S/cm)	B (K)	T_0 (K)	T_g–T_0 (K)	C_1^g	C_2^g	T_0	2.303 $C_1^g C_2^g$
PEVIM	0.96 (0.73)	1806 (1722)	230 (233)	113 (110)	6.89	114	229	1809
PPVIM	1.23 (1.09)	2219 (2186)	210 (211)	141 (140)	7.37	143	208	2429
PHVIM	0.28 (0.29)	1957 (1971)	209 (208)	133 (134)	6.81	151	191	2368
POVIM	1.77 (1.20)	2719 (2569)	179 (184)	165 (160)	7.43	178	166	3047
PHEVIM	3.38 (2.34)	2098 (1969)	201 (206)	120 (115)	7.75	131	190	2339
PHPVIM	0.11 (0.10)	1078 (1059)	262 (263)	54 (53)	8.46	71	245	1383
PHHVIM	0.10 (0.08)	1093 (1058)	243 (245)	44 (42)	9.56	44	243	969
PHOVIM	3.20 (0.55)	2163 (1535)	191 (222)	90 (59)	10.49	91	190	2198

T_g-independent ionic conductivities of room temperature ionic liquids with similar structural modifications commonly overlay onto a single master curve, which occurs when the viscous property of the ionic liquid dominates ionic conductivity.[59,60] Figure 6.8 shows the ionic conductivities of the HAVIM-Tf_2N and AVIM-Tf_2N homopolymers *versus* T-T_g. This T_g-

independent ionic conductivity plot confirmed a significant effect of substituent chain length and hydroxyl incorporation on the ionic conductivities of the imidazolium homopolymers.

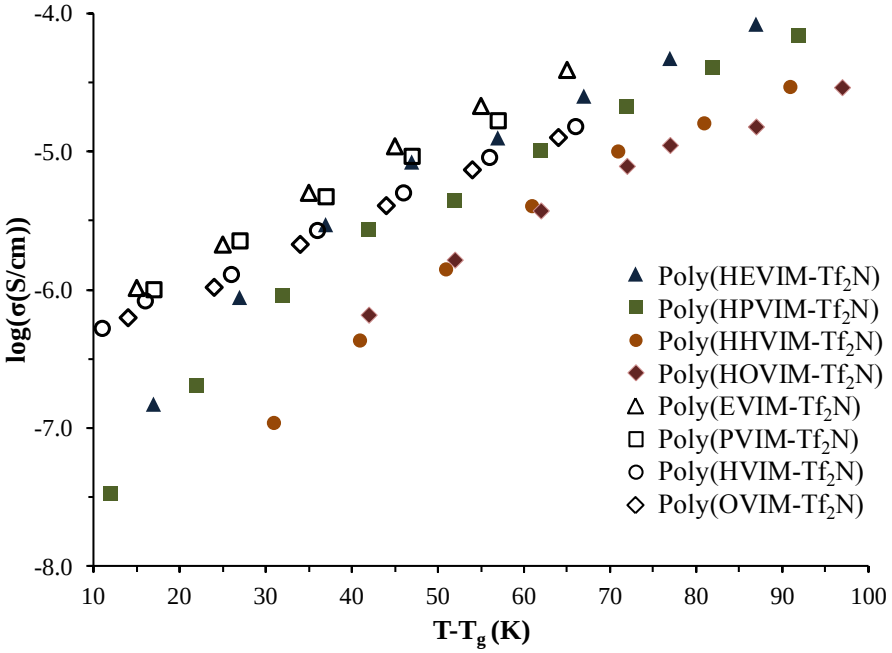

Figure 6.8. Ionic conductivities of (a) poly(HAVIM-Tf_2N) and (b) poly(AVIM-Tf_2N) as a function of T-T_g (T = 95 °C – 135 °C, < 10% RH) with various alkyl chain lengths.

The data for both the HAVIM-Tf_2N and AVIM-Tf_2N homopolymers failed to collapse onto a single curve, which indicated additional factors other than homopolymer T_g contributed to ion conduction. In each homopolymer system, as the substituent chain length decreased, the T_g-independent ionic conductivities increased accordingly: $\sigma_{(hydroxy)octyl} < \sigma_{(hydroxy)hexyl} < \sigma_{(hydroxy)propyl} < \sigma_{(hydroxy)ethyl}$. As discussed previously, Winey et al. determined intra- and inter-molecular spacings in amorphous imidazolium polymerized ionic liquids affected ion transport.[40] The AVIM-Tf_2N homopolymers displayed a smaller curve shift from the ethyl to octyl substituent compared to the HAVIM-Tf_2N homopolymers. X-ray scattering determined that the backbone-to-backbone spacing remained similar between each pair, suggesting additional factors influenced ionic conductivity between these homopolymers. The change in the macromolecular

nanoscale environment as the hydroxyalkyl-chain length increased presumably induced a larger curve shift in the HAVIM-Tf_2N homopolymers.

6.5 *Conclusions*

Incorporation of a polar, hydroxyl group into imidazolium homopolymers disrupted nanophase separation and improved ionic conductivity compared to traditional alkylated imidazolium homopolymers. Conventional free radical polymerization of imidazolium monomers afforded high molecular weight homopolymers to investigate the influence of hydroxyl substituent incorporation and (hydroxy)alkyl chain length on ionic conductivity. As expected, increasing the (hydroxy)alkyl chain length and counterion exchange lowered the T_g of the imidazolium homopolymers. More importantly, hydroxyl group incorporation dramatically reduced the T_g of the imidazolium homopolymers compared to the respective alkyl analogs. WAXS showed the increased polarity of the hydroxyl substituent diminished the nanophase-separated morphology present in the AVIM homopolymers. Consequently, the HAVIM homopolymers exhibited 10-fold higher ionic conductivities than the corresponding AVIM macromolecules through the facile attachment of a polar hydroxyl group onto the imidazolium homopolymers.

6.6 *Acknowledgements*

This material is also based upon work supported in part by the US Army Research Office under Grant No. W911NF-07-1-0452 Ionic Liquids in Electro-Active Devices (ILEAD) MURI. This work is on work partially supported by the U.S. Army Research Laboratory and the U.S. Army Research Office under the Army Materials Center of Excellence Program, contract W911NF-06-2-0014. This material is based on instrumentation supported by the Army Research Office (ARO) under Award No. W911NF-10-1-0307 (DURIP). We also acknowledge the

Institute for Critical Technology and Applied Science (ICTAS) at Virginia Tech for instrument support.

6.7 *References*

(1) Green, M. D.; Long, T. E. *Polym. Rev.* **2009**, *49*, 291-314.
(2) Mecerreyes, D. *Prog. Polym. Sci.* **2011**, *36*, 1629-1648.
(3) Armand, M.; Endres, F.; MacFarlane, D. R.; Ohno, H.; Scrosati, B. *Nat. Mater.* **2009**, *8*, 621-629.
(4) Anderson, E. B.; Long, T. E. *Polymer* **2010**, *51*, 2447-2454.
(5) Lu, J.; Yan, F.; Texter, J. *Prog. Polym. Sci.* **2009**, *34*, 431-448.
(6) Welton, T. *Chem. Rev.* **1999**, *99*, 2071-2084.
(7) Dupont, J.; de Souza, R. F.; Suarez, P. A. Z. *Chem. Rev.* **2002**, *102*, 3667-3692.
(8) Przemyslaw, K. *Prog. Polym. Sci.* **2004**, *29*, 3-12.
(9) Tokuda, H.; Hayamizu, K.; Ishii, K.; Susan, M. A. B. H.; Watanabe, M. *J. Phys. Chem. B* **2004**, *108*, 16593-16600.
(10) Tokuda, H.; Hayamizu, K.; Ishii, K.; Susan, M. A. B. H.; Watanabe, M. *The Journal of Physical Chemistry B* **2005**, *109*, 6103-6110.
(11) Seki, S.; Mita, Y.; Tokuda, H.; Ohno, Y.; Kobayashi, Y.; Usami, A.; Watanabe, M.; Terada, N.; Miyashiro, H. *Electrochem. Solid-State Lett.* **2007**, *10*, A237-A240.
(12) Dupont, J.; Fonseca, G. S.; Umpierre, A. P.; Fichtner, P. F. P.; Teixeira, S. R. *J. Am. Chem. Soc.* **2002**, *124*, 4228-4229.
(13) Ngo, H. L.; LeCompte, K.; Hargens, L.; McEwen, A. B. *Thermochim. Acta* **2000**, *357-358*, 97-102.
(14) Huddleston, J. G.; Visser, A. E.; Reichert, W. M.; Willauer, H. D.; Broker, G. A.; Rogers, R. D. *Green Chemistry* **2001**, *3*, 156-164.
(15) Yeon, S.-H.; Kim, K.-S.; Choi, S.; Lee, H.; Kim, H. S.; Kim, H. *Electrochim. Acta* **2005**, *50*, 5399-5407.
(16) Tang, S.; Baker, G. A.; Zhao, H. *Chem. Soc. Rev.* **2012**, *41*, 4030-4066.
(17) Branco, L. C.; Rosa, J. N.; Moura Ramos, J. J.; Afonso, C. A. M. *Chem. Eur. J.* **2002**, *8*, 3671-3677.
(18) Smith, G. D.; Borodin, O.; Li, L.; Kim, H.; Liu, Q.; Bara, J. E.; Gin, D. L.; Nobel, R. *PCCP* **2008**, *10*, 6301-6312.
(19) Triolo, A.; Russina, O.; Caminiti, R.; Shirota, H.; Lee, H. Y.; Santos, C. S.; Murthy, N. S.; Castner, J. E. W. *Chem. Commun.* **2012**, *48*, 4959-4961.
(20) Chiou, J. Y. Z.; Chen, J. N.; Lei, J. S.; Lin, I. J. B. *J. Mater. Chem.* **2006**, *16*, 2972-2977.
(21) Holbrey, J. D.; Turner, M. B.; Reichert, W. M.; Rogers, R. D. *Green Chemistry* **2003**, *5*, 731-736.
(22) Russina, O.; Triolo, A. *Faraday Discuss.* **2012**, *154*, 97-109.
(23) Russina, O.; Triolo, A.; Gontrani, L.; Caminiti, R. *J. Phys. Chem. Lett.* **2011**, *3*, 27-33.
(24) Zhang, S.; Qi, X.; Ma, X.; Lu, L.; Deng, Y. *J. Phys. Chem. B* **2010**, *114*, 3912-3920.
(25) Ficke, L. E.; Brennecke, J. F. *J. Phys. Chem. B* **2010**, *114*, 10496-10501.
(26) Matsumoto, K.; Endo, T. *Macromolecules* **2009**, *42*, 4580-4584.
(27) Chen, H.; Elabd, Y. A. *Macromolecules* **2009**, *42*, 3368-3373.
(28) Bara, J. E.; Carlisle, T. K.; Gabriel, C. J.; Camper, D.; Finotello, A.; Gin, D. L.; Noble, R. D. *Ind. Eng. Chem. Res.* **2009**, *48*, 2739-2751.

(29) Tang, J.; Tang, H.; Sun, W.; Radosz, M.; Shen, Y. *J. Polym. Sci., Part A: Polym. Chem.* **2005**, *43*, 5477-5489.
(30) Tang, J.; Radosz, M.; Shen, Y. *Macromolecules* **2007**, *41*, 493-496.
(31) Weber, R. L.; Ye, Y.; Banik, S. M.; Elabd, Y. A.; Hickner, M. A.; Mahanthappa, M. K. *J. Polym. Sci., Part B: Polym. Phys.* **2011**, *49*, 1287-1296.
(32) Chen, H.; Choi, J.-H.; Salas-de la Cruz, D.; Winey, K. I.; Elabd, Y. A. *Macromolecules* **2009**, *42*, 4809-4816.
(33) Vijayakrishna, K.; Mecerreyes, D.; Gnanou, Y.; Taton, D. *Macromolecules* **2009**, *42*, 5167-5174.
(34) Vidya, P.; Chadha, A. *J. Mol. Catal. B: Enzym.* **2009**, *57*, 145-148.
(35) Hunley, M. T.; England, J. P.; Long, T. E. *Macromolecules* **2010**, *43*, 9998-10005.
(36) Ye, Y.; Elabd, Y. A. *Macromolecules* **2011**, *44*, 8494-8503.
(37) Ohno, H. *Electrochim. Acta* **2001**, *46*, 1407-1411.
(38) Green, M. D.; Salas-de la Cruz, D.; Ye, Y.; Layman, J. M.; Elabd, Y. A.; Winey, K. I.; Long, T. E. *Macromol. Chem. Phys.* **2011**, *212*, 2522-2528.
(39) Ye, Y.; Elabd, Y. A. *Polymer* **2011**, *52*, 1309-1317.
(40) Salas-de la Cruz, D.; Green, M. D.; Ye, Y.; Elabd, Y. A.; Long, T. E.; Winey, K. I. *J. Polym. Sci., Part B: Polym. Phys.* **2012**, *50*, 338-346.
(41) Weber, R. L.; Ye, Y.; Schmitt, A. L.; Banik, S. M.; Elabd, Y. A.; Mahanthappa, M. K. *Macromolecules* **2011**, *44*, 5727-5735.
(42) Lee, M.; Choi, U. H.; Colby, R. H.; Gibson, H. W. *Chem. Mater.* **2010**, *22*, 5814-5822.
(43) Matsumoto, K.; Talukdar, B.; Endo, T. *Polym. Bull.* **2010**, *66*, 199-210.
(44) Rahman, M.; Brazel, C. S. *Prog. Polym. Sci.* **2004**, *29*, 1223-1248.
(45) Marcilla, R.; Alberto Blazquez, J.; Rodriguez, J.; Pomposo, J. A.; Mecerreyes, D. *J. Polym. Sci., Part A: Polym. Chem.* **2004**, *42*, 208-212.
(46) Salamone, J. C.; Israel, S. C.; Taylor, P.; Snider, B. *Polymer* **1973**, *14*, 639-44.
(47) Swain, C. G.; Kuhn, D. A.; Schowen, R. L. *J. Am. Chem. Soc.* **1965**, *87*, 1553-1561.
(48) Shostakovskii, M. F.; Glazkova, N. P.; Domnina, E. S.; Belousova, L. V.; Skvortsova, G. G. *Chem. Heterocycl. Compd.* **1971**, *7*, 894-896.
(49) Bonhôte, P.; Dias, A.-P.; Papageorgiou, N.; Kalyanasundaram, K.; Grätzel, M. *Inorg. Chem.* **1996**, *35*, 1168-1178.
(50) Nakamura, K.; Saiwaki, T.; Fukao, K.; Inoue, T. *Macromolecules* **2011**, *44*, 7719-7726.
(51) Urahata, S. M.; Ribeiro, M. C. C. *J. Chem. Phys.* **2004**, *120*, 1855-1863.
(52) Wang, Y.; Voth, G. A. *J. Am. Chem. Soc.* **2005**, *127*, 12192-12193.
(53) Wang, Y.; Voth, G. A. *J. Phys. Chem. B* **2006**, *110*, 18601-18608.
(54) Canongia Lopes, J. N. A.; Pádua, A. A. H. *J. Phys. Chem. B* **2006**, *110*, 3330-3335.
(55) Triolo, A.; Russina, O.; Bleif, H.-J.; Di Cola, E. *J. Phys. Chem. B* **2007**, *111*, 4641-4644.
(56) McBrierty, V.; Packer, K. *Nuclear Magnetic Resonance in Solid Polymers*; Cambridge 1993.
(57) Schmidt-Rohr, K.; Spiess, H. W. *Multidimensional Solid-State NMR and Polymers*; Academic Press, 1994.
(58) Laws, D. D.; Bitter, H.-M. L.; Jerschow, A. *Angew. Chem. Int. Ed.* **2002**, *41*, 3096-3129.
(59) Pitawala, J.; Matic, A.; Martinelli, A.; Jacobsson, P.; Koch, V.; Croce, F. *J. Phys. Chem. B* **2009**, *113*, 10607-10610.
(60) Martinelli, A.; Matic, A.; Jacobsson, P.; Börjesson, L.; Fernicola, A.; Scrosati, B. *J. Phys. Chem. B* **2009**, *113*, 11247-11251.

6.8 *Supporting Information*

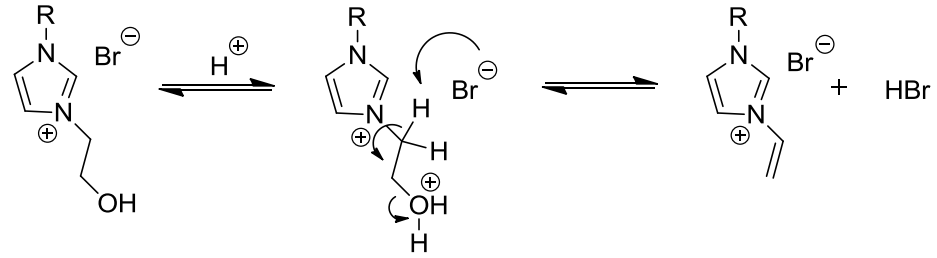

Figure S6.1. Proposed acid-catalyzed elimination reaction to generate a vinyl group which enables the generation of crosslinked homopolymers.

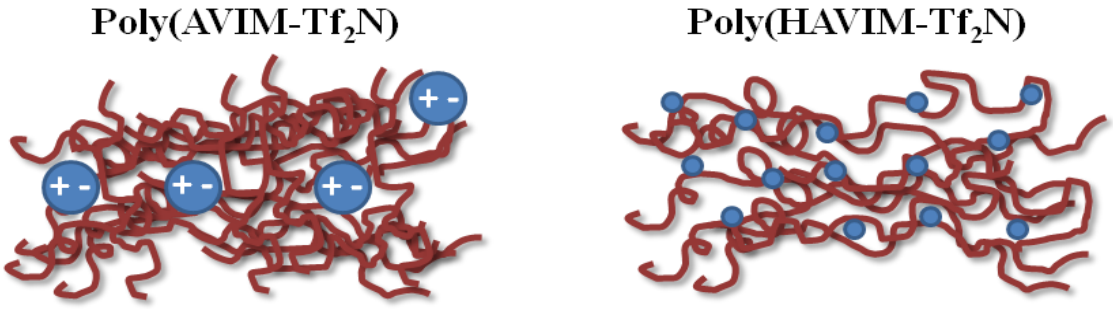

Figure S6.2. Schematic of nanophase separation in poly(AVIM-Tf_2N) and the solvation of the electrostatic interactions environment through the introduction of polar hydroxyl groups in poly(HAVIM-Tf_2N).

Chapter 7: Controlled Radical Polymerization of 4-Vinylimidazole

(Published in *Macromolecules*, **2012**, *45*, 3669-3676)

Michael H. Allen, Jr., Sean T. Hemp, Adam E. Smith, and Timothy E. Long
Department of Chemistry, Macromolecules and Interfaces Institute, Virginia Tech, Blacksburg, VA 24061

7.1 *Abstract*

We report the unprecedented controlled radical polymerization of 4-vinylimidazole (4VIM). Reversible addition-fragmentation chain transfer (RAFT) of 4VIM in glacial acetic acid afforded homopolymers with well-defined molecular weights and narrow polydispersity indices (PDIs). The polymerizations in acetic acid mediated with 4-cyano-4-(ethylsulfanylthiocarbonylsulfanyl)pentanoic acid (CEP) displayed linear pseudo-first order kinetics and linear molecular weight growth with monomer conversion. Systematic variation of numerous polymerization parameters included solvent composition, initiator concentration, monomer concentration, and the calculated degree of polymerization. Aqueous size exclusion chromatography (SEC) confirmed linear molecular weight growth to number-average molecular weights (M_n) of 65,000 g/mol with low PDIs (< 1.20). Subsequent monomer addition confirmed the presence of the trithiocarbonate functionality at the chain ends, which provided further evidence of controlled polymerization conditions. Polymerizations in traditional aqueous RAFT solvents (acidic buffers) failed to achieve controlled molecular weight growth. Effectively controlling 4VIM homopolymerizations enables the design of amphoteric block copolymers for emerging applications including nucleic acid delivery and electro-active membranes.

7.2 *Introduction*

Many researchers currently focus on the incorporation of the imidazole ring into a variety of macromolecules for biological and engineering applications.[1-4] The imidazole ring, which is found in the amino acid histidine, displays good biocompatibility and the capacity to condense and deliver DNA.[5,6] Additionally, quantitative alkylation imparts a permanent, cationic charge on the imidazole ring. These imidazolium salts, commonly referred to as ionic liquids, exhibit high ionic conductivities, high chemical and thermal stability, and negligible volatility.[7-10] Imidazole-containing ionic liquid monomers include (meth)acrylics,[11-13] styrenics,[14-17] and 1-, 2- and 4-vinylimidazoles (1VIM, 2VIM, 4VIM).[18-32] Conventional free radical polymerization of these ionic liquid monomers enables ionically conductive films,[33,34] microwave-absorbing materials,[35] and CO_2 capturing membranes.[36,37]

Although conventional free radical polymerization results in numerous polymerized ionic liquids, controlled radical polymerization (CRP) further enables the design of macromolecules with well-defined architectures and precise molecular weights.[38,39] Attempts to polymerize imidazole-containing monomers in a controlled fashion include atom transfer radical polymerization (ATRP), nitroxide-mediated polymerization (NMP), and reversible addition-fragmentation chain transfer (RAFT). Shen et. al polymerized 2-(1-butylimidazolium-3-yl) ethyl methacrylate tetrafluoroborate (BIMT) with ATRP with a Cu(I)Cl catalyst to control molecular weight.[40] Gnanou et al. homopolymerized BIMT employing RAFT polymerization and synthesized doubly hydrophilic block copolymers of BIMT with methacrylic acid.[41] Researchers also used NMP for styrenic-based imidazolium polymers of controlled architecture and well-defined molecular weights for CO_2 absorption membranes, poly(ionic liquid) brush coatings for surfaces, and micelle self-assembly.[16,17,42] Moreover, Mahanthappa and co-workers recently

studied the thermal, ion transport, and morphological properties of these charged homopolymers.[14,15]

N-vinyl radicals such as 1VIM form a highly reactive, unstable, propagating radical due to the absence of resonance stabilization, and the CRP of 1VIM proved difficult until only recently. Liu et al. utilized RAFT polymerization with a xanthate chain transfer agent (CTA) to synthesize poly(*N*-isopropylacrylamide-*b*-1VIM) block copolymers.[43] Thereafter, xanthate CTAs successfully mediated polymerization of three *N*-vinylimidazolium salts in a controlled fashion.[44] The polymerized ionic liquids however, displayed broad polydispersities (PDIs), and experimental molecular weights deviated from theoretical predictions. Cobalt-mediated controlled radical polymerization of 1-vinyl-3-ethylimidazolium bromide demonstrated improved polymer molecular weight control with narrow PDIs.[45]

Despite increased resonance stabilization of the propagating radical relative to 1VIM, CRP of 4VIM remains unexplored. Overberger and co-workers first polymerized 4VIM using conventional free radical polymerization in benzene.[27] They synthesized copolymers to examine the esterolytic activity of various imidazole-containing macromolecules.[20-26,28] Breslow et al. subsequently synthesized poly(4VIM) according to Overberger's methods to ascertain the catalytic effects on the reaction between pyridoxamines and pyruvic acid. Furthermore, they attempted RAFT polymerization of 4VIM to produce polymers with narrow PDIs; however, the polymerizations generated gels without molecular weight control.[46] In addition to catalysis studies, poly(4VIM) also displays potential as an effective non-viral gene transfection with minimal cytotoxicity.[47,48] Bozkurt and co-workers prepared 4VIM copolymers with acidic comonomers (vinylphosphonic acid, 4-vinylbenzylboronic acid) to generate anhydrous proton conducting membranes for methanol fuel cells.[49-52]

RAFT polymerization permits controlled polymerization of a variety of functional monomers including less stable *O*- and *N*-vinyl radicals.[39,53,54] RAFT imparts control of polymerizations through a series of reversible chain transfer reactions, which minimizes the instantaneous concentration of radicals, consequently reducing bimolecular termination.[55] An assortment of thiocarbonylthio compounds serve as CTAs including dithioesters, xanthates, dithiocarbamates, and trithiocarbonates to mediate and control RAFT polymerizations. Through CTA and solvent selection, initiator and monomer concentrations, and different target molecular weights, RAFT provides numerous avenues to control the polymerization of functionally rich monomers.[53]

In this manuscript, we demonstrate the unprecedented CRP of 4VIM. A trithiocarbonate, 4-cyano-4-(ethylsulfanylthiocarbonylsulfanyl)pentanoic acid (CEP), successfully mediated the controlled polymerization of 4VIM. We varied multiple reaction parameters including solvent, initiator concentration, monomer concentration, and target molecular weight to examine the efficacy of RAFT polymerization of 4VIM. Glacial acetic acid, which served as a unique solvent, maintained a homogeneous polymerization and allowed the synthesis of poly(4VIM) with controlled molecular weights and narrow PDIs. Successful chain extension experiments further demonstrated the integrity of the thiocarbonylthio end groups and the controlled nature of these polymerizations. RAFT polymerization of 4VIM enables the future design of block copolymers for advanced applications including pH-sensitive block copolymers for gene delivery and ionically conductive block copolymers for electro-active devices.

7.3 *Experimental Section*

7.3.1 Materials

Urocanic acid (Aldrich, 99%) was recrystallized from water and dried under reduced pressure for 18 h. 1VIM was distilled at 1 mmHg and 60 °C (Aldrich, 99%). 2,2'-

azobisisobutyronitrile (AIBN, Aldrich, 99%) and 4,4-azobis(4-cyanovaleric acid) (V-501, Aldrich, 98%) were recrystallized from methanol. CEP[56] and *N*-*tert*-butyl-*N*-(1-diethylphosphono-2,2-dimethylpropyl) nitroxide (SG1)[57] were synthesized according to literature procedures. Glacial acetic acid (Alfa Aesar, 99.7%), methanol (Fisher Scientific, HPLC grade), DMSO (Fisher Scientific, HPLC grade), and Blocbuilder® (Arkema Inc.) were used as received.

7.3.2 Analytical Techniques

^{1}H NMR spectroscopy (Varian Inova, 400 MHz, CD_3OD, d_6-DMSO) confirmed monomer and polymer structures and determined monomer conversion. Differential scanning calorimetry (TA Instruments, Q1000) determined thermal transitions. The molecular weight of the polymers was measured using aqueous size exclusion chromatography (SEC) (flow rate of 0.8 mL/min through two Waters Ultrahydrogel Linear and one Waters Ultrahydrogel 250 columns, solvent: 54/23/23 H_2O/MeOH/Acetic acid (v/v/v %), 0.1 M $NaNO_3$). SEC instrumentation included a Waters 1515 isocratic HPLC pump, Waters 717plus Autosampler, Wyatt miniDAWN multiangle laser light scattering (MALLS) detector operating at a wavelength of 690 nm, and a Waters 2414 differential refractive index detector. The specific refractive index increment values (*dn/dc*) were determined offline using a Wyatt Optilab T-rEX refractive index detector at 658 nm and 35 °C to obtain absolute polymer molecular weights using SEC. The *dn/dc* values for linear poly(1VIM) and poly(4VIM) were 0.2212 ± 0.0004 mL/g and 0.2296 ± 0.0008 mL/g, respectively. Absolute polymer molecular weights and PDIs were calculated using the Wyatt ASTRA SEC/LS software and compared to theoretical predictions. Dynamic light scattering with a Malvern Zetasizer NanoZS confirmed that the aqueous mobile phase prevented formation of large scale polymer aggregates.

7.3.3 Synthesis of 4VIM

4VIM was prepared according to a modified literature procedure.[27] Anhydrous urocanic acid (5.00 g, 53.0 mmol) was heated under vacuum (1 mmHg) at 220-240 °C to melt and decarboxylate the compound. After continuous heating, the product distilled as a colorless liquid that crystallized readily at 23 °C. The off-white powder sublimed at 80 °C under vacuum (0.5 mmHg) to further purify the 4VIM. White crystals (1.70 g, 53% yield) were collected on the cold finger and were dried under reduced pressure. ^{1}H NMR (400 MHz, d_6-DMSO):δ 12.11 (s, 1H), 7.59 (s, 1H), 7.04 (s, 1H), 6.55 (dd, 1H), 5.58 (dd, 1H), 4.98 (m, 1H).

7.3.4 Conventional Free Radical Homopolymerization of 1VIM and 4VIM

In a 25-mL, round-bottomed, flask equipped with a stir bar, each monomer (2.00 g, 21.3 mmol) was charged with 0.1 mol % AIBN (3.49 mg, 2.13 X 10^{-2} mmol) and dissolved in glacial acetic acid (8.00 g, 133 mmol). The reaction was sparged with argon at room temperature for 30 min and placed in an oil bath at 65 °C for 24 h. The reaction remained homogeneous and was precipitated into acetone, redissolved in methanol, and precipitated a second time into acetone. The polymer was dried 18 h under reduced pressure (1.80 g, 90 % yield). Absolute polymer molecular weights were determined using aqueous SEC. Typical M_n values were 5.00 x 10^4 g/mol and 1.10 x 10^6 g/mol with PDIs of 1.52 and 1.54 for poly(1VIM) and poly(4VIM), respectively.

7.3.5 NMP of 4VIM

In a representative NMP, 4VIM (0.600 g, 6.38 mmol), Blocbuilder® (2.43 mg, 6.37 μmol), SG1 (0.38 mg, 1.28 μmol), and glacial acetic acid (6.69 g, 111 mmol) were added to a 25-mL, round-bottomed, flask equipped with a stir bar. The reaction was sparged with argon for 30 min, and the reaction was subsequently immersed in an oil bath maintained at 110 °C. Aliquots were removed during the course of the reaction to obtain kinetics of the polymerization.

7.3.6 RAFT Polymerization of 4VIM

In a representative RAFT polymerization, 4VIM (0.250 g, 2.66 mmol), V-501 (2.98 mg, 10.6 μmol), CEP (2.80 mg, 10.6 μmol), and glacial acetic acid (2.79 g, 46.5 mmol) were added to a 25-mL, round-bottomed, flask equipped with a stir bar. The reaction was sparged with argon for 30 min, and the reaction was subsequently immersed in an oil bath thermostated at 70 °C. Samples were withdrawn during the course of the polymerization with an argon flushed syringe to monitor monomer consumption and polymer molecular weight increase as a function of reaction time. Monomer conversion was determined with ^{1}H NMR spectroscopy in CD_3OD. Aqueous SEC provided molecular weight data for the polymerization aliquots.

7.4 *Results & Discussion*

Three CRP techniques are commonly employed to produce functional polymers with tailored compositions and architectures, including ATRP, NMP, and RAFT. Heterogeneous polymerizations are also effective to control molecular weight, including dispersion, suspension, emulsion, and miniemulsion polymerizations; however, these techniques involve added surfactants and other stabilizers to intentionally create a two phase system.[58] Performing CRP in solution without additives, surfactants, and emulsifiers typically requires a good solvent to ensure homogeneous conditions. These conditions prevent the occurrence of uncontrolled molecular weight growth and broad PDIs. Numerous earlier studies performed conventional free radical polymerization of 4VIM in benzene; however, the polymerization was heterogeneous as the polymer precipitated during the process.[20-28,48] Ihm et al. reported a weight-average molecular weight (M_w) of 26,200 g/mol under these conditions (0.1 mol % AIBN, PDI not reported), which remains the only report of molecular weight data for a 4VIM homopolymer in literature.[48] It was necessary to identify a new solvent for 4VIM homopolymerizations to overcome these earlier heterogeneous reaction conditions.

Dissolution of 4VIM and its subsequent homopolymer proved difficult due to intermolecular hydrogen bonding, which prevented homogeneous polymerizations in organic (DMSO, DMF) and aqueous mixtures for the polymerization of 1VIM.[21] The conventional free radical polymerizations of 1VIM and 4VIM in glacial acetic acid afforded homopolymers under homogeneous reaction conditions as shown in Scheme 7.1a. Subsequent dialysis enables the recovery of the unprotonated poly(4VIM), which dissolves readily in methanol and DMSO.

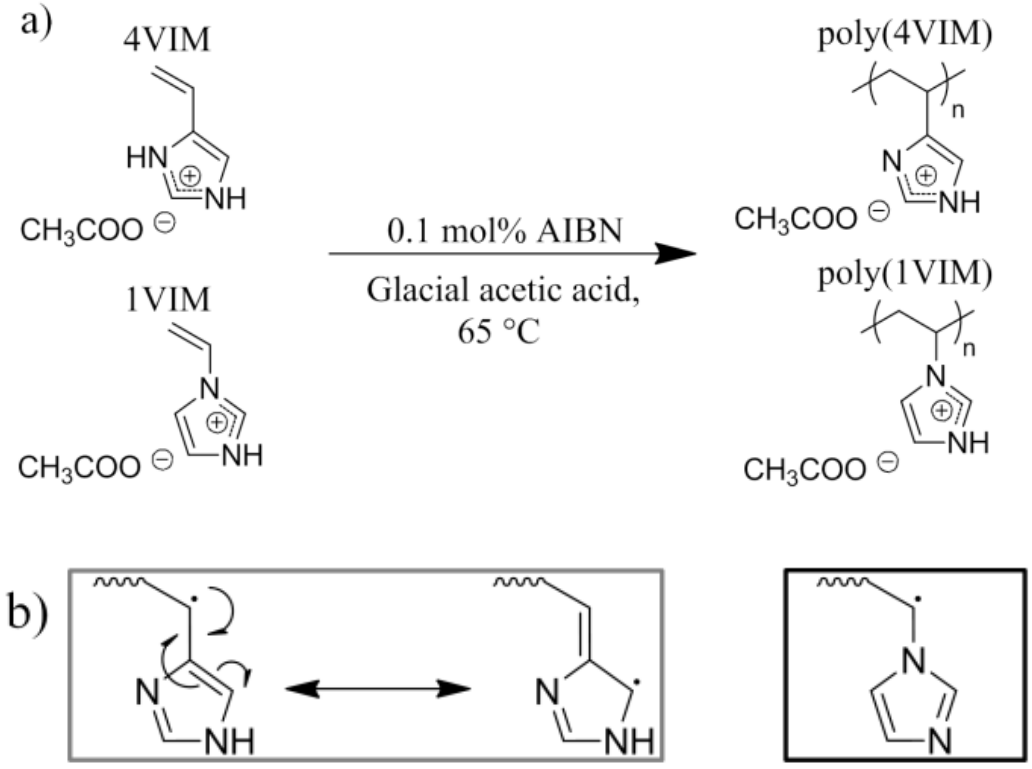

Scheme 7.1. (a) Conventional free radical homopolymerization of poly(4VIM) and poly(1VIM) in glacial acetic acid (b) resonance structures of the respective propagating radical.

In addition, Scheme 7.1b depicts the resonance contributors of the propagating radical for each monomer to illustrate 4VIMs increased radical stability relative to 1VIM. Aqueous size

exclusion chromatography determined the absolute molecular weight (M_n poly(4VIM) = 1.10 x 10^6 g/mol; M_n poly(1VIM) = 5.00 x 10^4 g/mol) of each polymer as shown in Figure 7.1.

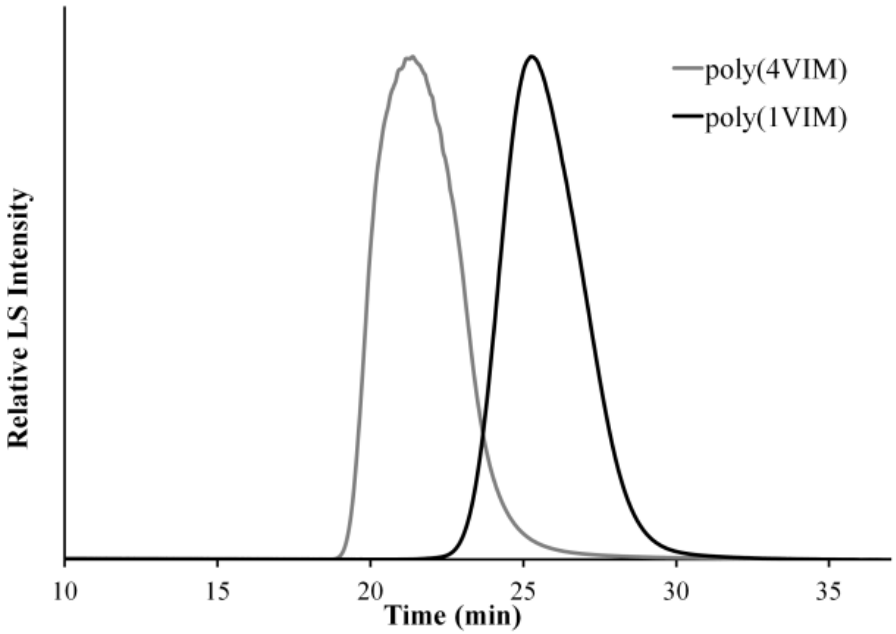

Figure 7.1. Aqueous SEC light scattering chromatograms of poly(4VIM) (M_n = 1,100,000 g/mol, PDI = 1.54) and poly(1VIM) (M_n = 50,000 g/mol, PDI = 1.52).

A higher k_t/k_p ratio for 1VIM relative to the more stable 4VIM propagating radical presumably accounted for the significant difference in polymer molecular weights. Moreover, comparing the experimentally obtained poly(4VIM) molecular weight (M_w = 1.69 X 10^6 g/mol) to previous literature (M_w = 2.26 X 10^4 g/mol) suggested the homogeneous polymerization conditions improved the range of attainable molecular weights. Similarly, conventional free radical polymerization of acrylamide affords high molecular weight polymers ($M_w > 10^7$ g/mol) due to the low k_t/k_p ratio.[70] The molecular weights reported above 10^6 g/mol approach the exclusion limit of the SEC columns potentially resulting in inefficient separation. Differential scanning calorimetry determined the glass transition temperatures (T_g) of each polymer (T_g poly(1VIM) = 175 °C; T_g poly(4VIM) = 218 °C), and the increased T_g of poly(4VIM) was attributed to the

presence of both a hydrogen bond donor and acceptor, leading to significant intra- and intermolecular hydrogen bonding. Interestingly, the specific heat capacities between each homopolymer appear different in the DSC thermograms and will undergo future investigation (Supporting Information). Additionally, poly(*p*-hydroxystyrene) (PHS) displays an elevated T_g (150 °C) compared to poly(styrene) (T_g = 100 °C) due to the presence of intra- and intermolecular hydrogen bonding.[71] Chang et al. demonstrated the mixing of polyhedral oligosilsesquioxanes (POSS) with PHS raised the T_g to ~ 200 °C through hydrogen bond interactions between the hydroxyl groups on the PHS and the POSS siloxane groups.[72]

The increased radical stability of the 4VIM propagating radical and the development of homogeneous polymerization conditions spurred our investigation of CRP in glacial acetic acid. For the polymerization of imidazole-containing monomers, ATRP remained problematic due to catalyst complexation;[59] therefore, we investigated the CRP of 4VIM utilizing NMP and RAFT polymerization strategies. NMP of 4VIM (Scheme 7.2) proved problematic as various SG1 and monomer concentrations resulted in less than 10% monomer conversion with higher molecular weights than theoretical predictions.

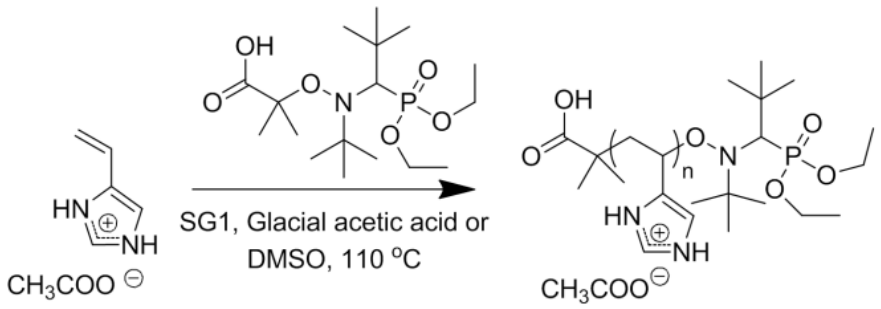

Scheme 7.2. NMP of 4VIM with Blocbuilder® and SG1.

The degradation of SG1 under acidic conditions contributed to this lack of control.[60] In addition, homogeneous polymerizations in DMSO at 110 °C also remained uncontrolled. We attributed

the absence of control to the decreased 4VIM propagating radical stability relative to monomers traditionally polymerized using NMP (acrylates and styrenics). NMP of 1VIM under similar conditions failed to produce polymer, which was also ascribed to decreased radical stability.

Due to the limitations of NMP to polymerize a variety of functional monomers, we probed the RAFT polymerization of 4VIM. Recently, numerous studies demonstrated the importance of fundamentally understanding RAFT polymerization kinetics of previously uncontrolled monomers.[44,61-63] These studies have accelerated the discovery of novel structures for many critical technologies. Careful selection of the CTA and polymerization reaction conditions remains a critical decision in performing successful RAFT polymerizations.[53] Numerous amine-containing monomers with RAFT polymerization conditions required an acidic buffer to prevent CTA aminolysis.[64] Thang et al. demonstrated that trithiocarbonate CTAs exhibited increased hydrolytic stability compared to the corresponding dithioesters.[65] In addition, Moad and McCormick discovered that trithiocarbonate CTAs effectively controlled more reactive monomers such as acrylamides and methacrylamides.[55,66] Endo et al. polymerized *N*-vinylimidazolium salts using xanthate-based CTAs; however, the more active xanthate CTAs proved unnecessary with the increased radical stability of 4VIM.[44]

As shown in Scheme 7.3, the RAFT polymerization of 4VIM occurred in an acetate buffer (pH = 5.2) with CEP as the CTA.

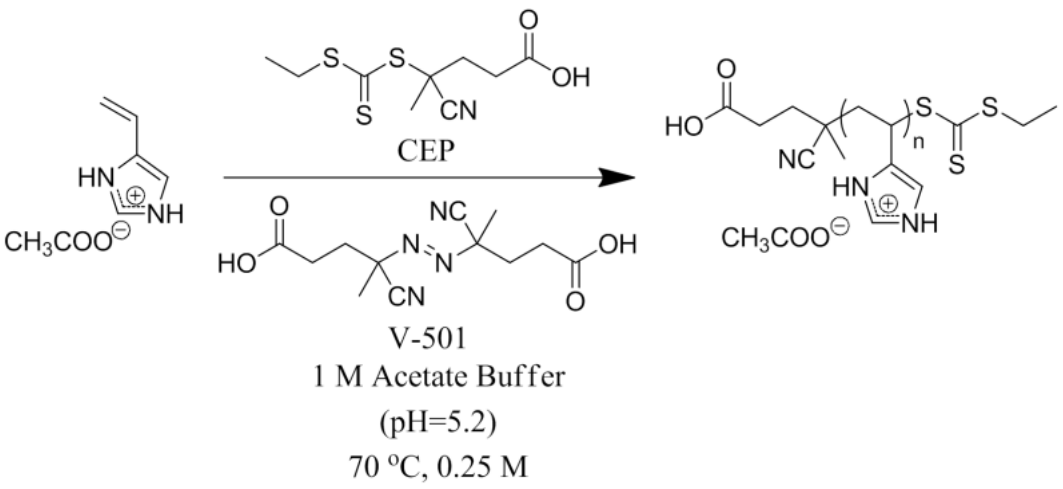

Scheme 7.3. Aqueous RAFT polymerization of poly(4VIM) in 1M acetate buffer.

The reaction conditions targeted an M_n of 23,500 g/mol at 100% conversion; however, as the reaction time increased, the polymer molecular weights exceeded target molecular weight and exhibited broad PDIs (>1.60) (

Table 7.1).

Table 7.1. Molecular weight analysis of 4VIM RAFT homopolymerization in 1M acetate buffer (pH = 5.2).[a]

Time (min)	M_n[b] (g/mol)	PDI
30	1,800	1.10
60	5,100	1.61
90	20,200	1.71
120	35,000	1.74
180	62,200	1.67
240	70,900	1.61

[a][4VIM]/[CEP]/[V-501] = 500:2:1, [4VIM] = 0.250 M.
[b]Absolute molecular weights determined with aqueous SEC-MALLS.

The uncontrolled molecular weight growth suggested that 4VIM remained partially unprotonated, contributing to CTA aminolysis during polymerization. To increase the acidity of

the solution and ensure complete protonation of 4VIM, we performed RAFT polymerizations in glacial acetic acid (Scheme 7.4).

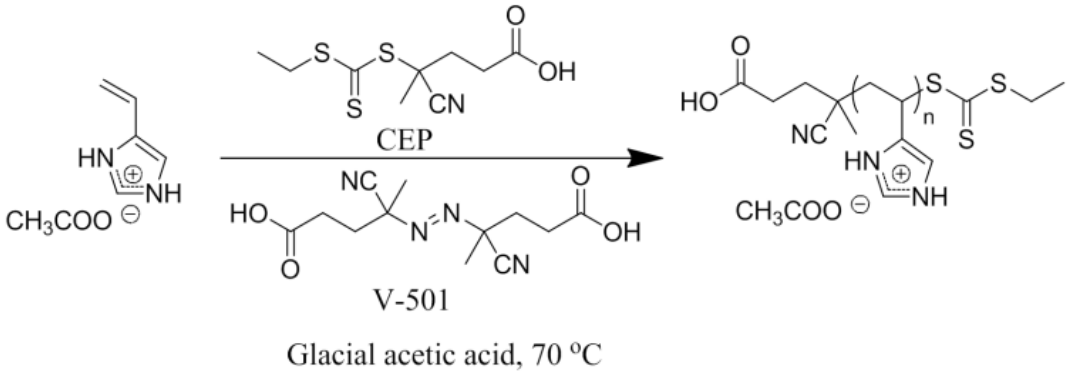

Scheme 7.4. RAFT polymerization of 4VIM at 70 °C in glacial acetic acid.

Initial experiments demonstrated the absence of CTA aminolysis under these conditions. The influence of initiator concentration, monomer concentration, and targeted molecular weight on the polymerization were studied to probe the feasibility of RAFT polymerization in this unconventional solvent.

Initial reaction conditions revealed the influence of increasing the initiator concentration (V-501) while maintaining a 250/1 [4VIM]/[CEP] molar ratio. Aqueous SEC-MALLS showed a shift in molecular weight distribution to shorter elution times as the 4VIM RAFT homopolymerization progressed (Figure 7.2a, [CEP]/[V-501] = 2). The unimodal SEC traces combined with the systematic shift in elution time indicated an absence of high molecular weight termination products and uncontrolled homopolymerization. Figure 7.2b shows the expected increase in the apparent polymerization rate as the initiator concentration increased.

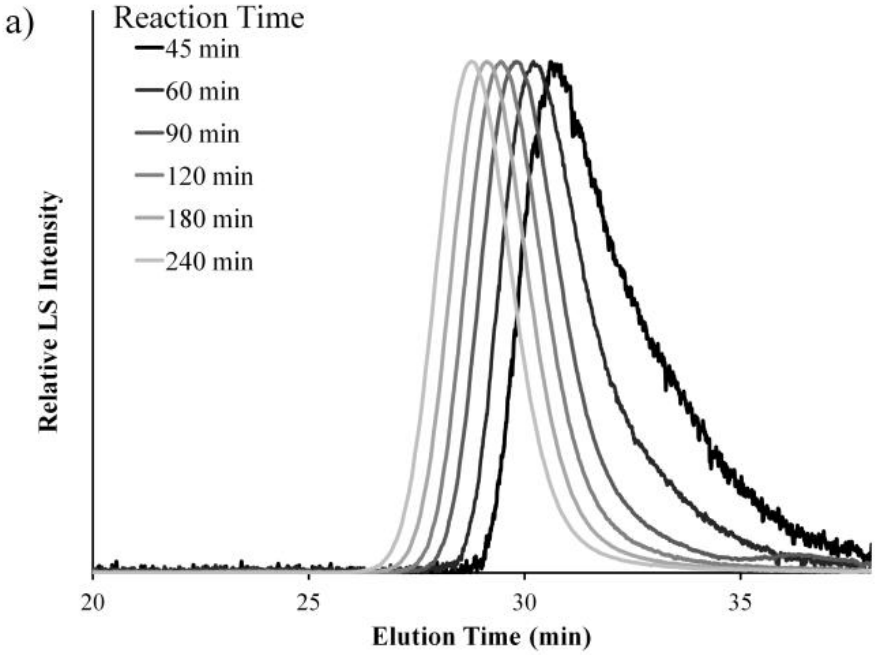
a)
Reaction Time
45 min
60 min
90 min
120 min
180 min
240 min
Relative LS Intensity
20
25
30
35
Elution Time (min)

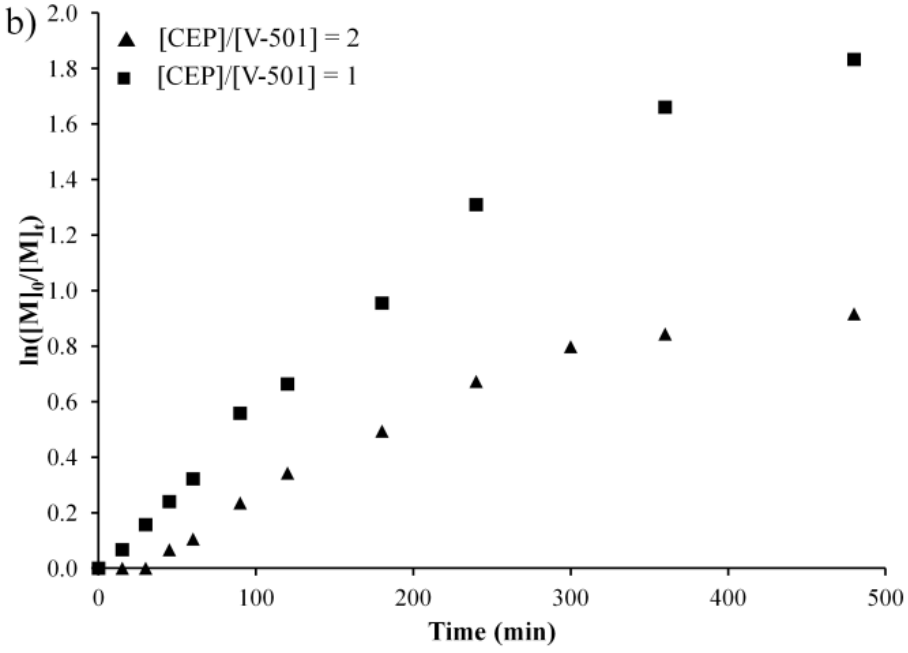
b)
[CEP]/[V-501] = 2
[CEP]/[V-501] = 1
ln([M]0/[M]t)
0.0
0.2
0.4
0.6
0.8
1.0
1.2
1.4
1.6
1.8
2.0
0
100
200
300
400
500
Time (min)

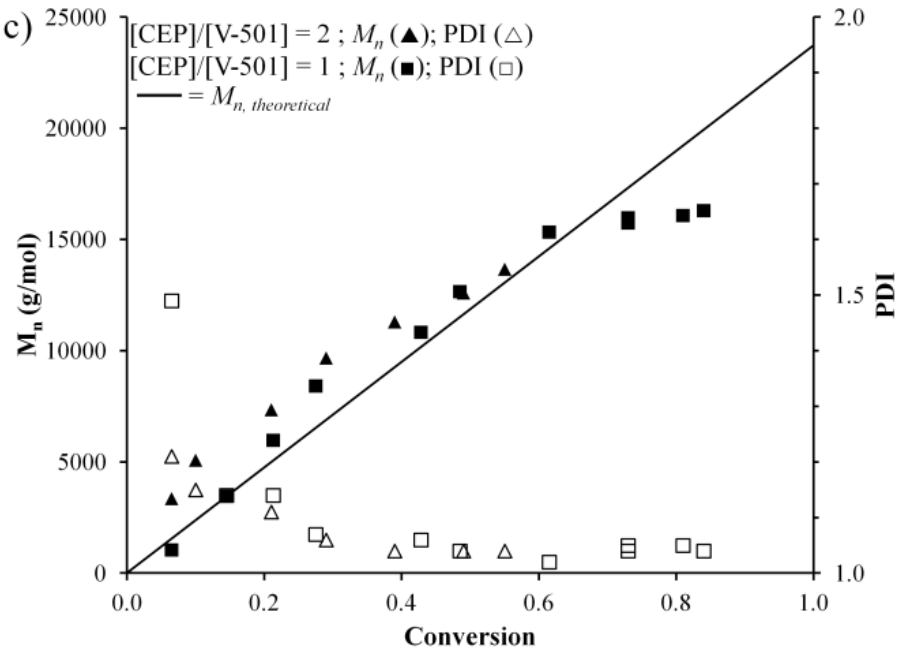

Figure 7.2. (a) Representative aqueous SEC light scattering chromatograms displaying the increase in polymer molecular weight as RAFT polymerization progressed. (b) Pseudo-first order kinetics plot for the RAFT polymerization of 4VIM (0.25 M) in glacial acetic acid at 70 °C employing various [CEP]/[V-501] concentrations while maintaining a target DP of 250. (c) Dependence of M_n and PDI on monomer conversion utilizing various [CEP]/[V-501] concentrations.

McCormick and co-workers ascribed the increasing slopes with increasing initiator concentration to the participation of more propagating chains during RAFT polymerization.[67] We examined various [CEP]/[V-501] molar ratios from 4 – 1; however, a [CEP]/[V-501] = 4 ratio exhibited inappreciable conversion over the 8 h experiment. The [CEP]/[V-501] = 2 molar ratio displayed an induction period of 45 min while a [CEP]/[V-501] = 1 molar ratio did not have an induction period. Literature suggests that induction periods occur when R• (from CTA) reinitiates slowly or preferentially combines with the CTA.[68] Increasing the number of radicals at the beginning of the reaction typically reduces or eliminates the inhibition period. The pseudo-first order kinetic plots for the different initiator concentrations remained linear for approximately 4 h where a change in slope occurred. The linear portion of the kinetic plot prior to the change in slope at 4 h

established the apparent rate constants, k_{app}, for each polymerization (Entries A and B in Table 7.2).

Table 7.2. Apparent rate constants (k_{app}) for the RAFT polymerization of 4VIM under various reaction conditions.

Entry	[CTA]/[I]	[4VIM] (M)	M_n @ 100% Conv.	k_{app} (s^{-1})
A	2	0.250	23,500 (DP = 250)	5.0×10^{-5}
B	1	0.250	23,500 (DP = 250)	9.2×10^{-5}
C	2	0.500	23,500 (DP = 250)	1.2×10^{-4}
D	2	0.500	47,000 (DP = 500)	2.5×10^{-5}
E	2	0.500	94,100 (DP = 1000)	0.7×10^{-5}

The RAFT polymerization of acrylamides and methacrylamides typically display a similar change in slope attributed to a reduction in radicals in the main RAFT equilibrium or a change in the propagation rate constant.[53,67,69] Figure 2c further demonstrates excellent molecular weight control, depicting linear increases in molecular weight with increasing conversion while maintaining narrow PDIs (< 1.20) up to 80% conversion. The overlap of experimental molecular weights with theoretical predictions also indicates a well-controlled polymerization.

In addition to varying the [CEP]/[V-501] molar ratio, we also studied the impact of 4VIM monomer concentration on the RAFT polymerization kinetics. The increased monomer concentration (0.25 M to 0.50 M) resulted in faster kinetics as expected (Figure 7.3a; Entries A and C in Table 7.2).

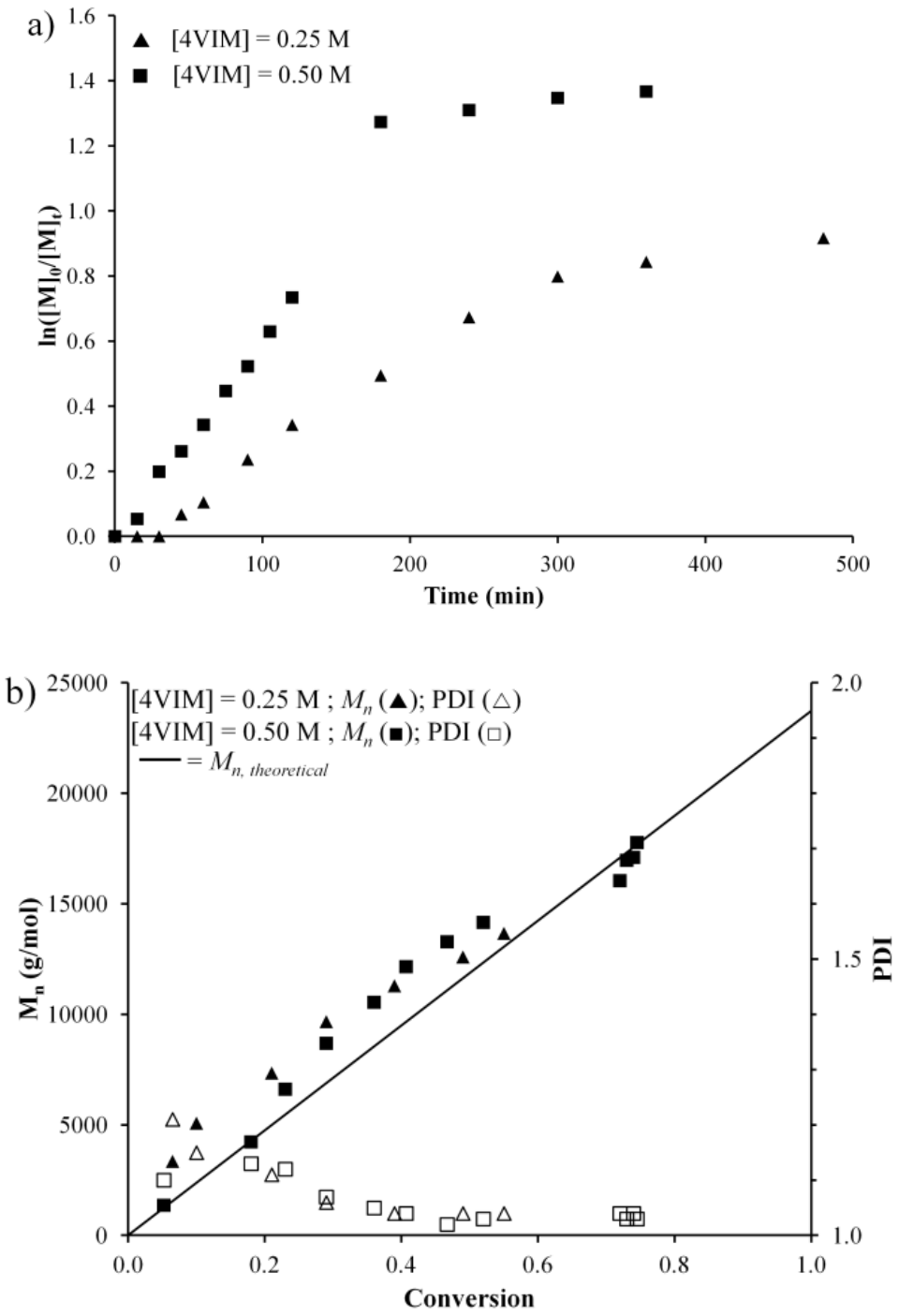

Figure 7.3. (a) Pseudo-first order kinetics plot for the RAFT polymerization of 4VIM in glacial acetic acid at 70 °C with various monomer concentrations ([CEP]/[V-501] = 2; [4VIM]/[CEP] = 250). (b) Dependence of M_n and PDI on monomer conversion at different reaction solution concentrations.

The linearity of the plots indicated pseudo-first order behavior. Likewise, a change in slope occurred for reaction times above 3 h, as discussed previously. The polymerizations proceeded to quantitative conversions with PDIs < 1.20. Figure 7.3b demonstrates good agreement between experimental and theoretical molecular weights.

The adjustment of the [4VIM]/[CEP] molar ratio while maintaining a constant [CEP]/[V-501] = 2 molar ratio targeted higher degrees of polymerization. Figure 7.4a shows linear pseudo-first order kinetics regardless of targeted degree of polymerization.

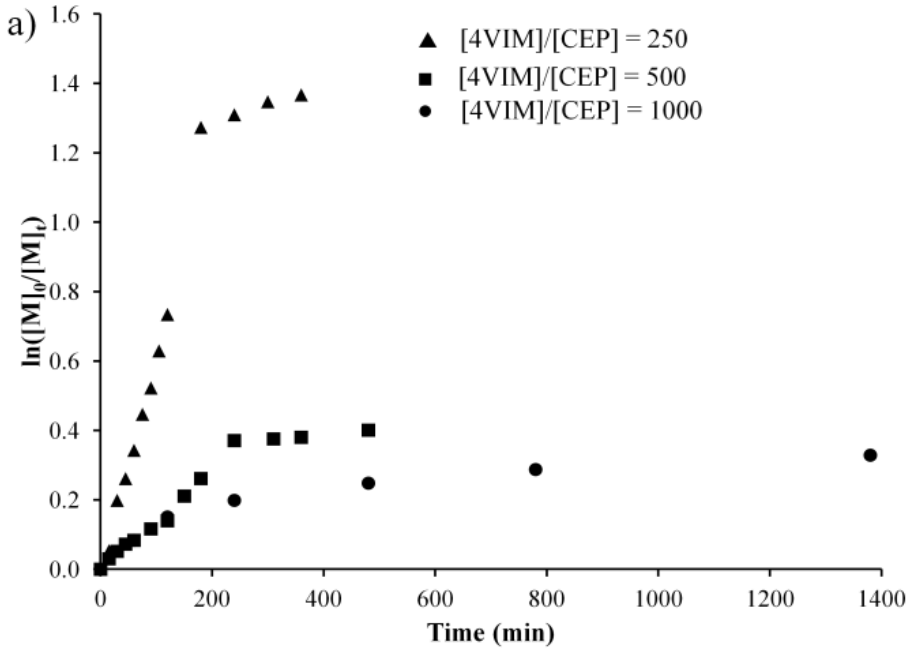

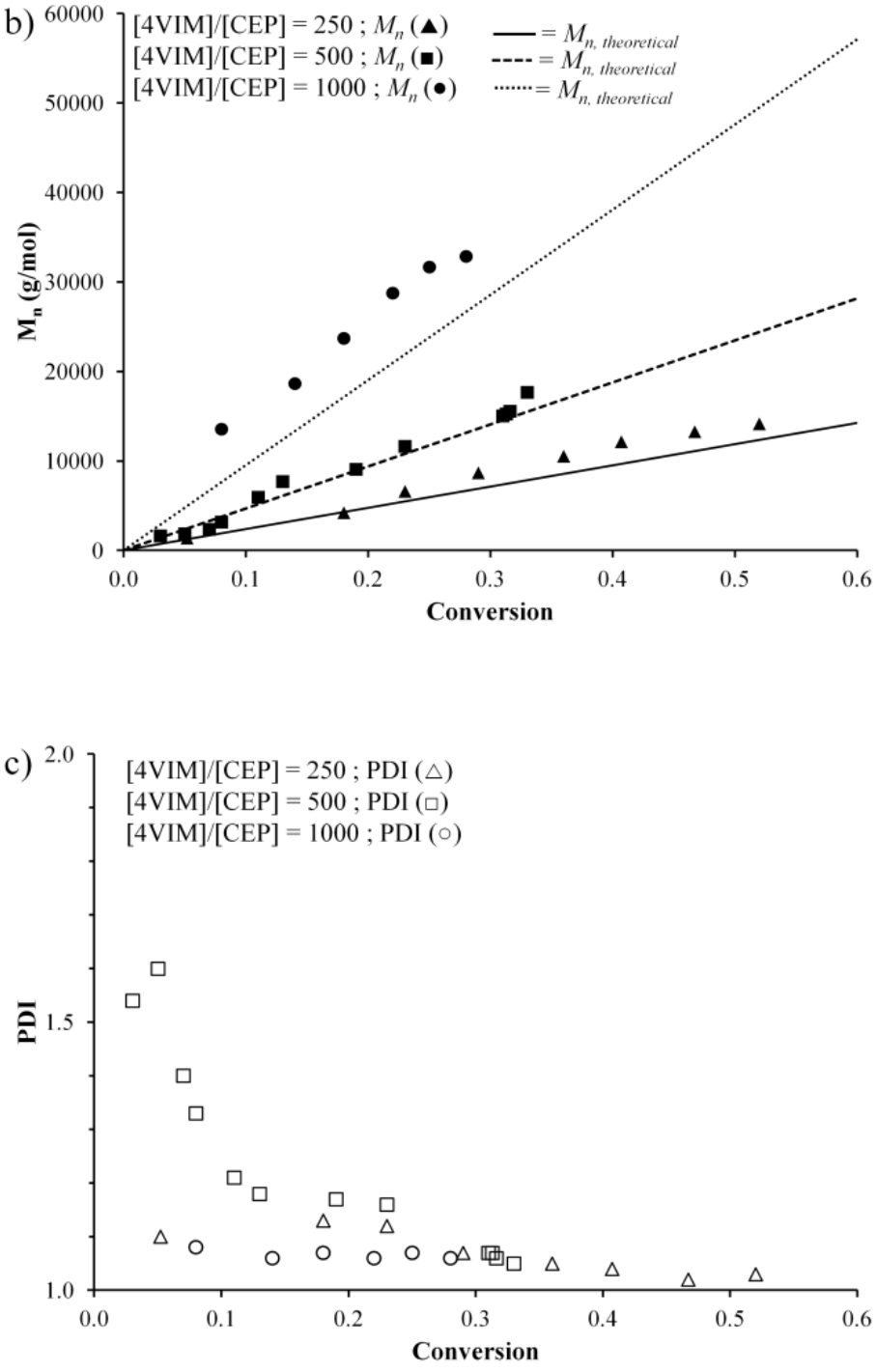

Figure 7.4. (a) Pseudo-first order kinetics plot for the RAFT polymerization of 4VIM in glacial acetic acid ([4VIM] = 0.50 M; [CEP]/[V-501] = 2) at 70 °C employing various [4VIM]/[CEP] concentrations. (b) Dependence of M_n on monomer conversion utilizing various [4VIM]/[CEP] concentrations. (c) Dependence of PDI on monomer conversion utilizing various [4VIM]/[CEP] concentrations.

As the target molecular weight increased, the reaction rates decreased significantly due to a reduction in the concentration of active propagating chains as explained previously (Entries A, D, and E in Table 7.2). The linear evolution of experimental molecular weights *versus* conversion occurred at all polymerization conditions with narrow PDIs as revealed in Figure 7.4b and c. The experimental molecular weights displayed good agreement with theoretical predictions, producing well-defined 4VIM homopolymers to 33,000 g/mol with PDIs as low as 1.06.

Upon identification of optimized reaction conditions for controlled RAFT polymerization of 4VIM, reaction conditions were identified to produce polymers with M_n's exceeding 30,000 g/mol. The reactions ([4VIM]/[CEP]/[V-501] = 2000/2/1 or 1000/1/1, 1.0 M, 17 h) produced higher molecular weight polymers (M_n = 51,000 and 65,000 g/mol ; PDI = 1.04, 1.02 respectively). These results confirmed that RAFT polymerization in glacial acetic acid produced precise 4VIM homopolymers under various conditions with a broad range of molecular weights with narrow PDIs (M_n = 1,000-65,000 g/mol; PDIs = 1.02-1.19). In sharp contrast, the RAFT polymerization of 1VIM failed to produce any polymer under similar conditions.

The synthesis of a 4VIM macroCTA and subsequent monomer addition with additional 4VIM produced a "diblock" copolymer, further demonstrating the controlled RAFT polymerization of 4VIM. The polymerization employed identical reaction conditions as discussed previously in Figure 7.2a utilizing a [CEP]/[V-501] = 2. Figure 7.5 shows an SEC chromatogram of the macroCTA (M_n = 16,900 g/mol; PDI = 1.02) with a clear shift in elution time when chain-extended with additional 4VIM.

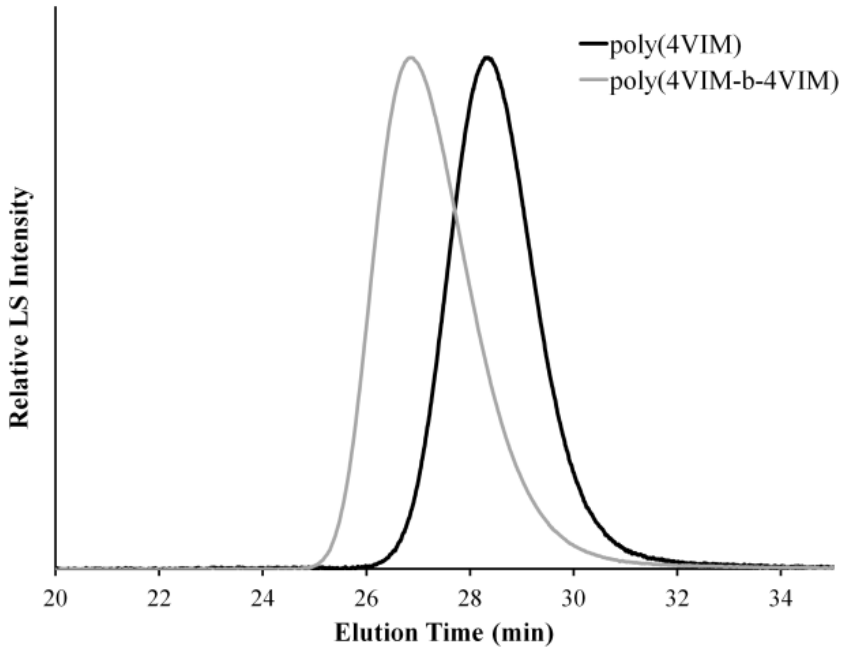

Figure 7.5. Aqueous SEC light scattering traces for the 4VIM macroCTA (M_n = 16,900 g/mol, PDI = 1.02) and the corresponding chain extended "block" copolymer (M_n = 37,300 g/mol, PDI = 1.04).

The chain-extension produced a "diblock" copolymer with an M_n = 37,300 g/mol and PDI = 1.04. The narrow PDI and absence of a high molecular weight shoulder suggested the macroCTA retained the trithiocarbonate functionality at the chain end. The lack of termination products demonstrated further proof of effective polymerization control.

7.5 *Conclusions*

The RAFT polymerization of 4VIM in glacial acetic acid produced well-defined, monodisperse homopolymers. We demonstrated, for the first time to our knowledge, the CRP of 4VIM. RAFT polymerization of 4VIM created macromolecules with an $M_n \leq$ 65,000 g/mol with PDIs below 1.20. We revealed through the variation of numerous reaction conditions that the RAFT polymerization of 4VIM remained controlled, however, NMP failed to control 4VIM homopolymerization. Aqueous SEC showed monomodal peaks with clear shifts in elution times

as monomer conversion increased. The experimental absolute molecular weights displayed excellent agreement with theoretical predictions. All reactions displayed linear, pseudo-first order kinetics. Chain extension experiments suggested the preservation of the trithiocarbonate functionality at the chain ends. The use of traditional aqueous RAFT solvents (acetate buffer) for amine-containing monomers exhibited uncontrolled molecular weight growth lending to the importance of glacial acetic acid as the reaction solvent. We plan to investigate the polymerization of 4VIM with additional comonomers using RAFT polymerization. CRP of 4VIM will enable the development of imidazole-containing block copolymers for various applications including non-viral gene delivery and electro-active device fabrication.

7.6 *Acknowledgments*

The authors acknowledge Arkema, Inc. for their generous donation of Blocbuilder® for controlled radical polymerization studies. This material is based upon work supported in part by the Macromolecular Interfaces with Life Sciences (MILES) Integrative Graduate Education and Research Traineeship (IGERT) of the National Science Foundation under Agreement No. DGE-0333378. This material is also based upon work supported in part by the US Army Research Office under Grant No. W911NF-07-1-0452 Ionic Liquids in Electro-Active Devices (ILEAD) MURI. This material is based on work partially supported by the U.S. Army Research Laboratory and the U.S. Army Research Office under the Army Materials Center of Excellence Program, contract W911NF-06-2-0014.

7.7 *References*

(1) Green, M. D.; Long, T. E. *Polymer Reviews* **2009**, *49*, 291 - 314.
(2) Anderson, E. B.; Long, T. E. *Polymer* **2010**, *51*, 2447-2454.
(3) Mecerreyes, D. *Prog. Polym. Sci.* **2011**, *36*, 1629-1648.
(4) Green, M. D.; Allen Jr, M. H.; Dennis, J. M.; Cruz, D. S.-d. l.; Gao, R.; Winey, K. I.; Long, T. E. *Eur. Polym. J.* **2011**, *47*, 486-496.
(5) Midoux, P.; Pichon, C.; Yaouanc, J.-J.; Jaffrès, P.-A. *British Journal of Pharmacology* **2009**, *157*, 166-178.

(6) Allen, M. H.; Green, M. D.; Getaneh, H. K.; Miller, K. M.; Long, T. E. *Biomacromolecules* **2011**, *12*, 2243-2250.
(7) Lu, J.; Yan, F.; Texter, J. *Prog. Polym. Sci.* **2009**, *34*, 431-448.
(8) Welton, T. *Chem. Rev.* **1999**, *99*, 2071-2084.
(9) Dupont, J.; de Souza, R. F.; Suarez, P. A. Z. *Chem. Rev.* **2002**, *102*, 3667-3692.
(10) Przemyslaw, K. *Prog. Polym. Sci.* **2004**, *29*, 3-12.
(11) Ye, Y.; Elabd, Y. A. *Macromolecules* **2011**, *44*, 8494-8503.
(12) Lee, M.; Choi, U. H.; Colby, R. H.; Gibson, H. W. *Chem. Mater.* **2010**, *22*, 5814-5822.
(13) Matsumoto, K.; Talukdar, B.; Endo, T. *Polym. Bull.* **2010**, *66*, 199-210.
(14) Weber, R. L.; Ye, Y.; Banik, S. M.; Elabd, Y. A.; Hickner, M. A.; Mahanthappa, M. K. *J. Polym. Sci., Part B: Polym. Phys.* **2011**, *49*, 1287-1296.
(15) Weber, R. L.; Ye, Y.; Schmitt, A. L.; Banik, S. M.; Elabd, Y. A.; Mahanthappa, M. K. *Macromolecules* **2011**, *44*, 5727-5735.
(16) Stancik, C. M.; Lavoie, A. R.; Achurra, P. A.; Waymouth, R. M.; Gast, A. P. *Langmuir* **2004**, *20*, 8975-8987.
(17) Stancik, C. M.; Lavoie, A. R.; Schütz, J.; Achurra, P. A.; Lindner, P.; Gast, A. P.; Waymouth, R. M. *Langmuir* **2003**, *20*, 596-605.
(18) Green, M. D.; Salas-de la Cruz, D.; Ye, Y.; Layman, J. M.; Elabd, Y. A.; Winey, K. I.; Long, T. E. *Macromol. Chem. Phys.* **2012**, *212*, 2522-2528.
(19) la Cruz, D. S.-d.; Green, M. D.; Ye, Y.; Elabd, Y. A.; Long, T. E.; Winey, K. I. *J. Polym. Sci., Part B: Polym. Phys.* **2012**, *50*, 338-346.
(20) Overberger, C. G.; Kawakami, Y. *Journal of Polymer Science: Polymer Chemistry Edition* **1978**, *16*, 1237-1248.
(21) Overberger, C. G.; Smith, T. W. *Macromolecules* **1975**, *8*, 416-424.
(22) Overberger, C. G.; Smith, T. W. *Macromolecules* **1975**, *8*, 401-406.
(23) Overberger, C. G.; Smith, T. W. *Macromolecules* **1975**, *8*, 407-415.
(24) Overberger, C. G.; Maki, H. *Macromolecules* **1970**, *3*, 214-220.
(25) Overberger, C. G.; Maki, H. *Macromolecules* **1970**, *3*, 220-223.
(26) Overberger, C. G.; Pierre, T. S.; Vorchheimer, N.; Lee, J.; Yaroslavsky, S. *J. Am. Chem. Soc.* **1965**, *87*, 296-301.
(27) Overberger, C. G.; Vorchheimer, N. *J. Am. Chem. Soc.* **1963**, *85*, 951-955.
(28) Overberger, C. G.; Pierre, T. S.; Vorchheimer, N.; Yaroslavsky, S. *J. Am. Chem. Soc.* **1963**, *85*, 3513-3515.
(29) Yoshizawa, M.; Ogihara, W.; Ohno, H. *Polym. Adv. Technol.* **2002**, *13*, 589-594.
(30) Ohno, H. *Electrochim. Acta* **2001**, *46*, 1407-1411.
(31) Johnson, D. M.; Rasmussen, P. G. *Macromolecules* **2000**, *33*, 8597-8603.
(32) Overberger, C. G.; Gerberding, K. *Journal of Polymer Science: Polymer Letters Edition* **1973**, *11*, 465-469.
(33) Matsumoto, K.; Endo, T. *Macromolecules* **2009**, *42*, 4580-4584.
(34) Chen, H.; Elabd, Y. A. *Macromolecules* **2009**, *42*, 3368-3373.
(35) Tang, J.; Radosz, M.; Shen, Y. *Macromolecules* **2007**, *41*, 493-496.
(36) Tang, J.; Tang, H.; Sun, W.; Radosz, M.; Shen, Y. *J. Polym. Sci., Part A: Polym. Chem.* **2005**, *43*, 5477-5489.
(37) Bara, J. E.; Carlisle, T. K.; Gabriel, C. J.; Camper, D.; Finotello, A.; Gin, D. L.; Noble, R. D. *Industrial & Engineering Chemistry Research* **2009**, *48*, 2739-2751.
(38) Matyjaszewski, K. *Curr. Opin. Solid State Mater. Sci.* **1996**, *1*, 769-776.

(39) Lowe, A. B.; McCormick, C. L. *Prog. Polym. Sci.* **2007**, *32*, 283-351.
(40) Ding, S.; Tang, H.; Radosz, M.; Shen, Y. *J. Polym. Sci., Part A: Polym. Chem.* **2004**, *42*, 5794-5801.
(41) Vijayakrishna, K.; Jewrajka, S. K.; Ruiz, A.; Marcilla, R.; Pomposo, J. A.; Mecerreyes, D.; Taton, D.; Gnanou, Y. *Macromolecules* **2008**, *41*, 6299-6308.
(42) He, X.; Yang, W.; Yuan, L.; Pei, X.; Gao, J. *Mater. Lett.* **2009**, *63*, 1138-1140.
(43) Ge, Z.; Xie, D.; Chen, D.; Jiang, X.; Zhang, Y.; Liu, H.; Liu, S. *Macromolecules* **2007**, *40*, 3538-3546.
(44) Mori, H.; Yahagi, M.; Endo, T. *Macromolecules* **2009**, *42*, 8082-8092.
(45) Detrembleur, C.; Debuigne, A.; Hurtgen, M.; Jérôme, C.; Pinaud, J.; Fèvre, M. v.; Coupillaud, P.; Vignolle, J.; Taton, D. *Macromolecules* **2011**, *44*, 6397-6404.
(46) Skouta, R.; Wei, S.; Breslow, R. *J. Am. Chem. Soc.* **2009**, *131*, 15604-15605.
(47) Ihm, J.-E.; Han, K.-O.; Han, I.-K.; Ahn, K.-D.; Han, D.-K.; Cho, C.-S. *Bioconjugate Chem.* **2003**, *14*, 707-708.
(48) Ihm, J. E.; Han, K.-O.; Hwang, C. S.; Kang, J. H.; Ahn, K.-D.; Han, I.-K.; Han, D. K.; Hubbell, J. A.; Cho, C.-S. *Acta Biomaterialia* **2005**, *1*, 165-172.
(49) Bozkurt, A.; Karadedeli, B. *React. Funct. Polym.* **2007**, *67*, 348-354.
(50) Bozkurt, A.; Meyer, W. H. *Solid State Ionics* **2001**, *138*, 259-265.
(51) Bozkurt, A.; Meyer, W. H.; Gutmann, J.; Wegner, G. *Solid State Ionics* **2003**, *164*, 169-176.
(52) Sezgin, A.; Akbey, Ü.; Graf, R.; Bozkurt, A.; Baykal, A. *J. Polym. Sci., Part B: Polym. Phys.* **2009**, *47*, 1267-1274.
(53) Smith, A. E.; Xu, X.; McCormick, C. L. *Prog. Polym. Sci.* **2010**, *35*, 45-93.
(54) Perrier, S.; Takolpuckdee, P. *J. Polym. Sci., Part A: Polym. Chem.* **2005**, *43*, 5347-5393.
(55) Moad, G.; Rizzardo, E.; Thang, S. H. *Aust. J. Chem.* **2005**, *58*, 379-410.
(56) Convertine, A. J.; Benoit, D. S. W.; Duvall, C. L.; Hoffman, A. S.; Stayton, P. S. *J. Controlled Release* **2009**, *133*, 221-229.
(57) Grimaldi, S.; Finet, J.-P.; Le Moigne, F. o.; Zeghdaoui, A.; Tordo, P.; Benoit, D.; Fontanille, M.; Gnanou, Y. *Macromolecules* **2000**, *33*, 1141-1147.
(58) Qiu, J.; Charleux, B.; Matyjaszewski, K. *Prog. Polym. Sci.* **2001**, *26*, 2083-2134.
(59) Edsall, J. T.; Felsenfeld, G.; Goodman, D. S.; Gurd, F. R. N. *J. Am. Chem. Soc.* **1954**, *76*, 3054-3061.
(60) Nicolas, J.; Charleux, B.; Guerret, O.; Magnet, S. p. *Macromolecules* **2004**, *37*, 4453-4463.
(61) Weber, C.; Neuwirth, T.; Kempe, K.; Ozkahraman, B.; Tamahkar, E.; Mert, H.; Becer, C. R.; Schubert, U. S. *Macromolecules* **2011**, *45*, 20-27.
(62) Chaduc, I.; Lansalot, M.; D'Agosto, F.; Charleux, B. *Macromolecules* **2012**, *45*, 1241-1247.
(63) Abreu, C. M. R.; Mendonça, P. V.; Serra, A. C.; Coelho, J. F. J.; Popov, A. V.; Gryn'ova, G.; Coote, M. L.; Guliashvili, T. *Macromolecules* **2012**, *45*, 2200-2208.
(64) Alidedeoglu, A. H.; York, A. W.; McCormick, C. L.; Morgan, S. E. *J. Polym. Sci., Part A: Polym. Chem.* **2009**, *47*, 5405-5415.
(65) Bicciocchi, E.; Chong, Y. K.; Giorgini, L.; Moad, G.; Rizzardo, E.; Thang, S. H. *Macromol. Chem. Phys.* **2010**, *211*, 529-538.
(66) Smith, A. E.; Xu, X.; Kirkland-York, S. E.; Savin, D. A.; McCormick, C. L. *Macromolecules* **2010**, *43*, 1210-1217.

(67) Thomas, D. B.; Convertine, A. J.; Myrick, L. J.; Scales, C. W.; Smith, A. E.; Lowe, A. B.; Vasilieva, Y. A.; Ayres, N.; McCormick, C. L. *Macromolecules* **2004**, *37*, 8941-8950.
(68) Coote, M. L. *Macromolecules* **2004**, *37*, 5023-5031.
(69) Scales, C. W.; Vasilieva, Y. A.; Convertine, A. J.; Lowe, A. B.; McCormick, C. L. *Biomacromolecules* **2005**, *6*, 1846-18
(70) Candau, F.; Leong, Y. S.; Fitch, R. M. *Journal of Polymer Science: Polymer Chemistry Edition* **1985**, *23*, 193-214.
(71) Nakamura, K.; Hatakeyama, T.; Hatakeyama, H. Polym. J. 1983, 15, 361-366.
(72) Xu, H.; Kuo, S.-W.; Lee, J.-S.; Chang, F.-C. *Polymer* **2002**, *43*, 5117-5124.

7.8 *Supporting Information*

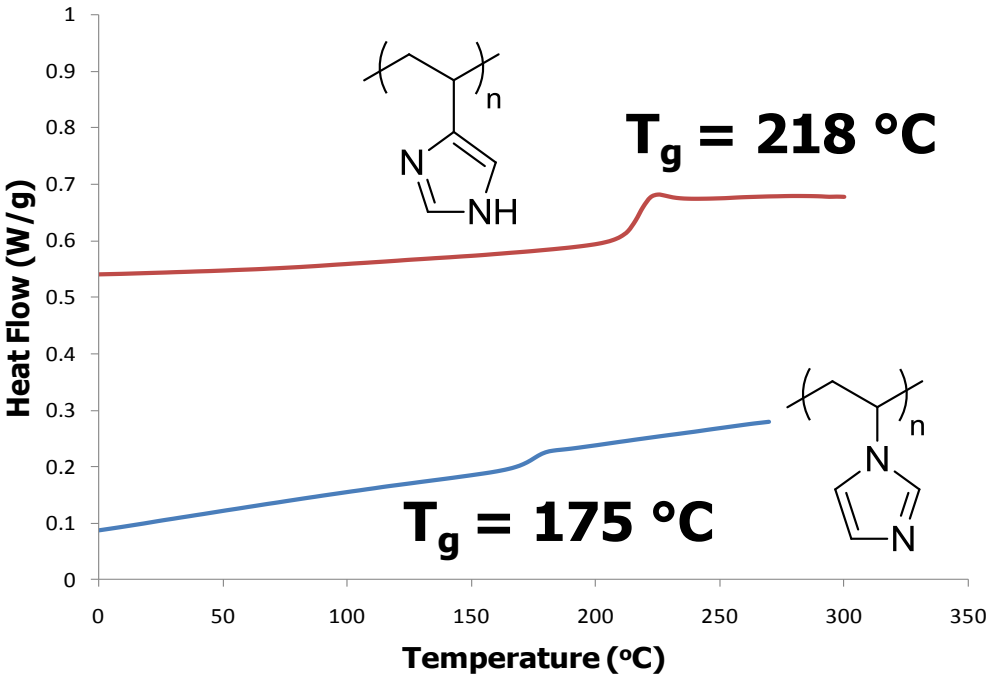

Figure S7.1. DSC thermogram of poly(1VIM) and poly(4VIM).

Chapter 8: Synthesis and Characterization of 4-Vinylimidazole ABA Triblock Copolymers Utilizing a New Difunctional RAFT Chain Transfer Agent

Michael H. Allen, Jr., Sean T. Hemp, Musan Zhang, Mingqiang Zhang, Adam E. Smith, [‡] Robert B. Moore, and Timothy E. Long
Macromolecules and Interfaces Institute, Department of Chemistry, Virginia Tech, Blacksburg, VA 24061
[‡]*Department of Chemical Engineering, The University of Mississippi, University, MS 38677*
Corresponding Author: telong@vt.edu

8.1 *Abstract*

Reversible addition-fragmentation chain transfer (RAFT) polymerization strategies enabled the unprecedented synthesis of 4-vinylimidazole (4VIM)-containing ABA triblock copolymers utilizing. The synthesis of a novel, difunctional trithiocarbonate RAFT chain transfer agent (CTA) controlled the divergent RAFT polymerization of methacrylic and 4VIM monomers with controlled molecular weights and narrow polydispersity indices (PDIs). The triblock copolymers consisted of a low-T_g di(ethylene glycol) methyl ether methacrylate (DEGMEMA) center block (M_n = 26,000 g/mol) and an amphoteric 4VIM external, mechanically reinforcing block (M_n = 6,500 – 16,500 g/mol). Varying the 4VIM content probed the influence of the triblock copolymer composition on the macromolecular thermomechanical and morphological properties. Dynamic mechanical analysis (DMA) of the triblock copolymers exhibited a rubbery plateau region over a wide temperature range (~200 °C), which confirmed the establishment of microphase-separated morphologies with flow temperatures above 200 °C. Transmission electron microscopy (TEM), atomic force microscopy (AFM), and small-angle X-ray scattering (SAXS) collectively probed the solid state morphologies of the triblock copolymers; all techniques revealed phase separation at nanoscale dimensions. The triblock copolymers with 40 wt. % 4VIM formed lamellar morphologies. Well-defined, amphoteric, 4VIM ABA triblock copolymers (PDIs < 1.10) with microphase-separated morphologies now

permits imidazole-containing macromolecules of controlled architectures for emerging applications.

8.2 *Introduction*

Tailoring noncovalent interactions for the design of well-defined supramolecular structures remains an area of intense focus for biological and engineering applications. Introduction of reversible, noncovalent interactions particularly through the addition of hydrogen bonding substituents enables the enhancement of morphology and physical properties of macromolecular structures.[1-3] The effects of multiple hydrogen bonding yield stronger intermolecular associations which enhance microphase separation within block copolymers compared to weaker van der Waals interactions.[4,5] Our research group and others previously demonstrated the addition of short hydrogen bonding blocks promotes microphase separation in step- and chain-growth polymers.[6-9] Complementary nucleobase triblock copolymers containing adenine or thymine residues with a soft *n*-butyl acrylate (*n*BA) center block required only 7 wt. % nucleobase monomer to achieve cylindrical morphologies.[10] In addition, Han et al. showed hydrogen bonding interactions in modified poly(styrene-*b*-isoprene) copolymers effectively increased the Flory-Huggins interaction parameter (χ), therefore promoting increased microphase separation.[11]

The amphoteric nature of the imidazole ring imparts unique properties for its incorporation into block copolymers. The association constant for the dimerization of imidazole (K_a = 15.9 M^{-1}) remains significantly larger than benzene (K_a = 0.85 M^{-1}) due to the complementary intermolecular hydrogen bonding interactions in the imidazole ring dimer.[12-14] The larger association constant for the imidazole ring would presumably allow for the synthesis of precise, nanophase-separated block copolymers as a superior alternative to traditional styrene-based block copolymers. Numerous imidazole-containing monomers are available for block

copolymer design utilizing controlled radical polymerization (CRP) including (meth)acrylics,[15-17] styrenics,[18-21] and 1-, 2-, and 4-vinylimidazoles (1VIM, 2VIM, 4VIM).[22-36]

Nitroxide-mediated polymerization (NMP), atom transfer radical polymerization (ATRP), and reversible addition-fragmentation chain transfer (RAFT) are versatile synthetic strategies to produce macromolecules with controlled architectures. Shen et al. mediated the polymerization of 2-(1-butylimidazolium)ethyl methacrylate tetrafluoroborate (BIMT) utilizing ATRP to generate homopolymers with precise molecular weights for CO_2 absorbing membranes.[37,38] Gnanou et al. polymerized BIMT with RAFT polymerization to synthesize stimuli-responsive block copolymers containing methacrylic acid.[39] Furthermore, Elabd, Winey and co-workers recently synthesized block copolymers containing 1-[(2-methacryloyloxy)ethyl]-3-butylimidazolium bis(trifluoromethane-sulfonyl)imide (MEBIm-TFSI) with methyl methacrylate (MMA) utilizing RAFT polymerization to understand the influence of phase separation on ionic conductivity.[40] The diblock copolymers weakly phase separated due to partial affinity between the MEBIM-TFSI and MMA blocks. NMP of styrenic-based imidazolium polymers also produced macromolecules with well-defined molecular weights suited for a variety of emerging applications including CO_2 absorbing membranes, electroactive materials, and micelle self-assembly.[18-21,41,42] Patrickios et al. utilized group transfer polymerization (GTP) to synthesize block copolymers containing 2-(1-Imidazolyl)ethyl methacrylate (ImEMA).[43] Incorporation of the imidazole ring into these systems relied upon functionality at the 1- and/or 3-positions, which eliminated the beneficial, amphoteric nature of the imidazole ring in producing microphase separated block copolymers.

1VIM monomer also contains functionality at the 1-position, which disrupts intermolecular hydrogen bonding. In addition, 1VIM forms a highly reactive, propagating

radical due to the lack of resonance stabilization, and controlled radical polymerization (CRP) of 1VIM is not achievable.[44-46] Substitution on the imidazole ring must reside on the 2-, 4-, or 5-positions to promote intermolecular hydrogen bonding between imidazole sites. 4VIM is a regioisomer that contains vinyl-functionality at the 4-position of the imidazole ring and includes two resonance contributors, for increased radical stabilization of the propagating chain end. The intermolecular hydrogen bonding in poly(4VIM) compared to poly(1VIM) is especially evident in the homopolymer thermal properties. Poly(1VIM) lacks intermolecular hydrogen bonding and exhibits a glass transition temperature (T_g) at ~180 °C, and in sharp contrast, poly(4VIM) displays a T_g near ~220 °C.[47] Due to the intermolecular hydrogen bonding present in poly(4VIM), Overberger and co-workers failed to achieve homogeneous polymerization conditions, which prevented subsequent CRP studies.[24,25,29-36,48] Recently, our research group successfully demonstrated the efficacy of glacial acetic acid for homogeneous free radical polymerization of 4VIM.[47] More importantly, RAFT polymerization of 4VIM in glacial acetic acid produced homopolymers with well-defined molecular weights and narrow polydispersity indices (PDIs). RAFT polymerization of histamine acrylamide with additional acrylamide comonomers remains the single report of the CRP of an amphoteric, imidazole-containing monomer.[49]

In this manuscript, we demonstrate the synthesis of novel 4VIM-containing ABA triblock copolymers for improved mechanical performance. A difunctional trithiocarbonate chain transfer agent (CTA) that allows divergent chain growth enabled the design of ABA triblock copolymers, poly(4VIM-*b*-DEGMEMA-*b*-4VIM). Glacial acetic acid maintained homogeneous polymerization conditions for the addition of 4VIM to the poly(DEGMEMA) macroCTA in the absence of CTA aminolysis or DEGMEMA esterolysis. ^{1}H NMR spectroscopy and size

exclusion chromatography (SEC) confirmed the well-controlled synthesis of poly(4VIM-*b*-DEGMEMA-*b*-4VIM) triblock copolymers with tunable 4VIM compositions to tailor polymer mechanical performance and morphology. Dynamic mechanical analysis (DMA) probed the thermomechanical properties of the ABA triblock copolymers. SAXS and complementary AFM and TEM examined the microphase separation of the thermoplastic elastomers. These amphoteric sequences offer unique potential for the design of thermoplastic elastomers for applications ranging from high temperature elastomers to drug delivery platforms.

8.3 *Experimental Section*

8.3.1 Materials

N, N'-dicyclohexylcarbodiimide (DCC, 99%), 4-(dimethylamino)pyridine (DMAP, ≥99.0%), 1,6-hexanediamine (98%), 1,6-hexanediol (99%) were purchased from Sigma-Aldrich and used as received. 4-cyano-4-(ethylsulfanylthiocarbonylsulfanyl)pentanoic acid (CEP)[50] and 4VIM[47] were synthesized according to previous literature. Anhydrous dichloromethane (DCM) was obtained from a solvent purification system (Pure Solv, Innovative Technology) and all other solvents were obtained from Fisher Scientific and used as received. Styrene (99.9%), *n*-butyl acrylate (*n*BA, > 99%), *t*-butyl acrylate (*t*BA, 98%), methyl methacrylate (MMA, 99%), 2-(dimethylamino)ethyl methacrylate (DMAEMA, 98%), glycidyl methacrylate (GMA, 97%), di(ethylene glycol) methyl ether methacrylate (DEGMEMA, 95%), and poly(ethylene glycol) methyl ether methacrylate (EG_9MEMA, average M_n = 475 g/mol) were purchased from Sigma-Aldrich and passed through alumina columns prior to use to remove inhibitors. 4,4-azobis(4-cyanovaleric acid) (V-501, Aldrich, 98%) was recrystallized from methanol.

8.3.2 Analytical methods

^{1}H NMR spectroscopy (Varian Inova, 400 MHz) determined CTA, monomer, and polymer composition. Mass spectrometry was performed with an Agilent 6220 LC-TOF-MS system to confirm material composition. Polymer molecular weight was measured using aqueous size exclusion chromatography (SEC) through two Waters Ultrahydrogel Linear and one Waters Ultrahydrogel 250 columns in a solvent consisting of 54/23/23 water/methanol/acetic acid (v/v/v %) with 0.1 M sodium acetate. The instrumentation consisted of a Waters 1515 isocratic HPLC pump operating at a flow rate of 0.8 mL/min, a Waters 717plus Autosampler, a Wyatt miniDAWN multiangle light scattering detector operating at a wavelength of 690 nm, and a Waters 2414 differential refractive index detector. Dynamic light scattering (Malvern Zetasizer NanoZS) confirmed the absence of polymer aggregation in the aqueous mobile phase prior to injection onto the columns. A Wyatt Optilab T-rEX refractive index detector operating at 658 nm and 35 °C determined the offline specific refractive index increment values. Wyatt ASTRA SEC/LS software calculated absolute polymer molecular weights and PDIs. Thermogravimetric analysis of the triblock copolymers was performed on a TA Instruments thermogravimetric analyzer (TGA) Q50 with a heating rate of 10 °C/min from 23 °C to 600 °C under a nitrogen atmosphere. Thermal transitions were determined on a TA Instruments Q1000 differential scanning calorimeter (DSC, heating rate 10 °C/min) utilizing a heat/cool/heat cycle to remove polymer thermal history. DMA (TA Instruments Q800, 3 °C/min heating rate, -80 °C to 250 °C) was performed on the triblock copolymer films in tension mode at 1 Hz frequency, an oscillatory amplitude of 10 μm, and a static force of 0.01N. T_g's were determined as the peak maximum of the tanδ curve. An Instron 4411 universal tensile testing instrument operating at a crosshead speed of 10 mm/min determined the tensile properties of the poly(4VIM-*b*-DEGMEMA-*b*-4VIM) triblock copolymer films. Tensile data represented an average of five samples. A TA

Instruments Q5000 sorption analyzer (TGA-SA) measured water uptake of homopolymer samples (relative humidity (RH) 0 – 95%, 5% increments) at 25 °C.

A Veeco MultiMode scanning microscope in tapping mode provided atomic force microscopy (AFM) images of the triblock copolymers. Samples were imaged with a set-point ratio of 0.6 at 3 μm x 3 μm and 1 μm x 1 μm magnifications using a nanosensor silicon tip with a spring constant of 42 N/m. A Rigaku S-Max 3000 3 pinhole small-angle X-ray scattering (SAXS) instrument outfitted with a rotating anode generated Cu Kα irradiation at a wavelength of 1.54 Å to perform bulk morphology analysis on the triblock copolymer films. The sample-to-detector distance was 1.5 m and was calibrated with a silver behenate standard. Two-dimensional data sets were collected using a fully integrated 2D multiwire area detector with an hour exposure time, which was corrected for detector noise, background scattering, and sample absorption. All data processing and analysis was performed with the SAXSGUI software package to obtain intensity versus scattering vector q plots, where $q=4\pi\sin(\theta)/\lambda$ and 2θ is the scattering angle.

8.3.3 Difunctional CTA synthesis

In a representative synthesis, CEP (5.00 g, 19.0 mmol) was dissolved in 50 mL anhydrous DCM in a dry 100-mL, round-bottomed flask and cooled to 0 °C. DMAP (catalyst) and 1,6-hexanediamine (0.735 g, 6.33 mmol) were dissolved in 20 mL DCM and added to the chilled CEP solution. Upon addition of DMAP and 1,6-hexanediamine, DCC (4.31 g, 20.9 mmol) was added immediately to the solution to prevent aminolysis of CEP. Under argon, the solution stirred at 0 °C for 4 h and then slowly warmed to room temperature to stir for an additional 20 h. The dicyclohexylurea precipitate was filtered and the resulting solution was washed three times with a saturated sodium bicarbonate solution. The organic layer was dried with $MgSO_4$ and the solution was concentrated under reduced pressure. The yellow solid

obtained was further purified with a silica gel column in 80/20 (v/v %) hexane/ethyl acetate to remove further impurities. Once the impurities eluted off the column, the mobile phase was changed to 50/50 (v/v %) ethyl acetate/methanol to elute the purified difunctional CTA. The solvent was removed with reduced pressure and the orange-yellow solid (47% yield) was dried overnight to obtain 1,6-bis(4-cyano-4-(ethylsulfanyl-thiocarbonylsulfanyl)pentanoic acid)-hexane diamide (dCEP-NH_2). ^{1}H NMR (400 MHz, d_6-DMSO): δ 7.95 (s, 2H), 3.37 (m, 4H), 3.00 (q, 4H), 2.31 (m, 8H), 1.83 (s, 6H), 1.35 (s, 6H), 1.26 (m, 8H). ^{13}C NMR: δ 218.8 (s), 170.0 (s), 119.6 (s), 47.5 (s), 34.3 (s), 31.5 (s), 31.0 (s), 29.4 (s), 26.5 (s), 24.4 (s), 24.2 (s), 13.2 (s). HRMS (ES+): m/z calcd for [M + H^+] 607.1409 g/mol; found 607.1407 g/mol. The synthesis of 1,6-bis(4-cyano-4-(ethylsulfanylthiocarbonylsulfanyl)pentanoic acid)-hexane diester (dCEP-OH) followed the same procedure replacing 1,6-hexanediamine with 1,6-hexanediol. The product obtained was an orange oil (50% yield). ^{1}H NMR (400 MHz, d_6-DMSO): δ 4.00 (t, 4H), 3.35 (q, 4H), 2.51 (m, 4H), 2.36 (m, 4H), 1.81 (s, 6H), 1.54 (t, 6H), 1.25 (m, 8H). ^{13}C NMR: δ 218.6 (s), 171.6 (s), 119.5 (s), 64.7 (s), 47.1 (s), 33.2 (s), 31.5 (s), 29.6 (s), 28.3 (s), 25.4 (s), 24.1 (s), 13.2 (s). HRMS (ES+): m/z calcd for [M + H^+] 608.1005 g/mol; found 608.1008 g/mol.

8.3.4 Synthesis of poly(4VIM-*b*-DEGMEMA-*b*-4VIM) triblock copolymers

The monofunctional CTA, CEP, contains one trithiocarbonate functionality ([TTC] = [CEP]). The difunctional CTA, dCEP-NH_2, contains two trithiocarbonate functionalities ([TTC] = 2[dCEP-NH_2]). In a representative polymerization, DEGMEMA (4.00 g, 21.3 mmol), dCEP-NH_2 (32.3 mg, 53.0 μmol dCEP-NH_2; 106 μmol TTC), V-501 (14.9 mg, 53.2 μmol), and DMSO (42.5 mL) were added to a 100-mL, round-bottomed flask equipped with a stir bar. The reaction was sparged with argon for 30 min and placed in a thermostated oil bath at 70 °C for 6 h. The resulting polymer was dialyzed (MWCO = 3500 g/mol) for 3 days against deionized water while changing the water every 24 h. The solution was lyophilized for 48 h to obtain a yellow oil.

Aqueous SEC determined the absolute molecular weight of the DEGMEMA macroCTA ($\overline{M_n}$ = 26,000 g/mol, PDI = 1.02).

The purified macroCTA (276 mg, 10.6 μmol macroCTA; 21.2 μmol TTC) was redissolved in glacial acetic acid (21.3 mL) in a 50-mL, round-bottomed flask equipped with a stir bar. 4VIM (0.500 g, 5.31 μmol) and V-501 (2.98mg, 10.6 μmol) were added to the flask and the reaction was sparged with argon for 30 min at room temperature. The reaction was immersed in an oil bath at 70 °C for 4 h to obtain the desired amount of 4VIM in the outer blocks. The polymer solution was dialyzed (MWCO = 3500 g/mol) for 3 d against deionized water to remove unreacted 4VIM and glacial acetic acid. Aqueous SEC confirmed successful chain extension (M_n= 35,800 g/mol, PDI = 1.03) producing a 30 wt. % 4VIM-containing triblock copolymer. Different weight percentages of 4VIM incorporation into the triblock copolymers were obtained with reaction time regulation.

8.3.5 Film Casting

All triblock copolymer were dissolved in methanol and cast from a 30 wt. % solution. Films were slowly dried at ambient conditions for 2 d followed with an additional 2 d of drying at room temperature under reduced pressure. The films were then stored in a dry box until analyzed. The films were not annealed as temperatures above 60 °C for an extended time (> 24 h) due to polymer crosslinking at higher temperatures (Supporting Information).

8.4 *Results and Discussion*

CRP enables the synthesis of a broad range of block copolymers with well-defined architectures and precise molecular weights.[51-53] RAFT remains one of the premiere strategies to polymerize vinyl-containing monomers under various conditions in a controlled fashion.[54,55] RAFT provides numerous avenues to effectively polymerize functional monomers with the proper CTA and monomer combination as well as solvent choice and initiator concentration.

The rapid development of numerous applications for ABA triblock copolymers including drug and gene delivery, thermoplastic elastomers, and electroactive devices requires effective and simple methods for producing these high performance polymers.[10,41,56]

Synthesis of ABA triblock copolymers with defined molecular weights suggests the need for difunctional CTAs in RAFT polymerization. Difunctional CTAs direct propagation in either a divergent or a convergent method as illustrated in Figure 8.1.

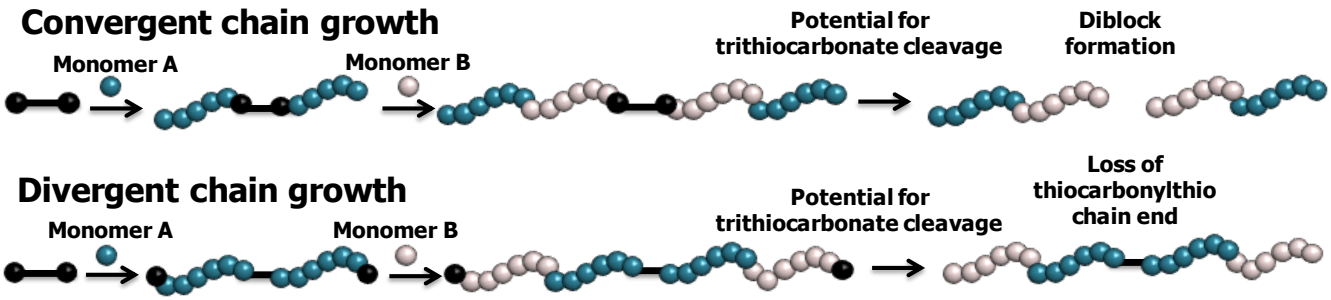

Figure 8.1. CTA design determines the growth of polymer chains in either a divergent or convergent fashion during RAFT polymerization.

Divergent growth involves propagation from the center, while maintaining the thiocarbonylthio groups at the propagating chain ends. On the other hand, a convergent strategy for propagation involves CTA design where the thiocarbonylthio group resides in the center of the propagating chain. Divergent growth is particularly advantageous since the polymer core remains thermally and hydrolytically stable due to the absence of thiocarbonylthio bonds at the center of the polymer, which prevents the deleterious degradation of triblocks into diblocks. The CTA, *S*,*S*'-bis(α, α'-dimethyl-α"-acetic acid) trithiocarbonate (BDAT), remains arguably the most commonly utilized difunctional trithiocarbonate CTA to produce ABA triblock copolymers.[57] Triblock copolymers produced with BDAT propagate according to the convergent strategy and in addition, fail to polymerize methacrylates. Currently, there remains an absence of

hydrolytically stable, difunctional trithiocarbonate CTAs, which effectively polymerize methacrylic monomers.

Our research group previously established ideal conditions for the RAFT polymerization of 4VIM in glacial acetic acid with CEP as a CTA.[47] The incorporation of a low-T_g center block into the 4VIM-containing triblock copolymers required a comonomer which exhibited stability in 5M and glacial acetic acid. In this case, methacrylate monomers display good stability under these conditions. Secondly, the order of monomer addition to synthesize diblock or triblock copolymers remains important; the first block must exhibit a higher transfer constant during RAFT polymerization with the second comonomer to achieve successful block copolymerization. Thus, the propagating radical of the first block must display a greater or equivalent radical stability compared to the propagating radical of the second monomer. Due to 4VIM's decreased radical stability and the necessary monomer order in RAFT polymerization, a divergent CTA was necessary to prepare the desired ABA triblock copolymers.

Scheme 8.1 depicts the synthesis of a novel, difunctional CTA to polymerize 4VIM-containing ABA triblock copolymers in a divergent fashion.

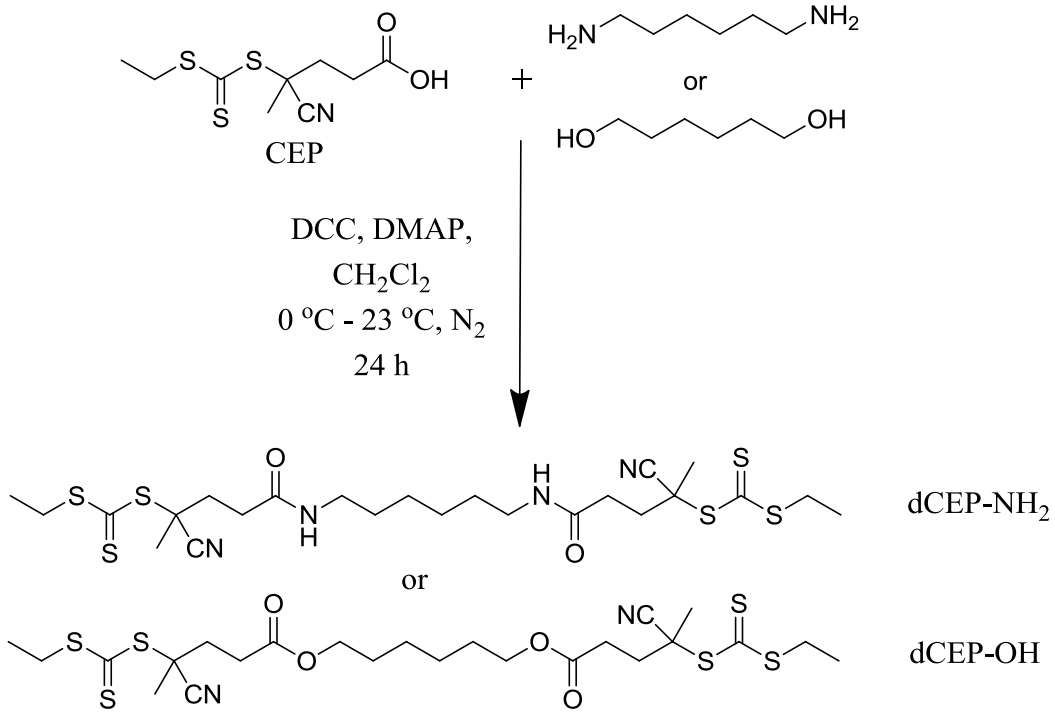

Scheme 8.1. Synthesis of difunctional trithiocarbonate CTAs utilizing DCC coupling with diamine- or diol-containing molecules for divergent RAFT polymerization.

The synthesis involved DCC coupling between CEP and a diamine or diol to generate hydrolytically stable amide (dCEP-NH_2) or degradable ester (dCEP-OH) containing CTAs in high yield. Sodium bicarbonate washings and silica gel column chromatography removed all traces of monofunctional CTA and residual impurities. ^{1}H NMR, ^{13}C NMR, and mass spectrometry confirmed the chemical structure and purity. These difunctional CTAs were ideal for the preparation of 4VIM-containing triblock copolymers due to the preservation of trithiocarbonate functionality, which successfully controlled previous 4VIM homopolymerizations.[47]

The polymerization of vinyl monomers with dCEP-NH_2 and dCEP-OH in a controlled fashion confirmed difunctionality and demonstrated the wide array of suitable monomers for these CTAs. DEGMEMA was ideal as a low-T_g middle block for 4VIM-containing ABA triblock copolymers due to its solubility in aqueous mobile phases for SEC characterization,

hydrolytic stability and solubility in glacial acetic acid, and homopolymer T_g ~ -40 °C. The homopolymerization of DEGMEMA under identical RAFT conditions ([DEGMEMA]/[TTC]/[V-501] ratio = 400/2/1) for both difunctional CTAs (dCEP-NH_2 and dCEP-OH) and CEP displayed similar linear pseudo-first-order kinetics (Figure 8.2a). All polymerizations proceeded to quantitative conversions with narrow PDIs and demonstrated good agreements between experimental and theoretical molecular weights (Figure 8.2b). Base stability studies showed the ability to cleave the dCEP-OH CTA to generate diblock copolymers from the triblock copolymer.

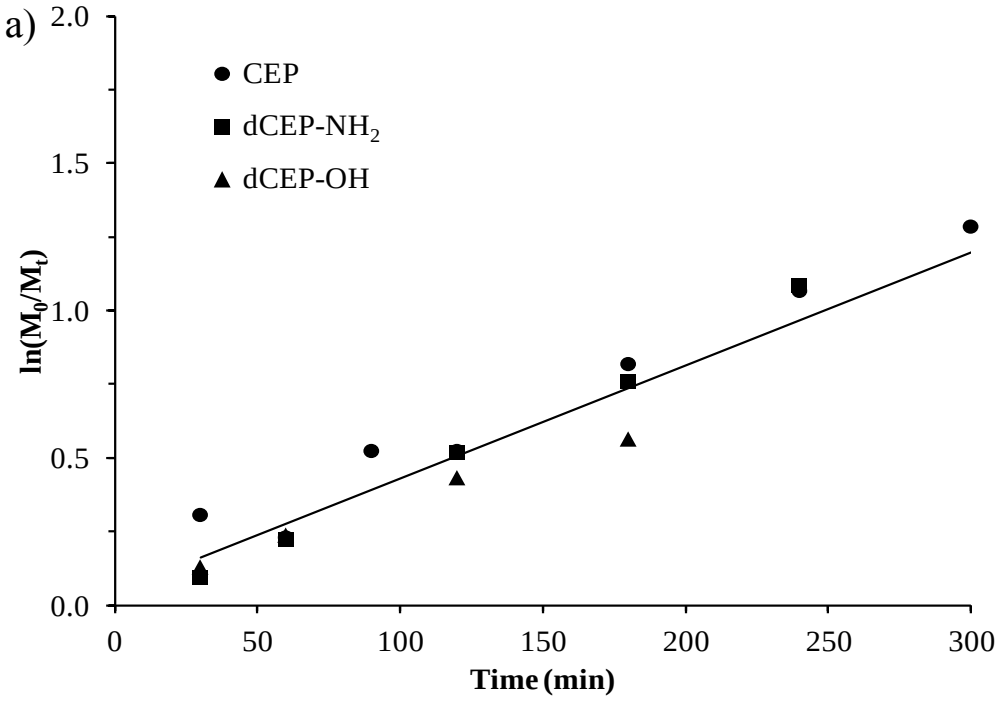

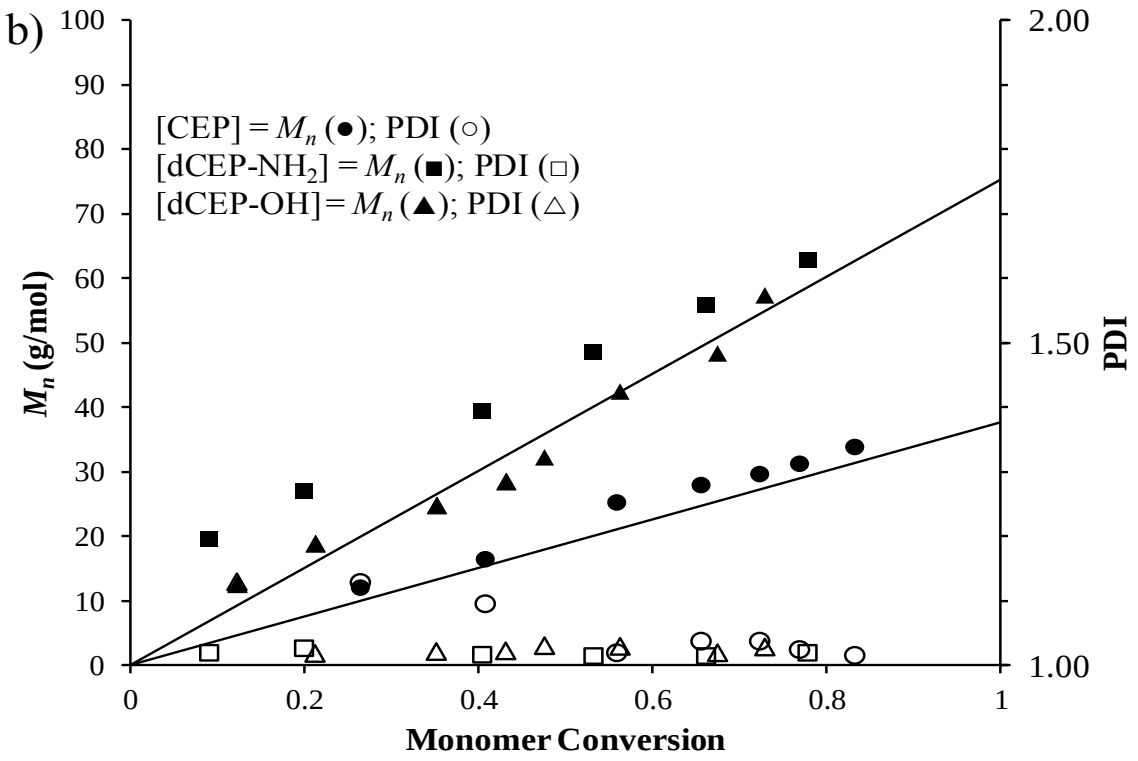

Figure 8.2. (a) Pseudo-first order kinetics plot for the RAFT polymerization of DEGMEMA in DMSO at 70 °C utilizing various CTAs (0.50 M; [TTC]/[V-501] = 2; DP = 200). (b) Dependence of M_n and PDI on monomer conversion utilizing various CTAs.

The synthesis of poly(4VIM-*b*-DEGMEMA-*b*-4VIM) triblock copolymers required the hydrolytic stability of dCEP-NH_2 in glacial acetic acid. Initial experiments involved the synthesis of a poly(DEGMEMA) macroCTA mediated with dCEP-NH_2 in DMSO to generate the low-T_g middle block as shown in Scheme 8.2. Our group has demonstrated previously the effectiveness of DMSO as a free radical polymerization solvent.[58]

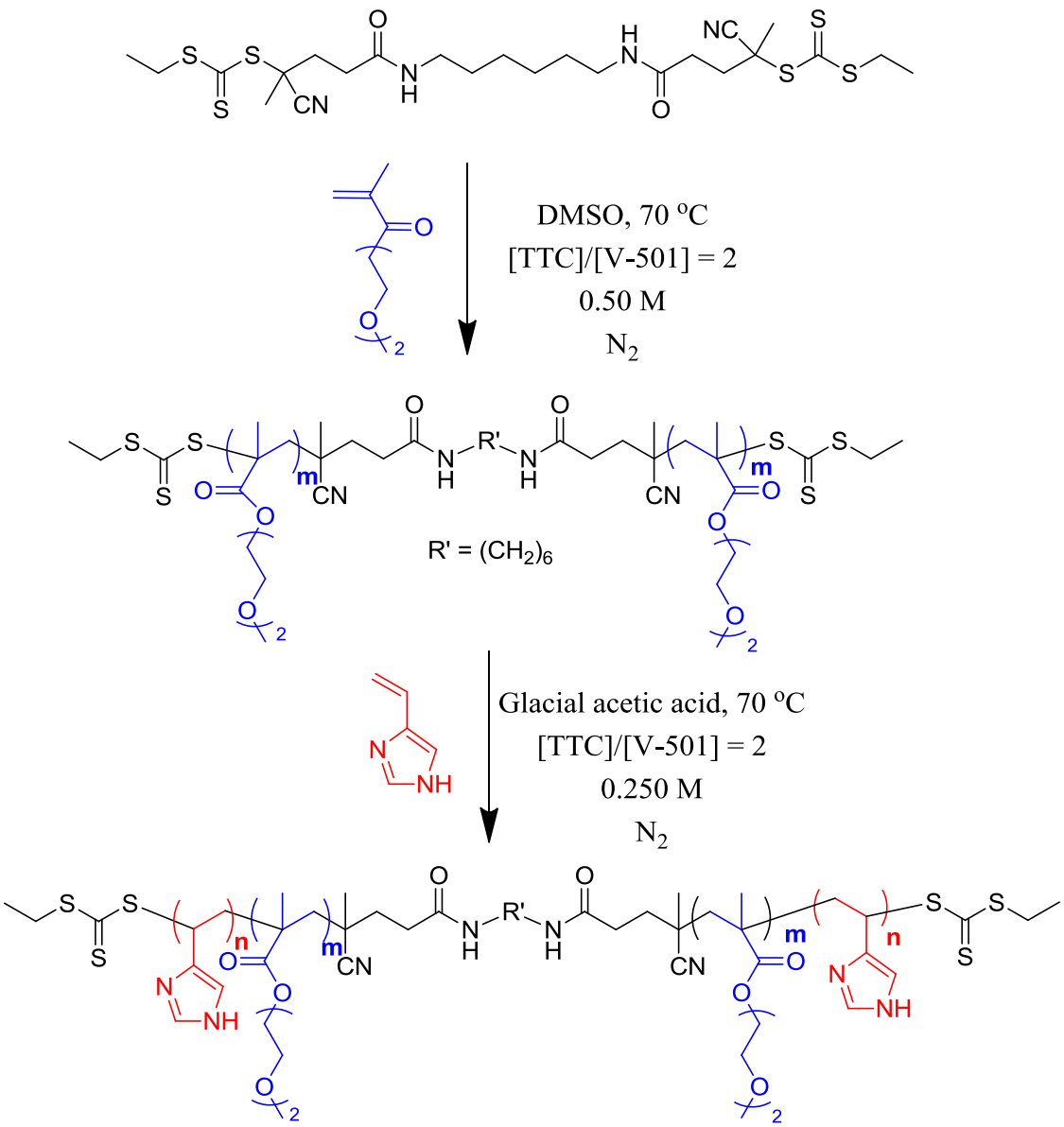

Scheme 8.2. Synthesis of amphoteric ABA triblock copolymers with RAFT polymerization.

The polymerization conditions resulted in a well-defined polymer with narrow PDIs (M_n = 26,000 g/mol; PDI = 1.02). The block copolymerization of 4VIM onto the DEGMEMA macroCTA was performed according to similar conditions previously established (Scheme 8.2; [4VIM]/[TTC]/[V-501] = 500/2/1; 0.25 M), which maintained excellent control of 4VIM polymerization.[47] The adjustment of polymerization reaction time enabled the synthesis of

different 4VIM outer block molecular weights. Aqueous SEC-MALLS confirmed a shift to shorter elution times as the triblock copolymer molecular weight increased (Figure 8.3).

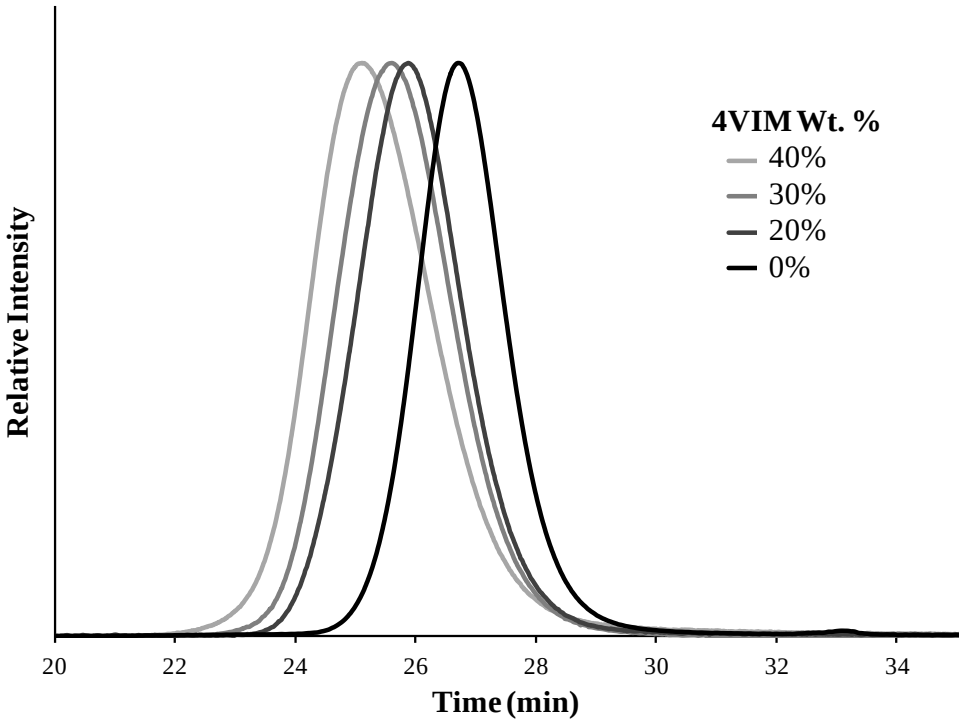

Figure 8.3. SEC light scattering chromatograms displaying the increase in polymer molecular weight to synthesize various amphoteric ABA triblock copolymers. The poly(DEGMEMA) macroCTA is represented as 0 wt. %.

The unimodal SEC chromatograms and narrow molecular weight distributions (PDIs < 1.10) indicated the absence of uncontrolled 4VIM homopolymerization and high molecular weight termination products. ^{1}H NMR spectroscopy verified the presence of 4VIM in the triblock copolymers and quantified the number-average molecular weight of the external blocks.

Table 8.1 shows the favorable agreement between the absolute molecular weights determined with both aqueous SEC-MALLS and ^{1}H NMR spectroscopy to generate approximately 20, 30, and 40 wt. % 4VIM triblock copolymers.

Table 8.1. Molecular weight analysis of 4VIM-containing ABA triblock copolymers.

Polymer	M_n **(g/mol)** ^{1}**H NMR**	M_n **(g/mol)** **SEC**	**PDI**
Poly(DEGMEMA) MacroCTA	----	26,000	1.02
Poly($4VIM_{41}$-*b*-$DEGMEMA_{134}$-*b*-$4VIM_{41}$)	33,700	32,500	1.03
Poly($4VIM_{62}$-*b*-$DEGMEMA_{134}$-*b*-$4VIM_{62}$)	37,700	35,800	1.04
Poly($4VIM_{100}$-*b*-$DEGMEMA_{134}$-*b*-$4VIM_{100}$)	44,800	42,500	1.09

Note: $4VIM_x$ represents the degree of polymerization in each block of the triblock copolymer.

DMA confirmed the presence of microphase separation in the triblock copolymers with various 4VIM contents. The storage modulus (E') and loss tangent (tanδ) *versus* temperature for the triblock copolymers are shown in Figure 8.4.

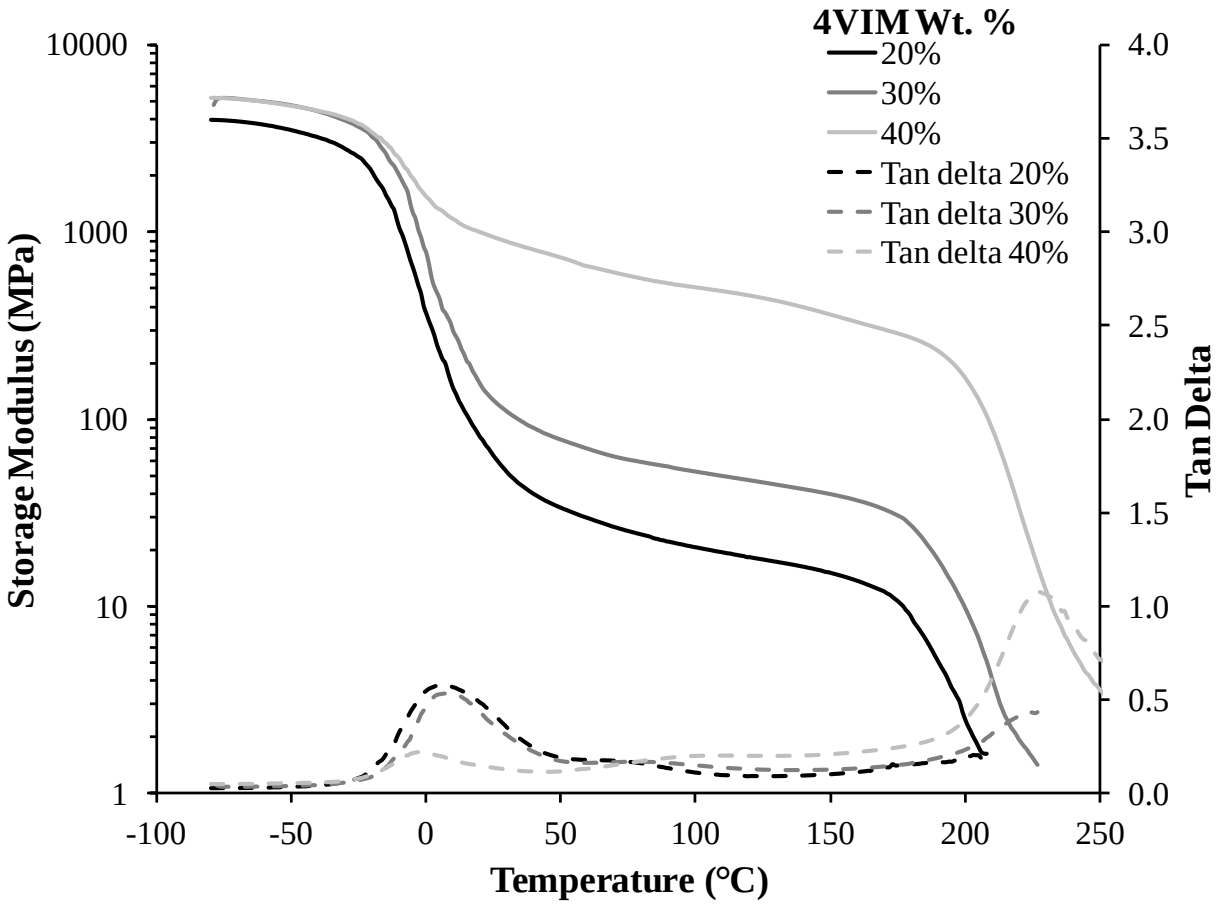

Figure 8.4. Dynamic mechanical analysis of 20, 30, and 40 wt. % 4VIM in poly(4VIM-*b*-DEGMEMA-*b*-4VIM) triblock copolymers. Dynamic mechanical properties analyzed in tension mode: 1 Hz, 3 °C/min.

The 40 wt. % triblock copolymer exhibited two distinctive tanδ peaks, while the 20 wt. % and 30 wt. % triblock copolymers displayed one tanδ maximum. The tanδ peak at ~ 2 °C corresponded to the T_g of the soft, DEGMEMA center block while the second tanδ peak at ~ 220 °C corresponded to the T_g of poly(4VIM) hard phase. An increase in the concentrations of 4VIM in the outer, reinforcing blocks dramatically increased the rubbery plateau storage modulus. The rubbery plateau extended for approximately 200 °C with a flow temperature exceeding 180 °C, which demonstrated the versatility of these triblock copolymers over a wide temperature range. Earlier literature on traditional poly(styrene-*b*-*n*BA-*b*-styrene) triblock copolymers, found

incorporations near 45 wt. % styrene produced weakly phase separated morphologies and poor thermomechanical properties (rubbery plateau storage modulus < 10 MPa) upon annealing.[59] In addition, the rubbery plateau only extended approximately 100 °C, which limited the temperature window for these thermoplastic elastomers.

Tensile testing evaluated the ultimate properties of triblock copolymer films at ambient conditions. Figure 8.5 shows representative stress *versus* strain curves for each triblock copolymer.

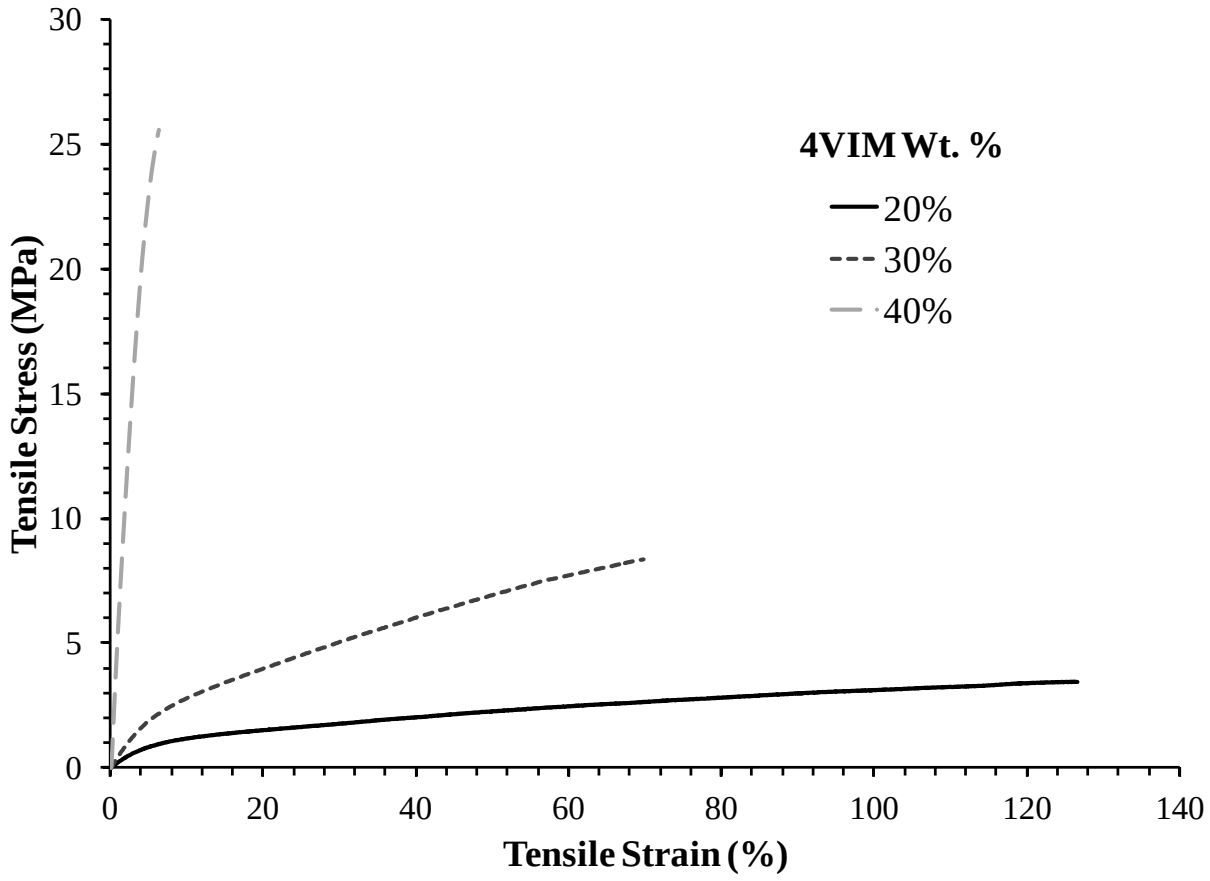

Figure 8.5. Tensile properties of 20, 30, and 40 wt. % 4VIM in poly(4VIM-*b*-DEGMEMA-*b*-4VIM) triblock copolymers. Tensile data are reported as an average of five samples under tensile mode and crosshead speed of 10 mm/min.

The triblock copolymer films exhibited significantly improved mechanical strength compared to either poly(4VIM) or poly(DEGMEMA) homopolymers as neither homopolymer formed an adequate film for mechanical property characterization. The tensile properties of the triblock copolymers exhibited an increase in Young's modulus and tensile stress and a decrease in tensile strain with increasing 4VIM content (Table 8.2). These triblock copolymers displayed improved mechanical properties compared to 45 wt. % styrene in poly(styrene-*b*-*n*BA-*b*-styrene) which exhibited a Young's modulus of 2.5 MPa with a tensile stress/strain at break of 0.85 MPa / 147%.[59] TGA-SA demonstrated despite arduous drying conditions that the homopolymer, poly(4VIM) absorbs water (< 10%) at ambient conditions, but, due to its amphoteric nature absorbs substantially less water than the regioisomer, poly(1VIM). To dry the polymers effectively prior to TGA-SA analysis, all polymers are dried at 100 °C under vacuum for 48 h and then dried to constant mass in the TGA-SA at 50 °C.

Table 8.2. Tensile properties of 4VIM-containing triblock copolymers.

4VIM Wt. %	Tensile Stress at Break (MPa)	Tensile Strain at Break (%)	Young's Modulus (MPa)
20%	3.73 $\pm$ 0.53	132 $\pm$ 18	19.9 $\pm$ 2.2
30%	8.72 $\pm$ 0.63	66.4 $\pm$ 6.4	39.6 $\pm$ 0.8
40%	23.7 $\pm$ 1.6	6.0 $\pm$ 1.0	631 $\pm$ 85

SAXS experiments revealed the triblock copolymer bulk morphology. X-ray scattering data plotted as intensity, $I(q)$, versus scattering vector, q (Figure 8.6) confirmed microphase separation in the ABA triblock copolymers.

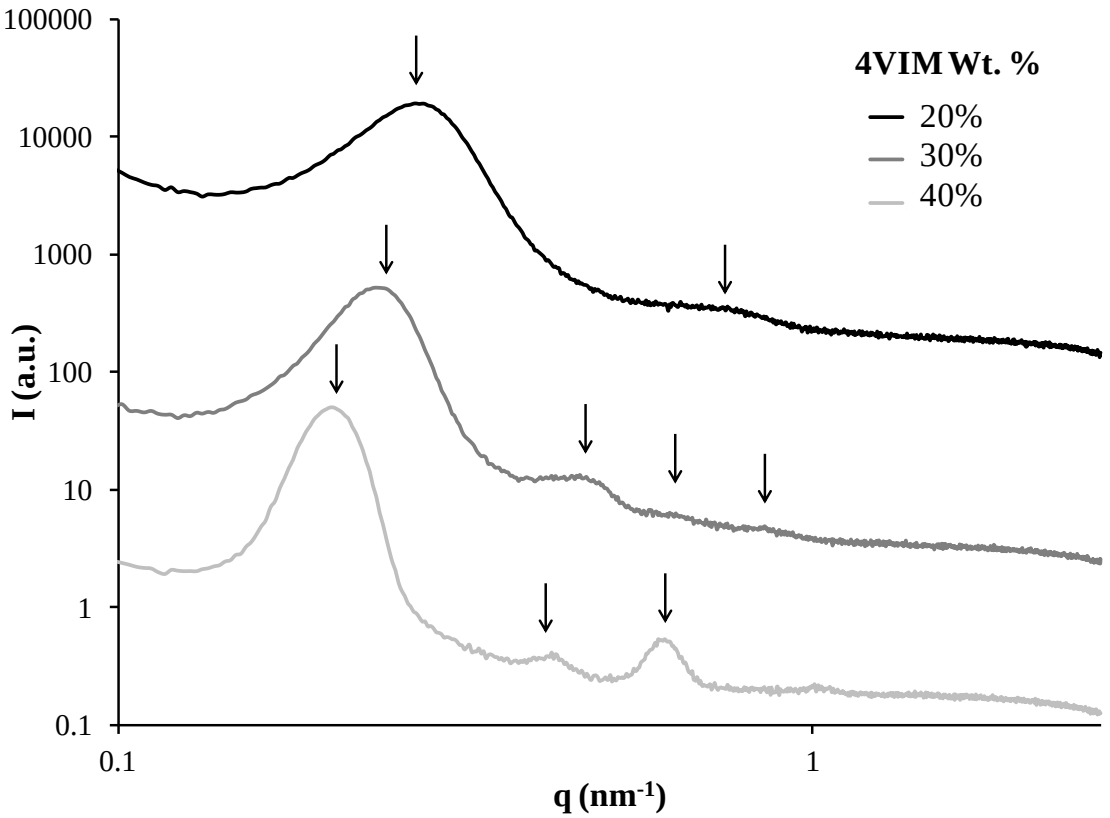

Figure 8.6. SAXS profiles of scattering intensity versus scattering vector for poly(4VIM-*b*-DEGMEMA-*b*-4VIM) triblock copolymers.

The apparent Bragg diffraction maxima observed with X-ray scattering of the 4VIM-containing triblock copolymers indicated the presence of well-defined, ordered morphologies. The 20 wt. % and 30 wt. % 4VIM-containing triblock copolymers failed to exhibit *q*-values characteristic of traditional block copolymer morphologies, presumably due to the lack of sufficient thermal annealing in these samples. Conversely, the 40 wt. % 4VIM triblock copolymer exhibited peak maxima at q^*, $2q^*$, $3q^*$, and $4q^*$, consistent with a lamellar morphology. The equation $2\pi/q^*$ calculated the average lamellar spacing of the 40 wt. % triblock copolymer (31.4 nm; Table 8.3). The principal q peak shifted to lower q values as the wt. % of 4VIM increased in the triblock copolymers indicating the formation of larger nanostructures. TEM and AFM (Figure 8.7)

confirmed the presence of lamellar morphologies present in the 40 wt. % 4VIM triblock copolymers.

Table 8.3. SAXS *q*-values and Bragg spacings.

4VIM Wt.%	q (nm^{-1}) (1st order peak)	Distance (nm)	q (nm^{-1}) (2nd order peak)	q (nm^{-1}) (3rd order peak)	q (nm^{-1}) (4th order peak)
20%	0.27	23.3	0.77	--	--
30%	0.24	26.2	0.47	0.64	0.85
40%	0.20	31.4	0.42	0.61	--

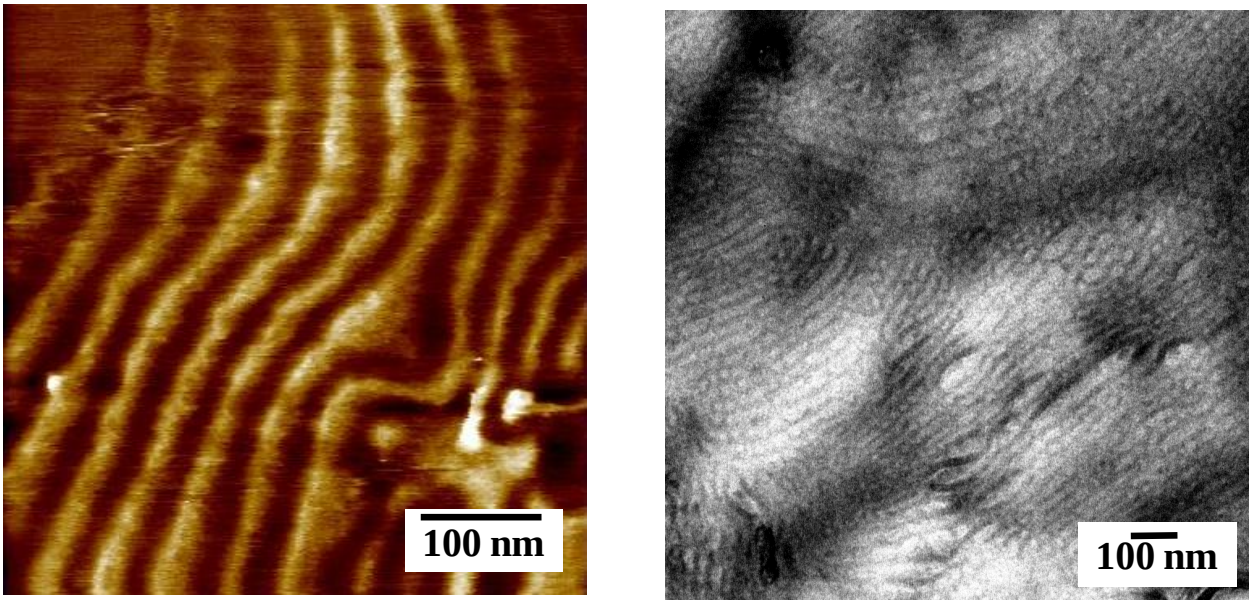

Figure 8.7. AFM phase image in tapping mode and TEM image of 40 wt. % 4VIM-containing ABA triblock copolymer.

The appearance of clear, well-defined lamellar morphologies in the triblock copolymers with higher incorporations of 4VIM indicated the high degree of nanophase separation in these triblock films, whereas, a majority of triblock copolymers require high annealing temperatures and/or long casting times to drive microphase separation.

8.5 *Conclusions*

RAFT polymerization strategies involving a newly synthesized difunctional CTA successfully synthesized 4VIM-containing triblock copolymers for the first time. These macromolecules currently are the only triblock copolymers which incorporate an amphoteric imidazole ring into the reinforcing, outer block. The difunctional CTA (dCEP-NH_2) demonstrated hydrolytic stability in glacial acetic acid and generated methacrylic macroCTAs in a living fashion with well-defined molecular weights and narrow PDIs. Additionally, dCEP-NH_2 successfully synthesized poly(4VIM-*b*-DEGMEMA-*b*-4VIM) triblock copolymers with various wt. % of 4VIM as the reinforcing, outer block with narrow molecular weight distributions. Controlling 4VIM incorporation enabled the tuning of triblock thermomechanical properties. These triblock copolymers exhibited microphase separated morphologies without annealing and displayed improved thermomechanical properties compared to traditional poly(styrene-*b*-*n*BA-*b*-styrene) triblock copolymers. SAXS and AFM confirmed microphase separation and showed high incorporations of 4VIM (40 wt. %) resulted in a well-defined lamellar morphology. The development of these new systems enables the design of future thermoplastic elastomers with amphoteric reinforcing blocks to tune macromolecular properties.

8.6 *Acknowledgements*

This material is also based upon work supported in part by the US Army Research Office under Grant No. W911NF-07-1-0452 Ionic Liquids in Electro-Active Devices (ILEAD) MURI. This material is based on work partially supported by the U.S. Army Research Laboratory and the U.S. Army Research Office under the Army Materials Center of Excellence Program, contract W911NF-06-2-0014. This material is based on work supported by the Army Research Office (ARO) under Award No. W911NF-10-1-0307 (DURIP). We also acknowledge the Institute for Critical Technology and Applied Science (ICTAS) at Virginia Tech for instrument

support. We acknowledge funding from NSF (CHE-0722638) for the acquisition of our Agilent 6220 LC-TOF-MS. We also acknowledge David Inglefield for performing and obtaining AFM and TEM images as well as Chainika Jangu for her help with RAFT polymerizations.

8.7 *References*

(1) Kim, J. K.; Yang, S. Y.; Lee, Y.; Kim, Y. *Prog. Polym. Sci.* **2010**, *35*, 1325-1349.
(2) Sijbesma, R. P.; Beijer, F. H.; Brunsveld, L.; Folmer, B. J. B.; Hirschberg, J. H. K. K.; Lange, R. F. M.; Lowe, J. K. L.; Meijer, E. *Science* **1997**, *278*, 1601-1604.
(3) Kato, T.; Kihara, H.; Kumar, U.; Uryu, T.; Fréchet, J. M. J. *Angew. Chem. Int. Ed.* **2003**, *33*, 1644-1645.
(4) Pan, J.; Chen, M.; Warner, W.; He, M.; Dalton, L.; Hogen-Esch, T. E. *Macromolecules* **2000**, *33*, 7835-7841.
(5) Kříž, J.; Dybal, J.; Brus, J. *J. Phys. Chem. B* **2006**, *110*, 18338-18346.
(6) Garrett, J.; Runt, J.; Lin, J. *Macromolecules* **2000**, *33*, 6353-6359.
(7) Mather, B. D.; Baker, M. B.; Beyer, F. L.; Berg, M. A. G.; Green, M. D.; Long, T. E. *Macromolecules* **2007**, *40*, 6834-6845.
(8) Cheng, S.; Zhang, M.; Dixit, N.; Moore, R. B.; Long, T. E. *Macromolecules* **2012**, *45*, 805-812.
(9) Leibler, L. *Macromolecules* **1980**, *13*, 1602-1617.
(10) Mather, B. D.; Baker, M. B.; Beyer, F. L.; Green, M. D.; Berg, M. A. G.; Long, T. E. *Macromolecules* **2007**, *40*, 4396-4398.
(11) Lee, K. M.; Han, C. D. *Macromolecules* **2002**, *35*, 3145-3156.
(12) Wang, S.-M.; Lee, L.-Y.; Chen, J.-T. *Spectrochimica Acta Part A: Molecular Spectroscopy* **1979**, *35*, 765-771.
(13) Tucker, E. E.; Lane, E. H.; Christian, S. D. *J. Solution Chem.* **1981**, *10*, 1-20.
(14) Tucker, E. E.; Christian, S. D. *J. Phys. Chem.* **1979**, *83*, 426-427.
(15) Ye, Y.; Elabd, Y. A. *Macromolecules* **2011**, *44*, 8494-8503.
(16) Lee, M.; Choi, U. H.; Colby, R. H.; Gibson, H. W. *Chem. Mater.* **2010**, *22*, 5814-5822.
(17) Matsumoto, K.; Talukdar, B.; Endo, T. *Polym. Bull.* **2010**, *66*, 199-210.
(18) Weber, R. L.; Ye, Y.; Schmitt, A. L.; Banik, S. M.; Elabd, Y. A.; Mahanthappa, M. K. *Macromolecules* **2011**, *44*, 5727-5735.
(19) Weber, R. L.; Ye, Y.; Banik, S. M.; Elabd, Y. A.; Hickner, M. A.; Mahanthappa, M. K. *J. Polym. Sci., Part B: Polym. Phys.* **2011**, *49*, 1287-1296.
(20) Stancik, C. M.; Lavoie, A. R.; Achurra, P. A.; Waymouth, R. M.; Gast, A. P. *Langmuir* **2004**, *20*, 8975-8987.
(21) Stancik, C. M.; Lavoie, A. R.; Schütz, J.; Achurra, P. A.; Lindner, P.; Gast, A. P.; Waymouth, R. M. *Langmuir* **2003**, *20*, 596-605.
(22) Green, M. D.; Salas-de la Cruz, D.; Ye, Y.; Layman, J. M.; Elabd, Y. A.; Winey, K. I.; Long, T. E. *Macromol. Chem. Phys.* **2011**, *212*, 2522-2528.
(23) Allen, M. H.; Green, M. D.; Getaneh, H. K.; Miller, K. M.; Long, T. E. *Biomacromolecules* **2011**, *12*, 2243-2250.
(24) Overberger, C. G.; Kawakami, Y. *Journal of Polymer Science: Polymer Chemistry Edition* **1978**, *16*, 1237-1248.
(25) Overberger, C. G.; Smith, T. W. *Macromolecules* **1975**, *8*, 416-424.

(26) Overberger, C. G.; Smith, T. W. *Macromolecules* **1975**, *8*, 401-406.
(27) Overberger, C. G.; Smith, T. W. *Macromolecules* **1975**, *8*, 407-415.
(28) Overberger, C. G.; Gerberding, K. *Journal of Polymer Science: Polymer Letters Edition* **1973**, *11*, 465-469.
(29) Okamoto, Y.; Overberger, C. *J. Polym. Sci., Part A: Polym. Chem.* **1972**, *10*, 3387-3395.
(30) Overberger, C. G.; Maki, H. *Macromolecules* **1970**, *3*, 214-220.
(31) Overberger, C. G.; Maki, H. *Macromolecules* **1970**, *3*, 220-223.
(32) Overberger, C. G.; Salamone, J. C. *Acc. Chem. Res.* **1969**, *2*, 217-224.
(33) Overberger, C. G.; Salamone, J. C.; Yaroslavsky, S. *J. Am. Chem. Soc.* **1967**, *89*, 6231-6236.
(34) Overberger, C. G.; Pierre, T. S.; Vorchheimer, N.; Lee, J.; Yaroslavsky, S. *J. Am. Chem. Soc.* **1965**, *87*, 296-301.
(35) Overberger, C. G.; Vorchheimer, N. *J. Am. Chem. Soc.* **1963**, *85*, 951-955.
(36) Overberger, C. G.; Pierre, T. S.; Vorchheimer, N.; Yaroslavsky, S. *J. Am. Chem. Soc.* **1963**, *85*, 3513-3515.
(37) Tang, H.; Tang, J.; Ding, S.; Radosz, M.; Shen, Y. *J. Polym. Sci., Part A: Polym. Chem.* **2005**, *43*, 1432-1443.
(38) Ding, S.; Tang, H.; Radosz, M.; Shen, Y. *J. Polym. Sci., Part A: Polym. Chem.* **2004**, *42*, 5794-5801.
(39) Vijayakrishna, K.; Jewrajka, S. K.; Ruiz, A.; Marcilla, R.; Pomposo, J. A.; Mecerreyes, D.; Taton, D.; Gnanou, Y. *Macromolecules* **2008**, *41*, 6299-6308.
(40) Ye, Y.; Choi, J.-H.; Winey, K. I.; Elabd, Y. A. *Macromolecules* **2012**, *45*, 7027-7035.
(41) Green, M. D.; Choi, J.-H.; Winey, K. I.; Long, T. E. *Macromolecules* **2012**.
(42) He, X.; Yang, W.; Yuan, L.; Pei, X.; Gao, J. *Mater. Lett.* **2009**, *63*, 1138-1140.
(43) Patrickios, C. S.; Simmons, M. R. *Colloids and Surfaces A: Physicochemical and Engineering Aspects* **2000**, *167*, 61-72.
(44) Ge, Z.; Xie, D.; Chen, D.; Jiang, X.; Zhang, Y.; Liu, H.; Liu, S. *Macromolecules* **2007**, *40*, 3538-3546.
(45) Mori, H.; Yahagi, M.; Endo, T. *Macromolecules* **2009**, *42*, 8082-8092.
(46) Detrembleur, C.; Debuigne, A.; Hurtgen, M.; Jérôme, C.; Pinaud, J.; Fèvre, M. v.; Coupillaud, P.; Vignolle, J.; Taton, D. *Macromolecules* **2011**, *44*, 6397-6404.
(47) Allen, M. H.; Hemp, S. T.; Smith, A. E.; Long, T. E. *Macromolecules* **2012**, *45*, 3669-3676.
(48) Schiavone, R.; Overberger, C. *J. Polym. Sci., Part A: Polym. Chem.* **1988**, *26*, 107-115.
(49) Liu, W.; Greytak, A. B.; Lee, J.; Wong, C. R.; Park, J.; Marshall, L. F.; Jiang, W.; Curtin, P. N.; Ting, A. Y.; Nocera, D. G.; Fukumura, D.; Jain, R. K.; Bawendi, M. G. *J. Am. Chem. Soc.* **2009**, *132*, 472-483.
(50) Convertine, A. J.; Benoit, D. S. W.; Duvall, C. L.; Hoffman, A. S.; Stayton, P. S. *J. Controlled Release* **2009**, *133*, 221-229.
(51) Matyjaszewski, K. *Curr. Opin. Solid State Mater. Sci.* **1996**, *1*, 769-776.
(52) Lowe, A. B.; McCormick, C. L. *Prog. Polym. Sci.* **2007**, *32*, 283-351.
(53) Hawker, C. J.; Bosman, A. W.; Harth, E. *Chem. Rev.* **2001**, *101*, 3661-3688.
(54) Chiefari, J.; Chong, Y. K.; Ercole, F.; Krstina, J.; Jeffery, J.; Le, T. P. T.; Mayadunne, R. T. A.; Meijs, G. F.; Moad, C. L.; Moad, G.; Rizzardo, E.; Thang, S. H. *Macromolecules* **1998**, *31*, 5559-5562.

(55) Moad, G.; Chiefari, J.; Chong, Y K.; Krstina, J.; Mayadunne, R. T A.; Postma, A.; Rizzardo, E.; Thang, S. H. *Polym. Int.* **2000**, *49*, 993-1001.
(56) Yu, J. M.; Dubois, P.; Jérôme, R. *Macromolecules* **1996**, *29*, 8362-8370.
(57) Lai, J. T.; Filla, D.; Shea, R. *Macromolecules* **2002**, *35*, 6754-6756.
(58) Yamauchi, K.; Lizotte, J. R.; Long, T. E. *Macromolecules* **2003**, *36*, 1083-1088.
(59) Cheng, S.; Beyer, F. L.; Mather, B. D.; Moore, R. B.; Long, T. E. *Macromolecules* **2011**, *44*, 6509-6517.

8.8 *Supporting Information*

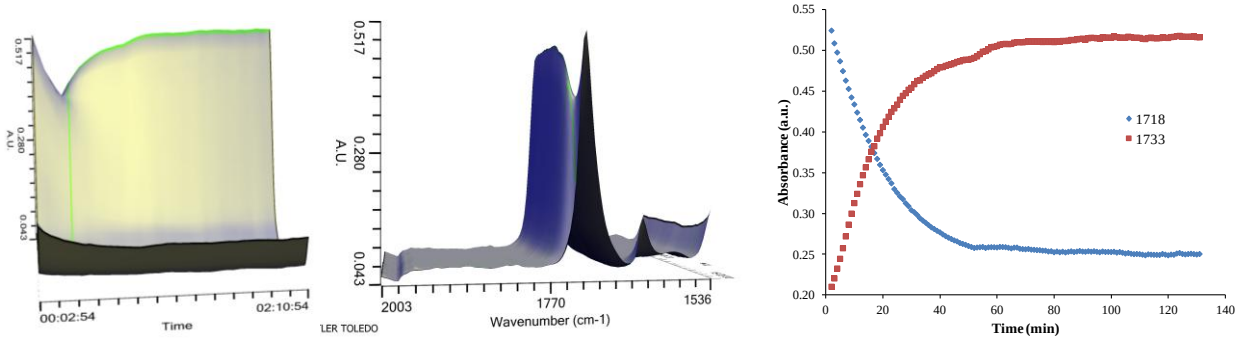

Figure S8.1. *In situ* FTIR of DEGMEMA in imidazole at 100 °C to probe possible reactions occurring during annealing of triblock copolymer films. Imidazole catalyzed the hydrolysis of DEGMEMA (1718 cm^{-1}) into an imidazole methacrylamide (1733 cm^{-1}) and di(ethylene glycol) methyl ether as evidenced in the *in situ* FTIR plots.

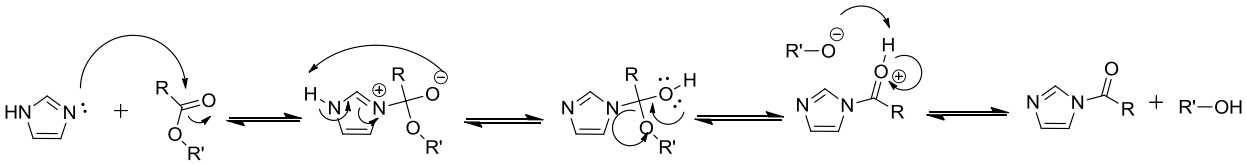

Scheme S8.1. Proposed crosslinking mechanism observed during annealing of triblock copolymer films.

Chapter 9: Overall Conclusions

The synthesis of functionalized vinylimidazole-containing polymers remains a unique area of macromolecular chemistry. First, 1-vinylimidazole (1VIM) was homopolymerized utilizing conventional free radical polymerization to generate linear macromolecules for nonviral gene delivery. Post-polymerization functionalization enabled the tailoring of macromolecular properties for improved DNA transfection efficiencies without varying polymer molecular weights. Increased cationic charge densities through post-polymerization functionalization increased the cytotoxicity of the copolymers. Charge densities over 25 mol % exhibited decreased transfection efficiencies due to high copolymer-DNA binding affinities preventing the release of the nucleic acid cargo. Varying hydrogen bonding substituent concentration provided an alternative route to tuning copolymer-DNA binding affinity. Substituents containing one hydroxyl group delivered DNA most effectively whereas zero or two hydroxyl groups per repeat unit delivered DNA ineffectively. The transfection efficiencies for both charge density and hydrogen bonding substituent variation suggested an intermediate copolymer-DNA binding affinity is required to effectively deliver DNA to cells. Advantageously, controlling hydrogen bonding substituent concentration does not impact copolymer cytotoxicity, therefore, providing a safe and effective alternative to tune copolymer-DNA binding affinities than the more conventional highly charged copolymer systems.

Functionalizing imidazolium copolymers enabled further investigation of copolymer composition on nonviral gene delivery. Several previous reports demonstrated specific cancerous tumors often over-express folate-receptors. The incorporation of folic acid onto therapeutic macromolecules allows for efficient delivery of genetic cargo into the cell through receptor-mediated endocytosis. For the first time, imidazolium-containing copolymers were functionalized with folic acid to explore the impact of folic acid incorporation on nucleic acid

delivery. The synthesis of these novel macromolecules remained difficult. Similar to previous studies, 1VIM was polymerized utilizing conventional free radical polymerization techniques to eliminate the effect of molecular weight on nonviral gene delivery. Post-polymerization functionalization with a *t*Boc-protected alkyl amine afforded charge densities up to 25 mol %, 10 times greater concentration than previously reported in literature. Acid deprotection generated alkyl-amine functionalized imidazolium copolymers for folic acid conjugations. Low concentrations of folic acid were conjugated onto the copolymers (4-8 molecules per polymer chain) to maintain water solubility. The copolymers transfected HeLa cells, which contain a high concentration of folate receptors on the cell membrane surface. Similar to other nonviral gene delivery vehicles functionalized with folic acid, the DNA delivery efficiency of the copolymers increased 250-fold with folic acid incorporation. Folic acid incorporation did not influence DNA binding affinity or copolymer cytotoxicity.

Functionalization of 1VIM with various hydroxyalkyl (HAVIM) and alkyl (AVIM) groups and subsequent conventional free radical polymerization afforded a series of imidazolium-containing polyelectrolytes. Counterion selection (Br^-, bis(trifluoromethane-sulfonyl)imide (Tf_2N^-)) enabled the tuning of polymer thermal transitions and thermal stabilities. Thermal analysis revealed the more hydrophobic, less basic counterion-containing homopolymers (Tf_2N^-) displayed increased thermal stabilities and lower glass transition temperatures (T_g's). More importantly, the HAVIM homopolymers exhibited significantly lower T_g's compared to their respective AVIM analogs. X-ray scattering determined the addition of the polar, hydroxyl group disrupted the nanophase-separated morphology present in the AVIM homopolymers. Furthermore, X-ray scattering determined the polymer chain backbone-to-backbone spacing of the HAVIM homopolymers was a similar spacing to the AVIM

homopolymers, even though the HAVIM homopolymers contained an additional hydroxyl group. These spacings suggested the hydroxyl group interacted and disrupted the electrostatic interactions in the homopolymer which lowered T_g and diminished nanophase separation compared to the commonly studied AVIM homopolymers. Impedance spectroscopy indicated the HAVIM-Tf_2N homopolymers exhibited an order of magnitude increase in ionic conductivity compared to AVIM-Tf_2N homopolymers. Control of macromolecular composition can eventually lead to the development of polyelectrolyte membranes for electroactive devices with improved ionic conductivity.

The functionalization of 1VIM for conventional free radical polymerization proves straightforward due to the availability of the tertiary amine for subsequent quaternization as discussed above. However, the design of macromolecules with advanced architectures and precise molecular weights remains difficult due to the radically unstable *N*-vinyl propagating radical. The regioisomer 4-vinylimidazole (4VIM) contains two resonance contributors providing increased propagating radical stability compared to 1VIM. Conventional free radical homopolymerizations generated poly(4VIM) with number-average molecular weights (M_n) greater than 1,000,000 g/mol compared to 50,000 g/mol for poly(1VIM). The use of an unconventional polymerization solvent, glacial acetic acid, was necessary due to the relative insolubility of poly(4VIM) in numerous organic and aqueous solvents. Utilizing RAFT polymerization strategies, the homopolymerization of 4VIM was controlled for the first time. The homopolymerizations displayed linear pseudo-first order kinetics which generated polymers with well-defined molecular weights and narrow PDIs.

Controlling the polymerization of 4VIM enabled the synthesis of triblock copolymer thermoplastic elastomers which incorporated 4VIM into the outer, reinforcing block. The design

of a new difunctional CTA afforded the synthesis of a low-T_g methacrylate center block followed with subsequent polymerization of 4VIM in glacial acetic acid. Controlling 4VIM incorporation enabled the tuning of triblock thermomechanical properties. These triblock copolymers exhibited microphase separated morphologies without annealing and displayed improved thermomechanical properties compared to traditional poly(styrene-*b*-*n*BA-*b*-styrene) triblock copolymers. Dynamic mechanical analysis confirmed the triblock copolymers exhibited microphase separation with a rubbery plateau modulus spanning ~200 °C. Transmission electron microscopy (TEM), atomic force microscopy (AFM), and small-angle X-ray scattering (SAXS) probed the solid state morphologies of the triblock copolymers, and all techniques revealed phase separation at nanoscale dimensions. These complementary techniques emphasize the strength of the association between amphoteric imidazole rings. Typically, most triblock thermoplastic elastomers require a lengthy annealing process at elevated temperatures to promote phase separation due to weak intermolecular interactions, while these triblock copolymers require only room temperature conditions. The triblock copolymers with higher concentrations of 4VIM (40 wt. %) showed lamellar morphologies. Effectively synthesizing well-defined, amphoteric 4VIM ABA triblock copolymers with microphase-separated morphologies (PDIs < 1.10) facilitates the design of imidazole-containing macromolecules of controlled architectures for emerging applications.

Chapter 10: Suggested Future Work

10.1 *Improved Nonviral Gene Delivery*

The polyelectrolytes presented in this work consisted of an imidazolium cation functionalized with a hydroxyalkyl group or aminoalkyl group for nonviral gene delivery. It was understood that hydrogen bonding significantly impacted the transfection efficiencies of the delivery vehicles, influencing most dramatically, polymer-DNA binding affinities without affecting copolymer cytotoxicity. An interesting study would investigate the effect of hydrogen bond donor and acceptor substituents attached to the imidazolium ring to establish a better understanding of structure-property-transfection relationships. Additionally, these cationic polyelectrolytes are not suitable for *in vivo* transfection due to a lack of colloidal stability; therefore, these macromolecules require the addition of a poly(ethylene glycol) substituent to prevent protein aggregation. Amine-functionalization would enable the prospective reductive amination reaction to attach a sugar or carbohydrate to the imidazolium polyelectrolyte for potentially improving colloidal stability and transfection efficiency. We also observed previously that folic acid incorporation led to improved DNA delivery. Further investigation into the uptake mechanism with flow cytometry and endocytic knockdown assays would enable the design of more effective delivery vehicles and elucidate the effect of folic acid concentration on gene delivery.

10.2 *Synthesis of Diblock Copolymers and Hydrophobic Triblock Copolymers*

The controlled radical polymerization of 4-vinylimidazole (4VIM) in Chapters 7 and 8 presented a thorough investigation into the reaction kinetics and design of macromolecules with precise molecular weights and well-defined structures. The successful synthesis of 4VIM-containing triblock copolymers provided experimental proof of a synthetic protocol to achieve various polymer architectures. Taking advantage of RAFT polymerization strategies, the

potential to generate numerous additional macromolecules exists. The synthesis of diblock copolymers remains an area of much interest especially for the design of polymeric "nanoreactors". The synthesis of a core-shell diblock in aqueous media as proposed in Scheme 10.1 would enable the design of stimuli-responsive micelles.

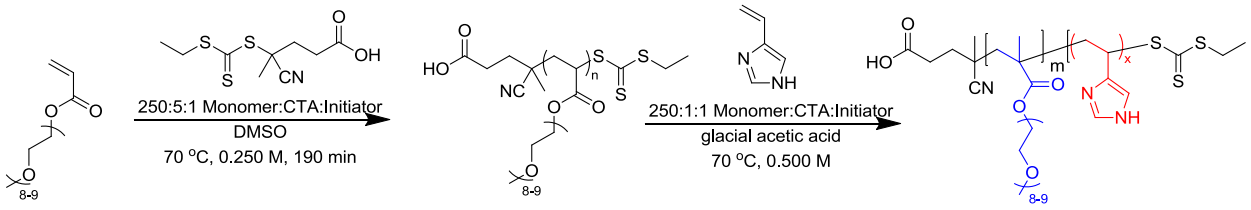

Scheme 10.1. Synthesis of pH-responsive 4VIM-containing micelles to catalyze various organic reactions or chelate metals.

The oligo(ethylene glycol) methyl ether methacrylate block remains soluble in aqueous solutions and 4VIM only dissolves in aqueous media when protonated (pH < 6). This allows for the generation of polymeric micelles in neutral and basic conditions enabling the catalysis of organic reactions in aqueous media as a replacement for expensive biological enzymes. Hydrophobic reactants would incorporate themselves into the hydrophobic 4VIM core where various reactions could occur (i.e. esterolysis). Additionally, atom transfer radical polymerization (ATRP) requires a coordinating ligand to complex the necessary copper catalyst to achieve well-defined polymer structures. The polymeric micelles or "nanoreactors" which incorporate 4VIM into the hydrophobic block would enable ATRP of hydrophobic monomers in aqueous solution and more importantly would facilitate the removal of the copper catalyst from the polymer due to imidazole's strong metal binding affinity. Furthermore, these designed polymeric micelles could also be employed for water purification due to imidazole's ability to chelate numerous heavy metals.

Further development of novel triblock copolymers with 4VIM also remains an important research topic in the future. Chapter 8 illustrates how incorporating 4VIM into the outer, reinforcing block of an ABA triblock copolymer dramatically improves thermomechanical properties. Scheme 10.2 shows the use of additional, hydrophobic methacrylate monomers to incorporate in the low-T_g center block.

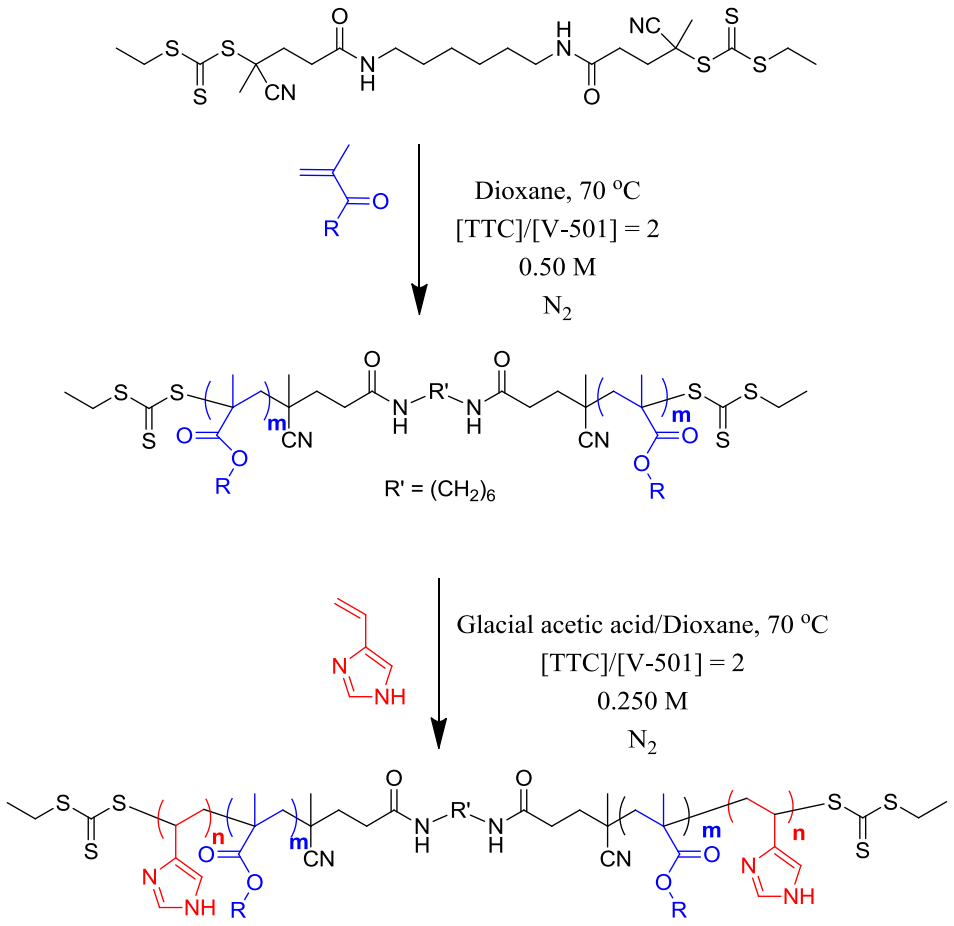

Scheme 10.2. Synthesis of ABA triblock copolymers with a hydrophobic center block to promote microphase separation.

The inspiration behind the use of more hydrophobic systems would allow for potentially better phase separation between the A- and B-blocks preventing covalent crosslinking and achieving more well-defined morphologies.

10.3 *Influence of Pendant Group Spacing on Hydrogen Bonding*

We have previously established the location of hydrogen bonding substituents in relation to the polymer backbone significantly impacted the association between pendant substituents. Scheme 10.3 depicts the synthesis of an imidazole-containing styrenic monomer enabling the design of a novel, amphoteric imidazole-containing monomer. This design advantageously places the imidazole ring further from the polymer backbone. Additionally, the incorporation of a styrenic functionality affords the design of additional block copolymers utilizing controlled free radical polymerization strategies, as styrenic monomers are easily controlled through various methods in polymer chemistry. The properties of this novel macromolecule could be compared to the regioisomer 4-vinylbenzyl-1-imidazole to study the effect of the amphoteric nature of the imidazole ring on macromolecular properties.

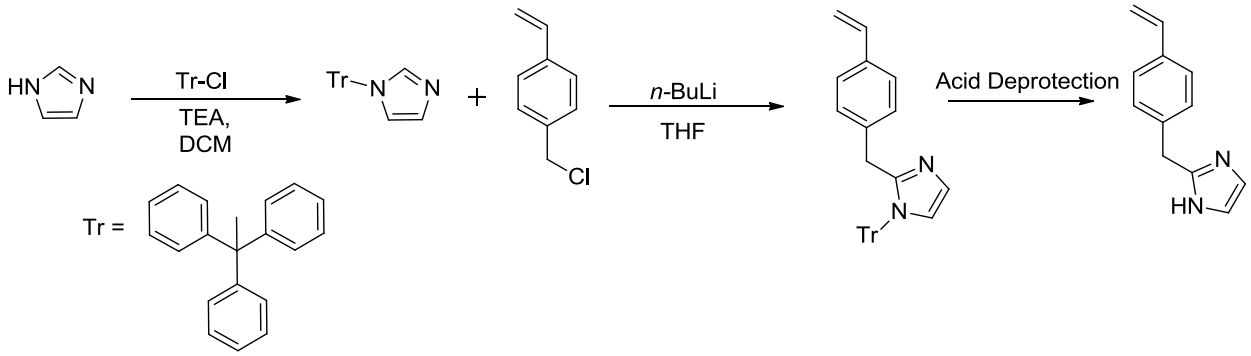

Scheme 10.3. Proposed synthesis of styrenic imidazole-containing monomers to study the impact of the amphoteric, imidazole ring on microphase separation.